

**EXPERIMENTAL AND NUMERICAL INVESTIGATION OF IMPACT  
LOADS ON A GROUP OF PILES**

A Dissertation

by

MOJDEH ASADOLLAHIPAJOUH

Submitted to the Office of Graduate and Professional Studies of  
Texas A&M University  
in partial fulfillment of the requirements for the degree of

DOCTOR OF PHILOSOPHY

Chair of Committee,	Jean-Louis Briaud
Committee Members,	Charles Aubeny
	Giovanna Biscontin
	Daren Cline
Head of Department,	Robin Autenrieth

December 2015

Major Subject: Civil Engineering

Copyright 2015 Mojdeh Asadollahipajouh

## **ABSTRACT**

Groups of in-line piles connected by beams are being used to contain errant vehicles for perimeter protection of infrastructures. Moreover, piles can be used as roadside safety devices resisting against impact loading. The effectiveness of in-line groups of piles to safely redirect or stop the approaching vehicles, however, has not been well investigated from the geotechnical point of view. The seriousness of the failure of such systems requires the development of reliable design guidelines for functional and cost-effective impact resistant systems. To date, such guidelines are limited and new barrier configurations rely mostly on full scale crash testing to be certified before they can be used. However, the extensive test setup, instrumentation and considerable cost of such crash tests have limited the practicality of running many of those tests. Numerical simulations are very useful to extend the values of the crash tests.

In this research, the performance of such barriers is examined through full-scale crash tests and numerical simulations. The full scale crash tests consisted of two different configurations of piles and beams: one was in loose sand and the other in hard clay. Both barriers were subjected to vehicle impact: one by a 6800 kg medium-duty truck traveling with the approaching velocity of 80 km/h and the other by a 2300 kg pickup truck with an approaching velocity of 100 km/h. Both barriers successfully contained the impacting vehicles. Detailed finite element models of the barriers and the soil were developed using LS-DYNA a powerful numerical package and then combined with the vehicle models to simulate the dynamic events. Comparison between predicted

and measured behavior was used to calibrate the models. Once calibrated, additional simulations were performed to create a comprehensive database to further study the impact response of these systems. Practical recommendations are drawn from the experimental and numerical work.

Using the numerical simulation results and the experimental data, a simple yet effective model TAMU-POST (Group) was successfully developed to predict the lateral response of in-line piles embedded in any soil type subjected to impact of a vehicle through a nonlinear impact analysis. It was shown that the developed simplified mass-spring-dashpot analogy method with the calibrated constants for damping gives a remarkably good estimate of the barrier deflection measured in the tests and simulations. Two full scale impact experiments and approximately 100 numerical simulations of impact events using LS-DYNA were used to assess the precision of TAMU-POST. After calibration against the full scale crash tests, additional numerical simulations were performed to study the influence of important design parameters including mass and velocity of vehicle, soil strength, pile spacing and embedment depth was performed. Finally, the uncertainties in estimates of the model inputs such as soil properties and the model parameters were acknowledged through a reliability analysis and the probability of failure provided. It is believed that the research outcome including the testing datasets, numerical experience and the proposed model serve a reliable means to design impact-resistant barriers and, in particular, facilitates future studies on impact performance of piles in better protecting assets.

## **DEDICATION**

I would like to dedicate this dissertation to my beloved parents. I cannot express my deep appreciation for their love, patience and their confidence in me. Without their sacrifice I would not be able to enjoy this amazing journey of education.

## **ACKNOWLEDGEMENTS**

First and foremost I would like to express my sincere gratitude to my wonderful supervisor Professor Jean-Louis Briaud. I am deeply grateful for his invaluable assistance, his patient advice and unfailing support through all my research without which this research would not have been possible. I also wish to thank Dr. Aubeny, Dr. Biscontin and Dr. Cline for their practical advice and comments throughout the course of this research.

I wish to acknowledge the funding I have received from the U.S. Department of State. The additional support from Texas A&M University in the form of scholarships, awards and teaching fellowship has greatly helped and motivated me over the time working on this research. I also wish to recognize our colleagues at the Texas A&M Transportation Institute especially Dr. Alberson and the crash test crew led by Gary Gerke for their invaluable technical support in conducting the crash tests. My sincere thanks go to Dr. Abu Odeh and Dusty Arrington who offered much helpful and timely advice in using LS-DYNA and simulating crash tests. I also want to thank Alireza Mirdamadi, Ghassan Akrouch and Charles Magbo for their help in the experiments.

I owe many thanks to my dear friends Maryam Rezvani and Mona Milani for their sincere friendship and my geotechnical fellows Ryan Beemer, Negin Yousefpour and Ajay Shastri and many other friends for the remarkable moments I have shared with. Finally, I am very deeply indebted to my parents for their love and support throughout my life, who kindly and patiently withstand time and long distance.

## TABLE OF CONTENTS

	Page
ABSTRACT .....	ii
DEDICATION .....	iv
ACKNOWLEDGEMENTS .....	v
TABLE OF CONTENTS .....	vi
LIST OF FIGURES.....	x
LIST OF TABLES .....	xviii
1. INTRODUCTION.....	1
1.1. Problem statement .....	1
1.2. Motivation of the study.....	2
1.2.1. Anti-ram barriers design.....	2
1.2.2. Roadside safety devices design .....	5
1.2.3. Bridge piers design under impact.....	6
1.3. Research objectives and the approaches.....	8
1.3.1. To provide experimental dataset.....	8
1.3.2. To perform numerical simulations validated against experiments.....	8
1.3.3. To develop a model to predict soil-pile-beam systems performance under impact .....	9
1.4. Dissertation organization.....	10
2. LITERATURE REVIEW .....	12
2.1. Piles static behavior .....	12
2.2. Piles dynamic behavior.....	15
2.3. Modeling soil-pile interaction .....	17
2.4. Piles impact behavior.....	18
2.5. Vehicle crash analysis .....	23
2.6. Anti-ram crash barrier .....	27
3. EXPERIMENTAL TESTS.....	31
3.1. Past experiments at TTI.....	35

3.1.1. Experiments on single piles .....	35
3.1.2. Experiments on group of piles: crash test on an eight-pile group (M50).....	39
3.2. Full scale impact test on group of four piles in hard clay (PU60).....	48
3.2.1. Full scale static test .....	49
3.2.2. Design of a four pile group .....	52
3.2.3. Geotechnical site characterization .....	61
3.2.4. Pile, beam and plates steel .....	66
3.2.5. Instrumentation and test set up .....	67
3.2.6. Test setup .....	71
3.2.7. Test vehicle .....	72
3.3. Group pile response under impact .....	72
4. NUMERICAL SIMULATION .....	85
4.1. Introduction .....	85
4.2. Introduction to LS-DYNA.....	86
4.2.1. Boundary.....	89
4.2.2. Constrained .....	89
4.2.3. Contact .....	90
4.2.4. Control .....	91
4.2.5. Element .....	92
4.2.6. Hourglass .....	92
4.2.7. Initial and interface .....	93
4.2.8. Section .....	94
4.3. Material models .....	94
4.3.1. Soil models .....	96
4.3.2. Steel (Piecewise Linear Plasticity) .....	104
4.4. Vehicle models .....	108
4.4.1. Single-unit flatbed truck .....	108
4.4.2. Chevrolet C2500 pickup truck .....	110
4.4.3. Geo Metro (reduced model).....	112
4.5. Simulation calibration.....	113
4.5.1. Medium duty truck M50.....	113
4.5.2. Pick-up truck PU60 calibration.....	117
4.6. Numerical simulations to calibrate TAMU-POST (Group) .....	131
4.6.1. Space-filling Latin Hypercube sample design .....	131
4.6.2. Experimental design for the TAMU-POST validation .....	132
4.6.3. Influence of some parameters .....	139
5. ANALYTICAL MODEL .....	144
5.1. Introduction .....	144
5.2. Modeling soil-structure interaction: Beam-on-Winkler Foundation ....	145

5.3. Model theory.....	153
5.4. Solution method.....	157
5.5. Model input parameters .....	159
5.5.1. Lateral static stiffness K .....	160
5.5.2. Ultimate failure load $H_{ou}$ .....	165
5.5.3. Damping coefficient C.....	167
5.5.4. Mass M .....	171
5.6. Energy absorption.....	173
5.7. Characterizing damping.....	178
5.8. Dynamic penetration.....	180
6. MODEL VALIDATION AND PARAMETRIC STUDY .....	184
6.1. Model validation.....	184
6.1.1. Maximum deflection.....	184
6.1.2. Maximum bending moment in the beam .....	188
6.1.3. Maximum bending moment in the pile.....	190
6.2. Parametric study and design insights.....	193
6.2.1. Effect of pile spacing and pile embedment depth.....	194
6.2.2. Effect of mass and velocity of vehicle.....	196
6.2.3. Effect of soil strength.....	198
6.2.4. Effect of pile and beam bending stiffness.....	200
6.2.5. Number of piles .....	202
6.2.6. Sensitivity analysis of M, C and K .....	203
6.3. Reliability analysis of TAMU-POST .....	205
6.3.1. Failure criterion.....	207
6.3.2. Random variables and the probability distributions .....	207
6.3.3. A design example.....	210
7. SUMMARY AND CONCLUSIONS.....	217
7.1. Experimental study .....	217
7.2. Numerical study.....	219
7.3. Analytical study.....	220
7.4. Recommendations for future studies .....	224
REFERENCES.....	227
APPENDIX A .....	244
APPENDIX B .....	250
APPENDIX C .....	257



APPENDIX D .....259

APPENDIX E.....278

## LIST OF FIGURES

	Page
Figure 1-1: Bollards with high-performance ratings (Secureusa Inc. and Delta Scientific Corp, FEMA 430).....	3
Figure 1-2: Typical bollard installation in concrete foundation (DOS, FEMA 430).....	4
Figure 1-3: U.S. embassy Bandar Seri Begawan, Brunei (left) U.S. embassy Oslo (right).....	5
Figure 1-4: Typical roadside safety hardwares (FHWA publications) .....	6
Figure 1-5: Collapse of I-80 bridge hit by tractor trailer, 2003 (El-Tawil, 2004, Photo Courtesy of NDOR).....	7
Figure 1-6: Bridge-vehicle crashes .....	7
Figure 2-1: Typical p-y curves for laterally loaded piles .....	13
Figure 2-2: The St. George Island causeway bridge .....	19
Figure 2-3: FB-MultiPier model (McVay et al. 2009).....	20
Figure 2-4: Lateral soil force on cap and seal (Mc Vay et al., 2009).....	20
Figure 2-5: Test setup and the finite element model in ABAQUS (Dezi et al. 2012) ....	22
Figure 2-6: Impact simulations of Chevy truck and the bridge pier (El-Tawil, 2004).....	24
Figure 2-7: Impact simulations of Ford truck and the bridge pier (El-Tawil, 2004) .....	25
Figure 2-8: Calculated impact forces versus approaching velocity for Ford truck (El-Tawil, 2004).....	26
Figure 2-9: Calculated impact forces versus approaching velocity for Chevy truck (El-Tawil, 2004).....	26
Figure 2-10: Design charts for group of piles embedded in sand and clay (Lim, 2011).....	29
Figure 3-1: The maximum allowable dynamic penetration (FEMA 430, Chapter 4).....	33

Figure 3-2: A Pendulum test on a single pile in loose sand (left); A bogie test on a single pile in stiff clay (right) .....	36
Figure 3-3: The test vehicle and the pile before and after the crash test (Alberson et al. 2007).....	36
Figure 3-4: The test vehicle and the pile before and after the crash test (Mirdamadi, 2014) .....	37
Figure 3-5: The load-deflection result in the static test on the single pile .....	37
Figure 3-6: The pickup truck impact test PU60 (Mirdamadi, 2014).....	38
Figure 3-7: The load-displacement curve of the static test on a pile in hard clay (left); The lateral displacement of the impact point in the crash test PU60 (right) .....	38
Figure 3-8: The loads derived from acceleration and strain in the test PU60 .....	39
Figure 3-9: Loose sand ditch (Lim, 2011).....	40
Figure 3-10: Side Elevation of the pile-beam structure .....	41
Figure 3-11: Side view and plan of the designed group piles .....	41
Figure 3-12: Instrumentations installed on the piles .....	42
Figure 3-13: The static test on the single pile and the results .....	43
Figure 3-14: The group pile after the crash test M50.....	44
Figure 3-15: The measured displacements of the piles .....	45
Figure 3-16: Dynamic penetration of the test vehicle .....	46
Figure 3-17: Measured vehicle displacement, velocity and acceleration.....	47
Figure 3-18: Obtained impact force on the barrier system.....	48
Figure 3-19: Static test design.....	49
Figure 3-20: The static test installation .....	50
Figure 3-21: The loading system.....	50

Figure 3-22: The data acquisition system .....	51
Figure 3-23: String potentiometer used for measuring lateral displacement .....	51
Figure 3-24: The load-displacement curve obtained in the static test.....	52
Figure 3-25: Pile driving into the hard clay .....	53
Figure 3-26: Installing the beams.....	54
Figure 3-27: Connections installations using bolts and welding.....	54
Figure 3-28: Details of the barrier: Front view .....	55
Figure 3-29: Details of the barrier: Elevation view.....	56
Figure 3-30: Details of the barrier: Plan view.....	57
Figure 3-31: The beams details .....	58
Figure 3-32: Details of mounting plates and pile-to-beam connections .....	59
Figure 3-33: Anchor bolts (left), the plates welded to beams (right).....	60
Figure 3-34: The barrier after installation .....	60
Figure 3-35: Field density test.....	61
Figure 3-36: Standard Penetration Testing and sampling .....	63
Figure 3-37: Pressuremeter apparatus .....	64
Figure 3-38: Pressuremeter test results .....	66
Figure 3-39: The accelerometer installed on the vehicle (rear axle).....	68
Figure 3-40: The strain gauges installed on the piles and beams.....	68
Figure 3-41: Strain gauges and accelerometer .....	69
Figure 3-42: High speed cameras .....	70
Figure 3-43: Vehicle guidance system .....	71

Figure 3-44: The test pickup truck .....	72
Figure 3-45: The barrier and test vehicle prior to testing.....	73
Figure 3-46: Vehicle and barrier after the impact on the group of piles system.....	74
Figure 3-47: Pile displacements .....	75
Figure 3-48: Permanent deflection of the piles and beams and barrier damage .....	75
Figure 3-49: Time history of the maximum displacements of piles at 1.3 m above the ground level.....	76
Figure 3-50: Vehicle acceleration signal.....	77
Figure 3-51: Vehicle velocity.....	78
Figure 3-52: Vehicle displacement .....	78
Figure 3-53: Measured dynamic penetration of the vehicle.....	79
Figure 3-54: The time history of 50msec average impact force .....	80
Figure 3-55: Piles after testing .....	81
Figure 3-56: Numerical model indicating the piles bending.....	81
Figure 3-57: The measured bending moment of beams .....	82
Figure 3-58: The plastic strain .....	82
Figure 3-59: The measured strains on gauges installed on beams .....	83
Figure 3-60: Sequential images of the crash test PU60.....	84
Figure 4-1: EOS: an IBM iDataplex Cluster provided by Texas A&M University.....	88
Figure 4-2: CONSTRAINED_NODAL_RIGID_BODY .....	90
Figure 4-3: Undetected interpenetration.....	91
Figure 4-4: a) Drucker Prager yield surface (Potts & Zdravkovic, 1999) b) Comparison of Mohr-Coulomb and Drucker Prager yield surface in 2D space (Alejano & Bobet, 2012).....	103

Figure 4-5: Finite element model of the test vehicle: Medium-duty truck .....	109
Figure 4-6: Finite element model of the test vehicles: Pickup truck for the PU60 test..	110
Figure 4-7: Validation of the vehicle finite element model for use in crash analysis....	111
Figure 4-8: FE model of the Geo Metro, reduced model (NCAC) .....	112
Figure 4-9: Finite element model of the test M50 installation .....	114
Figure 4-10: Numerical simulation of the impact test on a group of piles.....	115
Figure 4-11: Comparison between predicted and measured behavior .....	115
Figure 4-12: Comparison of measured and predicted displacements of piles No. 1,2,3 and 4 .....	116
Figure 4-13: Finite element models of the soil block and barrier .....	119
Figure 4-14: Soil, piles and beams mesh.....	121
Figure 4-15: Finite element models of the vehicle and the barrier .....	121
Figure 4-16: Mesh of 2.1 million elements and Mesh of 3.1 million elements .....	122
Figure 4-17: Comparison dynamic penetration in simulations of the design mesh and the finer mesh.....	123
Figure 4-18: Comparison contact forces in simulations of the design mesh and the finer mesh.....	123
Figure 4-19: Initialization of the soil-pile barrier.....	124
Figure 4-20: Numerical simulation of the impact test on a group of 4 piles.....	125
Figure 4-21: Measured and simulated vehicle acceleration .....	125
Figure 4-22: Measured and simulated vehicle velocity .....	126
Figure 4-23: Measured and simulated vehicle displacement .....	126
Figure 4-24: Measured and simulated dynamic penetration .....	127

Figure 4-25: Comparison of simulated and measured displacements of the inner pile (close to the impact).....	128
Figure 4-26: Comparison of simulated and measured displacements of the outer pile (end pile).....	128
Figure 4-27: Simulated and measured impact force.....	129
Figure 4-28: Sequential images of Test and Simulation PU60 .....	130
Figure 4-29: Three different sampling schemes a) Random sampling b) Full factorial sampling and c) Latin Hypercub Sampling (Hoare et al. 2008).....	132
Figure 4-30: LS-DYNA simulation of cases: 4, 6 and 8 in-line piles .....	135
Figure 4-31: LS-DYNA simulation of cases with the S/D (ratio of pile spacing to pile width) of 20, 35 and 50 .....	136
Figure 4-32: The effect of soil strength on the barrier deflection .....	140
Figure 4-33: The effect of pile spacing on the barrier deflection.....	141
Figure 4-34: The effect of vehicle velocity on the barrier deflection .....	142
Figure 4-35: The effect of piles number on the barrier deflection .....	143
Figure 5-1: Typical p-y curves (Meyer and Reese, 1979).....	147
Figure 5-2: Hysteric backbone curve (Kagawa and Kraft, 1981) .....	148
Figure 5-3: Soil-pile interaction model (Noghami et al. 1988).....	149
Figure 5-4: Far field soil-pile interaction models (Noghami et al. 1988) .....	149
Figure 5-5: Lysmer and Richart simplified model for dynamic elastic response of footing.....	150
Figure 5-6: Models suggested for the dynamic response of a rigid circular footing (Deeks & Randolph, 1995).....	151
Figure 5-7: Inelastic models developed by a) Smith b) Nguyen.....	152
Figure 5-8: The chosen single degree of freedom.....	152

Figure 5-9: Bending of an Euler–Bernoulli beam .....	154
Figure 5-10: Schematic presentation of the proposed analytical model for nonlinear dynamic analysis of lateral response of pile groups under impacts .....	156
Figure 5-11: Application of central finite difference approach.....	158
Figure 5-12: Conceptual soil resistance versus depth profile (Briaud, 1997).....	161
Figure 5-13: Horizontal load on a single pile.....	163
Figure 5-14: Soil model presented by Wolf and Somaini .....	170
Figure 5-15: Mobilized soil wedge .....	172
Figure 5-16: Crushing factor for vehicle classes M and P .....	175
Figure 5-17: Damping factor <i>Alpha</i> versus soil pressuremeter limit pressure $P_L$ .....	179
Figure 5-18: Dynamic penetration .....	181
Figure 5-19: The numerical simulation of a sedan (class C) impacting a rigid wall .....	182
Figure 5-20: The numerical simulation of a pickup truck (class P) impacting a rigid wall .....	183
Figure 5-21: The numerical simulation of a medium duty truck (class M) impacting a rigid wall .....	183
Figure 6-1: Predicted versus measured maximum deflection .....	185
Figure 6-2: Predicted versus measured maximum deflection (log scale) .....	186
Figure 6-3: The probability density function of the error in model prediction with respect to the maximum deflection.....	187
Figure 6-4: Ratio of predicted over measured maximum deflection for 95 cases .....	188
Figure 6-5: Ratio of predicted over measured maximum bending in the beam versus the soil pressuremeter limit pressure .....	189
Figure 6-6: Predicted over measured maximum bending in the beam versus soil pressuremeter limit pressure.....	190



Figure 6-7: Ratio of predicted over measured maximum bending in the beam versus soil pressuremeter limit pressure .....	191
Figure 6-8: Ratio of predicted over measured maximum bending moment in the beam versus the soil pressuremeter limit pressure .....	192
Figure 6-9: The effect of pile spacing and pile embedment depth for the four-pile group .....	195
Figure 6-10: The effect of pile spacing and pile embedment depth for the eight-pile group.....	196
Figure 6-11: The effect of mass and velocity of vehicle.....	197
Figure 6-12: The effect of soil strength and pile embedment depth for the four-pile group.....	199
Figure 6-13: The effect of soil strength and pile embedment depth for the eight-pile group.....	200
Figure 6-14: The effect of beam bending stiffness.....	201
Figure 6-15: The effect of pile bending stiffness .....	202
Figure 6-16: The effect of number of piles .....	203
Figure 6-17: The sensitivity of model result to mass, stiffness and damping estimation .....	204
Figure 6-18: The probability distribution of the random input parameter .....	209
Figure 6-19: PDE of the model parameter: crushing factor .....	210
Figure 6-20: The deterministic response by TAMU-POST .....	211
Figure 6-21: Comparison of MCS results with different numbers of sample .....	212
Figure 6-22: Probability Distribution Function of the dynamic penetration and the associated probability of failure, depth ranging from 1 m to 3 m .....	214
Figure 6-23: Probability Distribution Function of the dynamic penetration and the associated probability of failure, S/D ranging from 10 to 30.....	216

## LIST OF TABLES

	Page
Table 3-1: The ASTM impact condition designation.....	33
Table 3-2: The ASTM penetration ratings .....	34
Table 3-3: ASTM vs PAS 68 vehicle weights .....	34
Table 3-4: Details of the medium scaled tests on single piles (Lim 2011) .....	35
Table 3-5: Soil properties .....	40
Table 3-6: Response of the piles: displacement, rotation.....	44
Table 3-7: Field density test report .....	61
Table 3-8: SPT results .....	62
Table 3-9: PMT results.....	66
Table 3-10: The permanent deflection of the piles .....	76
Table 4-1: The material models employed in the numerical study .....	95
Table 4-2: LS-DYNA Material card for Isotropic Elastic-Plastic with Failure (LS-DYNA R7.1 Keyword Manual, 2014) .....	97
Table 4-3: Variables on Isotropic Elastic-Plastic with Failure (LS-DYNA R7.1 Keyword Manual, 2014) .....	97
Table 4-4: Summary of the material properties for the Isotropic Elastic Plastic soil model.....	97
Table 4-5: Material cards for Jointed Rock model (LS-DYNA R7.1 Keyword Manual, 2014).....	100
Table 4-6: Variables on Jointed Rock model (LS-DYNA R7.1 Manual, 2014).....	101
Table 4-7: Summary of the material properties for the Jointed Rock soil model .....	102
Table 4-8: Material cards for Piecewise Linear Plasticity model (LS-DYNA R7.1 Keyword Manual, 2014) .....	105

Table 4-9: Variables in Piecewise Linear Plasticity model (LS-DYNA R7.1 Keyword Manual, 2014) .....	106
Table 4-10: Material properties for steel piles, beams and plates .....	107
Table 4-11: The selected design strata for the LS-DYNA numerical study .....	133
Table 4-12: Soil strength categories and parameters - clay.....	133
Table 4-13: Soil strength categories and parameters - sand.....	133
Table 4-14: The simulations performed based on the experimental design SLHS .....	137
Table 5-1: Soil classification based on PMT data (Briaud, 2013) .....	166
Table 5-2: The recommended correlations for clay (Briaud, 2013).....	166
Table 5-3: The recommended correlations for sand (Briaud, 2013) .....	167
Table 5-4: Vehicle velocity reduction factor: Medium duty truck (M) .....	176
Table 5-5: Vehicle velocity reduction factor: Pickup truck (P) .....	177
Table 5-6: Vehicle velocity reduction factor: Passenger car (C) .....	178
Table 5-7: The obtained $L_{crushed}$ from the numerical simulations.....	182
Table 6-1: Coefficients of variation for in situ testing methods (Kulhawy and Trautmann 1996).....	208
Table 6-2: The random variables and their statistical features.....	210
Table 6-3: The cases studied .....	213

# 1. INTRODUCTION

## 1.1. Problem statement

The large and growing tragic consequences of vehicle crashes, ship collisions and similar extreme events have raised questions about the safety of the structures protected by roadside safety devices and anti-ram barriers against impact loading. “Anti-ram perimeter barriers” are typically composed of piles, rails, cables and bollards embedded in a foundation or directly placed in soil protecting the embassies or significant buildings against speeding vehicles. Proper design of these barriers becomes crucially important when the failure most likely involves huge loss of lives and tremendous economic destruction. In particular, when buildings are located in largely populated areas and urban environments, they are more vulnerable to extreme impact loading or vehicle crashes.

Among different possible systems capable of stopping vehicles, an efficient alternative is to make use of groups of piles tied together by beams. Since group piles directly embedded in soil require the least space underground, while providing adequate impact resistance with a visually friendly view, have the least interference with the infrastructure facilities. This is a major installation issue in urban areas.

Although extensive experiments have been performed on various anti-ram barriers by the U.S. Department of State and other research agencies, there is no analytical approach to investigate this soil-pile-beam performance under impact.

This research made comprehensive attempts to develop a general yet simple analysis-design methodology to predict the response of in-line piles impacted by a truck with a given mass traveling at a given velocity.

## **1.2. Motivation of the study**

The findings of this research offer an insight into barriers performance and in particular, soil contribution to the ultimate impact resistance. The model developed in this research is intended to be used by practitioners and designers to identify the minimum requirements for the impact resistant piles design. The recommendations facilitate a more reasonable and functional design with less cost and risk. The full scale tests datasets and the validated numerical models can also provide research tools for the further studies. In general, three areas as presented here will benefit from the implication of this research's outcomes:

### **1.2.1. Anti-ram barriers design**

A vehicle moving at high speed may reach a velocity to pass over the barrier and intrude the building. A key aspect of a safe, practical and efficient design of barriers is to identify the site conditions and the probable risk and accordingly propose a barrier which has been proved to provide adequate resistance using the available information, past testing, guidelines and new design methods.

In the recent years, novel functional and cost effective barriers have substituted the traditional high walls and huge bollards which are not visually pleasant in public and

also hard to install in urban areas. In 1985, the U.S. Department of State published the test standard SD-STD-02.01 “Standard Test Method for Vehicle Crash Testing of Perimeter Barriers and Gates” and then released several revised versions in 2003 and 2007.

Currently a widely used anti-ram barrier is a hard perimeter composed of bollards (Figure 1-1). The piles may be embedded in concrete mat foundation (Figure 1-2) or directly embedded in soil. However as mentioned, the underground facilities often do not leave enough space for large concrete foundations.



**Figure 1-1: Bollards with high-performance ratings (Secureusa Inc. and Delta Scientific Corp, FEMA 430)**

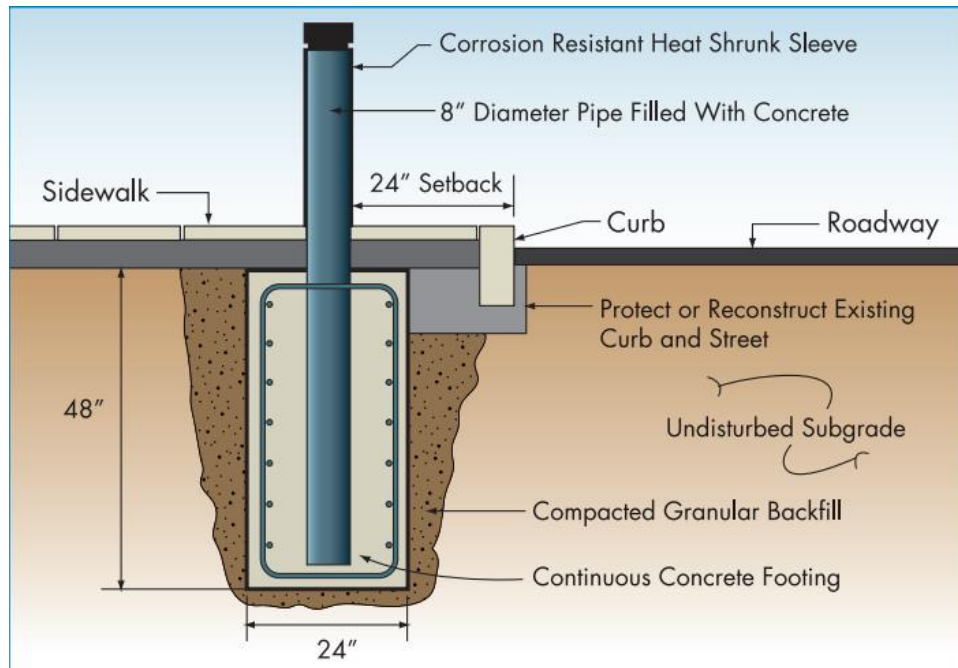


**Figure 1-2: Typical bollard installation in concrete foundation (DOS, FEMA 430)**

This research briefly reviews the impact performance of single piles given the soil is hard enough to stop the vehicle. In this respect, it is worthwhile to note that single piles' tests confirmed that soil strength, pile geometry and impact level significantly affect the impact performance and make this option less reliable and practical. So the major focus of this research is placed on investigation of group piles.



**Figure 1-3: U.S. embassy Bandar Seri Begawan, Brunei (left)  
U.S. embassy Oslo (right)**

### **1.2.2. Roadside safety devices design**

The significance of roadside safety has been recognized since 1960s. Since then many studies were directed to develop barriers guardrails or materials that make the roadways safer. The primary design loading is lateral impact loading. State departments of transportation (DOTs) and other research agencies such as the Federal Highway Administration (FHWA), the National Cooperative Research Program (NCHRP) have teamed up to take cost effective steps to advance roadside safety, improve system reliability and so reduce highway fatalities and injuries.





**Figure 1-4: Typical roadside safety hardwares (FHWA publications)**

### **1.2.3. Bridge piers design under impact**

When the crash events (ship or vehicle collisions) involve bridge piers and abutments, it would cause extremely catastrophic damage and design of impact resistant piers become more crucial. More than 2600 barge-bridge collisions over the period of time 1992 to 2001, reported by U.S. Coast Guard and American Waterways Operators (Allegretti and Pluta 2003) had FHWA to include the probability of extreme events in the existing design guideline. The impact characteristics studied in this research can be further evaluated in vehicle-pier crashes.



**Figure 1-5: Collapse of I-80 bridge hit by tractor trailer, 2003 (El-Tawil, 2004, Photo Courtesy of NDOR)**



**Figure 1-6: Bridge-vehicle crashes**

### **1.3. Research objectives and the approaches**

The objectives of this study fall into three sections investigating the vehicle-barrier crash from experimental, numerical and analytical aspects.

#### **1.3.1. To provide experimental dataset**

The most convincing datasets to study a complex and highly transient problem such as a vehicle crash can be obtained from full scale field tests. Real scale crash testing, though involves many difficulties in test design, setup and data acquisition, is found to be the most robust research tool to study such complicated events. Within the scope of this research and the available facilities, two full scale crash tests were planned on group piles with uniquely different conditions. Each of these impact tests were preceded by static loading tests.

#### **1.3.2. To perform numerical simulations validated against experiments**

Intensive 3D nonlinear numerical experience remarkably advances the knowledge and expertise required to explore crash events and affecting parameters. The refined element level simulations allow for examining measures which are difficult or impossible to obtain in experiments such as the energy absorbed by vehicle crushing. These numerical observations are to be applied in the analytical model development specifically in the model parameter optimizations. The fully nonlinear dynamic finite

element code LS-DYNA was utilized to simulate three dimensional barriers, vehicle and the whole crash.

### **1.3.3. To develop a model to predict soil-pile-beam systems performance under impact**

As modeling the whole system with finite element codes is not computationally efficient and hence is not a practical solution, it is critically necessary to establish a practical design method. In this respect, the soil-pile interaction mechanism and the key parameters which influence piles impact response should be thoroughly understood. This model based on theoretical concepts simulates the connecting beam supported by a number of Single Degrees of Freedom (SDOF) representing pile and associated soil. The response is governed by a number of factors including pile embedment and spacing, pile strength and stiffness, soil strength and stiffness, mass of the truck and its approach velocity. The method is then coded in MATLAB and an Excel spread sheet program called TAMU-POST (Group).

Once the model theoretical bases are established, the input parameters are then quantified using the datasets from the experiments and simulations. It was intended to correlate the model parameters to the geotechnical characteristics that can be obtained from routinely performed geotechnical tests (e.g. Standard Penetration Test SPT or Pressuremeter Test PMT).

The model is designed to reasonably predict the maximum displacement of the impact point and allow for analysis of any general crash scenario. The validation of the model should be evaluated using the available datasets.

#### **1.4. Dissertation organization**

This dissertation is structured in seven sections as follows: the relevant literature on group pile response under static, dynamic and impact loading is reviewed in Section 2. Particular emphasis is given to the recent impact experiments performed on piles and the associated findings. Section 3 fully describes two full scale tests, design and installation details, test setup, observations and the data obtained from the tests. Section 4 begins laying out the numerical study and then explains calibration of the developed numerical models against the experimental data. The detailed simulations results are reported accordingly.

The next part, Section 5 first introduces the analytical approach developed to predict the impact performance of pile groups. Then it moves to identify the model parameters and present the parameter optimization procedure using both experimentally and numerically collected data.

In Section 6, the model precision in response prediction is then critically examined by comparison with the measured data. Then it describes the sensitivity analysis and the parametric study carried out to derive design insights. The probability of failure associated with the proposed model through a simple reliability analysis is provided. The final part, Section 7 draws upon the entire research and discusses the research

significant findings, contributions and implications for practice. At the end, recommendations for future work are presented.

Appendices A through E provide the user's manual for the program, additional data such as soil profiles, the test designations and the standard documents for the laboratory and in situ investigations, those have been referred in the main text and the MATLAB code for the Monte Carlo Simulation and the TAMU-POST (Group).

## **2. LITERATURE REVIEW**

Dramatic damage caused by extreme events such as vehicle crashes has raised a strong need for an efficient design of protective barriers. Of the functional alternatives are groups of in-line piles, which are commonly installed in highways for roadside safety purposes as well as around significant buildings and facilities. However, very little on this topic is known. A considerable amount of literature has addressed the lateral response of pile groups under static loading and more recent, under lateral dynamic loading.

Perusal of literature suggests a lack of research in soil-pile interaction under impact loading. That calls for further full scale experiments to assess dynamic characteristics of piles and develop more numerical models.

### **2.1. Piles static behavior**

Research on the static behavior of laterally loaded piles either single or group piles has a long history, starting in the 1960s by researchers (Broms, 1964a; Broms, 1964b; Matlock, 1970; Poulos, 1971). Since then numerous studies have been carried out to predict lateral behavior (i.e. deflection, rotations, stresses and bending moment) of single piles and then followed by research focused on group piles. The oldest method is the Winkler Approach, based on the subgrade reaction theory. This method represents soil as a series of linear springs (Hetenyi 1946) and analyzes the single pile using the elastic beam equation with assumption of constant and linearly varied spring stiffness along pile

depth for clay and sands, respectively. Despite the method's shortcomings, such as using a non-unique soil property, discontinuous soil model and ignoring axial load effects, the Winkler method has been frequently used. Modification of the Winkler model led to the most popular method known as p-y approach, where the soil is represented by a series of nonlinear p-y curves (McClelland and Focht 1956). Following that, many analytical expressions and empirical curves were developed for typical soil types such as ones reported by Reese and Welch (1975). However the existing curves may not be reliably appropriate for any soil condition.

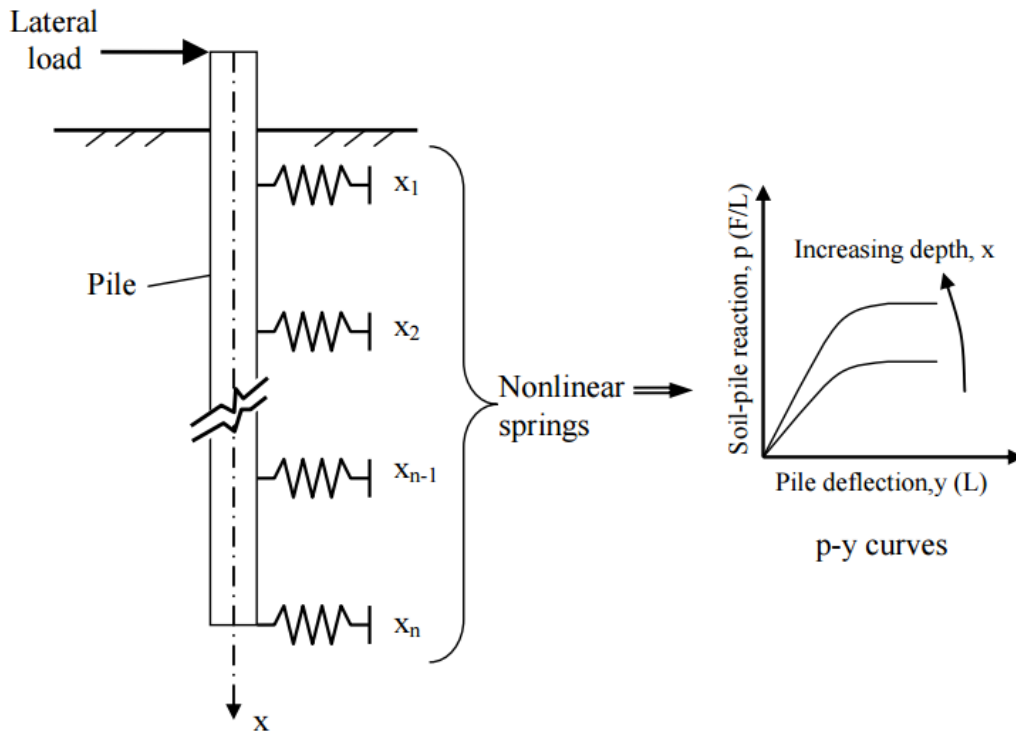


**Figure 2-1: Typical p-y curves for laterally loaded piles**



In 1971, Poulos first introduced the Elastic Column approach (Poulos, 1971 a,b). This method models the pile as a discretized thin rectangular strip, and solves the equilibrium equation of a beam element on a homogeneous, elastic and continuous soil using finite difference method. Novak (1974) proposed another continuum model that considered the soil as a set of independent horizontal layers. These layers are assumed to be in a plane strain state, isotropic and linearly elastic. These methods account for the continuous nature of soil and the boundary conditions effects but do not consider the local yielding of soil and assume the soil homogeneous. In addition to computational difficulties of these approaches, acquisition of an appropriate soil modulus also found to be a problem. Along with the analytical methods, many numerical efforts have intended to study a laterally loaded pile in a less approximate and less simplified way. Considering the soil as a continuum, numerical techniques would model soil-pile interaction through interface elements, allow any complex load conditions, and can perfectly represent the soil and structure nonlinearity.

For the group piles also there have been many methods proposed to explain pile-soil-pile interaction, shadow effects and group effects. Part of the studies made attempts to modify the single pile analytical methods with the empirically obtained factors (e.g. Bogard and Matlock 1983). A semi empirical-analytical approach known as the  $p$ -multiplier was proposed by O'Neill (1983), Brown and Reese (1988). This approach accounts for the shadow effects by reducing the soil resistance  $p$  in the single pile  $p$ - $y$  curves.

Novak and many researchers have made contributions to quantify group stiffness and damping in the case of static and dynamic lateral loading required in the analytical methods (Novak and Janes 1989).

Adopting the single pile continuum approach, Poulos and Davis (1980) introduced piles interaction factors to account for the additional displacements and rotations due to the adjacent piles movements (Pulikanti and Ramancharla, 2013)

Focht and Koch, in 1973, proposed the first combined analytical approach, which uses p-y curves to explain soil response close to piles and adopts elastic continuum principles to estimate soil-pile interaction effects in soil further from the piles. This hybrid approach was then evaluated in the following studies by Reese et al. (1984), O'Neill et al. (1977) and Ooi and Duncan (1994). Moreover, several parametric studies using finite element methods were performed to extend expressions for group interaction factors and investigate the group effects (Randolph 1981, Rao et al. 1996).

A number of researchers have used numerical approaches such as finite element simulations (e.g. Wu and Finn, 1997) or boundary element simulations (e.g. Kaynia and Kausel, 1982) that are computationally intense and time consuming to use in practice.

## **2.2. Piles dynamic behavior**

The literature is rich in studies on dynamic lateral response of single pile or pile groups. These studies are mostly focused on cyclic loading, earthquake and other vibration types of loading and less on impact loading. Early studies to evaluate the dynamic response and impedance function of piles include lumped mass models

(Penzien 1970), finite element models (Blaney 1974, Kuhlemeyer 1979; Manna and Baidya 2009), boundary element models (Kaynia & Kausel, 1982) and Winkler models (El Naggar and Novak 1995, 1996). It was found a difficult challenge to take into account soil nonlinearity in these analyses.

For years, load transfer curves known as p-y curves using the approximate Winkler model was commonly used for time domain nonlinear analysis. The early frequency domain solutions for dynamic lateral response of piles, introduced by Novak et al. (1978) and Nogami et al. (1991), could model the lateral behavior but approximated soil nonlinearity by equivalent linear models.

Afterwards, available powerful computers allowed researchers to develop analysis techniques in the time domain which facilitates modeling nonlinear behavior, energy dissipation (Nogami et al. 1992; El Naggar and Novak, 1996).

The continuum approach was first introduced by Baranov (1967) and simplified by Novak and his co-workers to calculate the impedance functions of piles considering soil-pile interaction and energy dissipation (Novak 1977; Nogami and Novak 1976; Novak and El Sharnouby 1984).

Dynamic response of piles was also studied through the experiments. In 1992, El-Marsafawi et al. executed two full scale tests one on a steel pile group embedded in sand and the other one on a concrete pile group in clay. Rollins et al. conducted a series of full scale cyclic lateral load tests on three pile groups with different longitudinal spacing as well as single piles for comparison purposes. In these experiments, the effects of group piles layout and spacing on the lateral load resistance were assessed. In addition, some

small scale experiments were performed to verify the available theoretical approaches (Novak and Grigg, 1976; Sheta and Novak, 1982).

### **2.3. Modeling soil-pile interaction**

Preliminary work on soil-pile interaction was first reported by Wolf (1980). After that, an increasing amount of analytical approaches have been suggested to evaluate soil-pile interaction under dynamic loads (Brown et al. 1988; Nogami et al., 1991; El Nagggar and Novak, 1996; Brown and Bollman; 1996; Wu and Finn, 1997). However, all the previously mentioned approaches carry serious limitations including high dependency on the estimated strength parameters such as dynamic stiffness and damping besides several simplification assumptions. Other studies have been made to offer a better estimate of input parameters required by the recommended analytical models (Nogami, 1980; Dobry and Gazetas, 1988; Wolf and Somaini, 1986).

All these studies have contributed significantly to the available knowledge on horizontal dynamic behavior of single piles and less extensively on groups of piles. Most of them, however, are related to cyclic horizontal loading and horizontal shaking of piles but not to impact loading. Today practical engineering design for soil-structure problems uses methods that assume the soil as a linear elastic medium. This would question the method prediction when the soil and structure undergo large deformation and exhibit fully nonlinear behavior.

## **2.4. Piles impact behavior**

Although fairly reliable methods have been well developed to predict lateral resistance of single and group piles, less research efforts have concerned the resistance of piles under impact loading. The number of extreme impact loading on structures either vehicle crashes in highways or ship-bridge collisions in waterways is progressively increasing and the current design guidelines are critically required to take into account the impact loading on buildings and bridge piers design. As the matter of roadside safety devices and anti-ram barriers, there is an ongoing research led by transportation research agencies and national laboratories that will be discussed later this section.

In literature, no single study investigates analytically the response of pile groups under extreme impact loading such as vehicle crashes. On the experimental side, the setup difficulties and significantly high cost of full scale testing have limited the experimental data on piles resistance in extreme events (Brown et al. 1988; Rollins et al. 1998; Ruesta and Townsend 1997; Rollins et al, 2003a, 2003b).

Halling et al. (2000) conducted a set of vibrational tests on a group of nine steel circular piles. The testing program included one static test, two series of statnamic tests, first without the pile cap (free-head) and then with the pile cap in place, two sinusoidal and one impact vibration tests. These series of testing results indicated that the dynamic response of a pile group significantly depends on the excitation frequency. Statnamic load testing consists of applying a rapid load on the pile vertically or laterally. It is not an impact but rather an impulse load with a typical duration of 0.5 second or less.

Basically in a static test, burning fuel generates high pressure and propels a reaction mass upward off the pile (ASTM D7383-08).

In the recent years, researchers from the University of Florida initiated a project to quantify the vessel impact forces on bridge piers and examine the soil-structure interaction during the impact (Consolazio et al. 2005 and McVay et al. 2009). A full scale barge impact test program was conducted on the main pier (Pier 1 as shown in Figure 2-2) at the St. George Island Causeway Bridge, Florida.



**Figure 2-2: The St. George Island causeway bridge**

Along with this research, the barge impact and the pier were also numerically analyzed using the FB-MultiPier finite element program (Florida Bridge Software Institute, 2005) indicated in Figure 2-3. The static soil resistance and damping were characterized using a Reese et al. (1974) P-y curve and viscous dashpots as identified by Smith (1962), respectively.

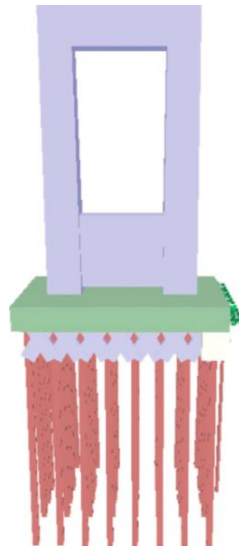


**Figure 2-3: FB-MultiPier model (McVay et al. 2009)**

According to the authors, the measured and numerically predicted soil response confirmed that inertia forces from the structural elements (i.e. columns, cap and piles) contributed significantly to the total resistance at the early part of the impact; however, the soil resistance was mainly provided through damping at peak impact loading. It was also reported that static soil stiffness controls the response at the peak displacement (Figure 2-4)

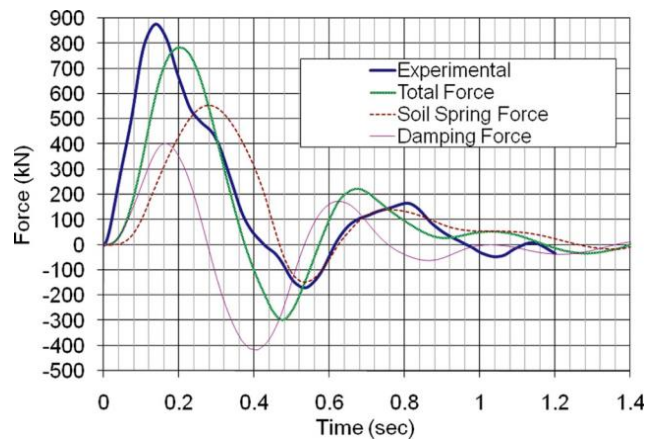


**Figure 2-4: Lateral soil force on cap and seal (Mc Vay et al., 2009)**

In the continue of this study, they characterized significant dynamic forces mobilized during the impact on the soil-structure system of interest, consisting of pier, cap, piles and soil providing the experimental and numerical results (McVay et al. 2009). The tests were primarily conducted to quantify the maximum dynamic loads during simulated slow impact collisions. They found that the maximum dynamic forces were much higher than the corresponding static forces and that soil damping is the primary component of the dynamic resistance.

Dezi et al. (2012) set up a series of full scale experiments on a group of three instrumented steel pipe piles subjected to a horizontal impact load (Figure 2-5). A 5.5 kg hammer equipped with a load cell was utilized to impact the piles heads. This study reports the soil-pile responses (e.g. time histories of strain gauges, pile heads acceleration, damping and mode shapes). These experiments data was then used to calibrate a finite element model of the system in ABAQUS.



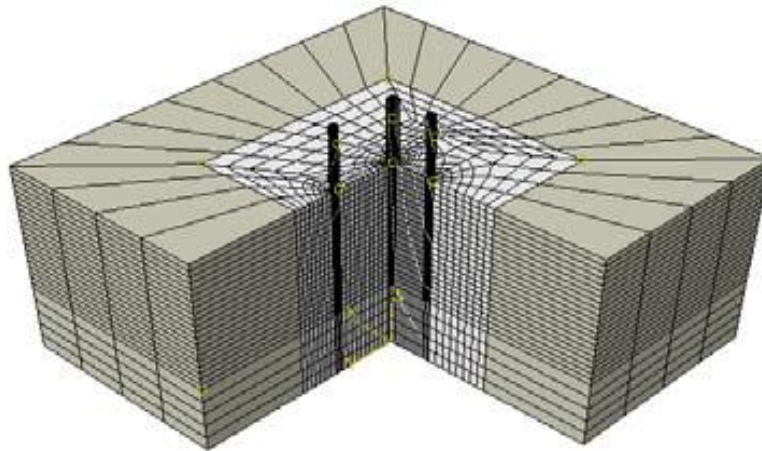


**Figure 2-5: Test setup and the finite element model in ABAQUS (Dezi et al. 2012)**

Further results of large scale static and impact tests on piles embedded in low liquid limit silt (ML) soil were reported by Zhu et al. (2011). The authors derived dynamic p-y curve with nonlinear static stiffness and damping coefficients.

## **2.5. Vehicle crash analysis**

These studies generally include three steps first a finite element model incorporating adequate details of all elements is developed, numerical study is then followed by a full-scale crash testing. The simulation results are then validated against the crash testing data. In automotive analyses such as crashworthiness and occupant safety as well as evaluation of roadside safety effectiveness, LS-DYNA has been successfully used to solve complex, nonlinear and large deformation crash problems.

The Texas A&M Transportation Institute has been pioneering experimental and numerical studies; TTI researchers have continued to working on finite element modeling using mostly a powerful finite element package LS-DYNA (Livermore Software Technology Corporation LSTC, 2013) and validation of roadside safety hardware devices along with performing small scale (e.g. pendulum), mid-scale (e.g. bogie) and full scale tests. These studies provide a valuable insight into design, analysis, testing, and evaluation of highway safety devices (Bligh R. et al. 2004; Abu-Odeh et al. 2015, Silvestri Dobrovolny et al. 2013, Brackin et al. 2013, and Arrington et al. 2011)

Researchers at National Crash Analysis Center, Worcester Polytechnic Institute and the University of Nebraska-Lincoln have also investigated the impact performance of roadside safety systems and improved finite element models of vehicles (Reid and Marzougui 2002, Mohan P. et al. 2009, 2010).

As part of a joint project by University of Michigan and University of Central Florida, numerical efforts were performed using LS-DYNA to investigate the structural design demands, impact forces and equivalent static forces generated in vehicle-bridge

pier collisions. Two finite element truck models crashed into bridge piers with various approaching velocities (Figure 2-7 and Figure 2-7). The calculated forces were then compared to the AASHTO-LRFD vehicle collision provisions. As the peak impact force occurs within a very short duration and the structural elements do not have time to respond to the loading, equivalent static forces are found to be a more proper design measure (Chopra 2001).

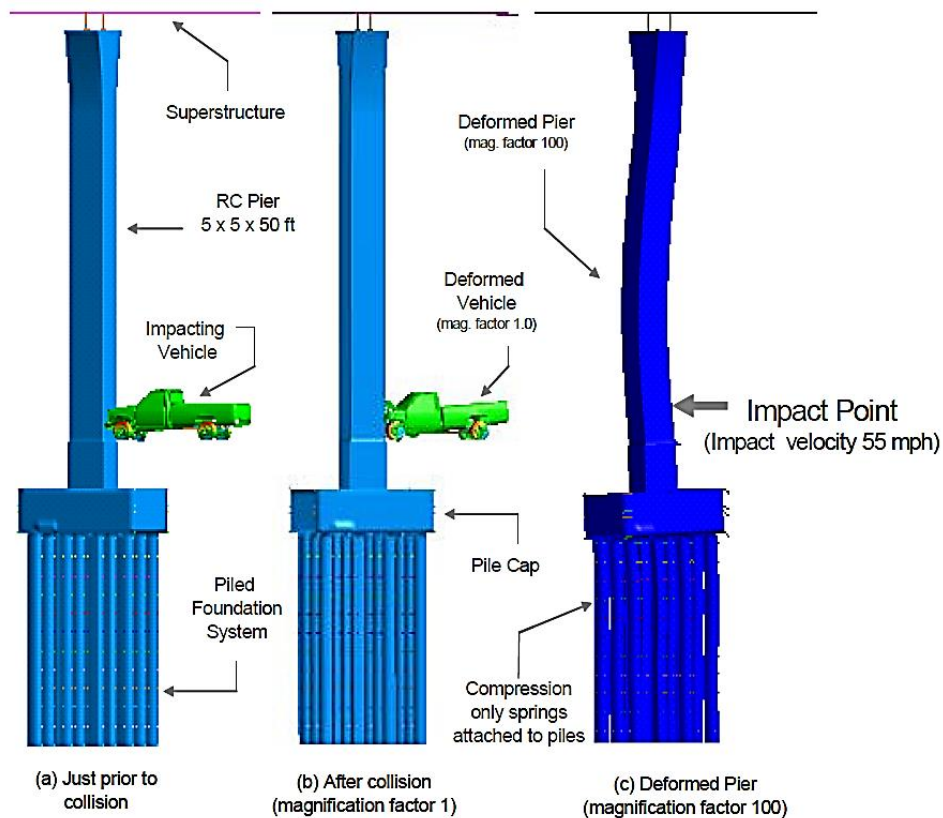


**Figure 2-6: Impact simulations of Chevy truck and the bridge pier (El-Tawil, 2004)**

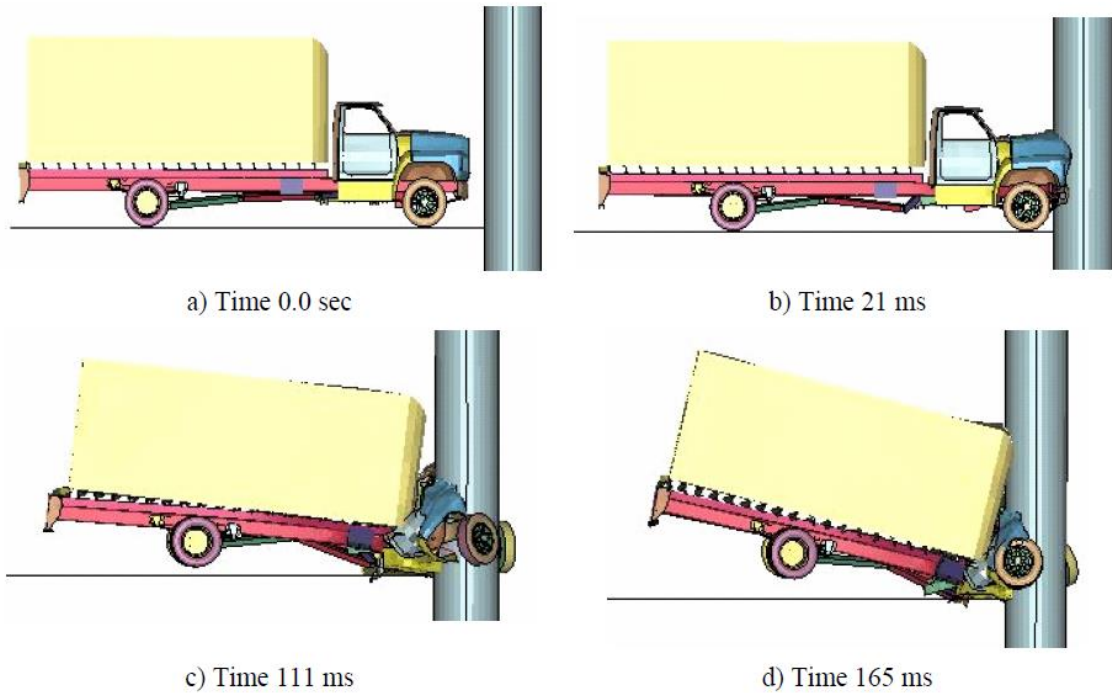


**Figure 2-7: Impact simulations of Ford truck and the bridge pier (El-Tawil, 2004)**

For a number of simulations, the equivalent static forces were computed significantly higher than the AASHTO-LRFD design forces (Figure 2-8, Figure 2-9).

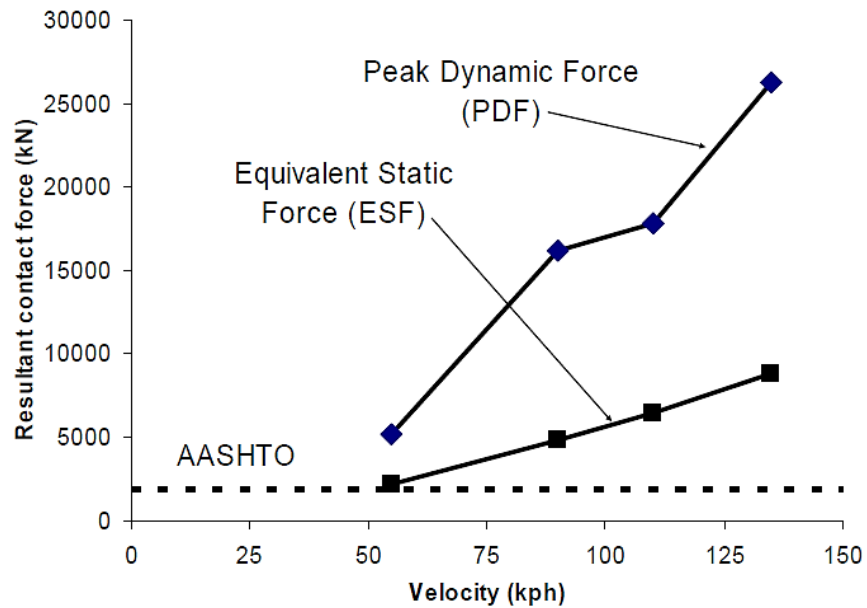


**Figure 2-8: Calculated impact forces versus approaching velocity for Ford truck (El-Tawil, 2004)**

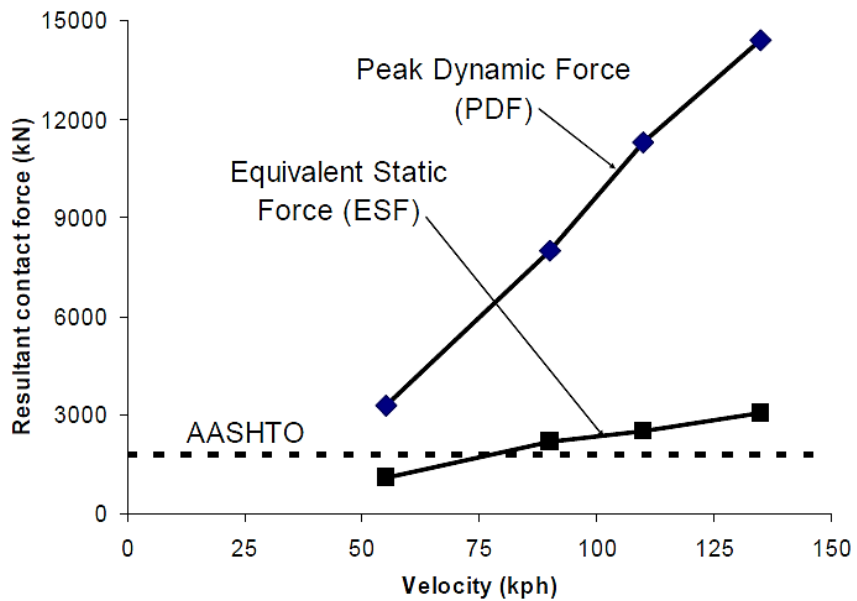


**Figure 2-9: Calculated impact forces versus approaching velocity for Chevy truck (El-Tawil, 2004)**

## **2.6. Anti-ram crash barrier**

The U.S. Department of State has set up rating standards for evaluating anti-ram barriers, depending on their performance in full scale crash tests. The standard in detail is introduced in Section 3. Typical testing procedure includes a finite element simulation followed by an actual crash test to verify the barrier performance. To date, Department of State certifies any new design of anti-ram perimeter in a fairly strong soil, while there are almost infinite soil conditions in the ultimate barrier installation sites. That draws the importance of soil effects on the barriers' response under vehicle impact.

In the recent years, the U.S. Department of State (DOS) and Texas Transportation Institute (TTI) have teamed up to develop efficient, functional and cost-effective perimeter-security devices around significant facilities and embassies.

In early the current project, several small-scale, mid-scale and full-scale tests were performed on single piles (10 pendulum impact tests, 2 bogie impact tests and 2 full scale impact tests) and one full scale impact test on a group of piles. The testing program was led by the crash crew in Texas Transportation Institute at Riverside Campus, College Station, TX.

Lim (2011) proposed a set of design charts to select the embedment of a single pile or group of piles embedded in soil of various strengths for a limited set of conditions using numerical simulations and experimental results (Figure 2-10).

The pile is a steel beam with an H shape cross section: W14X109 (14 inches wide and weighing 109 lbs/ft of length) for the single pile system and W14X90 (14 inches wide and weighing 90 lbs/ft of length) for the group system with a double beam made of

a hollow steel section HSS8x8x1/2 (8 inches wide, 8 inches high, and 1/2 inches wall thickness). The spacing of the piles for the group includes 2.44 m, 4.88 m, and 7.32 m. The truck has a mass of 6800 kg and the velocities include 50, 65, and 80 km/h.

The main limitation of the charts, however, is that the charts would help design of single piles and group of piles only for a certain pile profile given a limited soil condition. There is a critical need for a more general solution that allows for a wide range of pile and beams profiles and soil conditions.

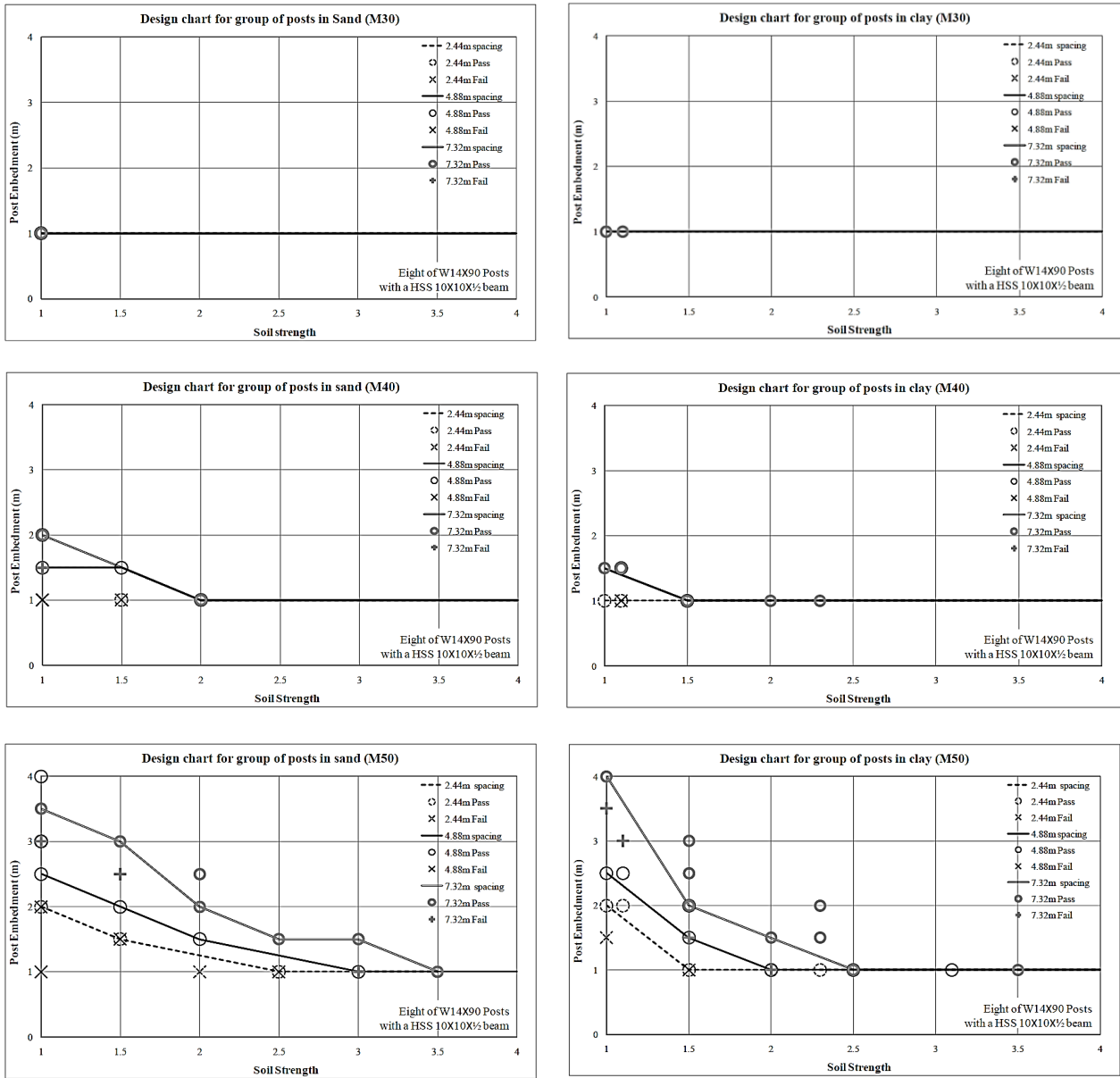


**Figure 2-10: Design charts for group of piles embedded in sand and clay (Lim, 2011)**

The work was then continued by Mirdamadi (2014) to develop an analytical solution for a single pile under impact loads. Although single piles can arrest vehicles in certain soil conditions, in general, they do not work as a cost-effective solution. In soft soil,



single piles should be designed so closely spaced for protecting purposes. In addition, single piles are more likely to fail to stop the vehicles. Therefore group of piles is widely preferred in practice.

Motivated by the limited amount of existing knowledge, the current study was conducted to structure a method to predict the response of in-line pile groups installed in soils with various levels of strength. The goal of this project is to lift the above mentioned limitations and develop a simple solution for the general case of a group of in line piles embedded in a given soil, connected by a beam and subjected to the impact of a vehicle with a given mass and approaching at a given velocity.

### 3. EXPERIMENTAL TESTS

The lack of studies on pile groups under lateral impact loading highlights a critical need for a comprehensive experimental work. Full scale testing allows researchers to study impact events and the barriers behavior both in qualitative and quantitative manners. Accordingly, a major part of this study is focused on conducting crash tests to examine the crashworthiness of the barriers and better understand the impact mechanism. This dataset was later used in development of an analytical design method.

The tests were performed in collaboration with the Texas A&M Transportation Institute (TTI) at Riverside Campus located in southwest of College Station, Texas. In order to observe the contribution of the effecting factors such as soil strength, number of in-line piles, pile embedment, pile width and impact level, two different full scale experiments were performed. Results of the preliminary crash simulations based on the initial finite element modeling using LS-DYNA led to select two barrier configurations for the crash tests. The impact tests were performed on: (i) a four-pile group embedded 2 m in hard clay with the spacing of  $S_p = 34B$ , where  $B$  is the pile diameter ; (ii) an eight-pile group embedded to a depth of 3 m in loose sand with the spacing of  $S_p = 14B$ . According to the ASTM F2656-07, these impact tests are denoted PU60 and M50, respectively. The letter followed by a number indicates the vehicle class (PU stands for the Pickup and M stands for the Medium-duty truck) and the latter numbers represent the impact velocity in unit of mph.

During each crash test, instrumentation and data acquisition systems were employed to quantify the barrier and soil responses.

Both tests were designed in compliance with the ASTM F2656-07 “Standard Test Method for Vehicle Crash Testing of Perimeter Barriers” test designation P1. ASTM F2656 was developed to standardize the tests conducted to validate the barriers’ efficiency to resist against the vehicle impacts. It specifies a range of vehicle impact designations and penetration levels. Kinetic energy level varies with the vehicle mass and vehicle velocity upon impact, assuming that the vehicle hits the barrier in the perpendicular direction. According to this standard, vehicles are categorized in four major classes: Heavy-duty truck (H), Medium-duty truck (M), Pickup truck (PU) and small passenger car (C). Each class has three levels of velocity: 65, 80 and 100 km/h (equal to 40, 50, and 60 mph). The standard currently requires the barriers not to allow more than one meter penetration from the perimeter of the barrier. The penetration distance is measured from the reference point on the leading edge of the testing vehicle and the reference point on the barrier. This distance is well-known as the dynamic penetration (Figure 3-1). Table 3-1 and Table 3-2 summarize the ASTM Impact Condition Designations and Penetration Ratings.

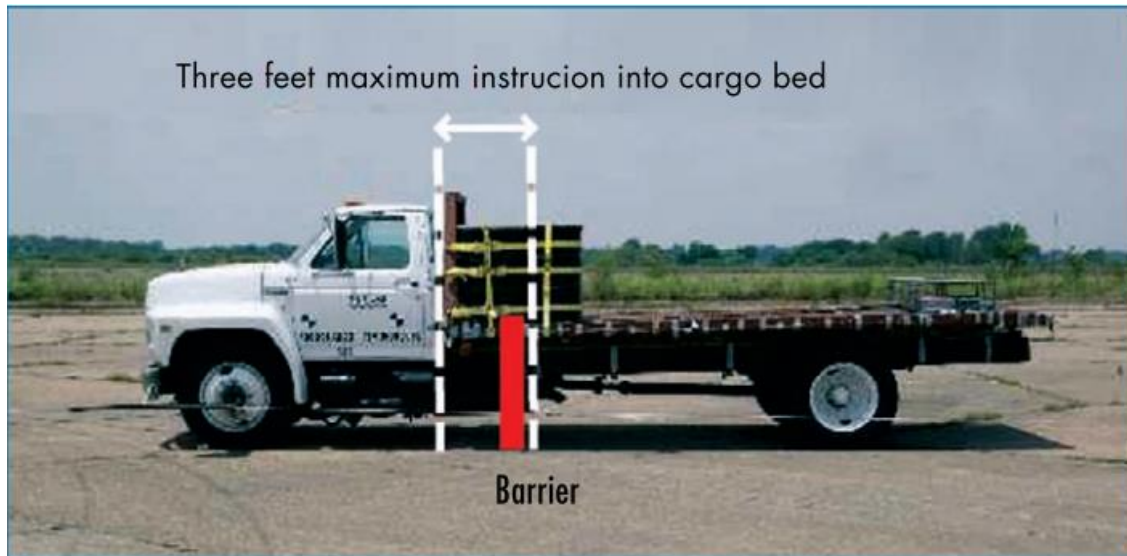


**Figure 3-1: The maximum allowable dynamic penetration (FEMA 430, Chapter 4)**

**Table 3-1: The ASTM impact condition designation**

<b>Test Vehicle type and weight</b>	<b>Nominal Impact Velocity km/h (mph)</b>	<b>Condition Designation</b>	<b>Kinetic Energy, KJ (ft-kips)</b>
Small passenger car 1100 kg (2430 lb)	65 (40)	C40	179 (131)
	80 (50)	C50	271 (205)
	100 (60)	C60	424 (295)
Pickup truck 2300 kg, (5070 lb)	65 (40)	PU40	375 (273)
	80 (50)	PU50	568 (426)
	100 (60)	PU60	887 (613)
Medium-duty truck (M) 6800 kg (15000 lb)	50 (30)	M30	656 (451)
	65 (40)	M40	1110 (802)
	80 (50)	M50	1680 (1250)
Heavy-duty vehicle (H) 29500 kg, (65000 lb)	50 (30)	H30	2850 (1950)
	65 (40)	H40	4810 (3470)
	80 (50)	H50	7280 (5430)

**Table 3-2: The ASTM penetration ratings**

<b>Designation</b>	<b>Penetration</b>
P1	<= 1 m (3.3ft)
P2	1.01 m to 7 m (3.3ft to 23.1ft)
P3	7.01 m to 30 m (23.1ft to 98.4ft)
P4	30 m (98ft) or greater

The United Kingdom anti-ram testing standard called as the Publicly Available Specification PAS 68:2007 also considers three classification systems: Vehicle Impact (V), Pendulum Impact (P) and Design method. The PAS 68 classification through the vehicle impact test is mostly similar to the U.S. DOS standard and the ASTM rating, while in PAS 68 the vehicles' weights are slightly larger than those of the United States ASTM standard.

**Table 3-3: ASTM vs PAS 68 vehicle weights**

<b>ASTM Test Vehicle Weights</b>	<b>PAS 68 Vehicle Weights</b>
1100 kg	1500 kg
2300 kg	2500 kg
	3500 kg
6800 kg	7500 kg
29500 kg	32000 kg

The following sections first review the past experiments performed on single piles and group piles in TTI under this project and then continues to the current work testing program, test setup and the obtained results.

### 3.1. Past experiments at TTI

#### 3.1.1. Experiments on single piles

Early in this project, eight medium scale tests summarized in Table 3-4 were conducted using a pendulum and a bogie. In these tests a steel pile HSS6x6x3/8 (152 mm wide and 9.5 mm thick) embedded in soil (loose sand and crushed limestone) was hit by a rigid mass such as a pendulum and a bogie (Figure 3-2) (Lim, 2011).

**Table 3-4: Details of the medium scaled tests on single piles (Lim 2011)**

<b>Test Number</b>	<b>Soil</b>	<b>Test Type</b>	<b>Mass of Pendulum (kg)</b>	<b>Impact Velocity (m/s)</b>	<b>Remarks</b>
P1	Crushed limestone	Pendulum	862	4.65	Backfilled
P2	Crushed limestone	Pendulum	862	2.41	Backfilled
P3	Crushed limestone	Pendulum	862	9.97	Backfilled
P4	Loose Sand	Pendulum	250	4.94	Driven
P5	Loose Sand	Pendulum	250	2.5	Driven
P6	Loose Sand	Pendulum	250	10.1	Driven
P10	Loose Sand	Pendulum	250	9.83	Backfilled
B1	Clay	Bogie	903	4.56	Driven



**Figure 3-2: A Pendulum test on a single pile in loose sand (left); A bogie test on a single pile in stiff clay (right)**

In 2007, a full scale crash test (M50) and a static test were performed on a single pile (Figure 3-3). During the impact, crushing the bumper of the vehicle covered the pile (I beam W14x90 embedded 3 m in crushed limestone) and therefore the pile displacement could not be captured by the cameras. Then, an identical test was performed in 2013 (Figure 3-4). Also, a static test was performed to obtain more information on the static stiffness of the soil-pile system, shown in Figure 3-5.



**Figure 3-3: The test vehicle and the pile before and after the crash test (Alberson et al. 2007)**



**Figure 3-4: The test vehicle and the pile before and after the crash test (Mirdamadi, 2014)**

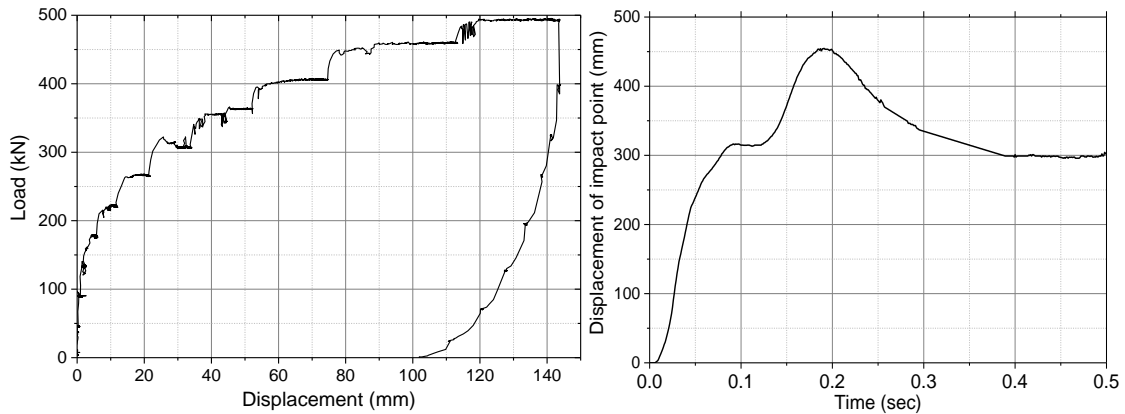


**Figure 3-5: The load-deflection result in the static test on the single pile**

Moreover, a full scale impact test was performed on a single pile with a pickup truck (Figure 3-6) to study a case with a different class of vehicle (Mirdamadi, 2014). In this test, a single pile (tube 14 inch in diameter and 0.5 inch thick) embedded 2 m in hard clay was impacted by a pickup truck with a mass of 2300 kg, traveling at a velocity of 60 mph (100 km/h). The selected results are shown in Figure 3-7 and Figure 3-8.





**Figure 3-6: The pickup truck impact test PU60 (Mirdamadi, 2014)**

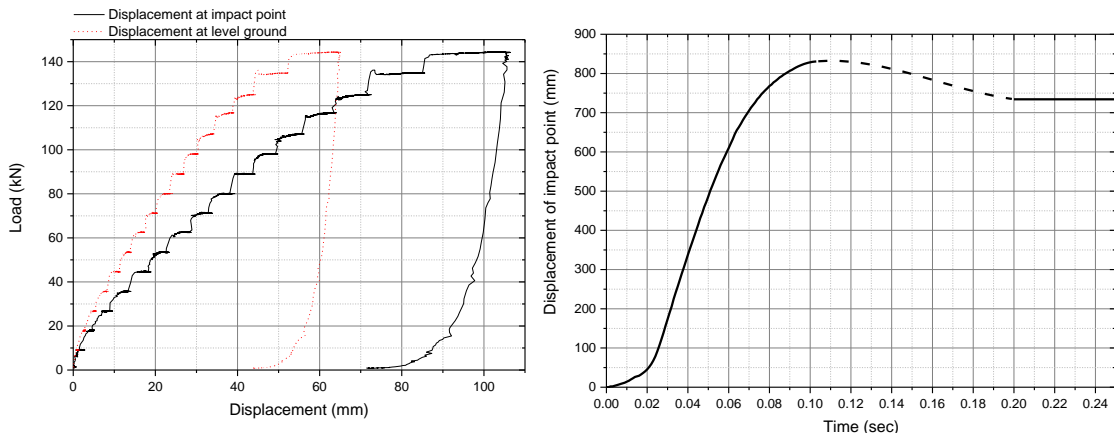


**Figure 3-7: The load-displacement curve of the static test on a pile in hard clay (left); The lateral displacement of the impact point in the crash test PU60 (right)**

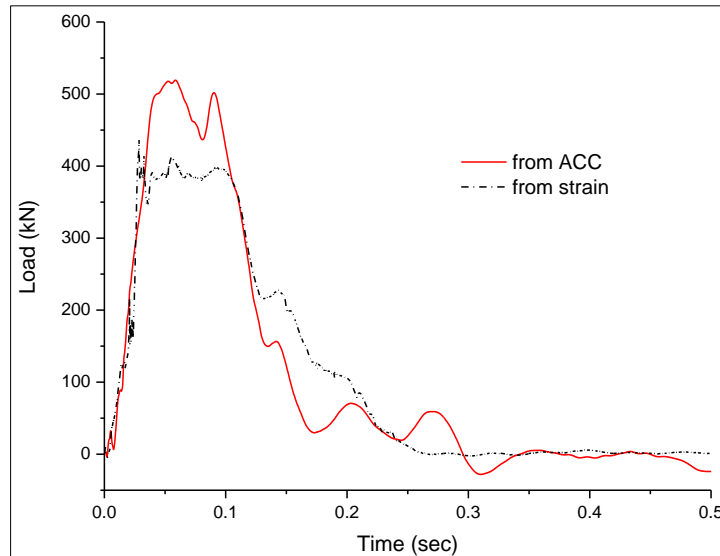


**Figure 3-8: The loads derived from acceleration and strain in the test PU60**

### **3.1.2. Experiments on group of piles: crash test on an eight-pile group (M50)**

Design of the pile group was initiated by running a set of LS-DYNA simulations to provide a preliminary prediction of the system response against a truck of 6800 kg mass with an approaching velocity of 80 km/h (50 mph). The test was planned to be conducted in a weak soil at the Texas A&M University Riverside Campus. A ditch of loose sand was constructed in the native hard clay by dumping the dry sand in place with no compaction as indicated in Figure 3-9. In order to characterize the soil properties a number of laboratory tests and in situ tests including the direct shear test and Pressuremeter test (PMT) were carried out. Table 3-5 summarizes the data collected on the soil properties. These values were then implemented as the reference in the finite element modeling. The loose sand utilized was classified as SP.



**Figure 3-9: Loose sand ditch (Lim, 2011)**

**Table 3-5: Soil properties**

<b>Depth (m)</b>	<b>Pressuremeter Limit pressure <math>P_L</math> (kPa)</b>	<b>Elastic Modulus <math>E</math> (kPa)</b>	<b>Standard Penetration Test SPT (bpf)</b>	<b>Water content (%)</b>
1.0	295	2800	1.5	3.5
2.0	190	1300	WOH*	5
3.0	175	1500	WOH*	5

\* Weight of hammer

The average unit weight and dry unit weight of the soil were measured as 17.6 kN/m<sup>3</sup> and 16.8 kN/ m<sup>3</sup>, respectively. From the direct shear tests, the friction angle of the soil was measured as 29 degrees.

In this test, a barrier consisting of two steel beams (HSS8x8x1/2) connecting eight steel piles (W14x90) embedded 3 m in loose sand with a spacing of 5.2 m was designed to contain a truck of 6800 kg mass with an approaching velocity of 80 km/h. The test configuration was considered to be representative of a relatively extreme condition. The barrier configuration is illustrated in Figure 3-10 and Figure 3-11.

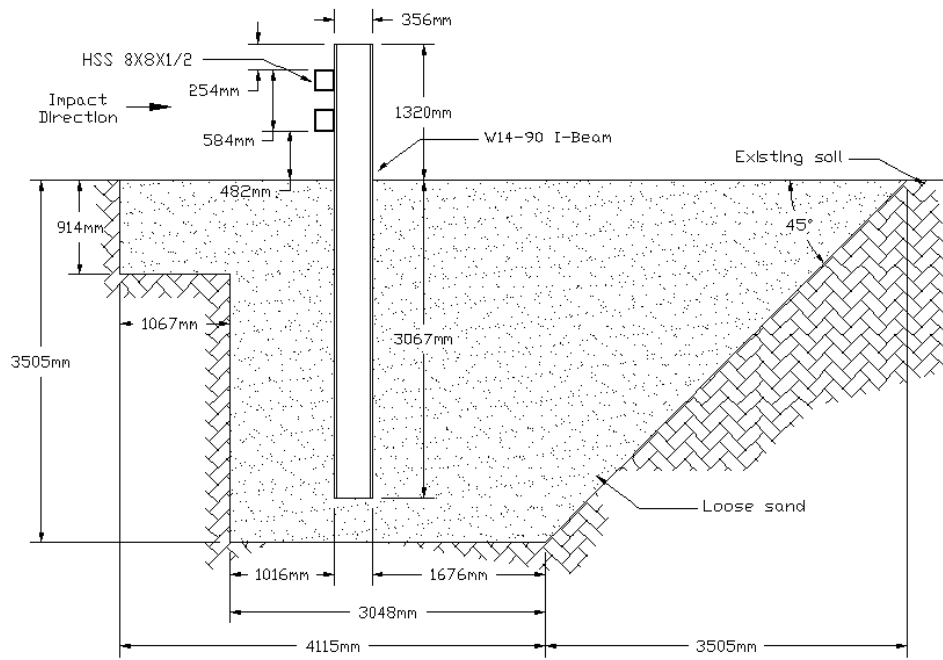


**Figure 3-10: Side Elevation of the pile-beam structure**

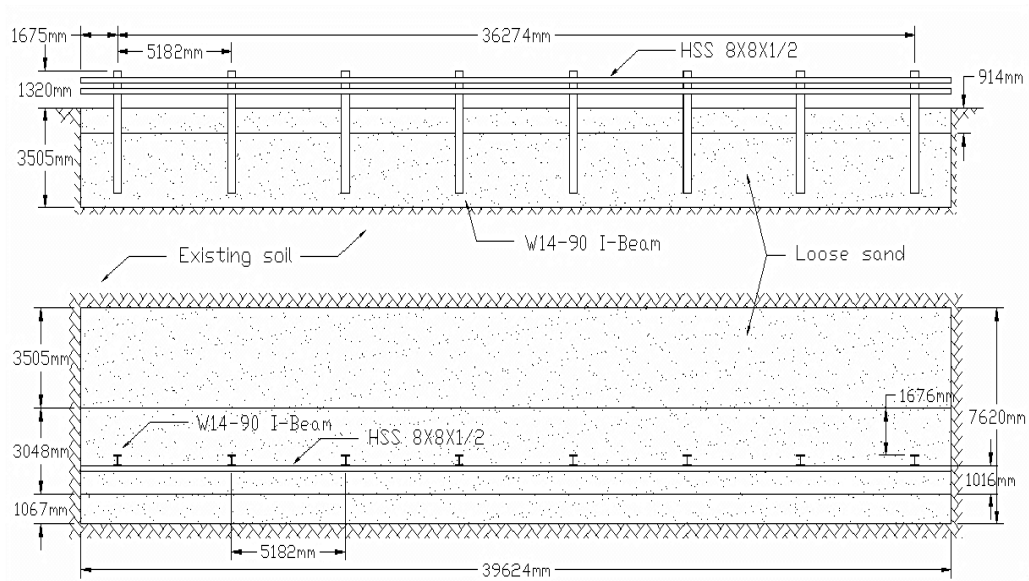


**Figure 3-11: Side view and plan of the designed group piles**

The beams were welded to the piles and anchored together with the plates. More details of the pile-beam installations are reported in Asadollahi Pajouh et al. 2014.

To meet the ASTM requirements of designation M50, a 2001 single-unit flatbed truck of 6800 kg mass was selected to hit the beams in the middle of the two center piles. In order to measure the system response, two accelerometers were installed on the vehicle as well as eight strain gauges on both sides of four of the piles. The strain gauges were welded with a micro welding method on the pile surface that has been smoothed with sandpaper (Figure 3-12). The strain gauges were installed on piles to measure the bending moment.



**Figure 3-12: Instrumentations installed on the piles**

The impact test was preceded by a static test on an isolated single pile at the end of the in-line group to determine the static lateral capacity. The load was applied by pulling horizontally on the pile at a slow and constant rate of displacement. Figure 3-13 shows

the static load-displacement curve. The total displacement was 65 mm or 0.2B where B is the width of the pile. The ultimate load defined at 10% of the pile width or 35.6 mm is 55 kN but smaller than the ultimate load of 60 kN at the final displacement of 65 mm or 0.2B. The secant static stiffness at 50% of the 0.1B ultimate load was calculated from the graph to be  $15.4 \times 10^6$  N/m. After the static test, the pile was pushed back to the original position.

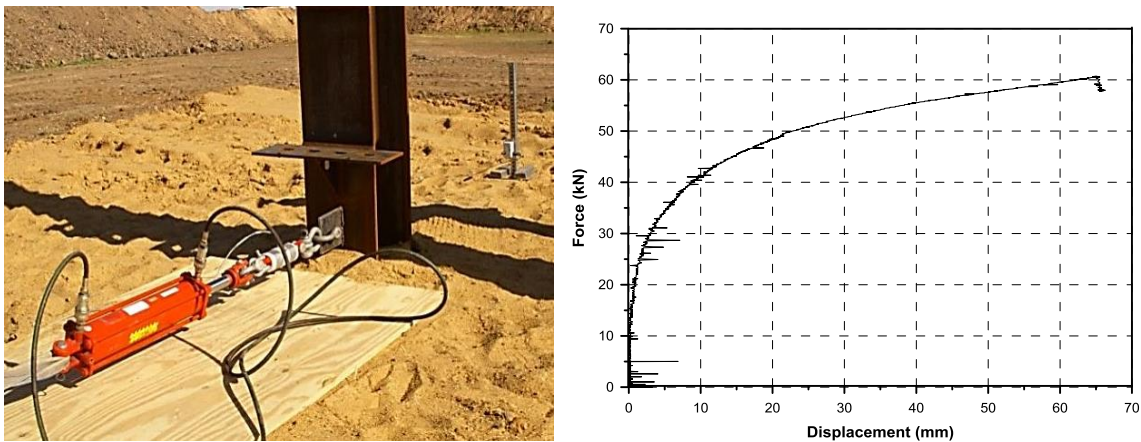


**Figure 3-13: The static test on the single pile and the results**

Figure 3-14 shows the system after the impact and Table 2 reports the pile response, displacement and rotation. As illustrated in Figure 3-11, piles are numbered from left to right in the impact direction view. The medium duty truck deflected the beams and the piles forward while the end piles deflected backward as a reaction. The forward movement lasted 400 ms at which time the vehicle started to rebound. The truck came to a complete stop at 5.7 sec. During the impact, the front edge of the vehicle flatbed passed the initial location of piles by less than 1m; therefore the barrier-piles system met

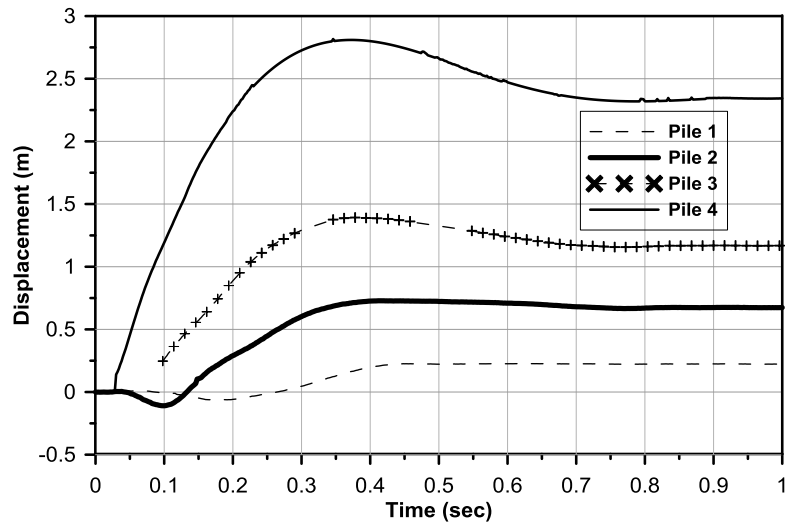
the ASTM F2656-07 penetration rating P1. Damage to the installation after the impact test is shown in Figure 3-14. Figure 3-15 indicates the maximum pile displacements.



**Figure 3-14: The group pile after the crash test M50**

**Table 3-6: Response of the piles: displacement, rotation**

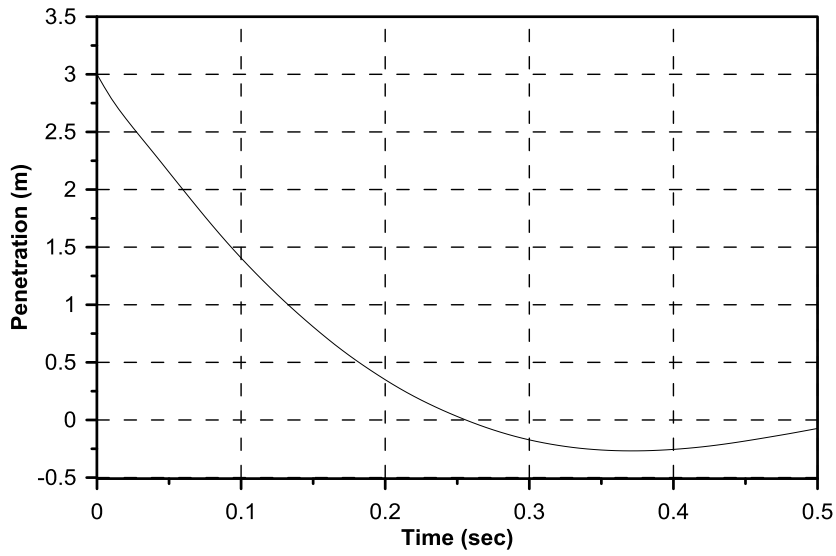
Pile No.	Permanent Rotation (degree)		Permanent pile displacement at the ground level (mm)
	Impact direction	Lateral	
1	2.2	2.3	76
2	8.6	2.5	333
3	17.7	7.5	775
4	38.1	6.4	1543
5	36.0	6.8	1492
6	18.1	3.5	845
7	9.9	3.3	400
8	3.3	2.3	135



**Figure 3-15: The measured displacements of the piles**

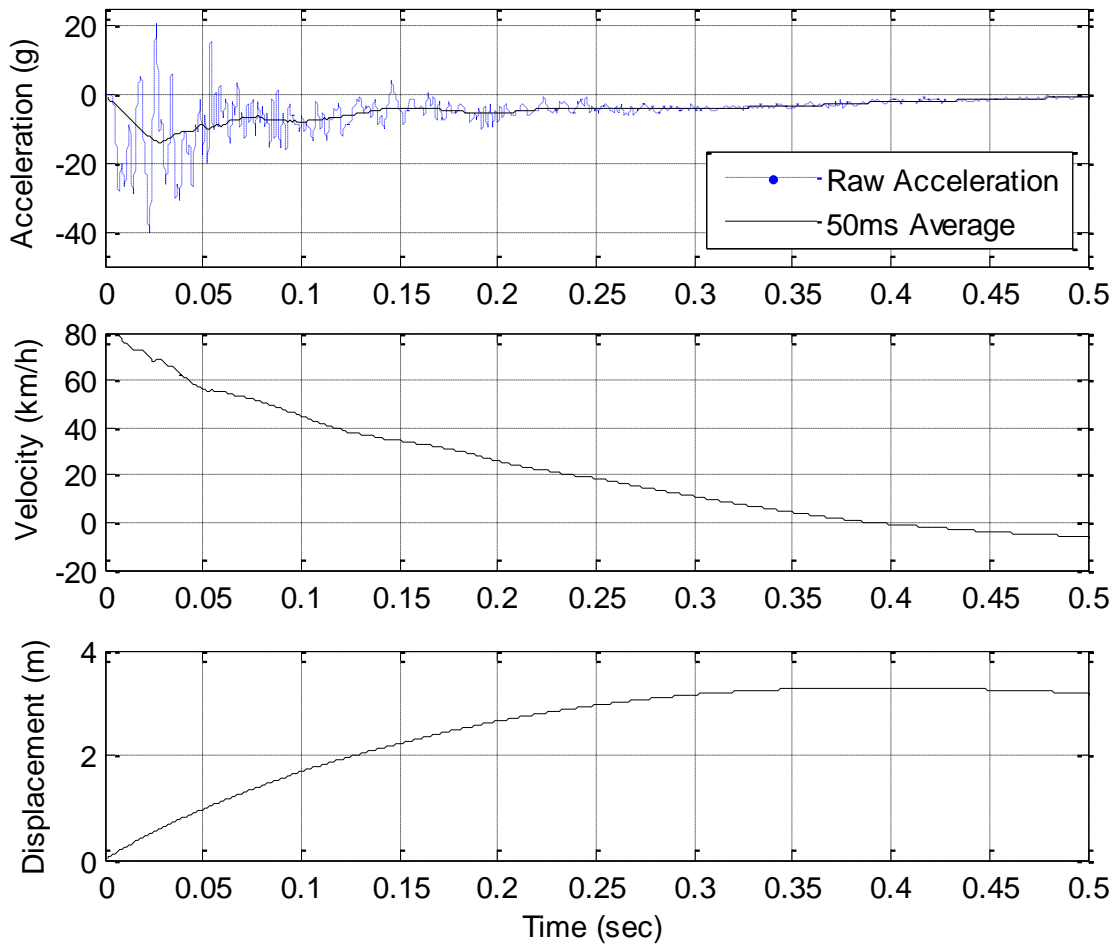
The horizontal deflection of the pile groups was 3.25 m and since the cab length was 3 m, the back of the cab did not penetrate more than 1 m past the original line of the pile group. The dynamic penetration of the test vehicle during the impact is presented in Figure 3-16. As observed that the piles were able to successfully stop the M50 designation vehicle within a distance less than one meter.





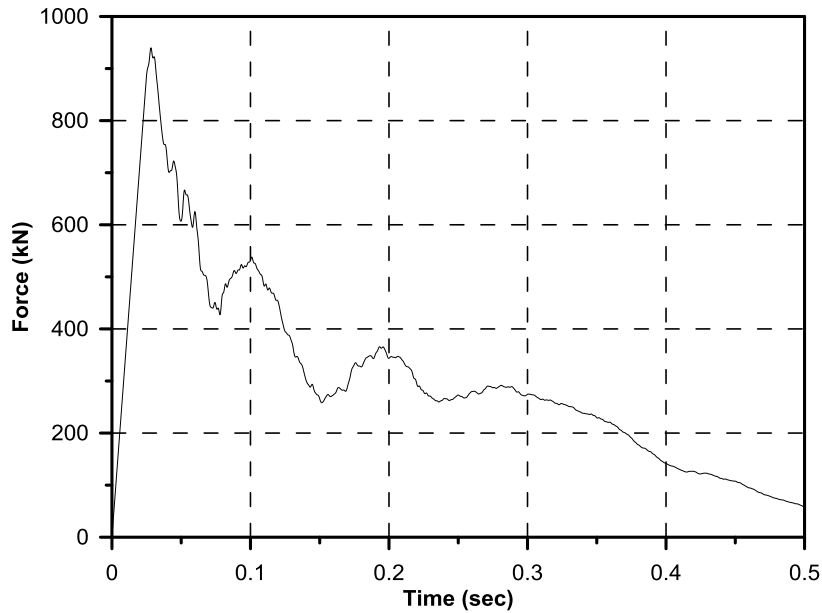
**Figure 3-16: Dynamic penetration of the test vehicle**

Figure 3-17 shows the vehicle deceleration and velocity as well as the barrier dynamic displacement at the point of impact after applying a 50-millisecond average smoothing on the raw acceleration. The longitudinal decelerations of the vehicle and 50 ms average one have the peaks of 40 g and 14 g, respectively. The maximum forward displacement of the barrier was 3.3 m. The strain gauges did not survive the test and no data could be recovered. Note that during the test, two of the connections between the piles and the beam failed.



**Figure 3-17: Measured vehicle displacement, velocity and acceleration**

Peak impact force calculated from the accelerometer readings and known mass of the vehicle is presented in Figure 3-18. Note that this is not necessarily the dynamic force at the contact between the truck and the barrier. Indeed the mass times acceleration assumes that the entire mass of the truck is subjected to the measured acceleration while in fact the crushing of the truck cabin decreases the average truck acceleration.



**Figure 3-18: Obtained impact force on the barrier system**

### **3.2. Full scale impact test on group of four piles in hard clay (PU60)**

In a subsequent full scale crash test, a four in-line pile group has been successfully impacted by a 2300 kg (5000 lb) pickup truck with an approaching speed of 100 km/h (60 mph), the common test setup for most roadside safety devices. The layout of piles, pile embedment and beams and the piles sections were determined on basis of the past experience and LS-DYNA simulations.

The test designation PU60 with the penetration rating P1 was considered. As defined earlier, the penetration rating P1 means that the barrier will stop the vehicle within less than one meter penetration. The following sections describe the design, static and dynamic tests.

### 3.2.1. Full scale static test

To comprehend the static nature of the soil-pile interaction, a full scale static test was conducted on a single pile with the same properties (steel tube of HSS6x6x1/2) and embedment depth (2 m) as the piles designed for the crash test. This test served as a reference for the dynamic pile behavior during the crash test and gave the static stiffness and ultimate static capacity of the pile-soil system. The horizontal load was applied in equal steps at a height of 0.75 m above the ground surface. More details about the loading system and its connection are illustrated in Figure 3-19, Figure 3-20 and Figure 3-21.

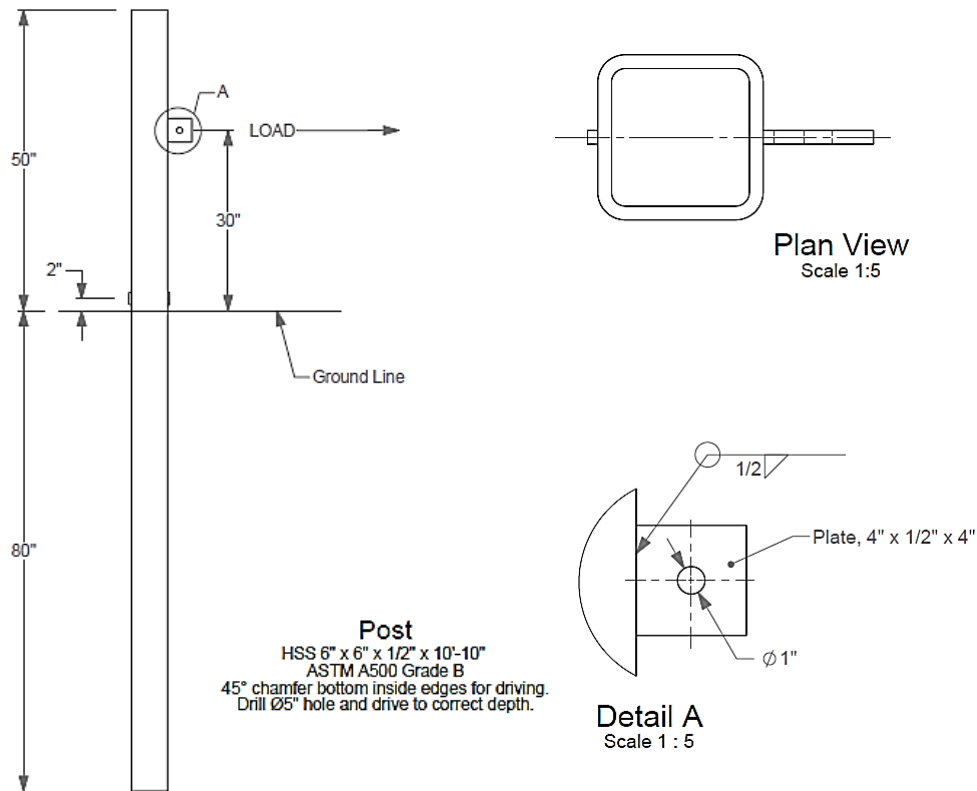


**Figure 3-19: Static test design**



**Figure 3-20: The static test installation**



**Figure 3-21: The loading system**

An amplifier was used to intensify and transfer the signals to the data acquisition system (Figure 3-22).

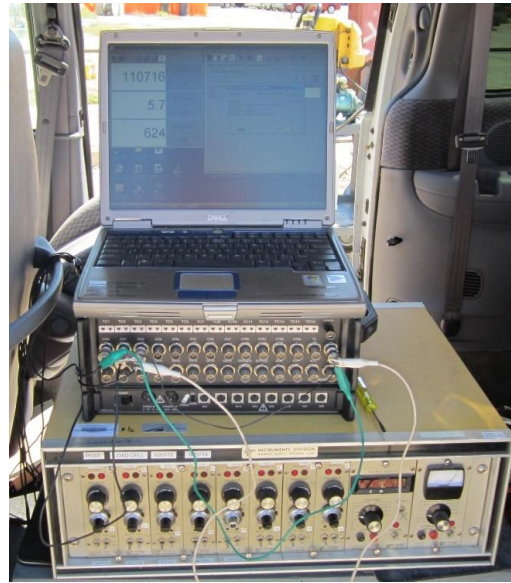


**Figure 3-22: The data acquisition system**

Displacement of the single pile at the load application point was measured by a string potentiometer with 50 inch range of measurement (Figure 3-23). String potentiometers measure the linear position using a flexible cable and spring-loaded spool.



**Figure 3-23: String potentiometer used for measuring lateral displacement**

Figure 3-24 shows the static test results. The ultimate horizontal load is typically defined at a displacement equal to one tenth of the pile width or 15.2 mm; in this case it is 22 kN but is far from the ultimate load measured at much larger displacement (53 kN at 128 mm or 0.8B). The static stiffness of the soil-pile system can be calculated from the graph as 1800 kN/m.

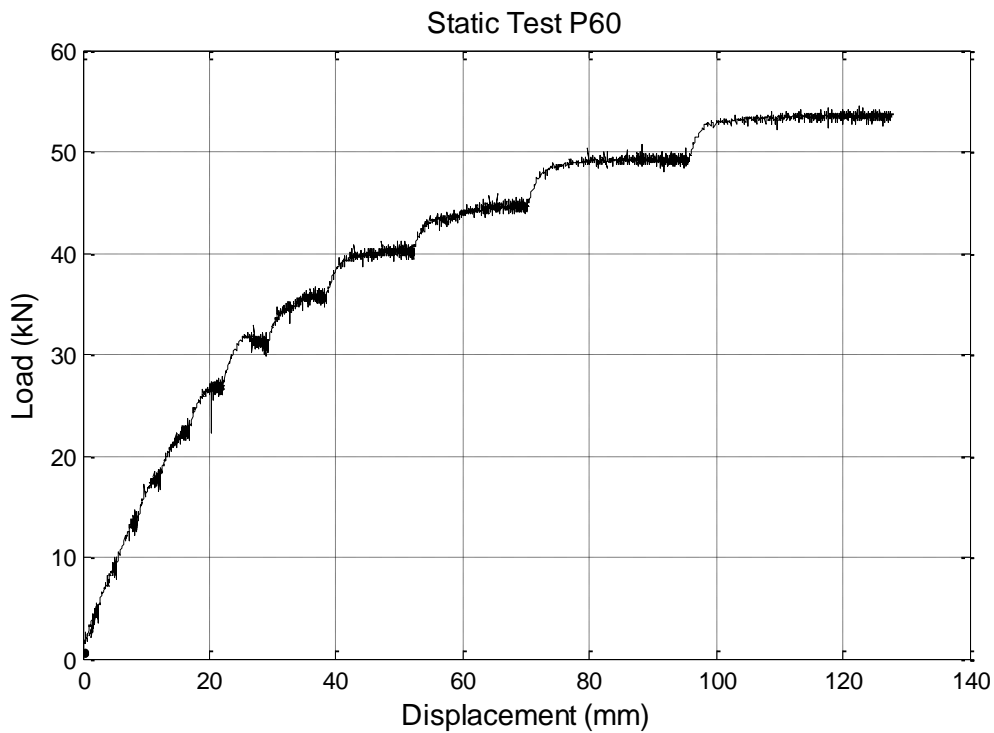


**Figure 3-24: The load-displacement curve obtained in the static test**

### 3.2.2. Design of a four pile group

A 2001 Chevrolet 2500 pickup truck, the primary test vehicle for roadside hardware evaluation (NCHRP Report 350) was directed into the barrier using a guidance system

and steel cable reverse tow system. The vehicle was released just prior to the impact traveling at the design velocity. The piles were designed as Hollow Steel Sections HSS6x6x1/2 (0.15 m wide, 0.15 m high, 12.5 mm thick and with a mass of 52 kg/m), spaced at 5.2 m on center apart, embedded 2 m in hard clay.

To install the piles, a 5-inch (12 mm) diameter hole was drilled with an auger, and then the pile was pushed into the hole to ensure a good contact with the surrounding clay. Figure 3-25 show the stages of the pile installation.



**Figure 3-25: Pile driving into the hard clay**



The piles were connected together with two beams of HSS8x8x1/2 (0.2 m wide, 0.2 m high, 12.5 mm thick with a mass of 72.5 kg/m). Figure 3-26 displays installing the beams.



**Figure 3-26: Installing the beams**

The piles and beams were connected by bolts holding two plates on both sides of the piles as shown in Figure 3-27. The beams are tied together with six steel plates.



**Figure 3-27: Connections installations using bolts and welding**

Considering the impact direction, the piles are numbered 1, 2, 3 and 4 from left to right. A front view and cross-sectional view of the barrier are shown in Figure 3-28 and Figure 3-29.

The lower beam has a distance of 0.5 m from the ground, which resolved concerns related to the test vehicle underriding the beams. Figure 3-30 through Figure 3-32 present the details of pile beam connections.

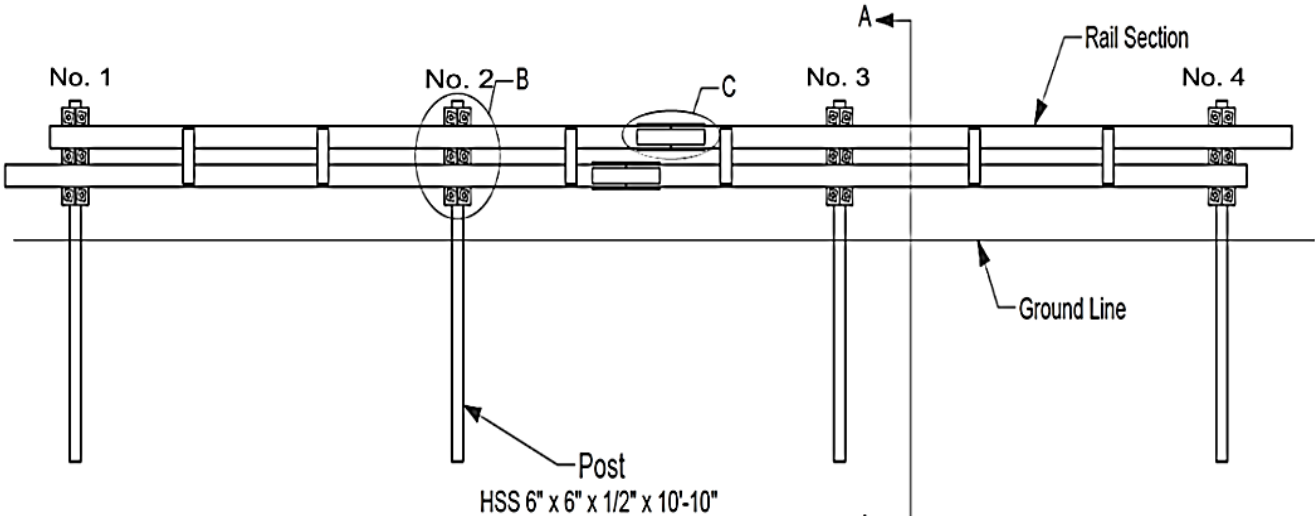


**Figure 3-28: Details of the barrier: Front view**

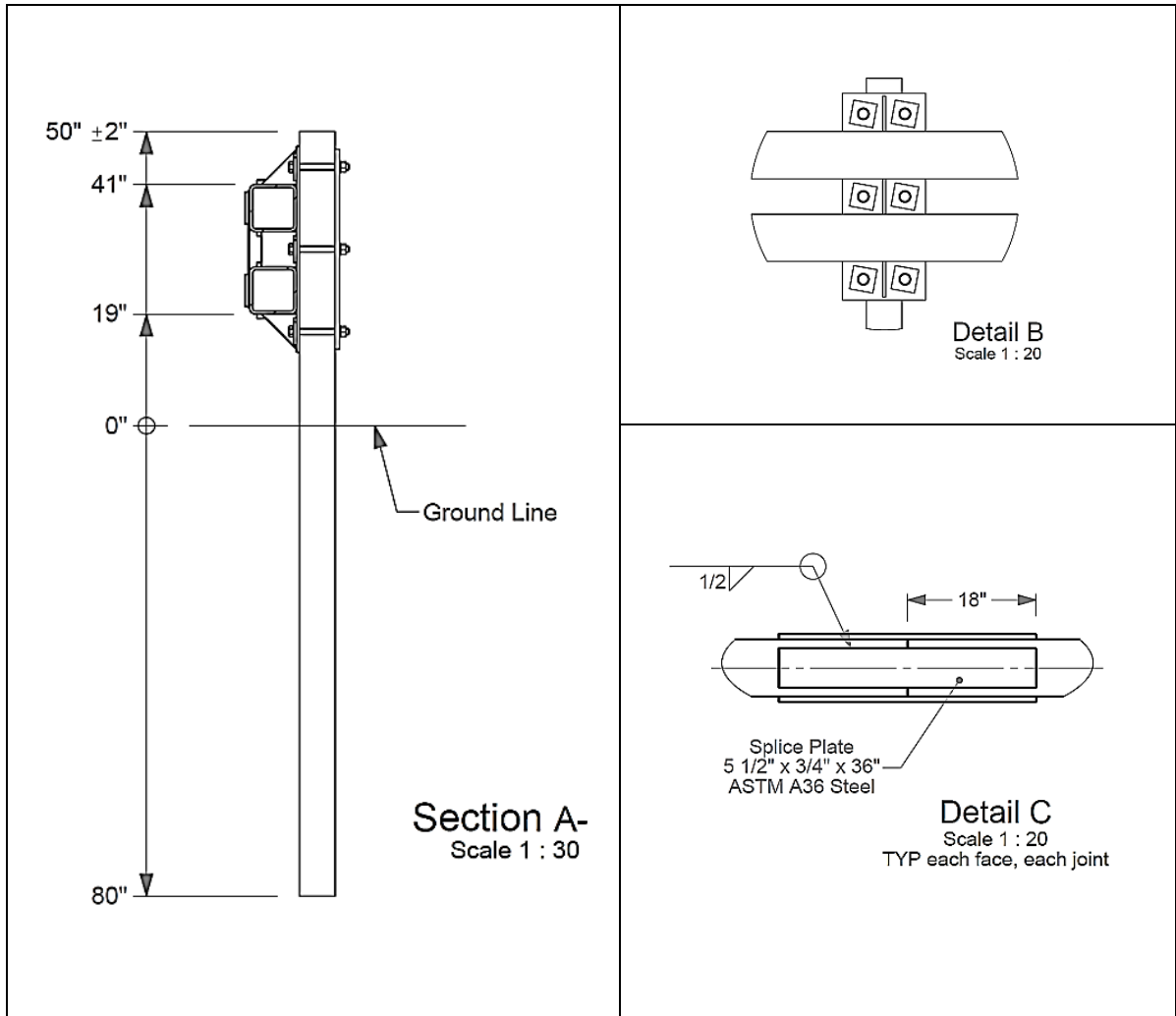


**Figure 3-29: Details of the barrier: Elevation view**

Plan View

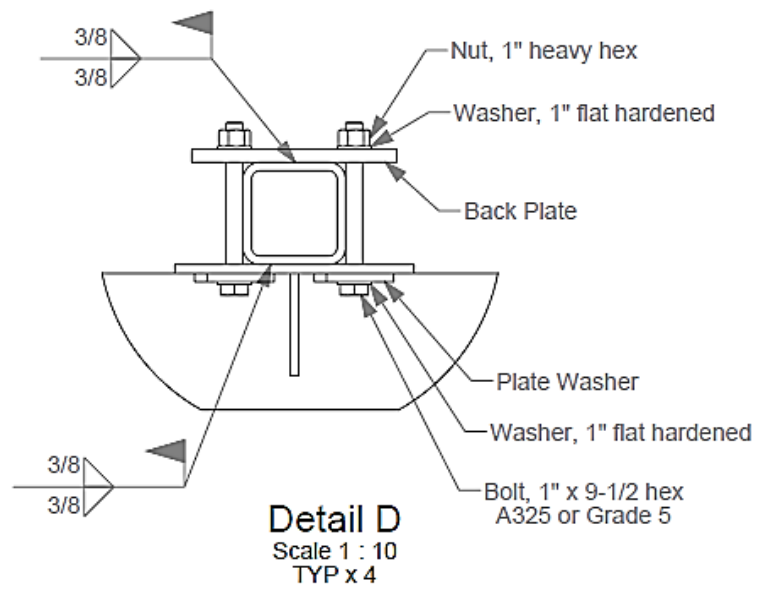
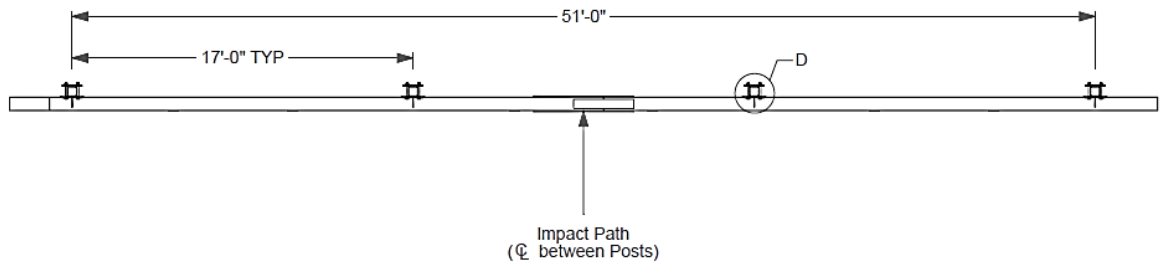
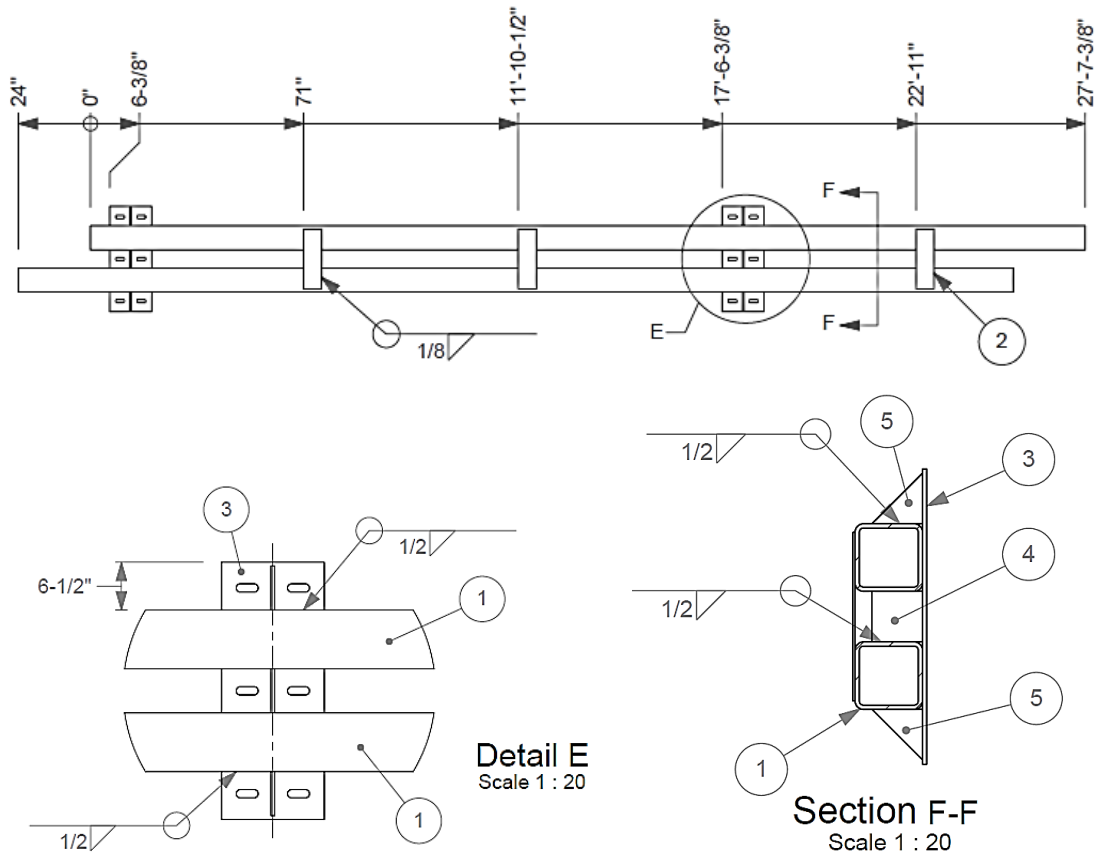


Figure 3-30: Details of the barrier: Plan view

RAIL SECTION PARTS					
#	Body Name	TYPE	LENGTH	MATERIAL	QTY.
1	Rail	HSS 8" x 8" x 1/2"	331 3/8"	ASTM A500 Grade B	2
2	Tie Plate	Plate, 6" x 1/4"	20"	ASTM A36 Steel	3
3	Mounting Plate	Plate, 14" x 1/2"	35"	ASTM A36 Steel	2
4	Middle Stiffener	Plate, 6" x 1/2"	6"	ASTM A36 Steel	2
5	Triangular Stiffener	Plate, 6" x 1/2"	6"	ASTM A36 Steel	4



**Figure 3-31: The beams details**

The beams are tied together with 6 steel plates 12X 3/4 X34 (Figure 3-32).

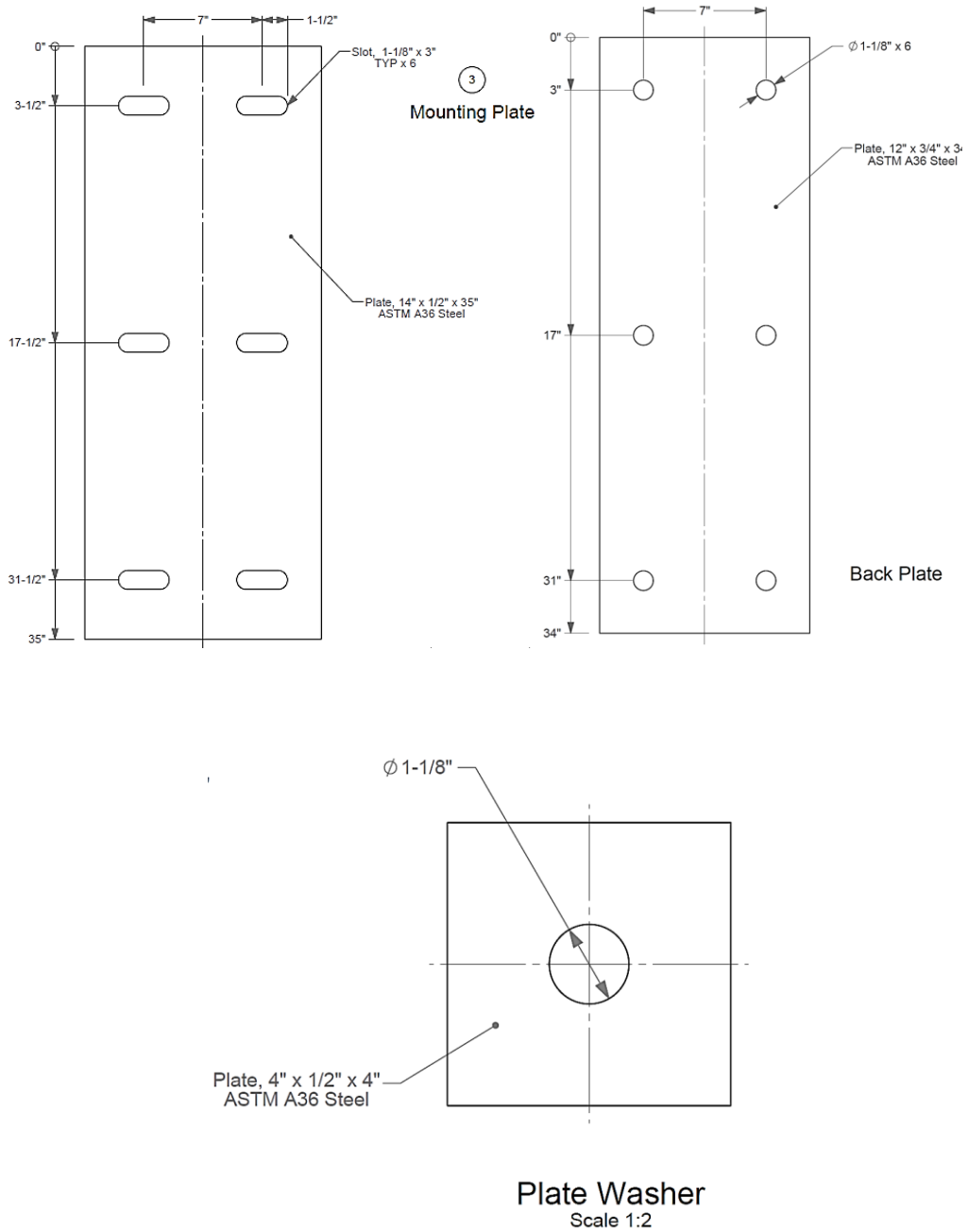


**Figure 3-32: Details of mounting plates and pile-to-beam connections**

The plates and the anchor bolts were fabricated from hot rolled carbon steel bars with high yield strength (Figure 3-33). The barrier prior testing is presented in Figure 3-34.



**Figure 3-33: Anchor bolts (left), the plates welded to beams (right)**



**Figure 3-34: The barrier after installation**

### 3.2.3. Geotechnical site characterization

A key factor that governs the impact performance of pile barriers is the soil properties and its interaction with the pile. The natural soil at the test site was dark grey sandy lean hard clay classified as CL according to the Unified Soil Classification system. Table 3-7 reports the data obtained from field density test performed at the site shown in Figure 3-35.



**Figure 3-35: Field density test**

**Table 3-7: Field density test report**

Depth (m)	Wet Density (kN/m <sup>3</sup> )	Percent Compaction (%)	Dry Density (kN/m <sup>3</sup> )	Water content (%)
0.2	19.6	99.9	16.9	16.3
0.25	19.3	100	16.9	14.1
0.25	19.6	100	17.9	11.9



Prior to the impact test, to characterize the site soil five borings were drilled and Shelby tube soil samples were recovered from two of the borings down to 2.5 m depth. Two Standard Penetration Tests (SPT) were performed at the location of piles No. 2 and 4 by Terracon Consulting Inc. The measured SPT N values are shown in Table 3-8.

**Table 3-8: SPT results**

<b>Depth (m)</b>	<b>N<sub>SPT</sub> @ Boring 2</b>	<b>N<sub>SPT</sub> @ Boring 4</b>
0.25	15	21
0.85	14	11
1.15	13	11

The SPT blow count and the PMT limit pressuremeter  $P_L$  averaged 14 blows per foot and 1400 kPa, respectively. The average unit weight measured as  $19.5 \text{ kN/m}^3$  and the undrained shear strength of 93.8 kPa was estimated using the correlation  $S_u \text{ (kPa)} = 6.7 \text{ N (bpf)}$  (Briaud, 2013). Moisture content of the soil was estimated 14.1%. The detailed soil profiles at the borings can be found in Appendix A.



**Figure 3-36: Standard Penetration Testing and sampling**

To better understand soil lateral resistance, Pressuremeter Test (PMT) was performed at the site. The test consists of lowering a 75 mm diameter, 0.6 m long cylindrical probe in a borehole and inflating it while recording the increase in volume and pressure of the probe. In this work, a small size of pressuremeter “Pencil Pressuremeter” was used for performing the PMT testing (Figure 3-37).

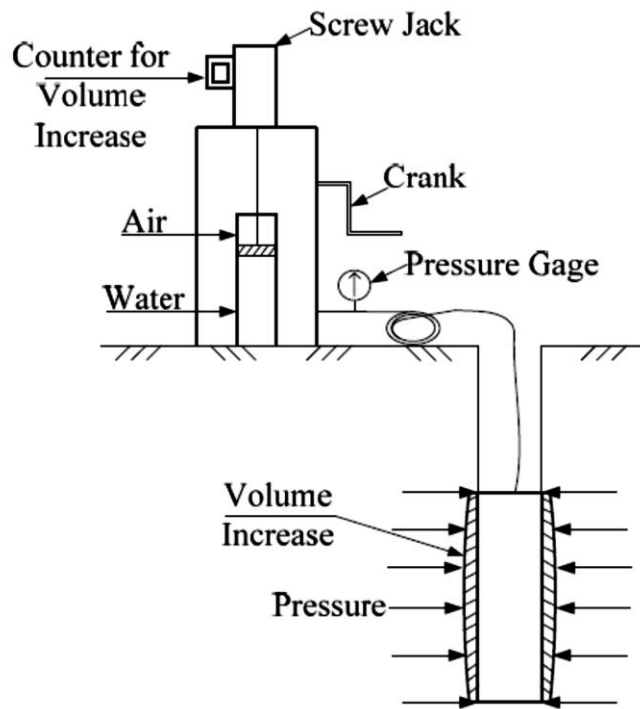
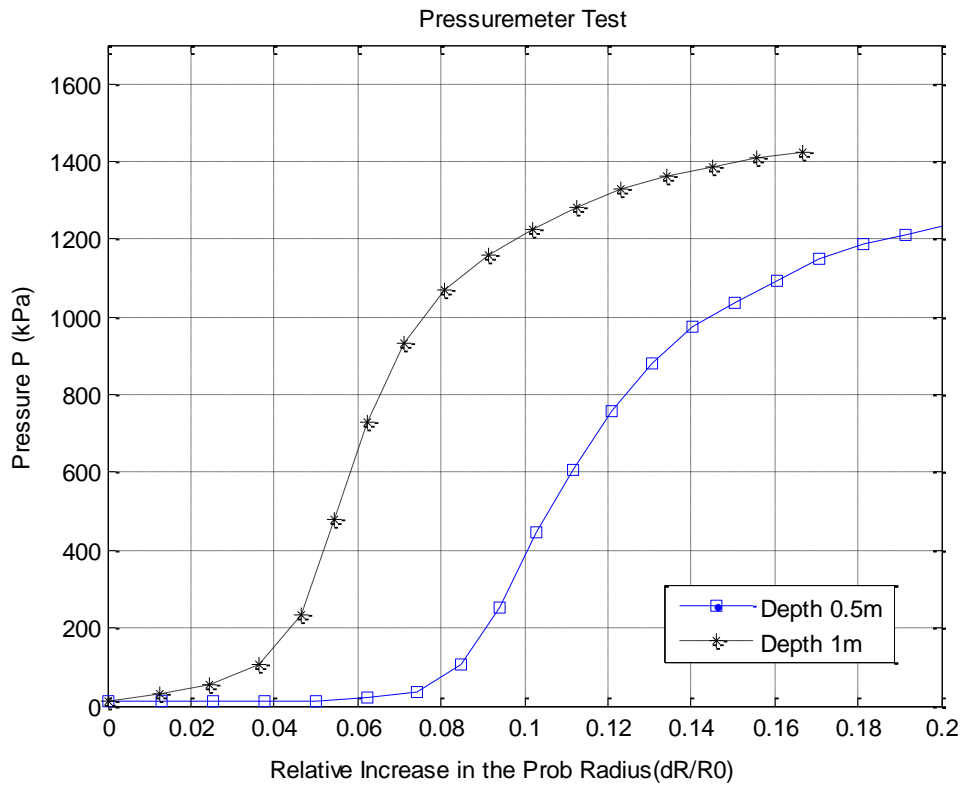


Figure 3-37: Pressuremeter apparatus

The probe had an outer diameter of 33 mm with a membrane of 1 inch (25.4 mm) diameter. The inflatable part is about 250 mm long. A maximum working pressure of 2500 kPa could be applied. This pressuremeter type can be used in both pre-bored hole (for high strength soils) and pushed in place (for low strength soils) down to 3m depth. Figure 3-37 indicates the test apparatus and the schematic of PMT testing procedure. More details on this in-situ test are provided in Appendix B. Two calibrations were performed to adjust the equipment effects on the test results: the compressibility calibration (volume calibration) and the membrane resistance calibration (pressure calibration).

**Table 3-9: PMT results**

Depth (m)	PMT Limit Pressuremeter $P_L$ (kPa)	PMT First Load Modulus $E$ (kPa)
0.5	1300	28
1	1450	38.5



**Figure 3-38: Pressuremeter test results**

### 3.2.4. Pile, beam and plates steel

Piles, beams and plates used in the barrier are fabricated of ASTM A-36 grade steel. According to ASCE LRFD Design Code, A-36 grade steel has a yield stress of 248 MPa and a tensile stress capacity of 400 MPa, however, it was observed that this grade

specifications are actually closer to the grade 50 steel with a yield stress of 345 MPa and a tensile stress capacity of 486 MPa. The piles and beams were assumed to have a modulus of elasticity of 29000 ksi, a Poisson ratio of 0.3 and a unit weight of 490 pcf. Researchers at Texas A&M Transportation Institute had performed several uniaxial tests of used steel materials to obtain a true stress-strain curve. The same curves have been applied for the LS-DYNA input in Steel material definition cards; that will be described in the following section.

### **3.2.5. Instrumentation and test set up**

To ensure capturing the vehicle and piles response, instrumentation including two accelerometers installed on the vehicle, one on the rear axle (Figure 3-39) and one near the center of gravity C.G., four strain gauges mounted on each pile (1/2 bridge bending on both front and back sides) at the ground level and two strain gauges installed on the beams at the mid-span was used. Figure 3-40 and Figure 3-41 illustrate the instrumentations.



**Figure 3-39: The accelerometer installed on the vehicle (rear axle)**

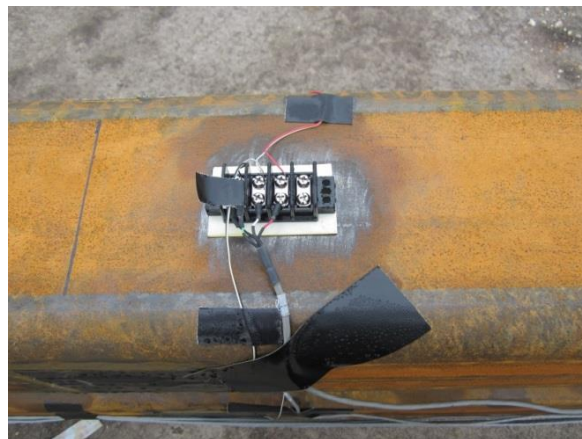


**Figure 3-40: The strain gauges installed on the piles and beams**

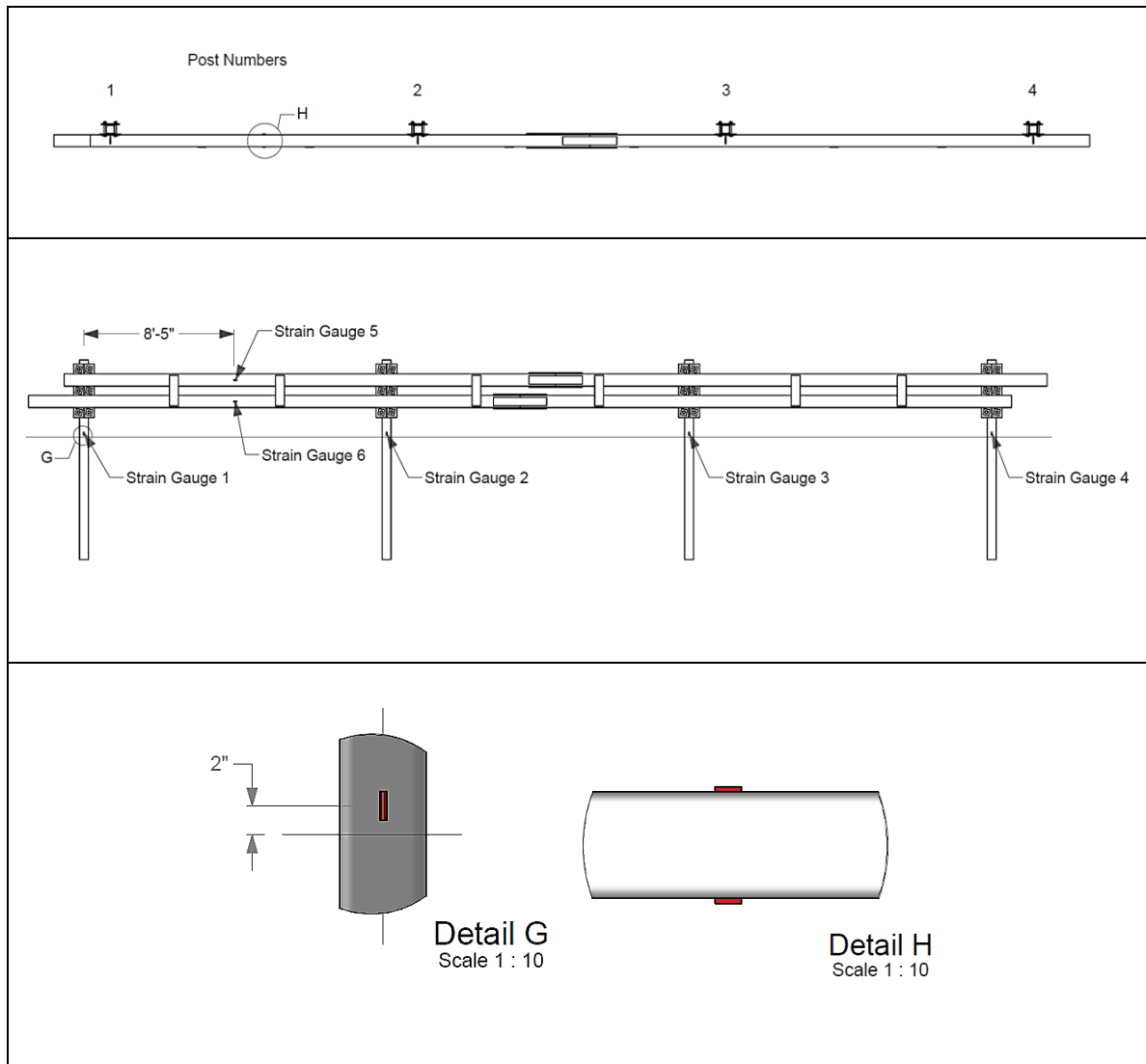


**Figure 3-41: Strain gauges and accelerometer**



Three 1000 fps high speed cameras (time interval for displacement is 1 ms) were set to record the experimental observations in three perpendicular directions: side, top and front view as shown in Figure 3-42. For the film analysis, the velocity of impactor and the distance between two targets at the same distance from the cameras are used to scale the measurements. Two film analysis software Phantom and Pro-analyst were used to track the target points and capture the deflection log by time. The accuracy of displacement is a function of distance between the cameras and the reference targets on the pile. Displacements were measured by tracking the reference points on the piles, the beams and the vehicle using the slow motion films.



**Figure 3-42: High speed cameras**

### 3.2.6. Test setup

In this test, a pickup truck approached the barrier with a 100 km/h (60 mph) impact velocity and targeting the center of the barrier between Pile 2 and 3. To direct the main vehicle toward the center of the barrier a ground cable system was utilized. The guidance cable and pulleys were installed on a concrete foundation buried in front of the impact point (Figure 3-43). Another vehicle travelling in the opposite direction towed the main vehicle towards the barrier at the desired velocity. Right before the impact, the guide cable was released and the main vehicle was set free to hit the target at the chosen location.



**Figure 3-43: Vehicle guidance system**

### 3.2.7. Test vehicle

The 2300 kg test vehicle was a 2001 year model Chevrolet pickup truck with a 5.7 liter, V8 engine and an automatic transmission. The C2500 pickup truck became the primary test vehicle for roadside hardware evaluation and certification crash tests, (NCHRP Report 350). The additional dimensions and information of the test truck is shown in Appendix C.



**Figure 3-44: The test pickup truck**

### 3.3. Group pile response under impact

The vehicle was successfully arrested by the barrier. The pickup truck did not roll over as was predicted in the preliminary simulations prior to testing. The front edge of the vehicle flatbed did not pass the initial location of piles, thereby the dynamic

penetration of the test vehicle was less than one meter and the barrier installation met the ASTM safety criterion. During the impact test, the data acquisition system recorded data from the accelerometers and the strain gauges for a total of 90 seconds at a rate of 10000 samples per second. Then the data was reduced and processed into acceleration, velocity, displacement, strain and force. In the following sections the collected data are compared to the numerically obtained results. The barrier and vehicle before the test and the damage to the barrier installation after the test are shown in Figure 3-45 and Figure 3-46.



**Figure 3-45: The barrier and test vehicle prior to testing**



**Figure 3-46: Vehicle and barrier after the impact on the group of piles system**

The strain gauges installed on the piles were damaged; however the gauges on the beams survived and measured the strains during the impact.

The deflections of piles presented in Figure 3-47 and Figure 3-48 were obtained by performing film analysis and tracking the target points.



**Figure 3-47: Pile displacements**



**Figure 3-48: Permanent deflection of the piles and beams and barrier damage**

The piles response, labeled from left to right of impact direction is presented in Table 3-10 and Figure 3-49.

**Table 3-10: The permanent deflection of the piles**

Pile No.	Permanent Rotation (Degrees)	Permanent Displacement at the ground level (mm)
1	19	165
2	23.9	304
3	24.4	298
4	20.3	155

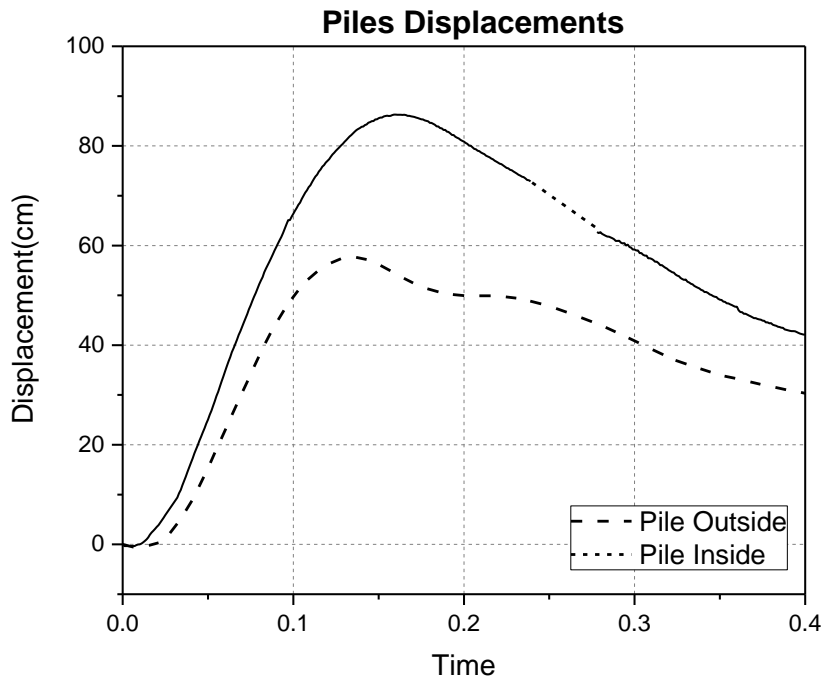


**Figure 3-49: Time history of the maximum displacements of piles at 1.3 m above the ground level**

The accelerometers attached on the flatbed above the rear axle of the vehicle and the one attached at the C.G. (Center of Gravity) measured the acceleration of the vehicle in three directions. The main concern is the longitudinal acceleration. The velocity and displacement of the vehicle are obtained through integration of this acceleration over

time. The deceleration comes from the accelerometer at the center of gravity of the truck. The raw signal was treated by applying a 50 ms average to remove excessive noise; this is a typical practice in this field. The velocity  $v$  was obtained by integration of the acceleration signal. The deflection  $y$  was obtained by double integration of the acceleration and by film analysis of the slow motion camera.

The recorded accelerations and calculated velocity, displacement and dynamic penetration of the vehicle are shown in Figure 3-50 through Figure 3-53. The maximum deceleration of the vehicle and the corresponding 50 ms average deceleration were recorded as 57 g and 29 g, respectively.

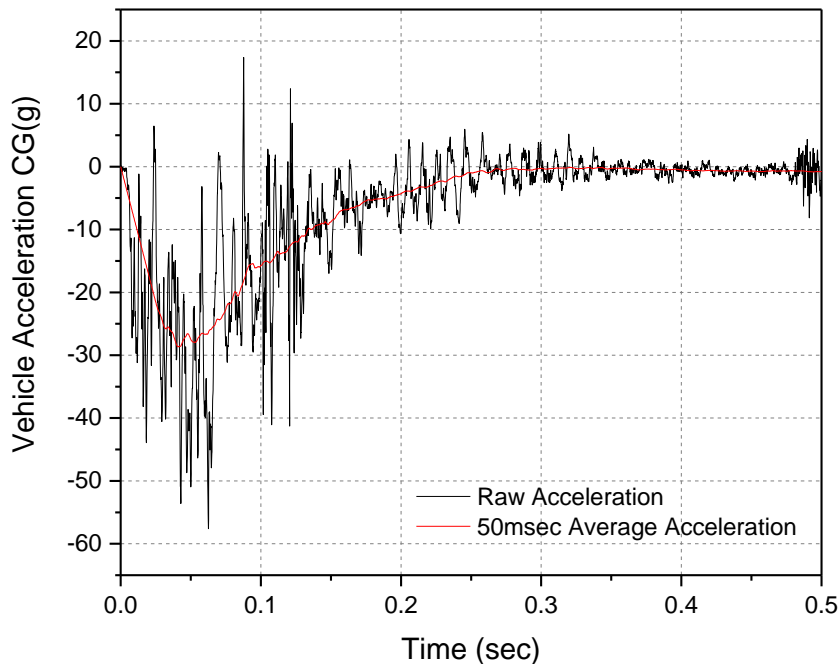


**Figure 3-50: Vehicle acceleration signal**



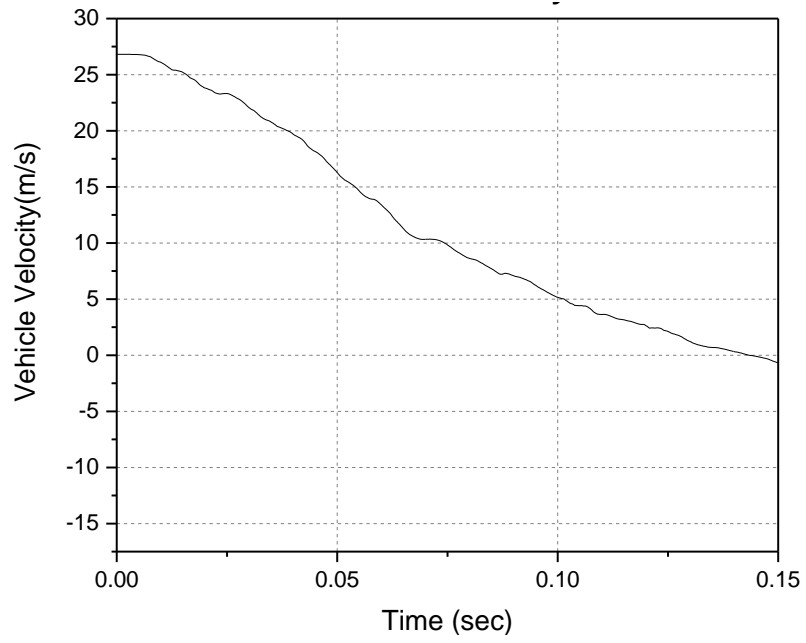


**Figure 3-51: Vehicle velocity**

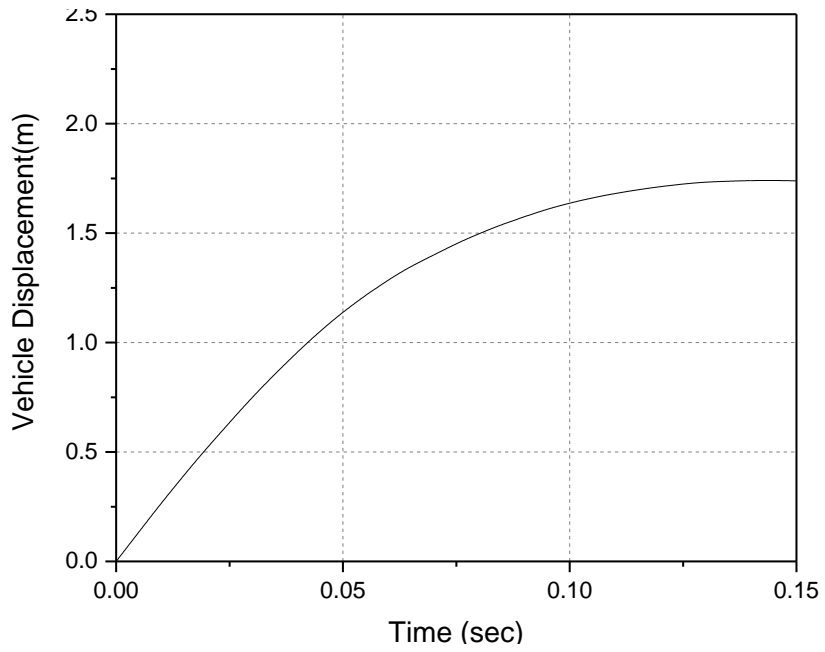


**Figure 3-52: Vehicle displacement**

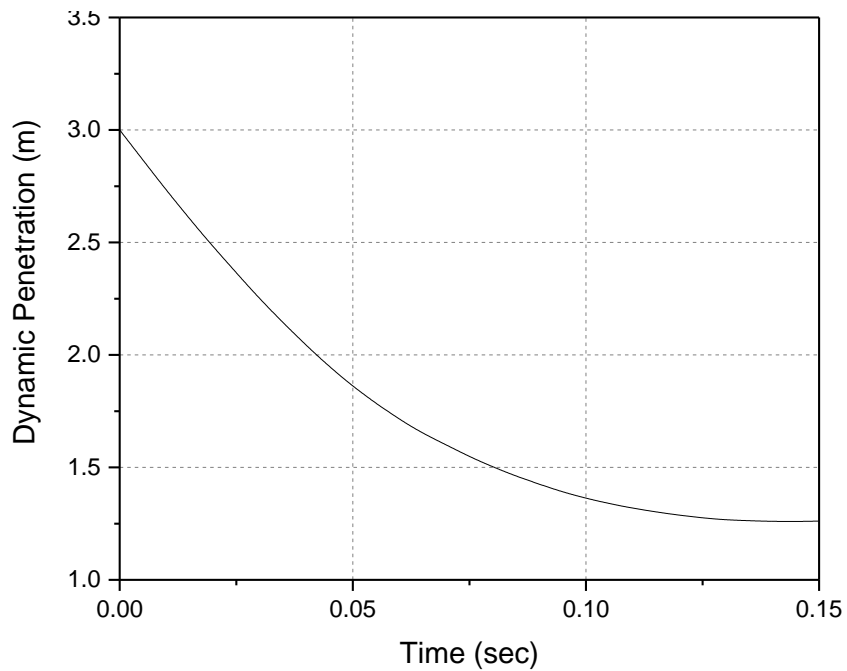


**Figure 3-53: Measured dynamic penetration of the vehicle**

The impact force (Figure 3-54) was obtained by multiplying the acceleration  $a$  by the mass  $M$  of the truck. Note that this approach is an approximation as the entire mass of the truck is not decelerating at  $a$ , since part of the mass is being crushed.

Note that the maximum pile displacement does not occur at the same time as the peak impact force. The impact force on the barrier is then quantified as the mass of the vehicle times its acceleration. The change in mass of the truck during the impact is assumed to be negligible.

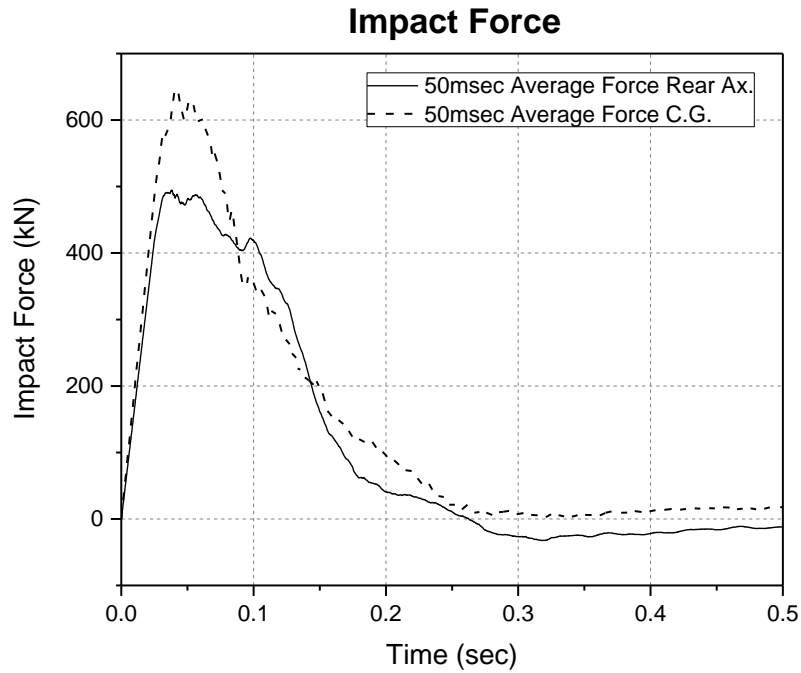


**Figure 3-54: The time history of 50msec average impact force**

All piles were failed due to the high bending moment caused by the impact loading (Figure 3-55). This failure bending is allowed as far as the piles do not rupture. Additionally in an optimum design, piles and beams are expected to bend and get plastified locally. The only concern is to assure the structural elements, i.e. piles, beams, plates and connections do not break or rupture during crashes. Piles are more likely to experience greater bending moment in stiffer soil, which in turn, result in more piles failing. Therefor structural strength of piles should be examined against rupture or breakage in a given impact level.



**Figure 3-55: Piles after testing**

LS-DYNA keyword deck by LS-PrePost  
Time = 0.13

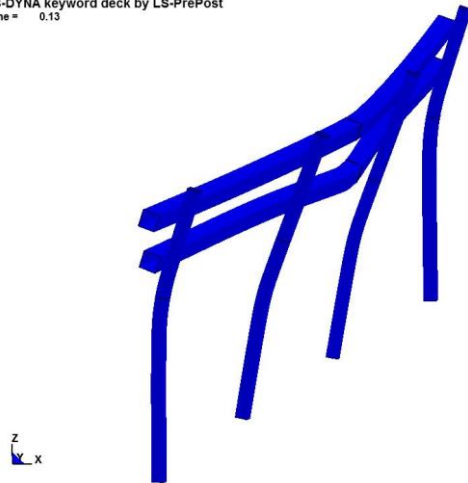


**Figure 3-56: Numerical model indicating the piles bending**

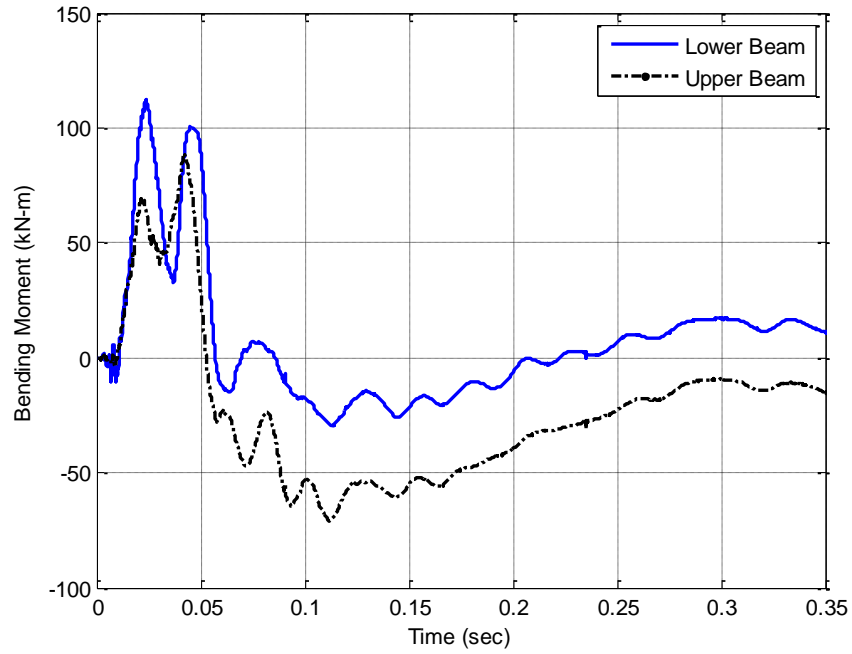


**Figure 3-57: The measured bending moment of beams**

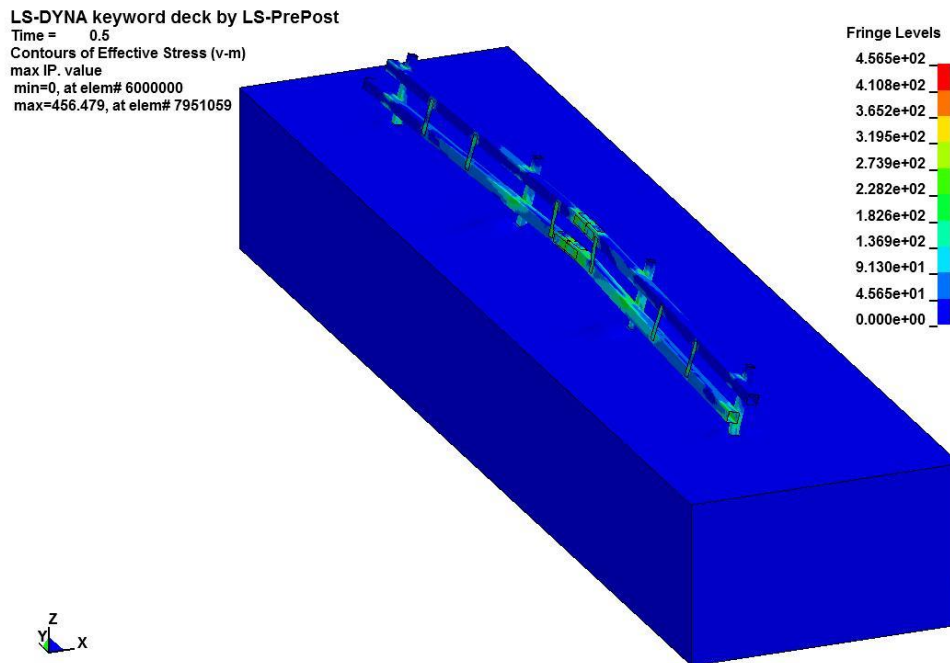


**Figure 3-58: The plastic strain**

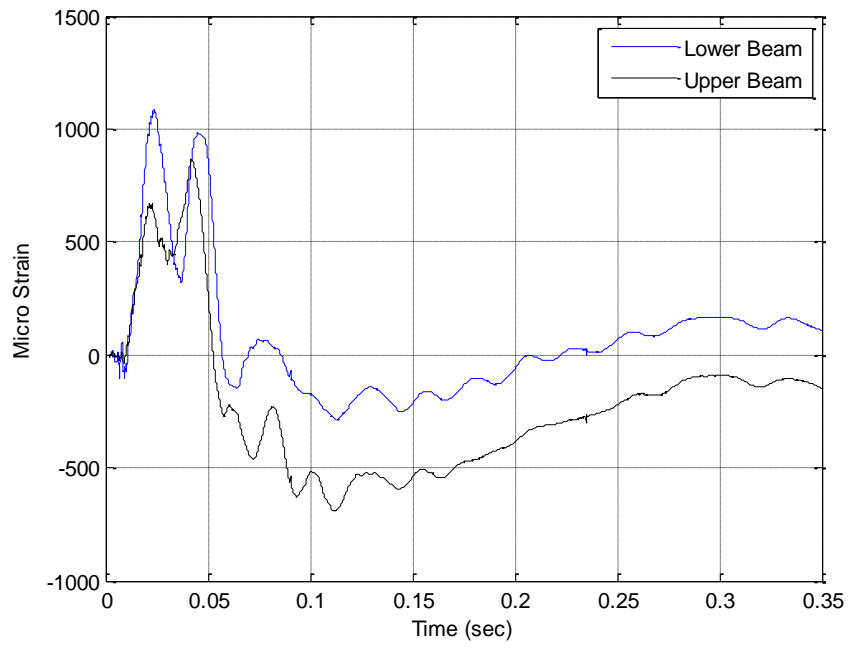


**Figure 3-59: The measured strains on gauges installed on beams**

Figure 3-60 shows sequential images of the crash test PU60.



**Figure 3-60: Sequential images of the crash test PU60**

## 4. NUMERICAL SIMULATION

### 4.1. Introduction

Crash events are complicated and difficult to study as they involve unknown interactions between the impacting mass (vehicle in this problem), structural elements (such as the barrier consisting of piles and beams) and soil supporting the structure. In addition, most elements in a vehicle-barrier crash, for instance, undergo extremely large deformations in a very short time and this transient extreme loading introduces substantial material nonlinearities. To accurately duplicate these complex behaviors in a crash event, use of advanced nonlinear codes is inevitable.

In this study, a state-of-art nonlinear finite element code LS-DYNA was used to simulate the crash experiments (PU60 and M50) described earlier in this dissertation. Parametric variation inherent in various in-line pile groups design makes numerical simulation an efficient tool for development a design process.

Lim (2011) at Texas A&M University conducted a number of simulations using LS-DYNA to model crash tests on either single or group of in-line piles. Based on this research, he developed design guidelines for certain cases of piles embedded in soils of different strengths. In these series of simulations, two material models were adopted to represent the soil behavior: Jointed Rock model for coarse-grained soils, and Isotropic Elastic-Plastic with Failure for clay. The results showed a reasonable agreement with the experiments. Mirdamadi (2014) also performed LS-DYNA simulations of the particular cases of single piles. Having those successful experiences in numerical modeling of



vehicles crashes, in the current study this package has been utilized to analyze the cases of group piles.

The main objective of this numerical study was first to develop detailed finite element models replicating the real impact tests and then examine other cases in general using the validated models. Additionally, comparing the numerical results help to draw practical recommendations to enhance safety of the anti-perimeter barriers.

#### **4.2. Introduction to LS-DYNA**

The finite element package LS-DYNA originates from the program DYNA3D (Hallquist 1976) which was primarily for the analysis of structures subjected to impact loadings. In the 1986 version of DYNA3D, introducing many new features such as beams, shells, rigid bodies, single surface contact, discrete springs and dampers, hourglass treatments expanded the code's applications (Hallquist and Benson 1986).

In development of the software, Livermore Software Technology Corporation was founded in 1988 to make more progress in solving crashworthiness problems and add more capabilities to the software. A commercial version called LS-DYNA3D (shortened LS-DYNA) was introduced. Since then many features such as more material models in the library, more capable contact interfaces, allowing for a variety of element types have been enhanced in new releases of the software to simulate the real crashes more properly (Hallquist, 1993).

LS-DYNA works with either implicit or explicit solver, either single or double precision. However the explicit time integration algorithms embedded in LS-DYNA

allows for accurate analysis, not sensitive to the machine precision. Therefore double precision is not generally required which greatly improves utilization of memory. LS-DYNA uses the explicit integration technique; this improves greatly its computation speed, in particular for very large and intensive models.

LS-DYNA having a comprehensive material models library, advanced contact algorithms and many different element formulations, allow for an accurate simulating of the actual impact mechanism. The primary capability of LS-DYNA is its accuracy in analyzing high speed events where inertia forces are important contributors. This code is well suited for the problems requiring computationally intensive time-domain analysis multi-physics simulations (Hallquist 2006, 2007, Livermore Software Technology). Other numerical codes such as FLAC-3D does not account for changes in material properties caused by the high strain rates that normally happen in crash events.

Traditional frequency domain solutions for numerical soil-structure interaction analysis were based upon linearization. This method does not work well in problems where any of the following behaviors: nonlinearity in structural elements, local soil failure and permanent deformations is expected. In time domain analysis solutions, nonlinearity of the soil and structure can be perfectly represented explicitly, given the boundaries of the finite soil model are cautiously simulated.

Also LS-DYNA can run on multiple processors clusters, which allows for an efficient use of Massively Parallel Processing (MPP) to solve complex problems within the least time and cost. All the analyses were performed by using LS-DYNA version 971 on a single precision SGI provided by Texas A&M supercomputing facilities, on EOS

cluster. Eos is an IBM "iDataPlex" cluster with nodes based on Intel's 64-bit Nehalem & Westmere processor. The cluster consists of 6 head nodes, 4 storage nodes, and 362 compute nodes. The storage and compute nodes have 24 GB of DDR3 1333 MHz memory while the head nodes have 48 GB of DDR3 1066 MHz memory (Texas A&M Supercomputing Facility, 2015). For this study, 32 CPUs (four nodes, eight processors) with 88 GB memory were used. 22 GB is the maximum memory that can be allocated to each node. For all the runs, MPP (Massive Parallel Processing) was used. This minimized the run time significantly. For example, a general model with intermediate level of complexity requires 800 BUs or 33 days of computing time, which is reduced to one day by using MPP Massive Parallel Processing.



Operating System: Linux
Number of Nodes: 372
Number of Processing Cores: 3168 (all@2.8GHz)
Total Memory: 9,056 GB
Total Disk: ~500 TB
File System: GPFS
Interconnect Type 4x QDR Infiniband

**Figure 4-1: EOS: an IBM iDataplex Cluster provided by Texas A&M University**

To facilitate preparing the input files including geometry, materials, loading and etc LSTC introduced a preprocessor Ls-Prepost 4.2 was used to generate the geometry and meshing the models and post process the results. LS-PrePost provides an efficient and

user friendly interface to pre and post processing files for the main solver of LS-DYNA. To run a problem with LS-DYNA, just a single executable file is required and all the input data is prepared in ASCII format using a text editor (e.g. Notepad).

For the models of more complex meshing HyperMesh was used. Altair Hypermesh is an advanced finite element pre-processor to generate the most complex and largest models with high quality meshes and maximum accuracy. Units in LS-DYNA models should be consistent for the whole simulations: for length the unit millimeter, for mass the unit ton (1000 kg), and for time the unit second were selected. The following sections overview the features of LS-DYNA that have been utilized in this numerical study.

#### **4.2.1. Boundary**

The keyword \*BOUNDARY provides a way to impose predefined motions on boundary nodes or a set of nodes. For the simulations, \*SPC\_SET\_BIRTH\_DEATH was used which allows birth and death times to be assigned to the associated nodes. The input “1” constrains the translation/rotation in the corresponding degree of freedom.

#### **4.2.2. Constrained**

In the current numerical models, to simulate the pile and beam rigid connections as well as the beam and plates connections the card \*CONSTRAINED\_NODAL\_RIGID\_BODY was utilized. This card allows defining a nodal rigid body with an arbitrary motion. It also provides the option “INERTIA” to

define constant translational and rotational velocities to the nodes predefined. The first picked node is treated as the master and the second one as the slave node.

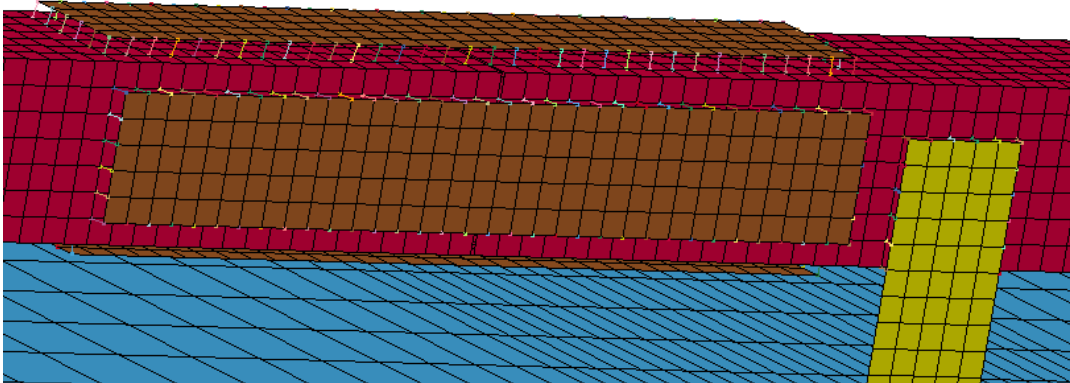


**Figure 4-2: CONSTRAINED\_NODAL\_RIGID\_BODY**

### **4.2.3. Contact**

Large deformations in crash events make it difficult or even impossible to predetermine where or how contact would occur. Therefore it is recommended to use the automatic contact options. The keyword `*CONTACT` was used to simulate interaction between disjoint parts. Different types of contact interfaces including `AUTOMATIC_NODES_TO_SURFACE` and `AUTOMATIC_SINGLE_SURFACE` were utilized. Unsuitable contacts and coarse mesh may result in initial undetected penetration (Figure 4-3). One side of the interface is treated as the master side and the other one as the slave side. In automatic contacts which are commonly used, the slave and master surfaces are introduced internally from the defined part ID's.

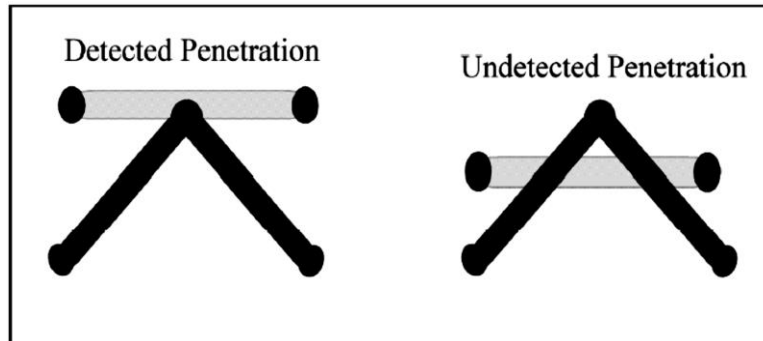


**Figure 4-3: Undetected interpenetration**

In automotive crash modeling, the entire vehicle is quite common to be assigned one single surface contact definition, where all the nodes and elements within the interface can interact independently. In this type of contact, no master surface is defined. Since this is a very reliable and accurate contact, if properly defined, it has been the most popular contact for crash analyses (DYNASUPPORT website).

#### **4.2.4. Control**

The keyword `*CONTROL` cards are optional but highly recommended. In this study several control cards were employed:

- `*CONTROL_TERMINATION` to set the termination time
- `*CONTROL_CONTACT` to change the computation features of contact surfaces
- `*CONTROL_MPP_IO_NODUMP` to suppress the output for dump files
- `*CONTROL_TIMESTEP` to set time step size control
- `*CONTROL_ENERGY` to set energy dissipation control
- `*CONTROL_ACCURACY` to improve the accuracy of the calculation

#### **4.2.5. Element**

The elements in the modeling are mainly generated by using cards \*SHELL and \*SOLIDS. In the vehicle FE model other types of elements were utilized including \*BEAM, \*DISCRETE, \*MASS, \*SEATBELT\_ACCELEROMETER.

The card \*SHELL allows to set the number of integration points across the 4 noded quadrilateral and 3 noded triangle shell elements. The card \*SOLID was employed to define three-dimensional 4 node tetrahedrons solid elements and 8-noded bricks.

#### **4.2.6. Hourglass**

The \*HOURGLASS card was applied to define hourglass and bulk viscosity properties of elements. The options IHG available in LS-DYNA are in both viscous and stiffness forms as following:

EQ.1: standard LS-DYNA viscous form,

EQ.2: Flanagan-Belytschko viscous form,

EQ.3: Flanagan-Belytschko viscous form with exact volume integration

EQ.4: Flanagan-Belytschko stiffness form,

EQ.5: Flanagan-Belytschko stiffness form with exact volume

For problems with high velocity deforming viscous hourglass control and for problems of lower velocities stiffness hourglass control is recommended. For solid element the option of exact volume integration treats the issues for highly distorted elements. The hourglass coefficient QM was picked as 0.1. Values of QM larger than 0.15 may cause instabilities for brick elements used with forms IHG=1-5. LS-DYNA

manual recommends the stiffness form of the hourglass control for automotive crash analysis. Bulk viscosity employed merely for solids controls shock waves propagation in solid materials. LS-DYNA manual suggests the default values.

#### **4.2.7. Initial and interface**

Pile and soil models have to be initialized for gravitational loading. In other words, soil stresses due to the self-weight should be taken into account before the primary crash analysis. Two approaches were adopted in simulations:

- Run the model including soil and piles under self-weight and generate the initial stresses, and then the obtained stresses are imported in the main model via \*INITIAL card

- Run the model using the card \*INTERFACE SPRINGBACK\_LSDYNA, this card generates a file (k file) under the name “dynain”. This file includes the elements stresses and strains from the initialization analysis for the part ID given. For the current case, initial stresses of soil part is desired.

Besides, the vehicle finite element models were given initial velocity to impact the barriers using \*INITIAL card.



#### **4.2.8. Section**

This card defines the element formulation, integration features, nodal thickness and cross sectional properties. Corresponding to the element type there is a \*SECTION card. There are several element formulation options such as EQ.1: Hughes-Liu, EQ.2: Belytschko-Tsay, EQ.3: BCIZ triangular shell, EQ.4: C0 triangular shell, EQ.5: Belytschko-Tsay membrane and etc. For solid elements ELFORM 1 (constant stress) and for shell elements ELFORM 2 (Belytschko-Tsay) were adopted. (Belytschko and Tsay, 1981)

NIP specifies number of through thickness integration points. For the current work NIP for shell elements is set to a value of 4 corresponding to a 2 by 2 Gaussian quadrature for the maximum accuracy. T1 to T4 indicate shell thickness at integration points.

#### **4.3. Material models**

LS-DYNA provides a variety of material models for clay, silt, sand and rock to simulate nonlinear behavior with a different degree of complexity. The card \*MAT describes the materials. LS-DYNA adopts Terzaghi's concept of effective stress to model materials with pore pressure. The pore pressure is calculated at nodes and then interpolated onto the elements. Table 4-1 lists the material models used among the large suite of models available in LS-DYNA. More detailed definition for each model parameters and the model theoretical base can be found in the LS-DYNA user's manual.

**Table 4-1: The material models employed in the numerical study**

Pickup truck	007-BLATZ-KO_RUBBER S02-DAMPER_VISCOUS 001- ELASTIC 026- HONEYCOMB 009-NULL 024-PIECEWISE_LINEAR_PLASTICITY 020-RIGID S01-SPRING_ELASTIC S04-SPRING_NONLINEAR_ELASTIC
Soil	013-ISOTROPIC_ELASTIC_FAILURE 198- JOINTED_ROCK
Pile, Beam and Plates	024-PIECEWISE_LINEAR_PLASTICITY

To select the soil model several factors were considered. First the list of available models in LSDYNA was examined. Then the complexity of some models was studied and the models which were either too complex in terms of formulation or in terms of the number of parameters required were abandoned; these included the “Honeycomb”, “Modified Honeycomb” and “Pseudo Tensor Geological” models. Then other soil models which work better under high confinement conditions were abandoned because the soil barrier system does not create very high confinement conditions; these included the “soil and foam” and the “soil concrete” models. Finally, the selected models because

of simplicity and robustness the “Elastic-Plastic with Failure” constitutive model was used for the hard clay in the PU60 test and the “Jointed Rock” model which is a modified “Drucker-Prager” model was used for the loose sand in the M50 test.

The efficiency of these material models are then examined through the experimental data. The values of the input parameters were selected to impose stiffness and strength corresponding to the data obtained in site investigations as the SPT blow count and the pressuremeter modulus and limit pressure in PMT tests.

#### **4.3.1. Soil models**

##### **Isotropic elastic-plastic with failure model**

The “Elastic-Plastic with Failure” model (MAT 013) assumes that the soil behavior is linear elastic up to a stress state where yield occurs. The material properties which were finally used are listed in Table 4-2 and Table 4-3. The mass density was measured in the field with the nuclear density probe and on samples in the laboratory. The elastic shear modulus was obtained directly from the pressuremeter tests. The Poisson’s ratio was estimated considering the fast loading condition. The undrained shear strength was estimated by correlation to the pressuremeter limit pressure. The bulk modulus was obtained from the formula linking it to the shear modulus.

**Table 4-2: LS-DYNA Material card for Isotropic Elastic-Plastic with Failure (LS-DYNA R7.1 Keyword Manual, 2014)**

<b>Variable</b>	<b>MID</b>	<b>RO</b>	<b>G</b>	<b>SIGY</b>	<b>ETAN</b>	<b>BULK</b>
Default	none	none	none	none	0.0	none
<b>Variable</b>	<b>EPF</b>	<b>PRF</b>	<b>REM</b>	<b>TREM</b>		
Default	none	0.0	0.0	0.0		

**Table 4-3: Variables on Isotropic Elastic-Plastic with Failure (LS-DYNA R7.1 Keyword Manual, 2014)**

<b>Variable</b>	<b>Description</b>
<b>MID</b>	Material identification
<b>RO</b>	Mass density
<b>G</b>	Shear modulus
<b>SIGY</b>	Yield stress
<b>ETAN</b>	Plastic hardening modulus
<b>BULK</b>	Bulk modulus
<b>EPF</b>	Plastic failure strain
<b>PRF</b>	Failure pressure ( $\leq 0.0$ )
<b>REM</b>	Element erosion option
<b>TREM</b>	dt for element removal

**Table 4-4: Summary of the material properties for the Isotropic Elastic Plastic soil model**

Mass Density (ton/m <sup>3</sup> )	Elastic Shear Modulus (MPa)	Poisson's Ratio	Undrained Shear Strength (kPa)	Bulk Modulus (MPa)
2.1	5.2	0.49	155	258

This material model follows von Mises yield condition given by:

$$\phi = J_2 - \frac{\sigma_y^2}{3} \quad (4-1)$$

Where  $\phi$  and  $\sigma_y$  are defined as yield function and yield stress and the second stress invariant is expressed in terms of the deviatoric stress components as Eq. 4-2 :

$$J_2 = \frac{1}{2} S_{ij} S_{ij} \quad (4-2)$$

Where the stress deviator tensor is expanded as Eq. 4-3

$$s_{ij} = \sigma_{ij} - \frac{\sigma_{kk}}{3} \delta_{ij} = \begin{bmatrix} \sigma_{11} & \sigma_{12} & \sigma_{13} \\ \sigma_{21} & \sigma_{22} & \sigma_{23} \\ \sigma_{31} & \sigma_{32} & \sigma_{33} \end{bmatrix} - \frac{\sigma_{11} + \sigma_{22} + \sigma_{33}}{3} \begin{bmatrix} 1 & 0 & 0 \\ 0 & 1 & 0 \\ 0 & 0 & 1 \end{bmatrix} \quad (4-3)$$

The yield stress,  $\sigma_y$ , is a function of the effective plastic strain  $\varepsilon_{eff}^p$  and the plastic hardening modulus,  $E_p$  as Eq.4-4:

$$\sigma_y = \sigma_0 + E_p \varepsilon_{eff}^p \quad (4-4)$$

The effective plastic strain is calculated as:

$$\varepsilon_{eff}^p = \int_0^t d\varepsilon_{eff}^p \quad (4-5)$$

$$\text{Where } d\varepsilon_{eff}^p = \sqrt{\frac{2}{3}} d\varepsilon_{ij}^p d\varepsilon_{ij}^p$$

The plastic modulus is defined in terms of the input tangent modulus,  $E_t$  as:

$$E_p = \frac{EE_t}{E - E_t} \quad (4-6)$$

Also pressure is obtained by the expression:

$$p^{n+1} = K \left( \frac{1}{V^{n+1}} - 1 \right) \quad (4-7)$$

Where  $K$  is the bulk modulus. Only one history variable  $\varepsilon_{eff}^p$  is stored with this model which makes this model the most cost effective plasticity model. This material model is not recommended for shell elements, because it might lead to inaccurate shell thickness updates and stresses after yielding.

In this model, either when the effective plastic strain reaches the failure strain failure or when the pressure reaches the failure pressure, the material fails to carry tension and the deviatoric stresses are set to zero ( $S_{ij} = 0$ ). The failed element can only carry loads in compression. Effective plastic strain  $\varepsilon_{max}^p$  and the failure pressure  $P_{min}$  are user-defined parameters (LS-DYNA R7.1 Keyword Manual, 2014).

$$\varepsilon_{eff}^p > \varepsilon_{max}^p \quad \text{Or} \quad P^{n+1} < P_{min} \quad (4-8)$$

In the case of uniaxial compression,  $\sigma_1 \neq 0, \sigma_2 = \sigma_3 = 0$ , hence the von Mises criterion is reduced to:

$$\sigma_1 = \sigma_y \quad (4-9)$$

where  $\sigma_1$  is the undrained compression strength (for the undrained case of clay is  $S_u$ ).

### Jointed Rock model

The “modified Drucker-Prager” model was chosen to characterize the sand behavior because it models the inability of the sand to resist tension, the increase in stiffness and strength of the sand with an increase in confinement and the volumetric dilation under shear (Drucker and Prager 2013). Additionally, this material model requires a limited number of input parameters that can be simply obtained through geotechnical tests. Table 4-5, Table 4-6, and Table 4-7 summarize the material properties implemented in the sand soil model. The mass density was measured in the field with the nuclear density probe. The elastic shear modulus was obtained directly from the pressuremeter tests. The Poisson’s ratio was estimated as a drained Poisson’s ratio for sand. The friction angle and dilation angle were obtained from direct shear tests. The cohesion value was used to avoid computational problems.

**Table 4-5: Material cards for Jointed Rock model (LS-DYNA R7.1 Keyword Manual, 2014)**

Card 1	1	2	3	4	5	6	7	8
Variable	MID	RO	GMOD	RNU	RKF	PHI	CVAL	PSI
Default					1.0			0.0
Card 2	1	2	3	4	5	6	7	8
Variable	STR_LIM	NPLANES	ELASTIC	LCCPDR	LCCPT	LCCJDR	LCCJT	LCSFAC
Default	0.005	0	0	0	0	0	0	0

**Table 4-5: Continued**

Card 3	1	2	3	4	5	6	7	8
Variable	GMODDP	PHIDP	CVALDP	PSIDP	GMODGR	PHIGR	CVALGR	PSIGR
Default	0.0	0.0	0.0	0.0	0.0	0.0	0.0	0.0
Card 4	1	2	3	4	5	6	7	8
Variable	DIP	STRIKE	CPLANE	FRPLANE	TPLANE	SHRMAX	LOCAL	
Default	0.0	0.0	0.0	0.0	0.0	1.0e+20	0.0	

**Table 4-6: Variables on Jointed Rock model (LS-DYNA R7.1 Manual, 2014)**

Variable	Description
MID	Material identification
RO	Mass density
GMOD	Shear modulus
RNU	Poisson's ratio
RKF	Failure surface shape parameter
PHI	Angle of friction (radians)
CVAL	Cohesion
PSI	Dilation angle (radians)
STR_LIM	Minimum shear strength of material is given by STR_LIM*CVAL
NPLANES	Number of joint planes (maximum 3)
ELASTIC	Flag = 1 for elastic behavior only
LCCPDR	Load curve for extra cohesion for parent material (dynamic relaxation)
LCCPT	Load curve for extra cohesion for parent material (transient)
LCCJDR	Load curve for extra cohesion for joints (dynamic relaxation)
LCCJT	Load curve for extra cohesion for joints (transient)
LCSFAC	Load curve giving factor on strength vs time
GMODDP	Depth at which shear modulus is correct
PHIDP	Depth at which angle of friction is correct
CVALDP	Depth at which cohesion is correct
PSIDP	Depth at which dilation angle is correct
GMODGR	Gradient at which shear modulus increases with depth
PHIGR	Gradient at which angle of friction increases with depth
CVALGR	Gradient at which cohesion increases with depth
PSIGR	Gradient at which dilation angle increases with depth
DIP	Angle of the plane in degrees below the horizontal
DIPANG	Plan view angle (degrees) of downhill vector drawn on the plane
CPLANE	Cohesion for shear behavior on plane
PHPLANE	Friction angle for shear behavior on plane (degrees)
TPLANE	Tensile strength across plane (generally zero or very small)
SHRMAX	Max shear stress on plane (upper limit, independent of compression)



**Table 4-7: Summary of the material properties for the Jointed Rock soil model**

Mass Density (ton/m <sup>3</sup> )	Elastic Shear Modulus (MPa)	Poisson's Ratio	Internal Friction Angle (degrees)	Dilation Angle (degrees)	Cohesion (kPa)
1.75	0.93	0.35	29	5	1

In this model a correction has been introduced into the Drucker Prager model, such that the yield surface never infringes the Mohr-Coulomb criterion. This means that the model does not give us the same results as a “pure” Drucker Prager model (LS-DYNA R7.1 Keyword Manual, 2014). The difference between Jointed Rock and Drucker-Prager model is that Jointed Rock model can consider joints inside the materials with properties of dip, plane and strength.

The Drucker-Prager yield criterion is a pressure dependent model suitable for granular soil materials that was established as a generalization of Mohr-Coulomb criterion. Similar to von Mises model the Drucker-Prager model has the advantage of smooth surface that does not exist in Mohr-Coulomb criterion. The sharp edges in Mohr-Coulomb model make the numerical analysis more difficult (Figure 4-4).

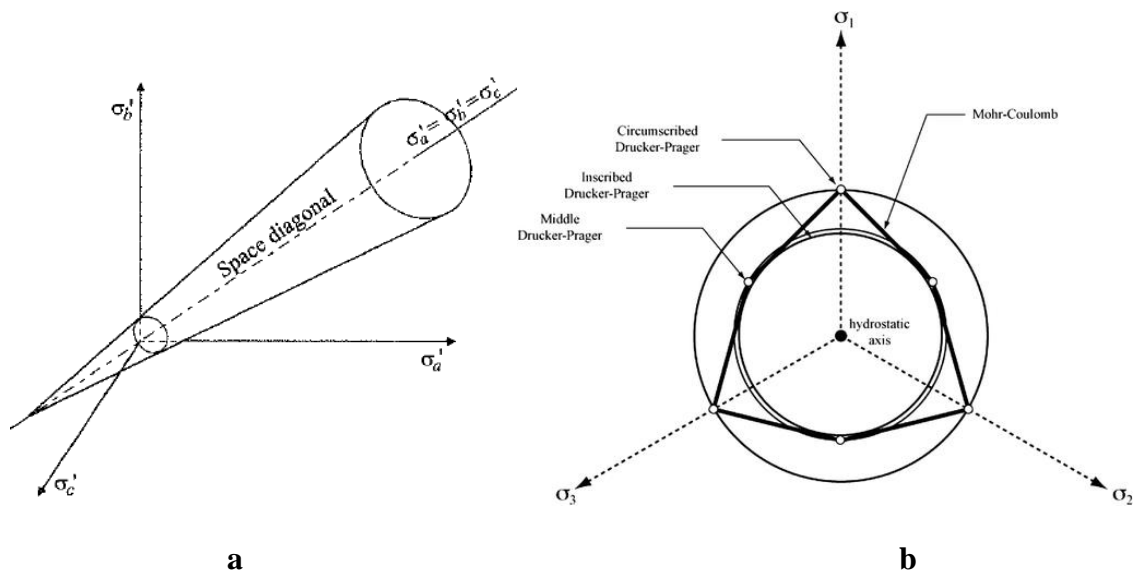


**Figure 4-4: a) Drucker Prager yield surface (Potts & Zdravkovic, 1999) b) Comparison of Mohr-Coulomb and Drucker Prager yield surface in 2D space (Alejano & Bobet, 2012)**

The yield criterion in Drucker-Prager model has the form:

$$\phi = \sqrt{J_2} - \lambda I_1 - \kappa \quad (4-10)$$

Where  $I_1$  and  $J_2$  are the first invariant of Cauchy stress and the second deviatoric stress invariant

$$I_1 = \frac{\sigma_{11} + \sigma_{22} + \sigma_{33}}{3} \quad (4-11)$$

$$J_2 = \frac{1}{2} S_{ij} S_{ij} = \frac{1}{6} [(\sigma_1 - \sigma_2)^2 + (\sigma_2 - \sigma_3)^2 + (\sigma_3 - \sigma_1)^2]$$

$\kappa$  and  $\lambda$ : model parameter determined from experiment

The parameters  $\kappa$  and  $\lambda$  can be obtained from standard compression triaxial test and expressed in term of soil friction angle ( $\phi$ ) and cohesion stress ( $c$ ):

Circumscribed Drucker-Prager:

$$\kappa = \frac{6c \cos \phi}{\sqrt{3}(3 + \sin \phi)} \quad \lambda = \frac{2 \sin \phi}{\sqrt{3}(3 + \sin \phi)} \quad (4-12)$$

Inscribed Drucker-Prager:

$$\kappa = \frac{6c \cos \phi}{\sqrt{3}(3 - \sin \phi)} \quad \lambda = \frac{2 \sin \phi}{\sqrt{3}(3 - \sin \phi)} \quad (4-13)$$

#### **4.3.2. Steel (Piecewise Linear Plasticity)**

The nonlinear elasto-plastic behavior of the steel was represented by a Piecewise Linear plasticity model (MAT 024). The yield criterion was Von Mises, and the model has the ability of modeling strain hardening behavior.

This is an elasto-plastic model with an arbitrary stress-strain curve and an arbitrary strain rate dependency. Failure can be defined upon reaching a plastic strain or a minimum time step size. The stress-strain, strain rate and the failure strain can be imported from user defined curves and tables.

Table 4-8 and Table 4-9 present the Piecewise Linear Plasticity model input parameters and description of each one. The material description includes elastic

modulus, Poisson's ratio, yield stress, hardening modulus, ultimate plastic strain and time step size for element deletion.

**Table 4-8: Material cards for Piecewise Linear Plasticity model (LS-DYNA R7.1 Keyword Manual, 2014)**

<b>Card1</b>	<b>1</b>	<b>2</b>	<b>3</b>	<b>4</b>	<b>5</b>	<b>6</b>	<b>7</b>	<b>8</b>
Variable	MID	RO	E	PR	SIGY	ETAN	FAIL	TDEL
Type	A8	F	F	F	F	F	F	F
Default	none	none	none	none	None	0	1.00E+21	0
<b>Card2</b>	<b>1</b>	<b>2</b>	<b>3</b>	<b>4</b>	<b>5</b>	<b>6</b>	<b>7</b>	<b>8</b>
Variable	C	P	LCSS	LCSR	VP	LCF		
Type	F	F	F	F	F	F		
Default	0	0	0	0	0	0		
<b>Card3</b>	<b>1</b>	<b>2</b>	<b>3</b>	<b>4</b>	<b>5</b>	<b>6</b>	<b>7</b>	<b>8</b>
Variable	EPS1	EPS2	EPS3	EPS4	EPS5	EPS6	EPS7	EPS8
Type	F	F	F	F	F	F	F	F
Default	0	0	0	0	0	0	0	0
<b>Card4</b>	<b>1</b>	<b>2</b>	<b>3</b>	<b>4</b>	<b>5</b>	<b>6</b>	<b>7</b>	<b>8</b>
Variable	ES1	ES2	ES3	ES4	ES5	ES6	ES7	ES8
Type	F	F	F	F	F	F	F	F
Default	0	0	0	0	0	0	0	0

**Table 4-9: Variables in Piecewise Linear Plasticity model (LS-DYNA R7.1  
Keyword Manual, 2014)**

Variable	Description
MID	Material identification
RO	Mass density
E	Young's modulus
PR	Poisson's ratio
SIGY	Yield stress
ETAN	Tangent modulus, ignored if (LCSS.GT.0) is defined
FAIL	Failure flag LT.0.0: User defined failure subroutine, matusr_24 in dyn21.F, is called to determine failure EQ.0.0: Failure is not considered. This option is recommended if failure is not of interest since many calculations will be saved. GT.0.0: Effective plastic strain to failure. When the plastic strain reaches this value, the element is deleted from the calculation.
TIDEL	Minimum time step size for automatic element deletion.
C	Strain rate parameter, C
P	Strain rate parameter, P
LCSS	Load curve ID defining effective stress versus effective plastic strain.
LCSR	Load curve ID defining strain rate scaling effect on yield stress.
VP	Formulation for rate effects: EQ.-1.0: Cowper-Symonds with deviatoric strain rate rather than total, EQ.0.0: Scale yield stress (default) EQ.1.0: Viscoplastic formulation
LCF	The equivalent plastic strain for failure may be specified with either a load curve or a table. (for heat affected zones)
EPS1-EPS8	Effective plastic strain values
ES1-ES9	Corresponding yield stress values to EPS1 - EPS8

Material properties for the piles, beams and plates are summarized in Table 4-10.

The actual stress-strain curve of the steel using the following equation was implemented in the material modeling.

$$\varepsilon_{xx}^{Plastic} = [\ln(1 + \varepsilon_{xx})] - \frac{\sigma_{xx}}{E} \quad (4-14)$$

**Table 4-10: Material properties for steel piles, beams and plates**

Mass Density (ton/m <sup>3</sup> )	Elastic Modulus (MPa)	Poisson's Ratio	Yield Stress (MPa)
7.850	210000	0.3	336

Effective Plastic Strain (mm/mm)	True Stress (MPa)
0.0	336
0.024	336.7
0.042	401.2
0.05	434.3
0.141	537.2
0.213	589.6
0.25	675.0
0.259	677.0

The yield criterion follows Von Mises in addition to having the capability of modeling the hardening behavior by using a hardening term in the expression of the yield stress ( $\sigma_y$ ):

$$\sigma_y = \beta[\sigma_0 + f_h(\varepsilon_{eff}^p)] \quad (4-15)$$

where the hardening function  $f_h(\varepsilon_{eff}^p)$  can be specified in tabular form as an option.

If rate effects in the problem are expected to be important, a table of curves can be defined for strain rates of interest.

The properties used for these materials were determined from the literature and data from the tests TTI team performed on similar steels.

#### **4.4. Vehicle models**

Once the structural model is completed, it should be combined with a vehicle model to simulate the whole test setup. Three vehicle classes were studied with their corresponding models: the single-unit flatbed truck, Chevrolet C2500 pickup truck, and Geo Metro, Sedan. These models were validated by the National Highway Traffic Safety Administration (NHTSA) New Car Assessment Program (NCAP). The vehicle models are continuously under study for improvement in terms of mesh size, mesh quality, contact algorithms and detailed modeling of various components. In vehicle FE models, the engine is not modeled in details since simulation experience has found that it reacts as a rigid mass in crashes.

##### **4.4.1. Single-unit flatbed truck**

To fully simulate the M50 test, a finite element model of a medium-duty truck created by the Texas A&M Transportation Institute, Roadside Safety Program was

combined with the barrier system model. This FE model for the medium duty truck consisted of 30295 elements and 33877 nodes.

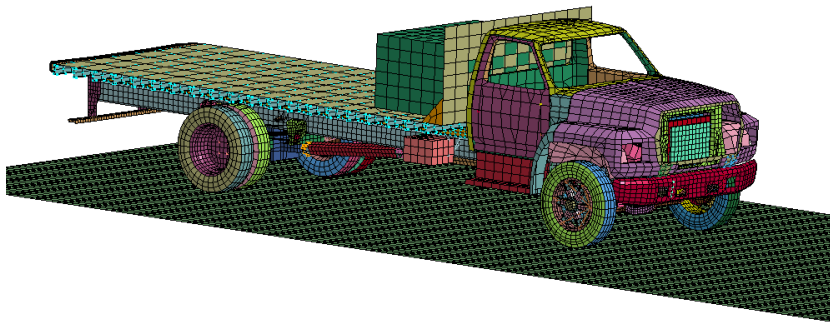


**Figure 4-5: Finite element model of the test vehicle: Medium-duty truck**



#### 4.4.2. Chevrolet C2500 pickup truck

A finite element model of a Chevrolet pickup truck developed at the National Crash Analysis Center (NCAC) was used for simulating the PU60 test. The model includes 58313 elements and 66586 nodes (Figure 4-6).

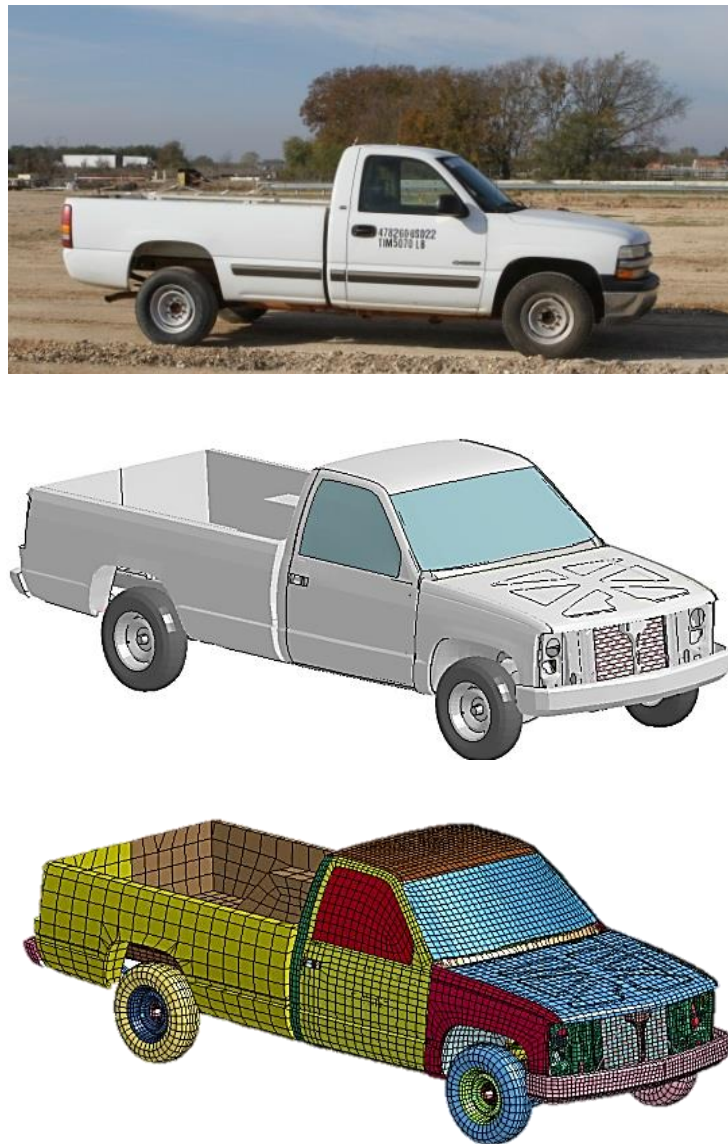


**Figure 4-6: Finite element model of the test vehicles: Pickup truck for the PU60 test**

The FE model consisting of 2.1 million elements (shell, beam and solid elements) presented in Figure 4-6 reflects all of the structural and mechanical features. Material properties were also determined through testing of samples taken from the vehicle. Several validations were conducted on the model by NCAC in terms of material stress-strain behavior in crash simulations, total energy and hourglass energy and acceleration match through crashing tests. More information of the vehicle model details can be found in Marzoughi et al. (2004).

The NCAC made efforts to verify the model efficiency using a rigid crash of this vehicle into a wall. The key crash reactions from simulation and the test were compared. This version of the C2500 pickup model was improved in terms of better tire meshing, side meshing, rear bumper and front and rear suspension. The model has been verified to NCAP test and many other roadside hardware impact tests.

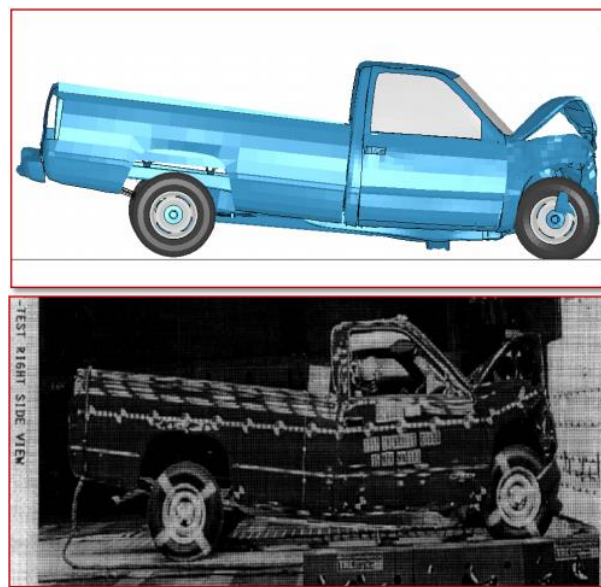


**Figure 4-7: Validation of the vehicle finite element model for use in crash analysis**

The mass of model was approximately 2000 kg (2023 kg). The mass was corrected to the required mass of 2300 kg, by changing the density of the cabin. Since most missing mass is linked to the un-modeled parts in the cabin, this adding mass to the cabin seems reasonable.

#### **4.4.3. Geo Metro (reduced model)**

For simulations involving the impact of a sedan, passenger car, an 820 kg small car model known as Geo Metro developed by NCAC (National Crash Analysis Center) was utilized. Figure 4-8 shows the FE model of this vehicle which includes 16000 elements and 19000 nodes.

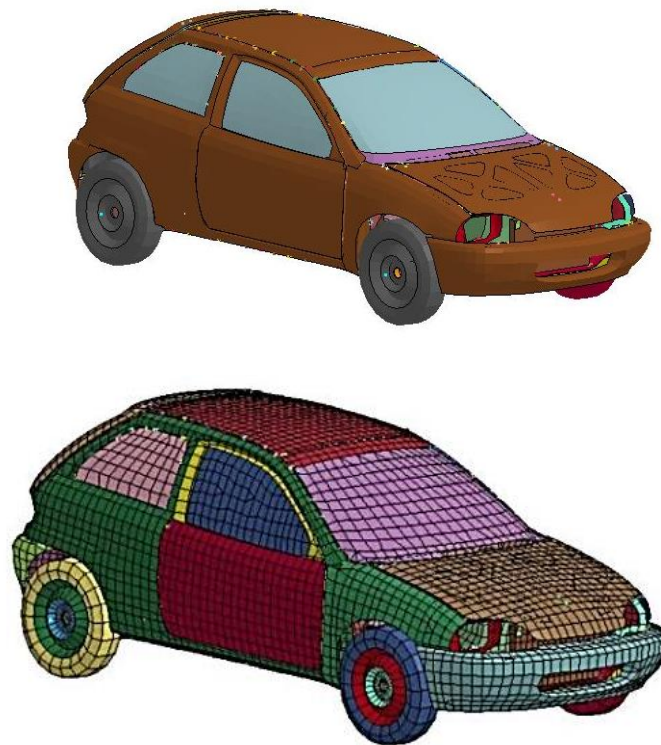


**Figure 4-8: FE model of the Geo Metro, reduced model (NCAC)**

## **4.5. Simulation calibration**

Two full scale crash M50 and PU60 tests described in Section 3 were simulated using LS-DYNA and the results were compared to the experiments. Herein validation of the numerical models is presented in details. The calibrated models would then be used to develop a design method.

### **4.5.1. Medium duty truck M50**

A mesh consisting of solid elements was used to represent the soil surrounding the piles. Among the soil models implemented in LS-DYNA, the Jointed Rock model (Livermore Software Technology Corporation, 2007) modified with the Drucker-Prager model (Drucker and Prager, 1952) was selected; in addition a non-tensile behavior of the sand was enforced. Soil model input parameters were identified based on past laboratory and in-situ tests. The unit weight, elastic modulus and friction angle of the soil were considered to be  $17.5 \text{ kN/m}^3$ ,  $2.5 \text{ MPa}$  and  $29 \text{ degree}$ , respectively.

In the finite element model of the Test M50 installation, a continuum of soil elements with the size of  $41.5 \times 8.25 \text{ m}$  and depth of  $3.6 \text{ m}$  was modeled. These dimensions were adopted such that the true behavior of soil and its interaction with piles can be captured with reasonable computation cost. The boundary surfaces are constrained from horizontal translation, however the surface nodes are free to rotate or displace in the vertical plane. The elements at the base are constrained in all degrees of freedom. The contact algorithm “Automatic-Nodes-to-Surface” was used for the contact between the vehicle and the barrier.

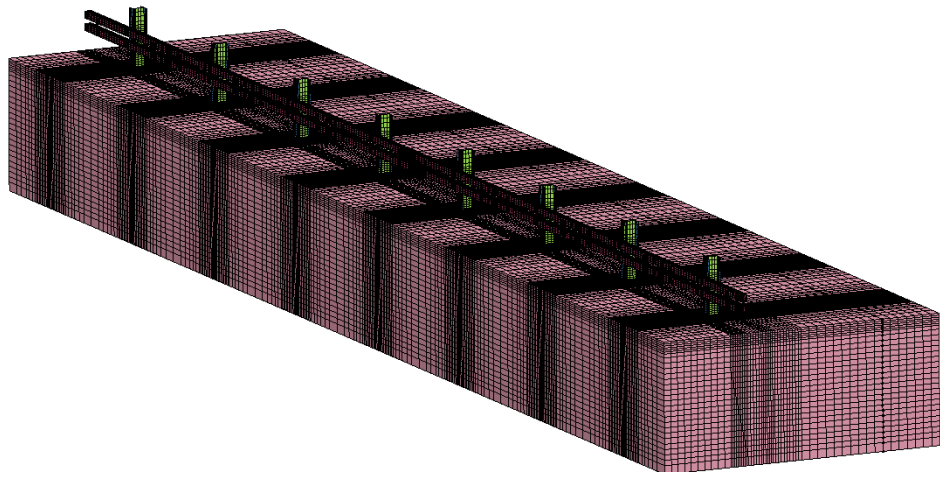


**Figure 4-9: Finite element model of the test M50 installation**

The deformed simulated vehicle and pile system after impact are presented in Figure 4-10. It shows that the impact force was well transferred to all the piles and that noticeable soil resistance was mobilized. Compared results (velocity and acceleration of the vehicle, dynamic penetration and the impact force applied on the barrier) shown in Figure 4-11 indicates a significant similarity between the simulated results and those obtained in the field. It also shows a close match between the simulation and measured impact force versus time curve. Again a 50 millisecond average is used to present the acceleration which is multiplied by the mass to obtain the force.



**Figure 4-10: Numerical simulation of the impact test on a group of piles**

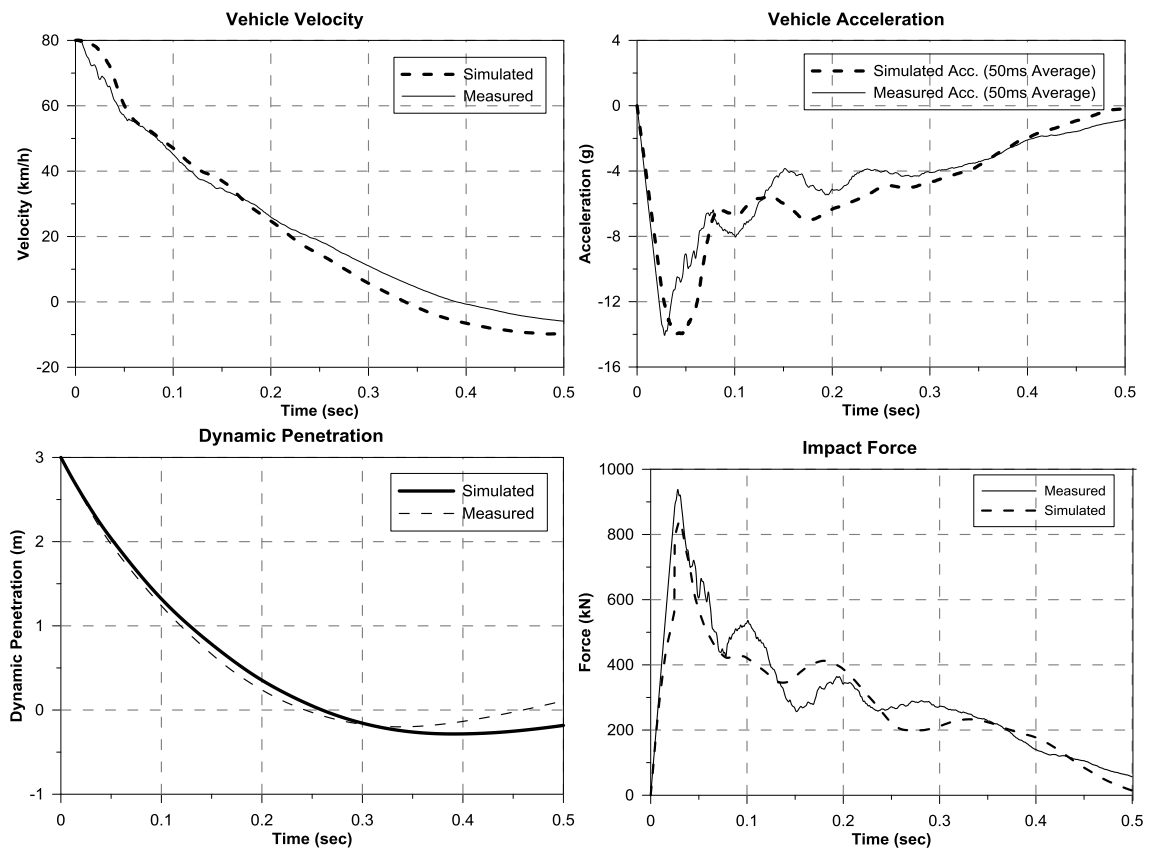


**Figure 4-11: Comparison between predicted and measured behavior**

Additional results of the simulations are shown in Figure 4-12. In general, the simulation results show good agreement with those obtained from the field experiment. During the full scale impact test, one of the connections between the beams and the outside pile (Pile 1) failed which may explain some of the discrepancy. The performance of the barrier system could be improved prior to testing by revising the connection designs to increase their strength. The deflection of that pile is consequently overestimated numerically (Figure 4-12).

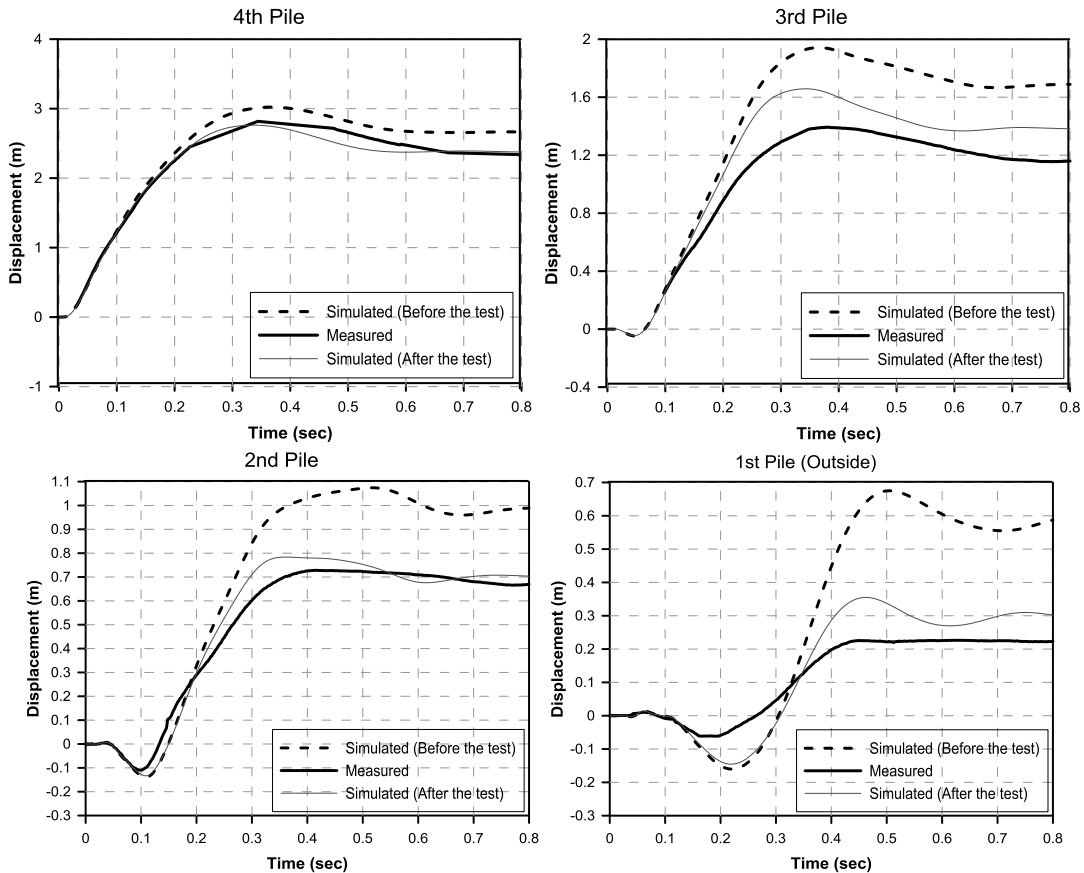


**Figure 4-12: Comparison of measured and predicted displacements of piles No. 1,2,3 and 4**

We note that the difference between the simulated deflection and the measured deflection gets worse for piles further away from the impact. In particular the side pile deformation is over-predicted compared to the measured deflection. As discussed before, the connection between that pile and the beam failed during the impact so that the pile experienced a lower force. In LS-DYNA the connections were featured as Nodal-rigid body contact which did not allow for failure. Overall, the results obtained by numerical simulations are in a reasonable agreement with the measurements.

#### **4.5.2. Pick-up truck PU60 calibration**

As described earlier, in 2014 a full scale crash test was performed on a group of four in-line piles embedded in hard clay. The piles and beams were modeled using shell elements while the soil was modeled by solid elements. The soil boundaries and the mesh refinement near the piles were examined and optimized. Prior to the main impact simulation an initialization under gravitational loading was performed.

The total duration of the simulation was 500 milliseconds to capture the initial impact until the rebounding of the vehicle from the barrier. Computation time to run this model using 4 processors on a single precision SGI workstation was approximately 30 hours.

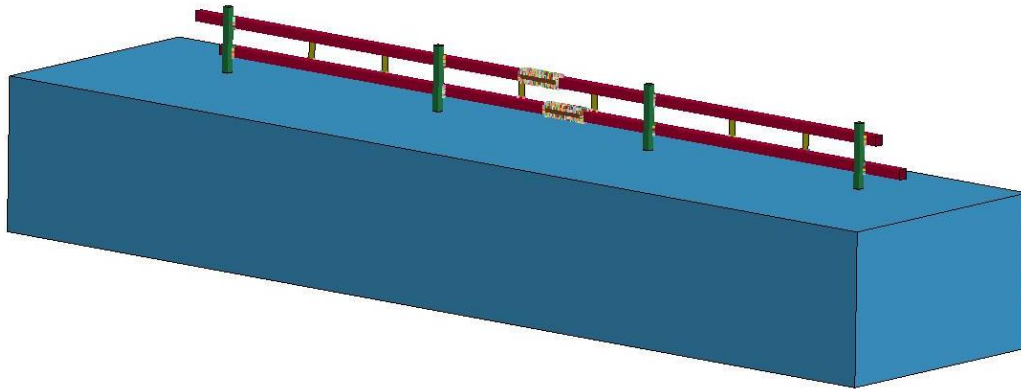
#### **Pile, beam and soil modeling**

Piles, beams and plates were meshed using shell elements with two integration points through the thickness of the elements. To avoid numerical instabilities and eliminate



zero-energy hourglass modes incited by this under-integrated element formulation, meshing, geometry and hourglass control cards were closely examined. The nonlinear elastoplastic behavior of steel parts was modeled using a Piecewise Linear plasticity material model (material number 24 in LS-DYNA). The yield criterion follows Von Mises in addition to having the capability of modeling the hardening behavior by using a hardening term in the expression of the yield stress ( $\sigma_y$ ). The stress/strain constitutive relationship of the steel (graded A36) has been examined by TTI researchers by actual material testing and was readily used as a reference in modeling.

In the test PU60 modeling, 44826 shell elements comprising the piles, beams and plates are squares of 300 mm wide with thickness of 12.7 mm. The soil was modeled using solid elements structuring a rectangular soil block as shown in Figure 4-13. Given the pile embedment depth, pile spacing, number of piles, in the PU60 simulation, the soil block is 3 m (10 ft) deep, 5 m (16.4 ft) wide and 21 m (69 ft) long with a spatial mesh.



LS-DYNA keyword deck by LS-PrePost

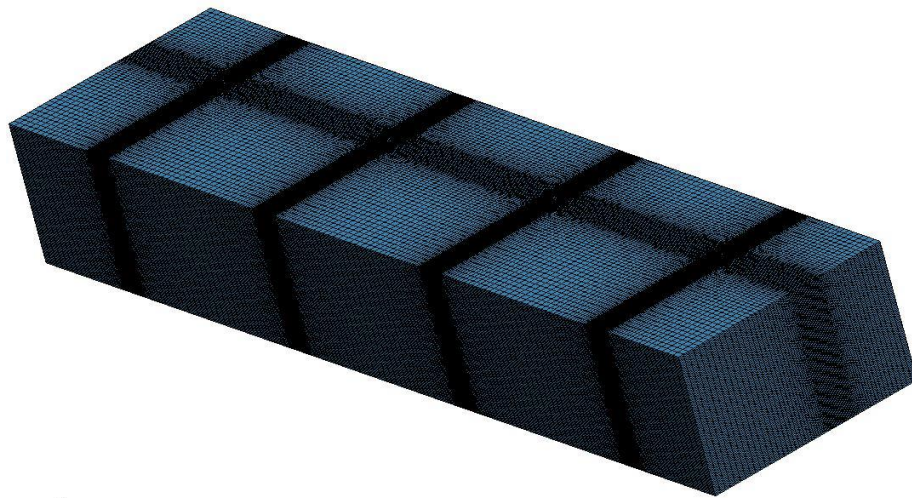


**Figure 4-13: Finite element models of the soil block and barrier**

The pile shells and the soil solids merged in the contact faces. The nodes on the lateral and bottom surfaces of the soil block were constrained using \*SPC card specified boundary conditions. The lateral face nodes were constrained in the transnational degree of freedom in the direction perpendicular to the lateral surfaces of soil block and the

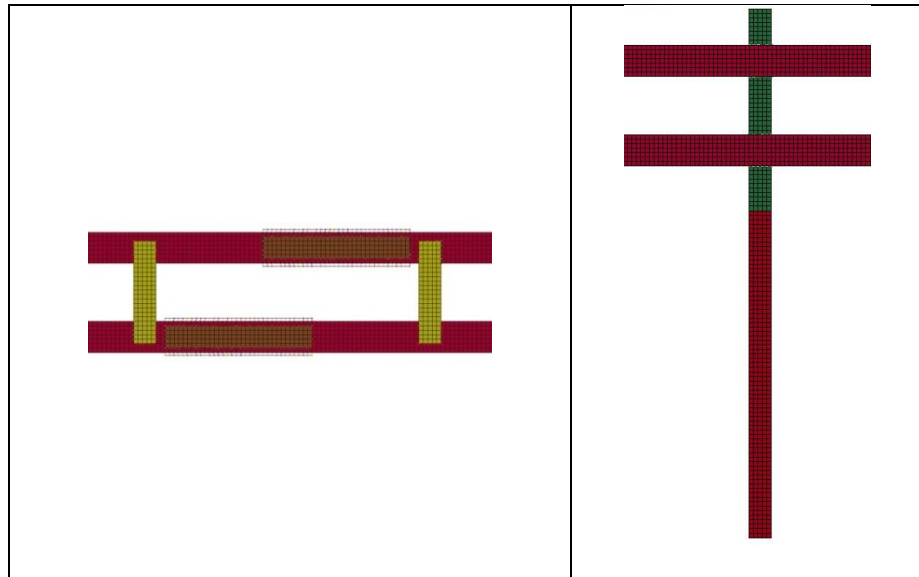
bottom nodes were constrained only in the z-translational displacement. The barrier and soil model consist of 2.1 million elements. To eliminate the boundary effects, the outer sides of the soil block were constraint using a nonreflecting boundary feature.

Size of the soil buckets varied in cases of different pile embedment, different spacing and number of piles. A sensitivity analysis was performed to determine the computationally efficient size of soil block. After couple of simulations and checking the stress zones, a soil block with 20.8m length, 5 m width and 3m height was finalized.

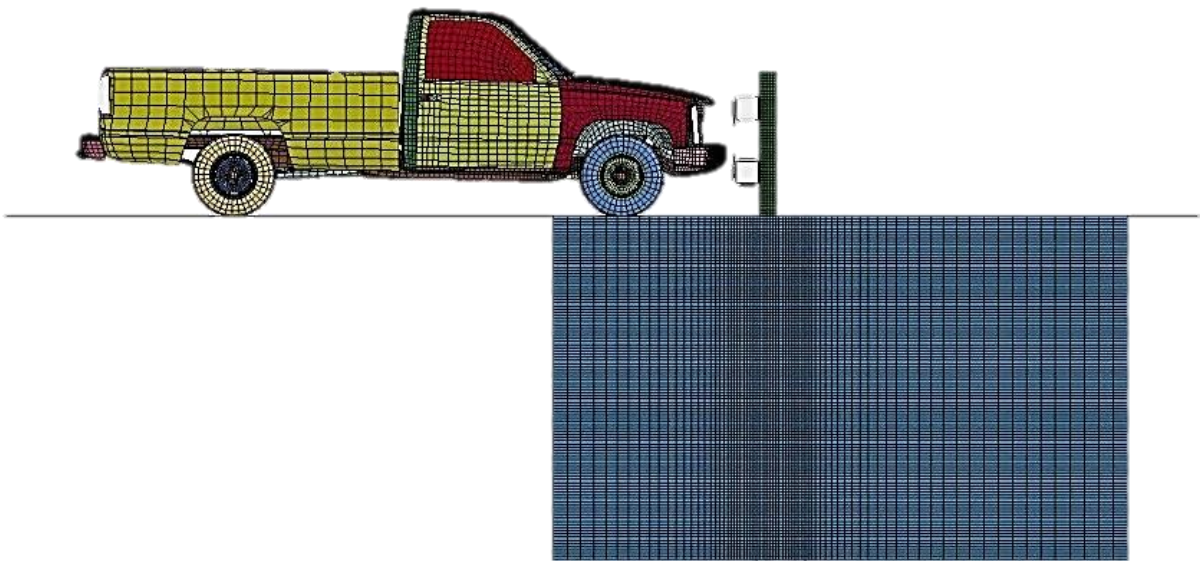
Ls-Prepost was used to mesh the soil, pile and beams parts. To reduce the hourglass energy and help numerical instability a refined mesh with a reasonable increase in computational time and cost was adopted. For the soil block, the element size was finer where large deformation and local failure were expected such as around the piles.

### **Connection modeling**

Since pile-beam connections failure was not expected nor observed during the crash testing, these connections were simply modeled using Constrained Nodal Rigid Body (CNRB) rather than modeling welding, thereby decreasing computational cost. CNRBs which are internally treated as rigid parts in LS-DYNA can well reflect short welded parts behavior. Following comparison of test and simulation results confirms the connection validity.



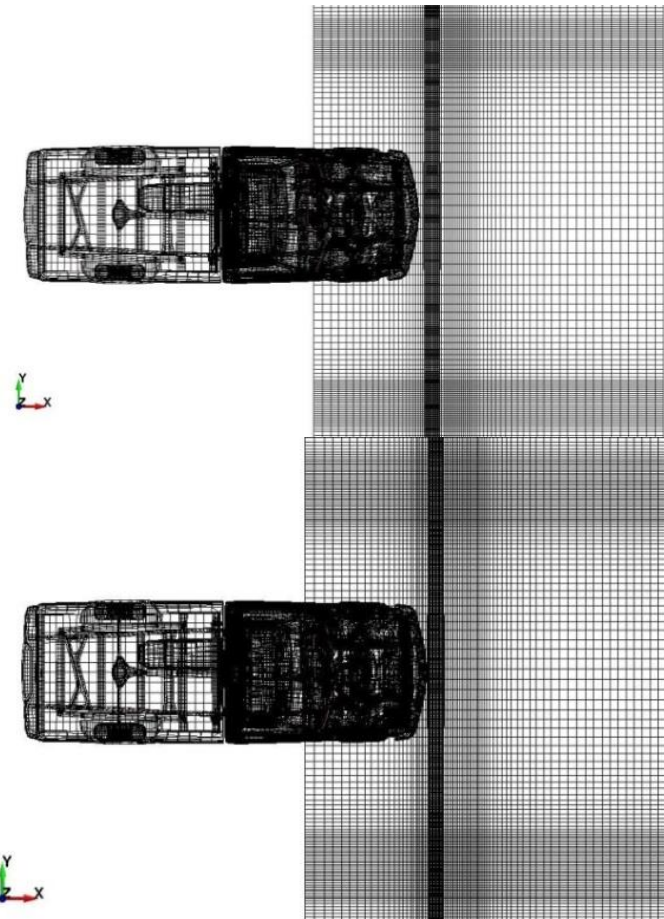
**Figure 4-14: Soil, piles and beams mesh**



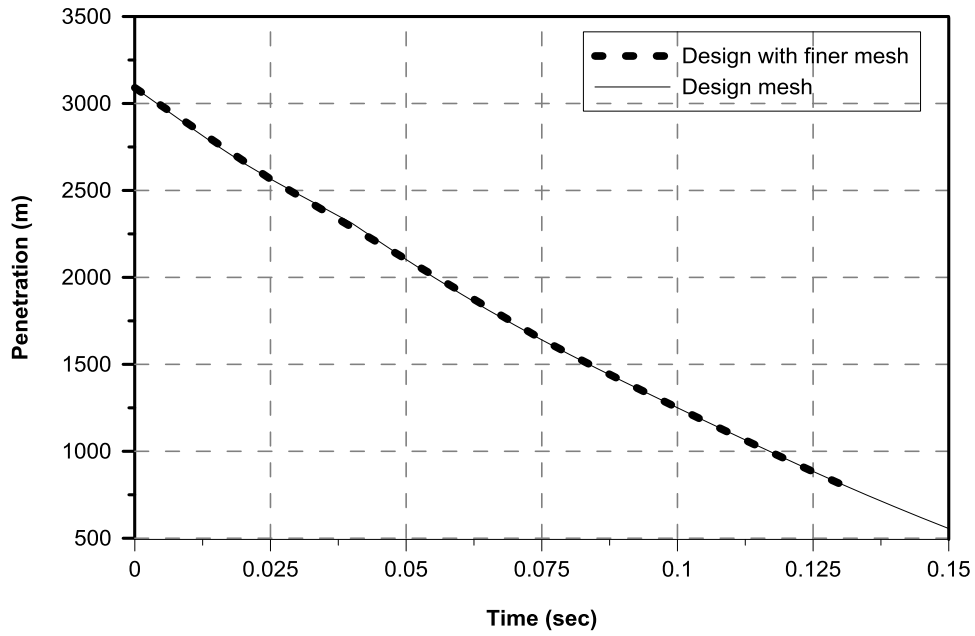
**Figure 4-15: Finite element models of the vehicle and the barrier**

### Mesh size sensitivity

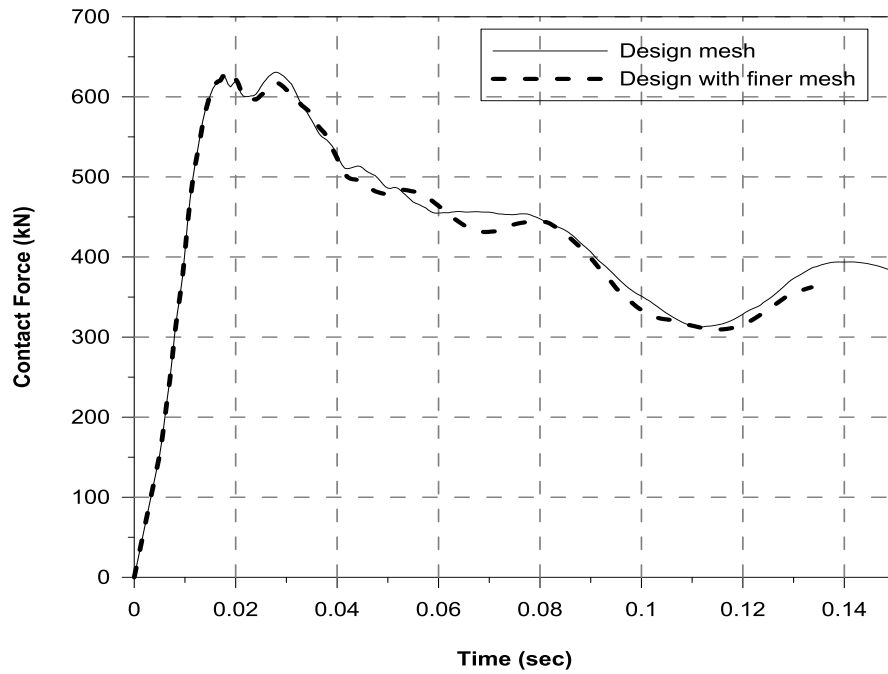
Soil boundaries and mesh refinement are examined to finalize an optimum model in terms of run time and accuracy of the results. Herein the effects of element size and refinement of the mesh on crash simulation results are studied to check the accuracy of the results. The original design model has a fine soil mesh consisting of a total number of elements as 2.1 million. In order to investigate the mesh refinement, results of another model of finer mesh, consisting of 3.1 million elements, was compared to the original one.



**Figure 4-16: Mesh of 2.1 million elements and Mesh of 3.1 million elements**



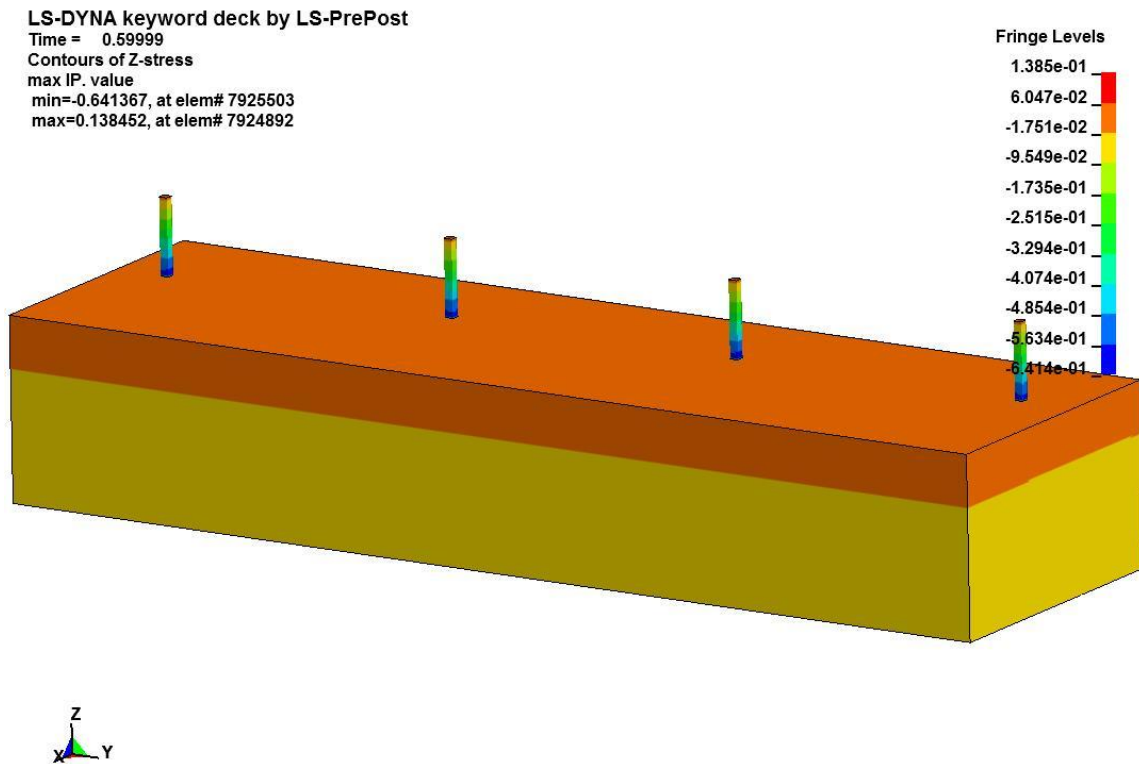
**Figure 4-17: Comparison dynamic penetration in simulations of the design mesh and the finer mesh**



**Figure 4-18: Comparison contact forces in simulations of the design mesh and the finer mesh**

## Initialization

Before running the main impact simulation, the soil-pile system was initialized for the gravitational loading including the soil pressure due to its self-weight. The stress-strain state of the elements reached after gravity initialization was then imported as a starting point of the primary impact run (Figure 4-19).



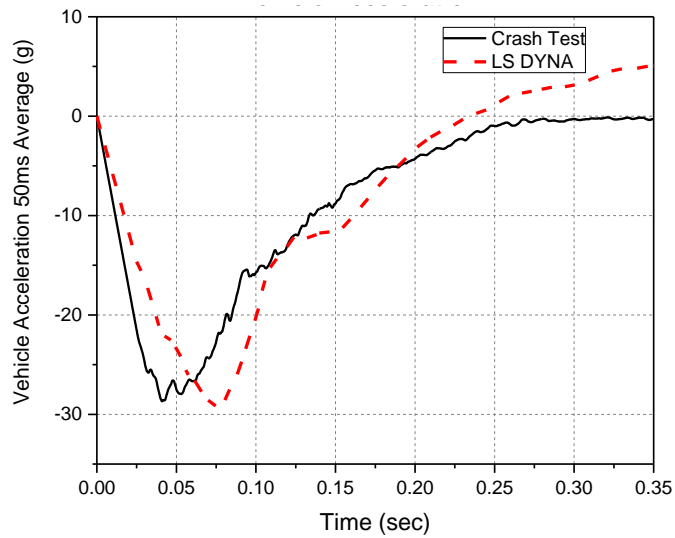
**Figure 4-19: Initialization of the soil-pile barrier**

Figure 4-20 shows the numerical simulation of the PU60 test. Figure 4-21 through Figure 4-24 compare measured and predicted vehicle response versus time. It indicates that the simulation captured most of the crash test characteristics. Various aspects of the

testing and simulations are compared favorably up to 500 ms, however the results are shown up to 350 ms. After this time no significant change was observed.



**Figure 4-20: Numerical simulation of the impact test on a group of 4 piles**



**Figure 4-21: Measured and simulated vehicle acceleration**



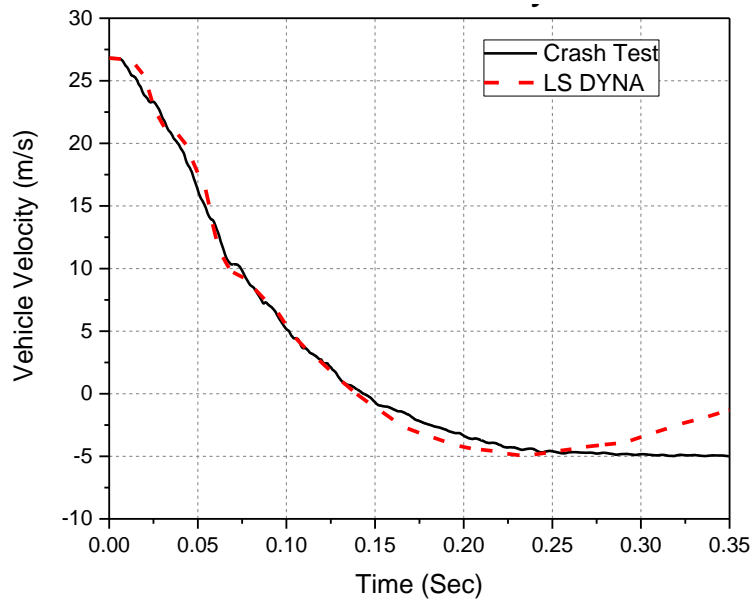


**Figure 4-22: Measured and simulated vehicle velocity**

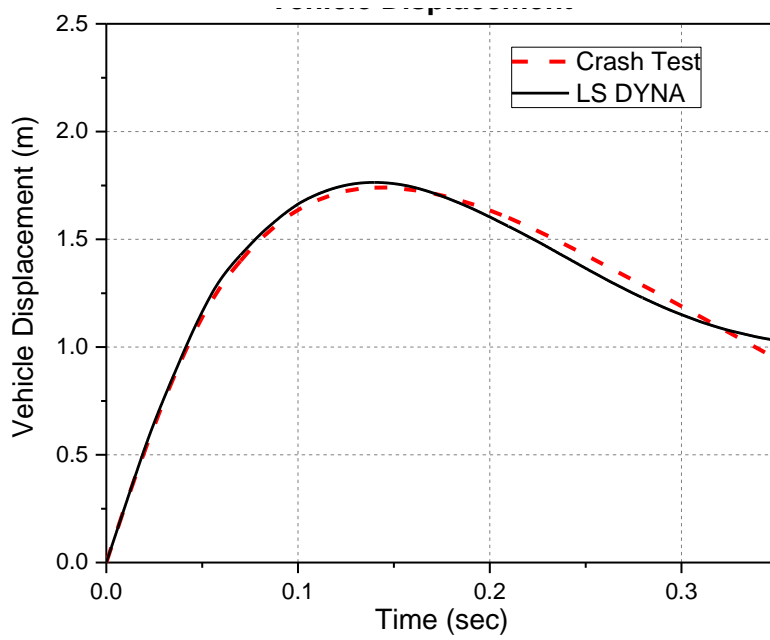


**Figure 4-23: Measured and simulated vehicle displacement**

Note that the measured acceleration, velocity and displacement of vehicle recorded at Center of Gravity seem closer to the predicted by LS-DYNA. This might be due to probable damage to instrumentation during the impact.

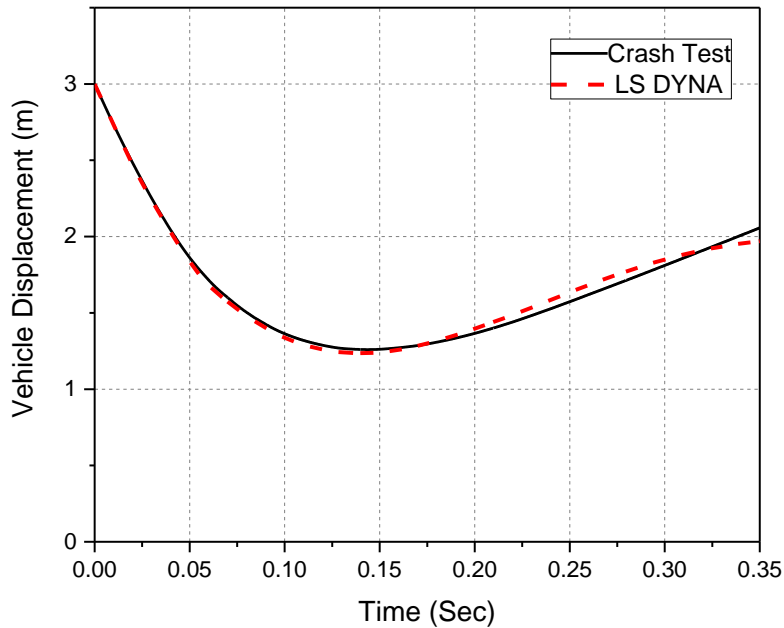


**Figure 4-24: Measured and simulated dynamic penetration**

Since some of the strain gauges installed on the piles reached the ultimate threshold the strains were not recorded for the duration of impact. Hence, the deflections of piles are captured through film analysis of cameras. Comparison of measured and predicted pile displacements shows the ability of the numerical model to reflect the barrier response.

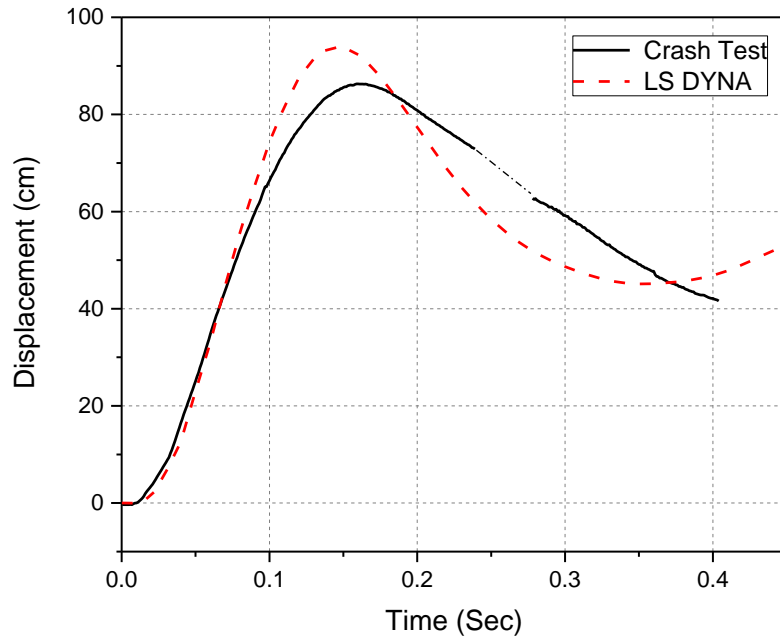


**Figure 4-25: Comparison of simulated and measured displacements of the inner pile (close to the impact)**

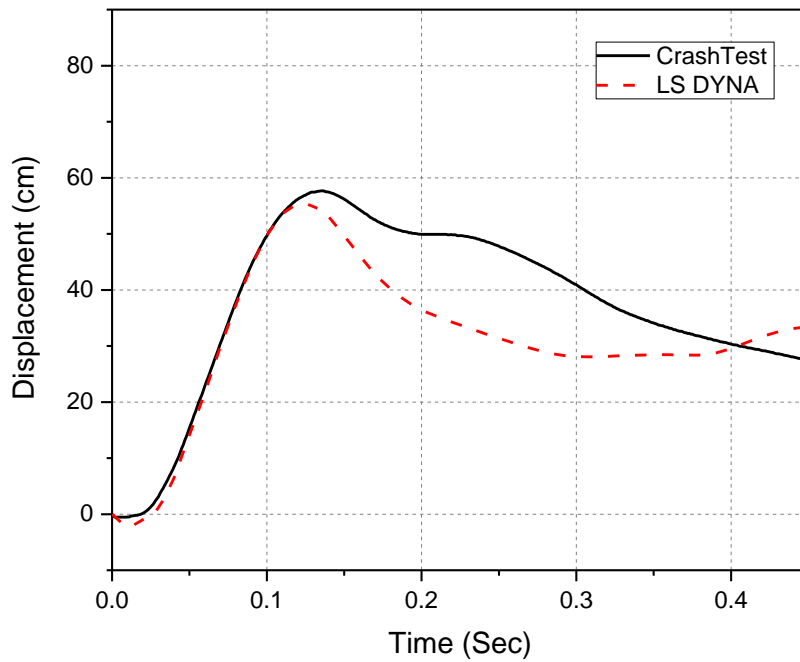


**Figure 4-26: Comparison of simulated and measured displacements of the outer pile (end pile)**

Overall the predicted behavior of the pile group agrees well with the measured ones. A critical measure in design of barriers is a robust estimate of the impact force. The current LS-DYNA model replicates the total force applied on the barrier relatively well. Figure 4-27 compares measured and predicted 50msec average force.

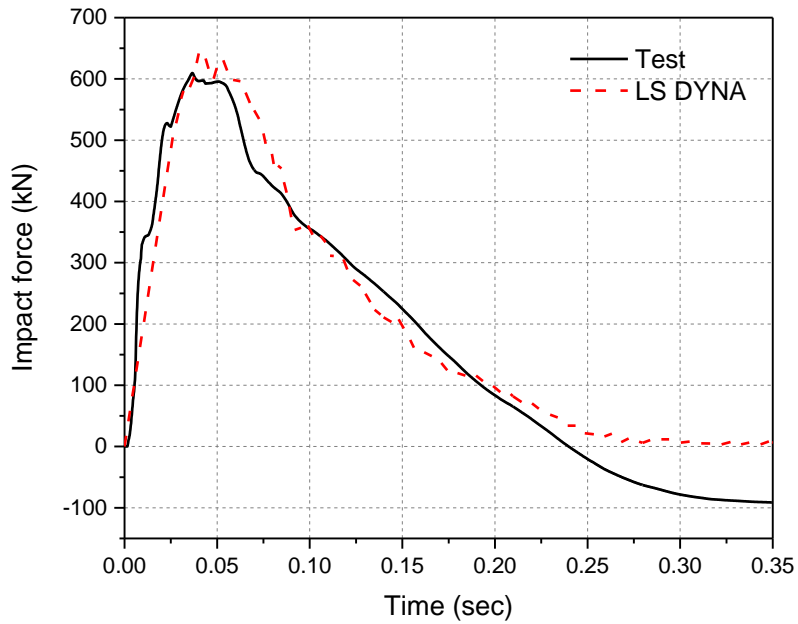
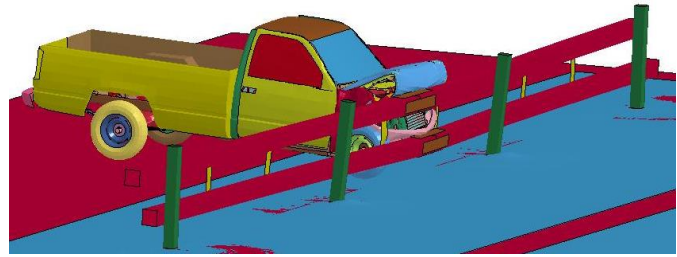
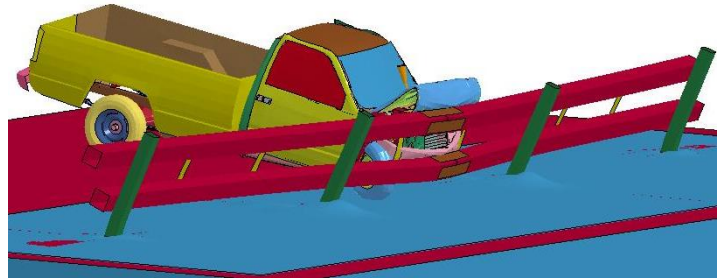


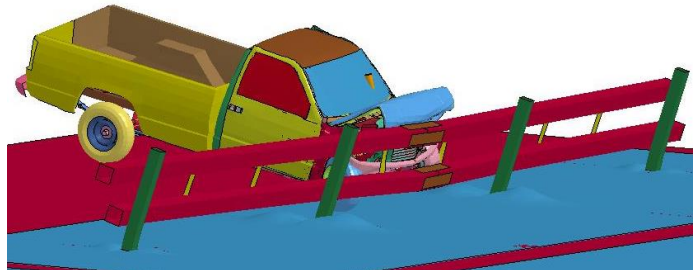
**Figure 4-27: Simulated and measured impact force**



**(a) Test and Simulation set-up at 0.05 seconds**



**(b) Test and Simulation set-up at 0.15 seconds**



**(c) Test and Simulation set-up at 0.5 seconds**

**Figure 4-28: Sequential images of Test and Simulation PU60**

#### **4.6. Numerical simulations to calibrate TAMU-POST (Group)**

Full scale experiments are the best data to calibrate a method. However they are costly, time consuming and not a practical solution to study various cases. Numerical simulations are less expensive and typically less time consuming. Therefore, a series of numerical simulations were performed using LS-DYNA to augment the databank that would be used to calibrate the new method.

##### **4.6.1. Space-filling Latin Hypercube sample design**

In the parameter optimization of the proposed model TAMU-POST, one problem was to select the cases for simulation to best cover the possible cases. In this respect, an experimental design using the stratified Latin hypercube sampling technique was adopted.

Latin hypercube sampling extended from Latin Square sampling was first introduced by McKay et al. and later developed by Inman et al. (McKay 1979, Inman, 1981, McKay et al. 2000). This refined sampling technique compared to the other sampling schemes, shown in Figure 4-29, was observed to adequately give sampling over the entire parameter space. Only one sample is randomly chosen from every interval of each parameter.

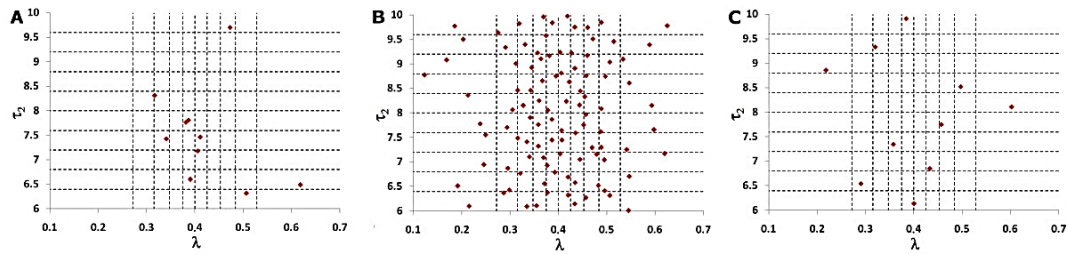


**Figure 4-29: Three different sampling schemes a) Random sampling b) Full factorial sampling and c) Latin Hypercube Sampling (Hoare et al. 2008)**

Several studies have demonstrated the advantage of the LHS method over Monte Carlo Sampling which is the most universally admitted method in uncertainty quantification. It was shown that the mean error in MCS drops more slowly with the number of samples and identical parameters are likely to be selected, while the stratification and random sampling within the strata incorporated in SLHS guarantees a better convergence and ensures that the selected random samples represent the real variability. Stratified Latin Hypercube Sampling (SLHS) intends to maximize the minimum distance between the model inputs in a multivariate space and minimize the root mean square (RMS) variation of the cumulative distribution function (CDF).

#### **4.6.2. Experimental design for the TAMU-POST validation**

The TAMU-POST (Group) model involves numerous input variables. The governing variables based on the experience and the test observations were stratified into adequate serial intervals. Table 4-11 lists the selected design strata and the parameters ranges. The parameters such as the vehicle mass, vehicle speed, ratio of the pile spacing to pile width or diameter and soil strength were chosen as the significant scenario dimensions.

**Table 4-11: The selected design strata for the LS-DYNA numerical study**

Variable	Range	number of strata
Vehicle mass	4pile: 808 kg, 2300 kg 8pile: 2300 kg, 6800 kg	2
Soil strength	Clay: soft- very hard (Table 4-12) Sand: loose- very dense (Table 4-13)	5
Spacing to pile width	4pile: 20, 35 and 50 8pile: 7, 13 and 19	3
Vehicle speed	40, 50 and 60 mph	3

This sampling has been repeated for both clay and sand. Table 4-12 and Table 4-13 show the soil strength categories and the associate parameters.

**Table 4-12: Soil strength categories and parameters - clay**

Number	Soil Strength	PL (kPa)	Su (kPa)	E (MPa)	$\gamma$ (kN/m <sup>3</sup> )
1	Soft	300	50	5	17
2	Medium Soft	800	100	10	18
3	Medium	1300	150	15	19
4	Hard	2000	200	20	21
5	Very Hard	2500	250	25	22

**Table 4-13: Soil strength categories and parameters - sand**



Number	Soil Strength	PL (kPa)	E (MPa)	C (kPa)	$\phi$ Degrees	$\psi$ Degrees	$\gamma$ (kN/m <sup>3</sup> )
1	Loose	400	5	5	35	0	17
2	Medium Loose	700	10	10	35	10	18
3	Medium	1100	15	20	40	10	19
4	Dense	1700	20	30	40	12	21
5	Very Dense	2500	30	40	40	15	22

In the 4 pile cases, piles are HSS 6x6x1/2 and in 8 pile cases, piles are I-beam W14x90. In all cases beam is a square steel tube 8x8x1/2. In most of the cases, the pile embedment depth is 2 m, which is considered to be the minimum embedment (based on the previous experience) and in some other cases the pile embedment is 3 m. Figure 4-30 and Figure 4-31 indicate the models of these numerical efforts.

In overall, 60 cases for clay and 60 cases for sand were selected and numerically simulated. After running the simulations, the cases involving the sedan were found not to contribute significantly to the model parameter optimizing, because the sedan (with a mass of 800 kg) could not displace pile groups significantly. Therefore, the number of useful simulation was reduced to 95 as listed in Table 4-14.

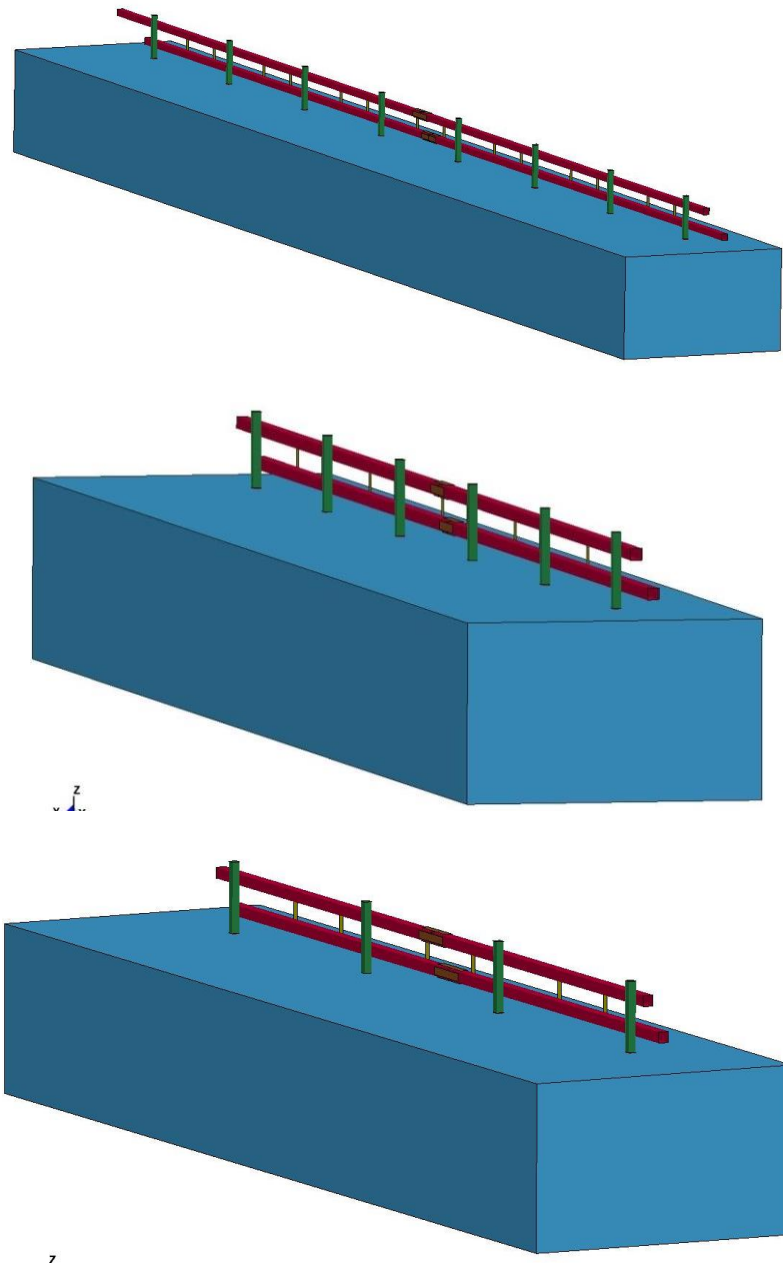


**Figure 4-30: LS-DYNA simulation of cases: 4, 6 and 8 in-line piles**

Besides these simulations, two full scale tests were used as other sources of data to obtain an expression for the simple model parameters and the damping coefficient  $C$ , in particular.

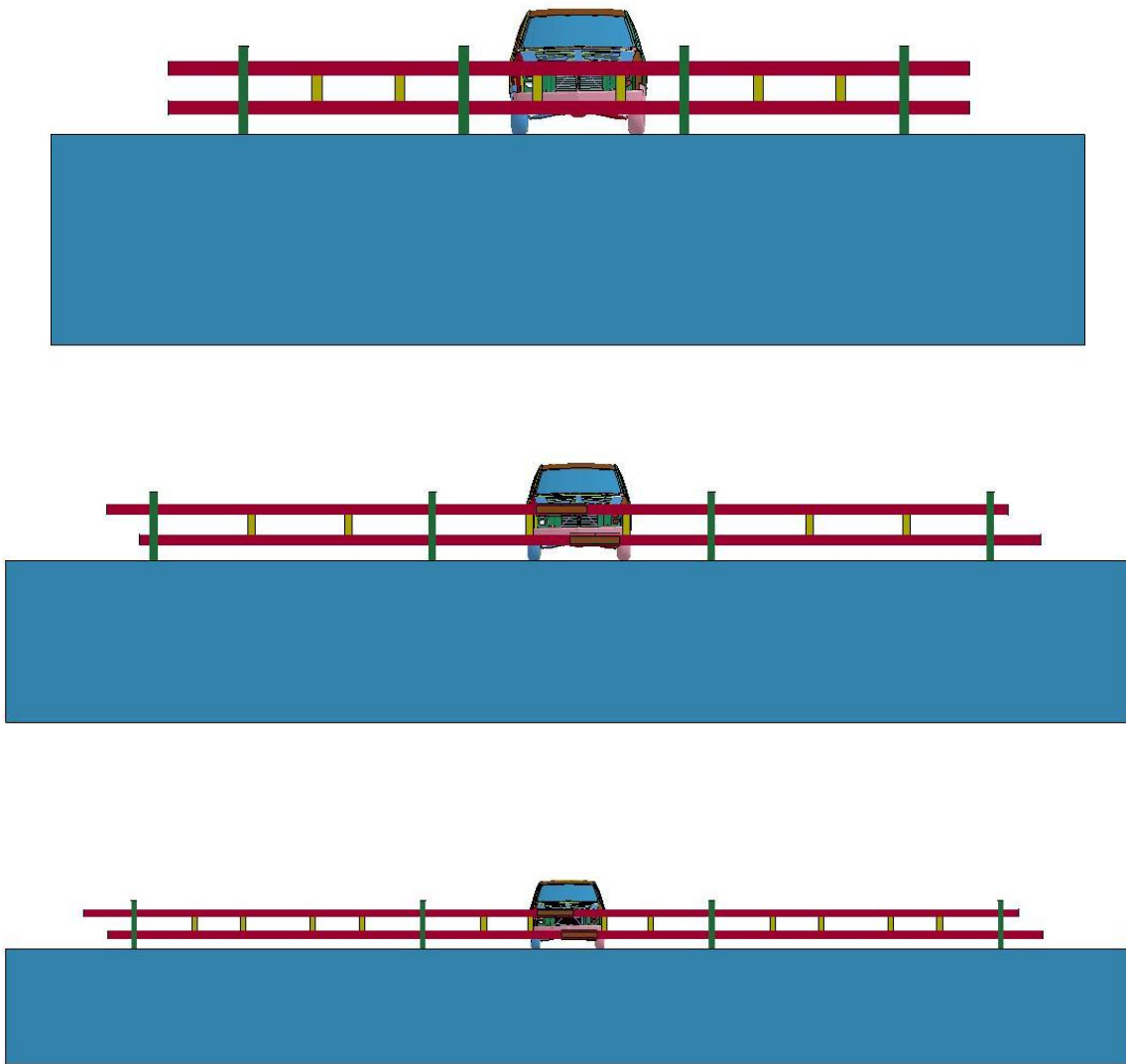


**Figure 4-31: LS-DYNA simulation of cases with the S/D (ratio of pile spacing to pile width) of 20, 35 and 50**

**Table 4-14: The simulations performed based on the experimental design SLHS**

No. Test	Vehicle Mass (kg)	Vehicle Velocity (m/s)	Number of Piles	Spacing (m)	PMT E <sub>0</sub> (Mpa)	PMT P <sub>L</sub> (Mpa)	Soil Density (kN/m <sup>3</sup> )	Pile Width B <sub>p</sub> (m)	Pile Embedment D (m)
1	2300	17.88	8	2.8	5	0.3	1800	0.35	2
2	6800	26.82	8	5.2	20	2	2000	0.35	2
3	2300	22.35	8	2.8	15	1.3	1900	0.35	2
4	2300	22.35	8	5.2	5	0.3	1800	0.35	2
5	6800	26.82	8	7.6	25	2.5	2100	0.35	2
6	2300	26.82	8	7.6	5	0.3	1800	0.35	2
7	2300	17.88	8	5.2	15	1.3	1900	0.35	2
8	2300	26.82	8	5.2	10	0.8	1800	0.35	2
9	2300	26.82	8	7.6	10	0.8	1800	0.35	2
10	6800	22.35	8	7.6	15	1.3	1900	0.35	2
11	2300	22.35	8	2.8	20	2	2000	0.35	2
12	6800	22.35	8	7.6	10	0.8	1800	0.35	2
13	6800	26.82	8	2.8	15	1.3	1900	0.35	2
14	6800	17.88	8	5.2	25	2.5	2100	0.35	2
15	6800	26.82	8	5.2	5	0.3	1800	0.35	2
16	2300	17.88	8	5.2	20	2	2000	0.35	2
17	6800	26.82	8	7.6	25	2.5	2100	0.35	2
18	6800	17.88	8	2.8	20	2	2000	0.35	2
19	6800	22.35	8	7.6	5	0.3	1800	0.35	2
20	2300	17.88	8	7.6	25	2.5	2100	0.35	2
21	6800	17.88	8	2.8	15	1.3	1900	0.35	2
22	2300	22.35	8	7.6	10	0.8	1800	0.35	2
23	6800	26.82	8	2.8	25	2.5	2100	0.35	2
24	6800	22.35	8	5.2	10	0.8	1800	0.35	2
25	2300	17.88	8	2.8	20	2	2000	0.35	2
26	2300	17.88	8	2.8	5	0.4	1800	0.35	2
27	6800	26.82	8	5.2	20	1.7	2000	0.35	2
28	2300	22.35	8	2.8	15	1.1	1900	0.35	2
29	2300	22.35	8	5.2	5	0.4	1800	0.35	2
30	6800	26.82	8	7.6	30	2.5	2100	0.35	2
31	2300	26.82	8	7.6	5	0.4	1800	0.35	2
32	2300	17.88	8	5.2	15	1.1	1900	0.35	2
33	2300	26.82	8	5.2	10	0.7	1800	0.35	2
34	2300	26.82	8	7.6	10	0.7	1800	0.35	2
35	6800	22.35	8	7.6	15	1.1	1900	0.35	2
36	6800	22.35	8	7.6	10	0.7	1800	0.35	2
37	6800	26.82	8	2.8	15	1.1	1900	0.35	2
38	6800	17.88	8	5.2	30	2.5	2100	0.35	2
39	6800	26.82	8	5.2	5	0.4	1800	0.35	2
40	2300	17.88	8	5.2	20	1.7	2000	0.35	2
41	6800	26.82	8	7.6	30	2.5	2100	0.35	2
42	6800	17.88	8	2.8	20	1.7	2000	0.35	2
43	6800	22.35	8	7.6	5	0.4	1800	0.35	2
44	2300	17.88	8	7.6	30	2.5	2100	0.35	2
45	6800	17.88	8	2.8	15	1.1	1900	0.35	2
46	2300	22.35	8	7.6	10	0.7	1800	0.35	2

**Table 4-14: Continued**

No. Test	Vehicle Mass (kg)	Vehicle Velocity (m/s)	Number of Piles	Spacing (m)	PMT E <sub>0</sub> (Mpa)	PMT P <sub>L</sub> (Mpa)	Soil Density (kN/m <sup>3</sup> )	Pile Width B <sub>p</sub> (m)	Pile Embedment D (m)
47	6800	26.82	8	2.8	30	2.5	2100	0.35	2
48	6800	22.35	8	5.2	10	0.7	1800	0.35	2
49	2300	17.88	8	2.8	20	1.7	2000	0.35	2
50	2300	26.82	4	3	10	0.8	1800	0.15	2
51	2300	26.82	4	7.5	20	2	2000	0.15	2
52	2300	26.82	4	7.5	5	0.3	1800	0.15	2
53	2300	22.35	4	7.5	10	0.8	1800	0.15	2
54	2300	26.82	4	5.2	5	0.3	1800	0.15	2
55	2300	26.82	4	5.2	5	0.3	1800	0.15	2
56	2300	17.88	4	5.2	25	2.5	2100	0.15	2
57	2300	26.82	4	3	5	0.3	1800	0.15	2
58	2300	26.82	4	5.2	15	1.3	1900	0.15	2
59	2300	17.88	4	7.5	20	2	2000	0.15	2
60	2300	17.88	4	7.5	25	2.5	2100	0.15	2
61	2300	17.88	4	7.5	20	2	2000	0.15	2
62	2300	26.82	4	5.2	10	0.8	1800	0.15	2
63	2300	26.82	4	3	10	0.7	1800	0.15	2
64	2300	26.82	4	7.5	5	0.4	1800	0.15	2
65	2300	22.35	4	7.5	10	0.7	1800	0.15	2
66	2300	26.82	4	7.5	30	2.5	2100	0.15	2
67	2300	26.82	4	5.2	5	0.4	1800	0.15	2
68	2300	17.88	4	5.2	30	2.5	2100	0.15	2
69	2300	26.82	4	3	5	0.4	1800	0.15	2
70	2300	17.88	4	7.5	20	1.7	2000	0.15	2
71	2300	17.88	4	7.5	30	2.5	2100	0.15	2
72	2300	17.88	4	7.5	20	1.7	2000	0.15	2
73	2300	26.82	4	5.2	10	0.7	1800	0.15	2
74	2300	26.82	6	5.2	5	0.3	1800	0.15	2
75	2300	17.88	6	5.2	25	2.5	2100	0.15	2
76	2300	26.82	6	5.2	25	2.5	2100	0.15	2
77	2300	26.82	6	5.2	10	0.8	1800	0.15	2
78	2300	26.82	6	5.2	15	1.3	1900	0.15	2
79	2300	17.88	6	5.2	30	2.5	2100	0.15	2
80	2300	26.82	6	5.2	15	1.1	1900	0.15	2
81	2300	26.82	4	5.2	15.5	1.5	2100	0.15	2
82	6800	22.35	8	5.2	2.5	0.2	1760	0.35	3
83	2300	26.82	4	5.2	15.5	1.3	2100	0.15	2.5
84	2300	26.82	4	5.2	15.5	1.3	2100	0.15	3
85	2300	26.82	8	5.2	15.5	1.3	2100	0.15	2
86	2300	22.35	4	5.2	15.5	1.3	2100	0.15	2
87	2300	17.88	4	5.2	15.5	1.3	2100	0.15	2

**Table 4-14: Continued**

No. Test	Vehicle Mass (kg)	Vehicle Velocity (m/s)	Number of Piles	Spacing (m)	PMT E <sub>0</sub> (Mpa)	PMT P <sub>L</sub> (Mpa)	Soil Density (kN/m <sup>3</sup> )	Pile Width B <sub>p</sub> (m)	Pile Embedment D (m)
88	2300	26.82	4	3	15.5	1.3	2100	0.15	2
89	2300	26.82	4	7.5	15.5	1.3	2100	0.15	2
90	2300	26.82	6	5.2	15.5	1.3	2100	0.15	2
91	2300	17.88	4	5.2	5	0.4	1800	0.15	3
92	2300	26.82	4	5.2	25	2.5	2100	0.15	3
93	2300	26.82	4	5.2	20	1.7	2000	0.15	3
94	6800	26.82	8	2.8	15	1.3	1900	0.35	3
95	6800	17.88	8	7.6	5	0.3	1800	0.35	3

#### 4.6.3. Influence of some parameters

Additional PU60 and M50 simulations were carried out to study the effect of critical design parameters on the barrier performance. The first parameter to be studied was the soil strength. For this the PU60 and M40 (40 mph instead of 50 mph) were selected with the same pile configuration as in the crash tests. Several runs were simulated for different soil strength characterized by a limit pressure ranging from 0.4 MPa to 2.5 MPa. The results are show in Figure 4-32. As can be expected, the maximum deflection of the barrier decreases as the soil strength increases. There seems to be a point of diminishing return around a limit pressure value of about 1 MPa in these simulations.

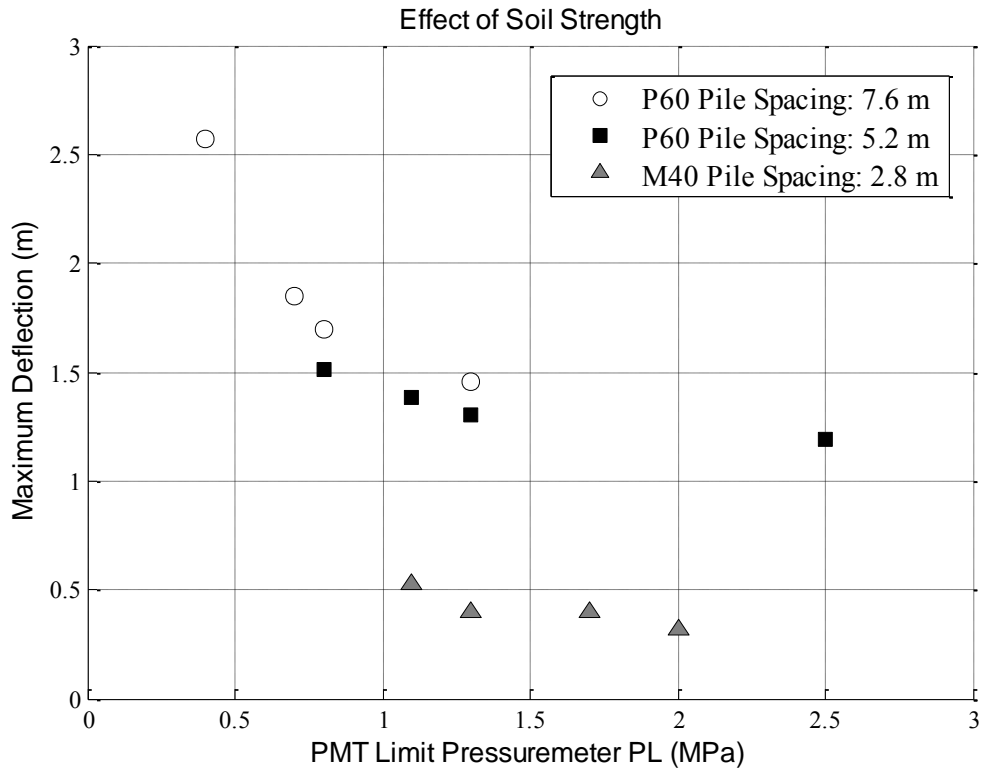


**Figure 4-32: The effect of soil strength on the barrier deflection**

The second parameter to be studied was the pile spacing. The PU60 configuration was selected: 4 pile group barrier impacted by a 2300 kg pickup truck at 60 mph. The pile spacing was varied from a spacing to diameter ratio  $s/d$  of 20, 35, and 50. Two soil strength cases were selected, one with a limit pressure  $P_L$  of 0.3 MPa and one with a  $P_L$  of 1.3 MPa. Figure 4-33 shows that the maximum deflection of the barrier continuously increases with the spacing to diameter ratio.

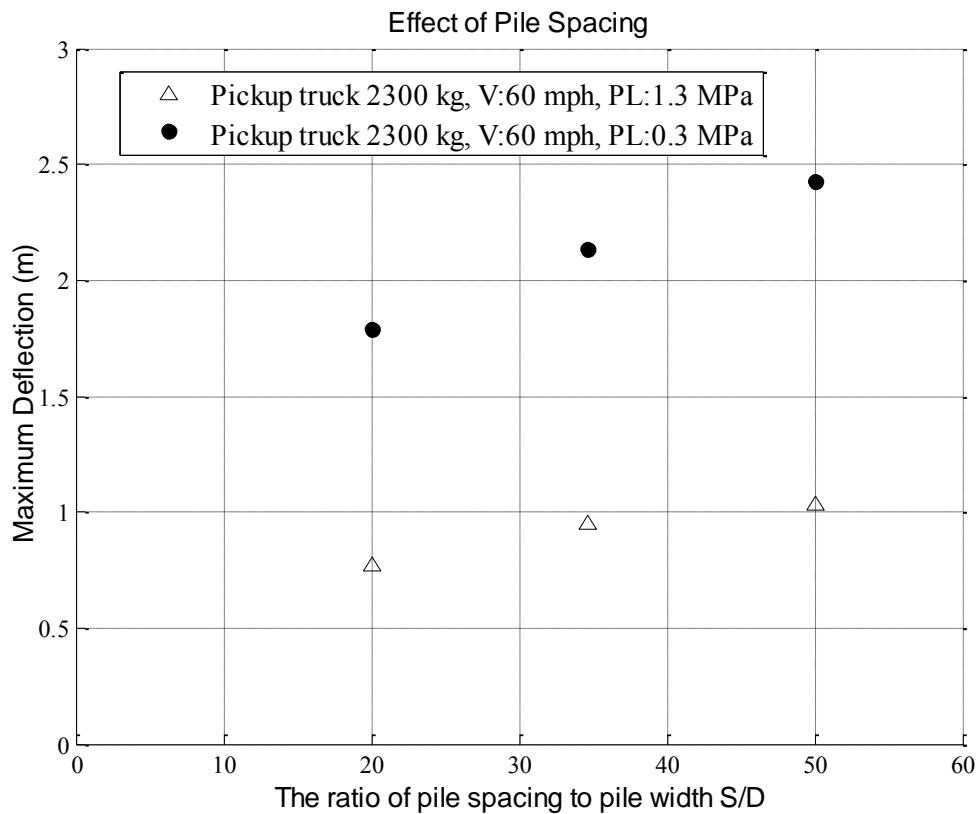


**Figure 4-33: The effect of pile spacing on the barrier deflection**

The third parameter which was studied was the impact velocity of the vehicle. Two configurations were selected: a PU60 barrier installation and a modified M50 barrier installation. The velocities were 64, 80, and 96 km/h. Figure 4-34 shows the barrier deflection increases linearly with the vehicle velocity for the two vehicle classes: the pickup truck and the medium-duty truck.



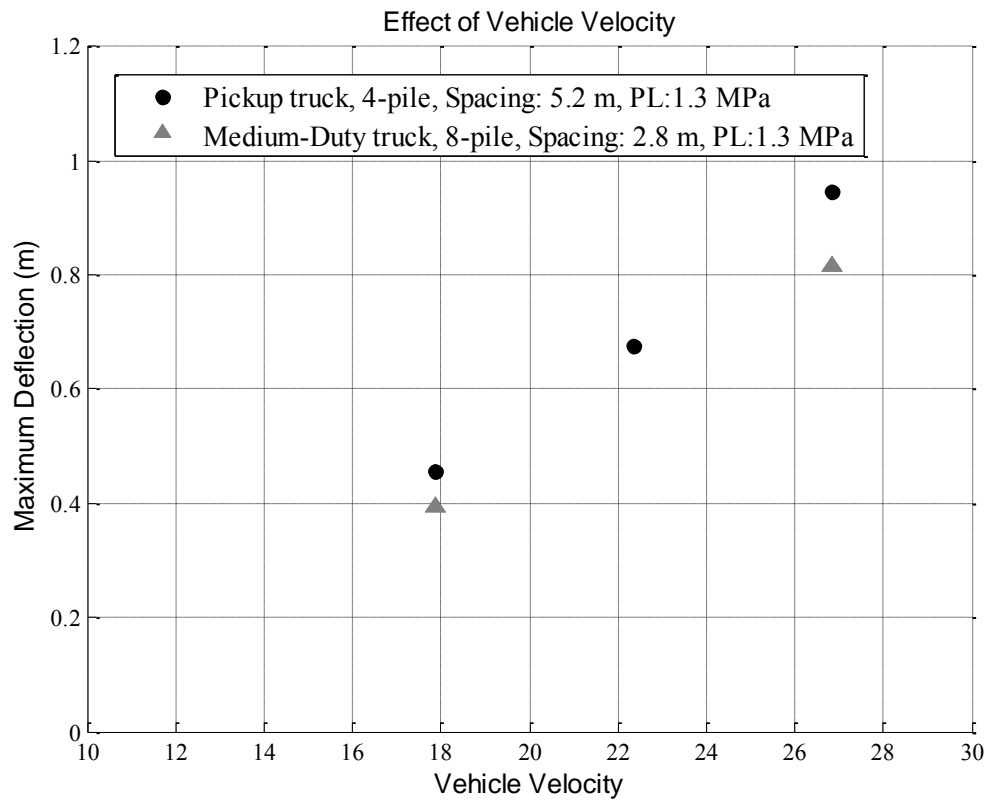


**Figure 4-34: The effect of vehicle velocity on the barrier deflection**

The fourth parameter to be studied was the number of piles for a given spacing. The PU60 configuration was selected and the number of piles was 4, 6, and 8. Figure 4-35 shows that the maximum deflection decreases as the number of piles increases but that there is a point of diminishing return around 6 piles. This indicates that in order to simulate a long row of piles, using 6 piles may be sufficient to capture the complete response of the long barrier.

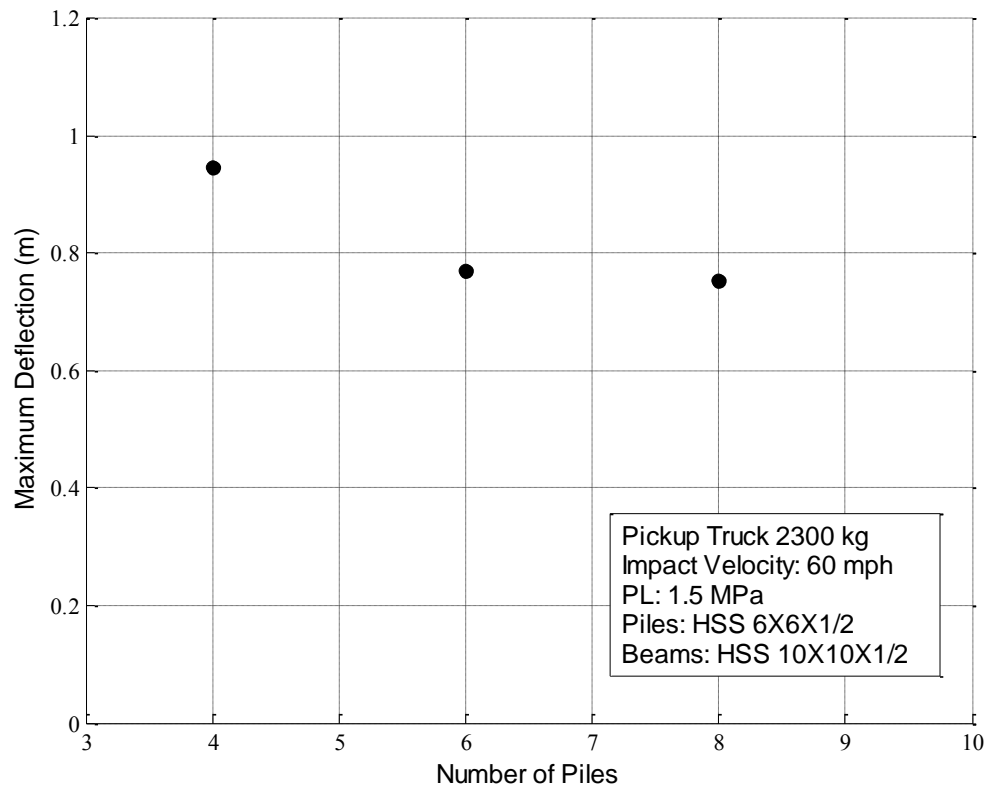


**Figure 4-35: The effect of piles number on the barrier deflection**

## 5. ANALYTICAL MODEL

### 5.1. Introduction

Single piles might be capable of arresting vehicles in high strength soils; but in general, they are not a practical solution. For protection purposes, piles have to be designed close to each other to function properly. Therefore, groups of in-line piles are preferred in practice.

This work has been primarily motivated by the lack of a model to design such pile systems under impact loading. A semi empirical semi theoretical model so called “TAMU-POST (Group)” has been developed to predict the response of a group of in-line piles connected by a beam subjected to a vehicle impact. This simple analytical model is designed to offer major benefits in modelling nonlinear soil-pile interaction and reasonable precision in estimation of impact performance. The model has been developed while satisfying two goals: to be fundamentally sound and to be able to predict reasonably well the experimental data and numerical simulations accumulated. The proposed model has been shown to work for a wide range of soil strength, impact loading levels for any pile or beam section. The main advantage of the model is that it requires the least yet adequate number of input parameters that could be easily obtained from common laboratory and in situ tests.

The computational approach to develop the model is described in this section. The required inputs and the model parameters calibration are discussed. The necessary laboratory and in-situ tests to obtain the parameters are explained in more details in

Appendix B. Novel formulations are proposed to approximate dynamic damping, mass and stiffness based on existing well-established methods and also utilizing the static and crash test results as well as extensive advanced numerical simulations.

As earlier mentioned, the ASTM F2656-07 defines failure when the dynamic penetration is more than one meter. In this respect, the model is aimed to best predict the dynamic penetration as the main output. The method also gives an estimate of the maximum bending moment in the piles and beam. In the following section, Section 6, the precision of the model TAMU-POST in predicting the barrier response is evaluated in comparison with the available data. Indeed, it is shown that the proposed model combined by a Monte Carlo Simulation method provides a simple means to estimate the probability of failure associated with a variety of soil-pile system design cases.

## **5.2. Modeling soil-structure interaction: Beam-on-Winkler Foundation**

Soil-pile interaction under vertical loading was first addressed in pile driving models using an empirical model proposed by Smith 1962 and after that many progresses have been made towards developing improved models to account for interaction between the pile and the surrounding soil (e.g. Novak 1974). In respect of laterally loaded piles, also considerable efforts have been made to study the soil-pile interaction in various levels of analysis in the 1960's and 1970's. Hetenyi (1946) was the first researcher introduced the beam-on-elastic-foundation method to solve the governing differential equation (Eq. 5-1) for the pile deflection ( $y$ ).

$$EI \frac{d^4 y}{dx^4} = p \text{ where } p = -E_s y \quad (5-1)$$

With E the pile elastic modulus, I moment of inertia.  $E_s$  is the modulus of subgrade reaction and p is soil reaction on the pile. As this solution does not allow for varying soil and pile stiffness, its application has been limited to the static lateral loading cases. Matlock and Reese (1960) developed a solution with varying soil modulus with depth while Broms (1964 a,b) presented a method for rigid and flexible piles in both cohesive and cohesionless soils, using the modulus of subgrade reaction with values recommended by Terzaghi (1955).

In 1876, the concept of the beam on Winkler foundation was introduced and has become popular and widely accepted to model the pile lateral loading problems by an elastic beam and a series of lumped mass connected by springs and dashpots. These springs may be assumed linear elastic or nonlinear using empirical p-y curves. This allows for including pile installation effects on the soil response. The main disadvantage of the Winkler method is the two dimensional approximation of the soil-pile contact. The p-y method for laterally loaded pile analysis (McClelland and Focht 1958) offers a load-deflection curve developed by the triaxial test data at different depths and estimating the corresponding modulus of subgrade reaction. Figure 5-1 shows a typical set of p-y curves. Matlock (1970) conducted a series of static and cyclic tests on piles embedded in soft clays and accordingly suggested p-y curves for the cases of interest. Likewise, Reese et al. (1974, 1975) reported the characteristic p-y curves in sand and

clay based on the lateral pile load tests. The p-y method has been established in API Recommended Practice, (API, 2002).

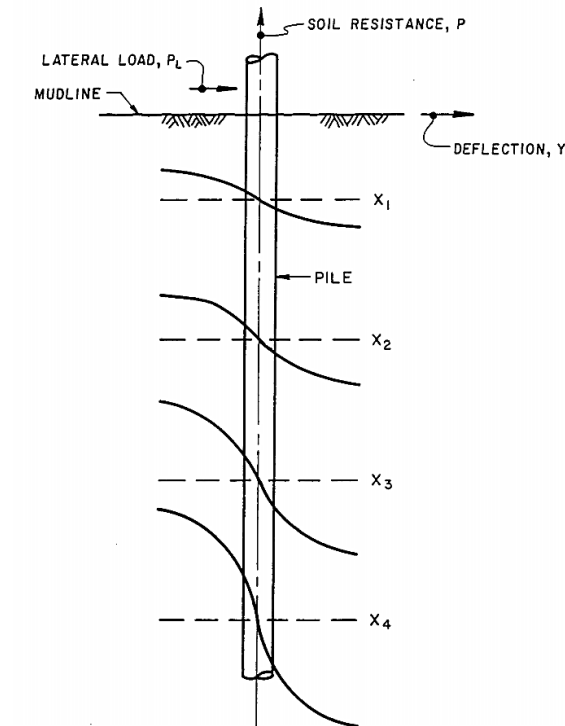


**Figure 5-1: Typical p-y curves (Meyer and Reese, 1979)**

Kagawa and Kraft (1981) presented a nonlinear Winkler model with a continuous beam representing the pile supported by a set of parallel springs and dashpots indicating near field soil elements. This model was combined with the superstructure elements accounting for the inertial resistance. The stiffness and radiation damping coefficients were respectively determined from the hysteric curve shown in Figure 5-2 and the following equation:

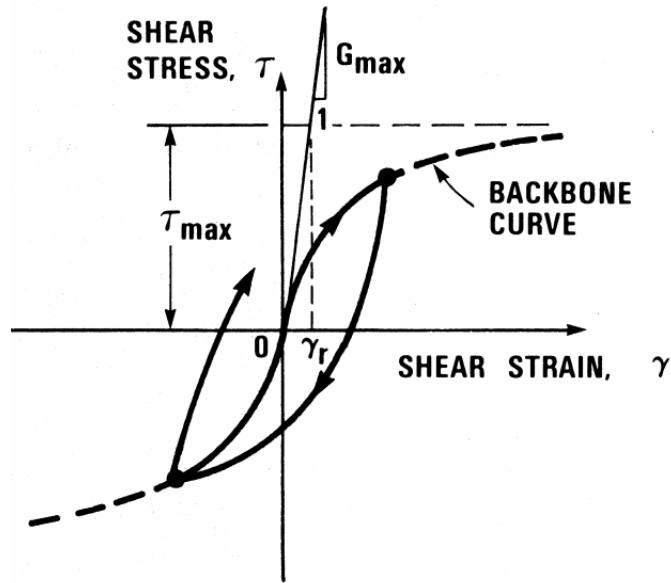


Figure 5-2: Hysteric backbone curve (Kagawa and Kraft, 1981)

$$c = 2\rho_s B(V_p + V_s) \quad (5-2)$$

Where  $\rho_s$  denotes soil density,  $B$  is the pile diameter,  $V_p$  and  $V_s$  are the compression and shear wave velocities, respectively.

Noghami et al. (1991, 1992) presented near field-far field solutions for laterally and axially loaded single pile and group piles including nonlinear soil-pile interaction and other significant features such as rate dependency effects, soil-pile gapping, slip and radiation damping (Figure 5-3).

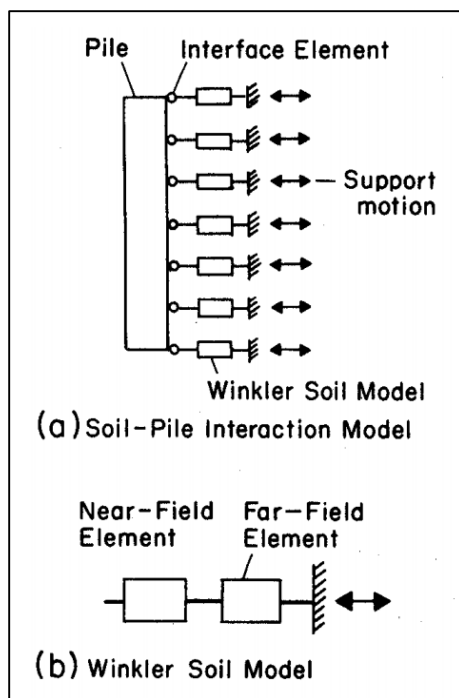


Figure 5-3: Soil-pile interaction model (Noghami et al. 1988)

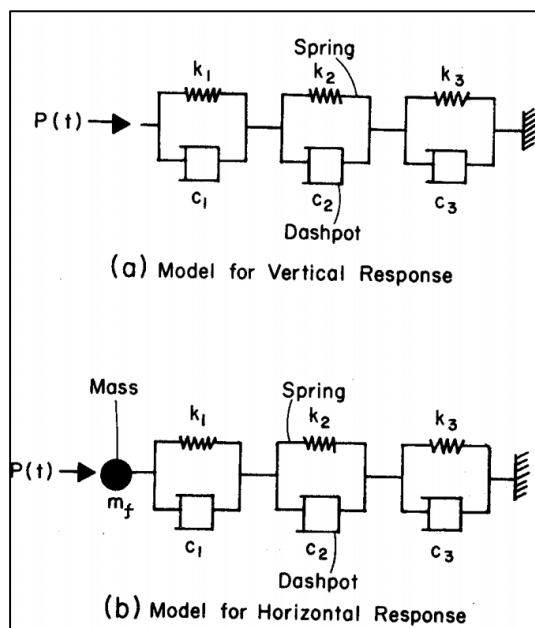
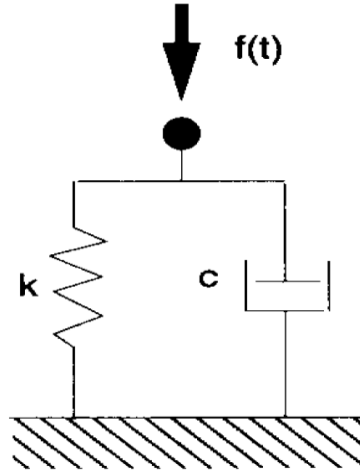


Figure 5-4: Far field soil-pile interaction models (Noghami et al. 1988)



As shown in Figure 5-4, the parallel Kelvin-Voigt spring-dashpots simulate an infinite elastic medium and the shear element incorporated in series accounts for the effects of adjacent soil layers. Overtime numerous studies were designed to develop simplified lumped-parameter models capable of simulating dynamic soil-pile interaction adequately. Lysmer and Richart (1966) originally proposed a simplified one-dimensional spring-dashpot model for analysis of elastic response of rigid footings (Figure 5-6 a) wherein spring stiffness  $k$  and damping constant  $c$  were obtained as following:

$$k = \frac{4GR}{1-\nu} \quad \text{and} \quad c = 0.85k \frac{R}{c_s} \quad \text{Where } c_s = \sqrt{\frac{G}{\rho}} \quad (5-3)$$



**Figure 5-5: Lysmer and Richart simplified model for dynamic elastic response of footing**

Where  $G$  refers to the soil shear modulus,  $R$  is the footing radius,  $\nu$  is Poisson ratio,  $c_s$  is the shear wave velocity and  $\rho$  denotes for the soil bulk density. More complicated

mechanical models introduced by different researchers are demonstrated in Figure 5-6. Velestos and Verbic (1974) and later Wolf and Hall (1988) attempted to derive parameters for the model (b) which has two lumped masses, two dashpots and two degrees of freedom. In another study, De Barros and Luco (1990) analyzed a model with an additional spring. Given proper selection of parameters these models were found to work adequately.

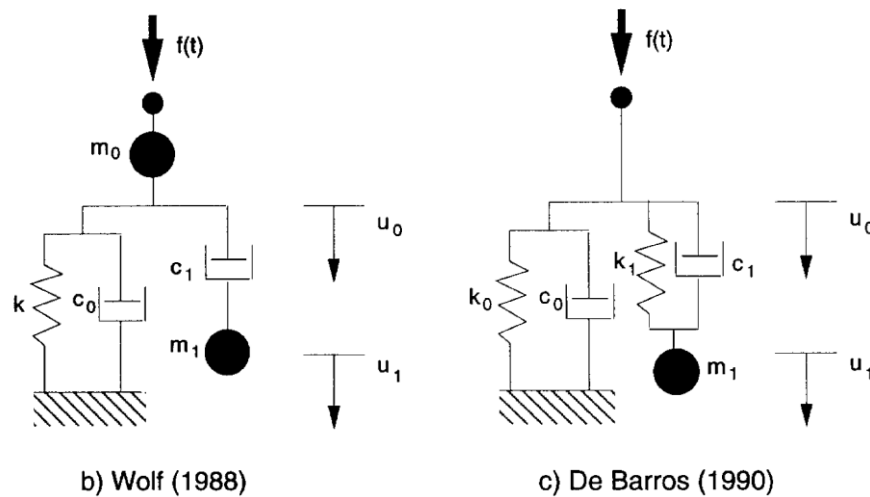


**Figure 5-6: Models suggested for the dynamic response of a rigid circular footing (Deeks & Randolph, 1995)**

Moving to model the inelastic response, Smith (1962) presented a model shown in Figure 5-7 (a) similar to Lysmer's analogue with an additional plastic slider connected to the spring to account for the effect of soil inelasticity. This slider has a slip load equal to the ultimate static failure load. Once the failure load is reached the slider displaces so that the force maintain constant. Nguyen et al. (1988) modified the model by relocating

the slider (Figure 5-7 b) and later on Deeks & Randolph (1995) examined these models placing the slider at different locations.

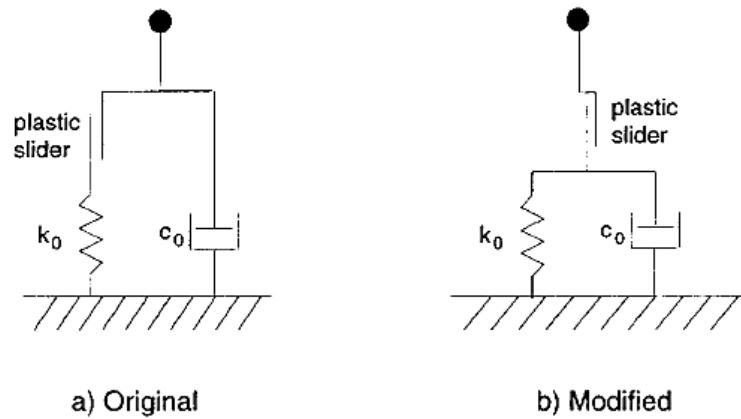


**Figure 5-7: Inelastic models developed by a) Smith b) Nguyen**

In this research, a lumped-parameter model derived from Smith (1962) was adopted to simulate soil, pile and the corresponding interaction. This model as illustrated in Figure 5-8 consists of a parallel dashpot, visco-elstic spring and a lumped mass with one degree of freedom.

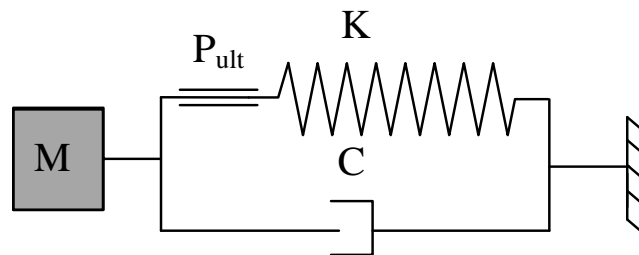


**Figure 5-8: The chosen single degree of freedom**

As earlier mentioned, when the soil surrounding pile fails, defined as the force exceeds the ultimate failure load or the deflection reaches the failure displacement, the spring stiffness becomes zero. In computational respect, the slider displaces and the spring cannot contribute to the ultimate resistance.

### 5.3. Model theory

For the present impact loading problem, the governing equation is derived from the Euler-Bernoulli beam theory. The beam connecting the piles is modeled as an elastic Euler-Bernoulli beam supported by a series of Single Degrees of Freedom (SDOFs) representing piles embedded in soil. Although the beam is assumed to behave elastically, the model parameters are identified using an actual nonlinear dynamic test data, in such a way that nonlinearity of soil-pile-beam system is included.

The Euler-Bernoulli static equation for an elastic beam relates beam's deflection ( $y$ ) shown in Figure 5-9 to the applied lateral load  $q(x)$  expressed as:

$$\frac{\partial^2}{\partial x^2} \left( E_b I_b \frac{\partial^2 y}{\partial x^2} \right) = q(x) \quad (5-4)$$

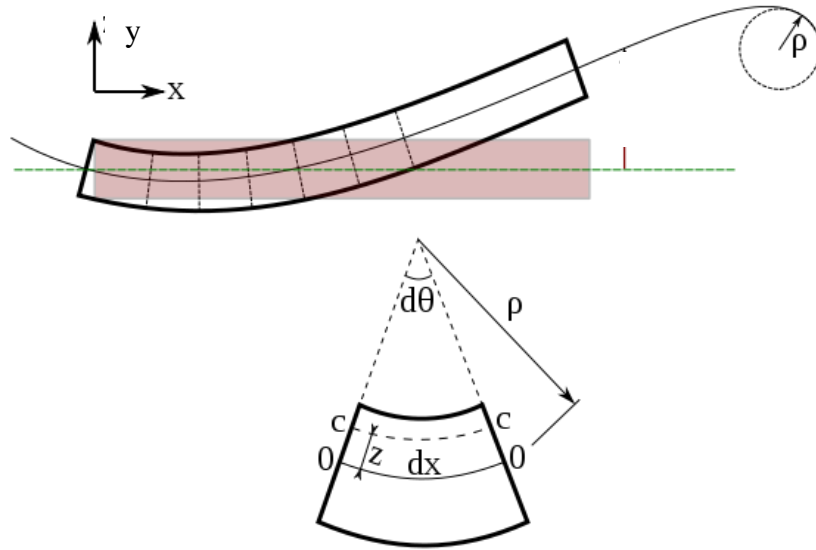


**Figure 5-9: Bending of an Euler–Bernoulli beam**

Where  $E_b$  is the elastic modulus of the beam,  $I_b$  the second moment of area (moment of inertia) of the beam with respect to the axis perpendicular to the applied load.

In dynamic loading, the Euler-Bernoulli equation, assuming constant bending stiffness (EI), is modified by adding the inertia term:

$$E_b I_b \frac{\partial^4 y}{\partial x^4} + m \frac{\partial^2 y}{\partial t^2} = q(x, t) \quad (5-5)$$

Where  $m$  is mass per unit length of the beam and  $q(x, t)$  is the transverse load applied at a distance  $x$  and at time  $t$ .

Let's consider a SDOF system (as shown in Figure 5-8) with a moving mass  $M$ , a damping coefficient  $C$ , and an elastic stiffness coefficient  $k$ . For this system, kinetic

energy, potential energy and the external loading and dissipative forces can be computed as:

$$T(y, \dot{y}) = \frac{1}{2} m \dot{y}^2(t) \quad (5-6)$$

$$V(x) = \frac{1}{2} k y^2(t) \quad (5-7)$$

$$D(y, \dot{y}) = -c \dot{y}(t) + f(t) \quad (5-8)$$

From the Lagrange's equation, the differential equation of dynamic motion is given by:

$$\frac{d}{dt} \frac{\partial T(y, \dot{y})}{\partial \dot{x}} - \frac{\partial T(y, \dot{y})}{\partial x} + \frac{\partial V(y)}{\partial x} - P(y, \dot{y}) = 0 \quad (5-9)$$

In another expression, writing equilibrium of the applied forces (inertia force  $f_I$  , stiffness  $f_S$  , damping  $f_D$  and external load  $f$  ) on the mass results in the dynamic equilibrium equation:

$$f_{inertia} + f_{Damping} + f_{static} = f_{impact} \rightarrow M \frac{\partial^2 y}{\partial t^2} + c \frac{\partial y}{\partial t} + ky = f \quad (5-10)$$

M is the mass, c and k are the equivalent stiffness of the system and dashpot constant, respectively.

Figure 5-10 schematically illustrates the model structure for a group of in-line piles tied together by a beam. It is worth noting that the ratio of the pile spacing to the pile width or diameter in anti-ram barriers is often far larger than 10, so that it seems

justifiable to neglect group effects and the interaction between the piles (Rollins et al., 2005).

As the maximum deflection of the barrier is the critical measure in design of such barriers, the present analysis does not include the unloading phase where the vehicle is rebounded and redirected against the barrier.

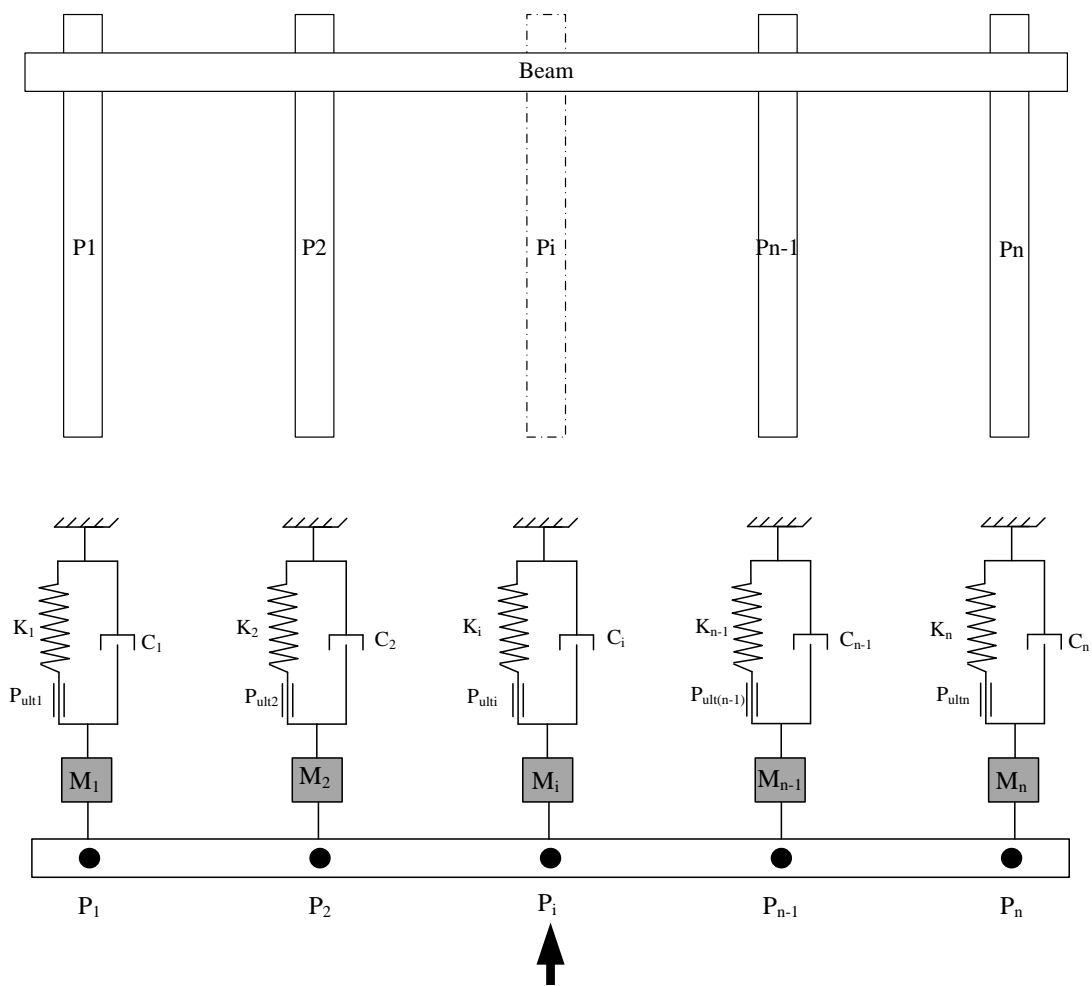


**Figure 5-10: Schematic presentation of the proposed analytical model for nonlinear dynamic analysis of lateral response of pile groups under impacts**

#### 5.4. Solution method

To solve the governing equation (Eq.5-10) a numerical solution is applied. The PDE is solved for the deflection of beam ( $y$ ) by implementing the Central Finite Difference Method, applying the corresponding initial values and boundary conditions.

For this purpose, the beam is discretized into a number of equal length elements (Figure 5-11). Considering accuracy and computational efforts, it has been chosen to consider 15 nodes and 14 elements as it allows for various layouts from 3 to 8 piles accommodating impact nodes both on the piles and between the piles. The seven different pile configurations are described in detail in Appendix D.

Therefore, the stiffness matrix is defined by a fifteen by fifteen matrix, which relates the lateral displacement of each node to the associated load  $P$ .

For each node  $i$  at time  $j$  the deflection of beam  $y$  is computed explicitly using the approximate central finite difference solution, given by:

$$E_b I_b y'' + M_G \ddot{y} + C_G \dot{y} + K_G y_{i,j} = 0 \rightarrow$$

$$E_b I_b \left( \frac{y_{i+2,j} - 4y_{i+1,j} + 6y_{i,j} - 4y_{i-1,j} + y_{i-2,j}}{h^4} \right) + M_G \left( \frac{y_{i,j+1} - 2y_{i,j} + y_{i,j-1}}{\Delta t^2} \right) + C_G \left( \frac{y_{i,j+1} - y_{i,j-1}}{2\Delta t} \right) + K_G y_{i,j} = 0$$

(5-11)



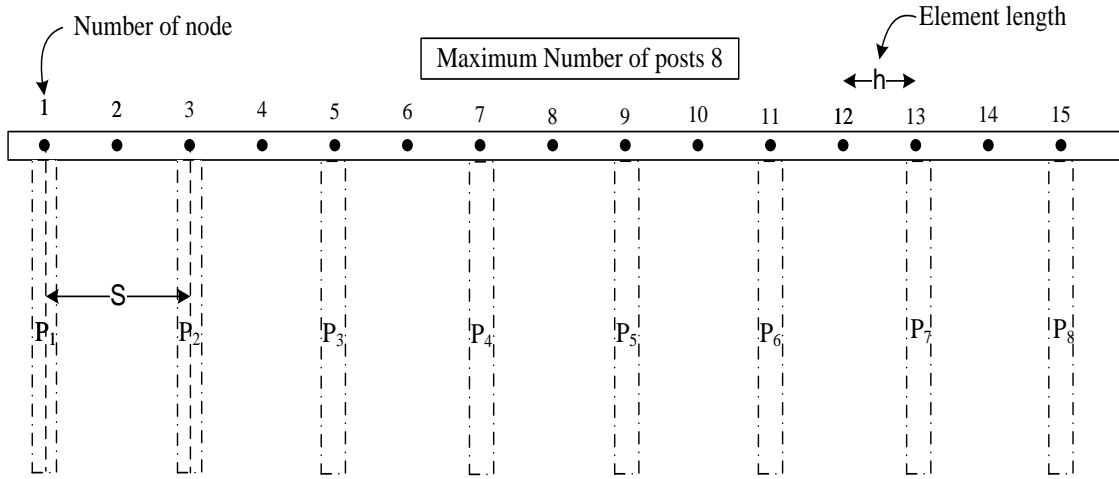


**Figure 5-11: Application of central finite difference approach**

Where the subscripts  $i$  and  $j$  are the counters for nodes and time, respectively. In order to facilitate the numerical solution the parameters  $m, e$  and  $c$  are introduced as following:

$$m = \frac{M}{\Delta t^2}, \quad e = \frac{EI}{h^4} \quad \text{and} \quad c = \frac{C}{2\Delta t} \quad (5-12)$$

Then the deflection at node  $i$  at the current time step is computed based on the deflections of that node and the adjacent nodes in previous time steps as below:

$$(m+c)y_{i,j+1} = (c-m)y_{i,j-1} - ey_{i+2,j} + 4ey_{i+1,j} - (6e-2m+k)y_{i,j} + 4ey_{i-1,j} - ey_{i-2,j} \quad (5-13)$$

In Eq.5-13 all quantities are known except for  $y_{i,j+1}$ . A Matlab code and an Excel Spreadsheet were written to automate the solution.

- Initial Conditions

The node under impact displaces as  $y_{i,-1} = -\Delta t.V_0$  during the first time step where  $V_0$  the velocity of the approaching vehicle. This applies an extremely large acceleration at that node. To avoid convergence issues associated with this problem, a very small time step  $\Delta t 10^{-5}$  is used in the explicit solution.

- Boundary Conditions

Boundary conditions enforce that the shear force ( $\partial^3 y / \partial x^3$ ) and the bending moment ( $\partial^2 y / \partial x^2$ ) at both ends of beam be zero. Therefore, the following conditions should be met:

$$V|_{node0} = 0 \rightarrow y_{3,j} - 2y_{2,j} + 2y_{0,j} - y_{-1,j} = 0 \quad (5-14)$$

$$M|_{node0} = 0 \rightarrow y_{2,j} - 2y_{1,j} + y_{0,j} = 0 \quad (5-15)$$

$$V|_{nodeN} = 0 \rightarrow y_{N+2,j} - 2y_{N+1,j} + 2y_{N-1,j} - y_{N-2,j} = 0 \quad (5-16)$$

$$M|_{nodeN} = 0 \rightarrow y_{N+1,j} - 2y_{N,j} + y_{N-1,j} = 0 \quad (5-17)$$

Solving the equation for all the nodes deflection requires solving a simple diagonal matrix equation without need to inverse the matrices. However attention should be paid to choose very small time steps.

### 5.5. Model input parameters

The simplified analytical model results appreciably depend on parameters selection. Hereby, special attention was paid to formulate the parameters including static stiffness, mass and dynamic damping using theoretically grounded methods and a databank of full scale tests and numerical simulations. The proposed expressions are functions of characteristics which can be easily obtained from field, common laboratory and in situ testing data.

### **5.5.1. Lateral static stiffness K**

Spring stiffness in the lumped-parameter model represents the soil-pile static stiffness. It has been known that the static stiffness is roughly equivalent to dynamic stiffness in the loading frequency range of interest. Stiffness is relatively easier to quantify rather than damping coefficient and associated soil mass, as there is more experience in determining stiffness.

Behavior of laterally loaded piles has received a lot of attention (Broms 1964, Matlock 1970, Briaud et al. 1996). By further reviewing of the literature, the SALLOP method (Simple Approach for Lateral Load on Piles) developed by Briaud (1997) is found the best method for this investigation. SALLOP has been proven to give a reliable estimate of lateral static stiffness  $K$  of a pile subjected to a horizontal load  $H_0$  and a moment  $M_0$ . This semi-theoretical semi-empirical method makes use of pressuremeter limit pressure  $P_L$  and pressuremeter modulus  $E_0$  that can be obtained from Pressuremeter Test. It is recommended to take an average of the PMT measures within the influence depth,  $D_v$  so-called zero-shear depth. This depth is defined in the following.

More details on the test operation and its data reduction are provided in Appendix B. In the PMT test, since the applied load on soil is mostly radial, it is more reasonable to use the PMT test data to quantify lateral stiffness of the soil embedded piles.

The P-Z curve (soil resistance P per length of pile versus depth Z), shown in Figure 5-12 indicates that the soil resistance to horizontal loading comes mostly from shallow layers (Baguelin et al. 1978, Briaud 1992).

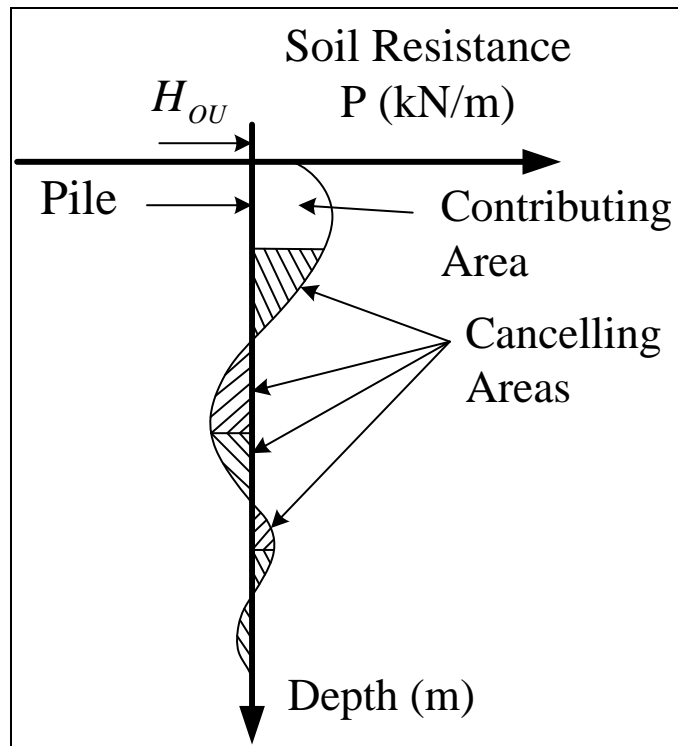


**Figure 5-12: Conceptual soil resistance versus depth profile (Briaud, 1997)**

Pile deflection, slope, bending moment, and shear force can be obtained from the theoretical solution of the governing differential equations with the following

simplification assumptions: uniform soil, linear behavior, long pile or short pile (Briaud, 1992).

The depth to the point where the shear force is zero  $D_v$ , can be calculated for the two cases: a) Long and flexible piles (Hetenyi 1946, Baguelin et al. 1978; Briaud 1992), b) Short and rigid piles (Baguelin et al. 1978; Briaud 1992). Pile is assumed to be long if its length is larger than  $3l_0$  and is short when the pile length is less than  $l_0$ , where  $l_0$  refers to the transfer length defined as a function of the relative stiffness of the pile and soil:

$$l_0 = \left( \frac{4EI}{K_s} \right)^{1/4} \quad (5-18)$$

E and I are elastic modulus and moment of inertia of the pile, respectively.  $K_s$  the spring constant represents the soil stiffness.  $K_s$  is obtained from the initial pressuremeter modulus  $E_0$  as proposed by Briaud, 1997:

$$K_s = 2.3E_0 \quad (5-19)$$

In the case of long flexible piles subjected to a horizontal load  $H_0$  and a moment  $M_0$ , shear force V at a depth Z and the zero-shear depth  $D_v$  are computed using Eq.5-20 and Eq. 5-21, respectively:

$$V = H_0 e^{-(z/l_0)} \left( \cos \frac{z}{l_0} - \sin \frac{z}{l_0} \right) - \frac{2M_0}{l_0} e^{-(z/l_0)} \sin \frac{z}{l_0} \quad (5-20)$$

$$D_v = l_0 \cdot \tan^{-1} \left( \frac{1}{1 + \frac{2M_0}{l_0 H_0}} \right) \quad (5-21)$$

Similarly, in the case of short rigid piles, shear force and zero-shear depth can be obtained as following:

$$V = H_0 + \frac{6(H_0L + 2M_0)}{L^3} \frac{z^2}{2} - \frac{2(2H_0L + 3M_0)}{L^2} z \quad (5-22)$$

$$D_v = \frac{H_0L^2}{3(H_0L + 2M_0)} \quad (5-23)$$

For piles with a length  $L$  such that  $l_0 < L < 3l_0$ , a linear interpolation between the long flexible case and the short rigid case is suggested.

In the current study, the horizontal impact load  $H_0$  is applied on the pile at the impact height above the ground surface. This load is transferred to the ground level along with the corresponding moment  $M_0 = H_0 \times h$ , where  $h$  is the impact height (Figure 5-13).

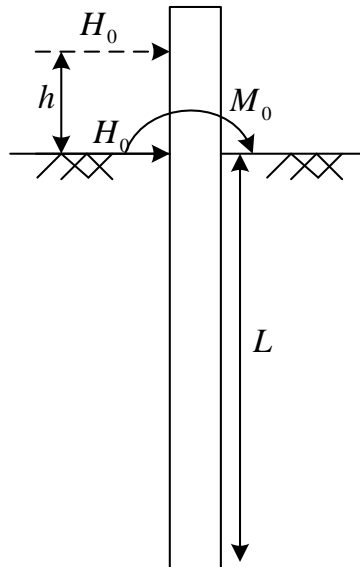


**Figure 5-13: Horizontal load on a single pile**

Using  $M_0$  equal to the product of  $H_0$  by the impact height  $h$ , Eq. 5-24 and 5-25 are introduced for long-flexible and short-rigid piles, respectively:

$$D_v = l_0 \cdot \tan^{-1} \left( \frac{1}{1 + \frac{2h}{l_0}} \right) \quad (5-24)$$

$$D_v = \frac{L^2}{3(L+2h)} \quad (5-25)$$

The pile lateral deflection can be obtained using Eq. 5-26 and Eq. 5-27:

$$\text{Deflection for Short Rigid Piles} \quad y_0 = \frac{2(2H_0L + 3M_0)}{K_s L^2} \quad (5-26)$$

$$\text{Deflection for Long Flexible Piles} \quad y_0 = \frac{2H_0}{l_0 K_s} + \frac{2M_0}{l_0^2 K_s} \quad (5-27)$$

Static stiffness of the pile-soil system is defined as the ratio of the horizontal force to the associated deflection. Therefore, the equivalent stiffness  $K$  can be given by Eq. 5-28 and 5-29:

$$\text{Stiffness for Short Rigid Piles} \quad K = \frac{H_0}{y_0} = \frac{K_s L^2}{4L + 6h} \quad (5-28)$$

$$\text{Stiffness for Long Flexible Piles} \quad K = \frac{H_0}{y_0} = \frac{l_0^2 K_s}{2(l_0 + h)} \quad (5-29)$$

These values of  $K$  have been successfully compared to the full-scale static tests performed in this project.

### 5.5.2. Ultimate failure load $H_{ou}$

In SALLOP, the lateral pile capacity is defined as the load corresponding to the pile deflection equal to one-tenth of pile diameter or width. Note that this ultimate load refers to the soil failure and does not incorporate pile failure. Pile must be designed to resist the bending moment without breaking. The SALLOP method predicts the pile capacity  $H_{ou}$  as a function of soil and pile properties as follows:

$$H_{ou} = 0.75P_L B_p D_v \quad (5-30)$$

Where  $P_L$  is the pressuremeter limit pressure,  $B_p$  is pile diameter or width, and  $D_v$  is zero-shear depth obtained as described in the previous section. If  $P_L$  is not available, other in situ or laboratory tests results such as SPT blow count  $N$  (corrected  $N$ ,  $N_{60}$ ), undrained shear strength  $S_u$  or CPT point resistance  $q_c$  can be used to estimate  $P_L$  (Briaud, 2013). Finally, the deflection at failure  $y_f$  for the elastic perfectly plastic soil-pile model is given by:

$$y_f = \frac{H_{ou}}{K} \quad (5-31)$$



This failure deflection accounts for the discontinuity conditions of the motion between pile and soil caused by gap opening at the pile-soil interface. If the soil deformation exceeds the deflection at failure, i.e. soil-pile separation occurs; the spring stiffness will be excluded from the resistance computation.

**Table 5-1: Soil classification based on PMT data (Briaud, 2013)**

CLAY					
Soil strength	Soft	Medium	Stiff	Very Stiff	Hard
$\dot{p}_L$ (kPa)	0 – 200	200 – 400	400 – 800	800 – 1600	> 1600
$E_0$ (kPa)	0 - 2500	2500 - 5000	5000 - 12000	12000 - 25000	> 25000
SAND					
Soil strength	Loose	Compact	Dense	Very Dense	
$\dot{p}_L$ (kPa)	0 – 500	500 - 1500	1500 - 2500	> 2500	
$E_0$ (kPa)	0 - 3500	3500 - 12000	12000 - 22500	> 22500	

**Table 5-2: The recommended correlations for clay (Briaud, 2013)**

Correlations for Clay (Column A = Number in Table x Row B)							
B	$E_0$	$E_R$	$\dot{p}_L$	$q_c$	$f_s$	$s_u$	N
A	(kPa)	(kPa)	(kPa)	(kPa)	(kPa)	(kPa)	(bl/30 cm)
$E_0$ (kPa)	1	0.278	14	2.5	56	100	667
$E_R$ (kPa)	3.6	1	50	13	260	300	2000
$\dot{p}_L$ (kPa)	0.071	0.02	1	0.2	4	7.5	50
$q_c$ (kPa)	0.4	0.077	5	1	20	27	180
$f_s$ (kPa)	0.079	0.0038	0.25	0.05	1	1.6	10.7
$s_u$ (kPa)	0.01	0.0033	0.133	0.037	0.625	1	6.7
N (bl/30 cm)	0.0015	0.0005	0.02	0.0056	0.091	0.14	1

**Table 5-3: The recommended correlations for sand (Briaud, 2013)**

Correlations for Sand (Column A = Number in Table x Row B)							
B	$E_0$	$E_R$	$\dot{p}_L$	$q_c$	$f_s$	$s_u$	N
A	(kPa)	(kPa)	(kPa)	(kPa)	(kPa)	(kPa)	(bl/30 cm)
$E_0$ (kPa)	1	0.278	14	2.5	56	100	667
$E_R$ (kPa)	3.6	1	50	13	260	300	2000
$\dot{p}_L$ (kPa)	0.071	0.02	1	0.2	4	7.5	50
$q_c$ (kPa)	0.4	0.077	5	1	20	27	180
$f_s$ (kPa)	0.079	0.0038	0.25	0.05	1	1.6	10.7
$s_u$ (kPa)	0.01	0.0033	0.133	0.037	0.625	1	6.7
N (bl/30 cm)	0.0015	0.0005	0.02	0.0056	0.091	0.14	1

### 5.5.3. Damping coefficient C

Damping in impact problems is difficult to identify because of the complexity of the impact loading. Basically the term damping is used to approximate the unknown nonlinear energy dissipation in the system. It is possible to estimate an effective damping through calibration of the model against full-scale tests and numerical models. This section describes an approximate quantification method of the system damping and its effect on the pile group performance. Accordingly expressions are proposed to relate soil-pile system damping to the most contributing variables.

The phenomenon of soil damping under dynamic loading has been discussed in numerous studies (Roesset et al. 1973, Rainer 1975, Wolf and Somaini 1986). Wolf has verified that in the case of shallow layers of soil the primary source of energy dissipation in the soil medium is material damping. In dynamic problems a coupled analysis of damping known as Rayleigh damping is commonly used. In Rayleigh damping formulation the mass coefficient controls response at low frequencies, while the stiffness

contributes more at high frequencies. Many analyses indicated that dynamic resistance is largely attributed to damping (e.g. Rollins et al. 2003).

Nevertheless, to date there is no well-developed approach to define soil dynamic damping under impact loading. In this project, the interaction between the soil and the pile adds more complexity to the problem. This work attempts lead to an indirect estimation of soil-pile damping when the structure is subjected to impact loading.

In the literature on damping, a variety of damping types have been identified including Viscoelastic Damping (or material damping), Hysteric Damping (or inelasticity damping), and Radiation Damping (or geometric damping). The damping associated with impact tests originates from energy dissipation either through wave propagation in the soil medium known as radiation damping, or through viscous damping associated with rate effects in soil. Herein, the effect of soil viscosity is small compared to the radiation damping and dissipating energy in wave propagation. It is believed that the major part of the impact energy is damped through radiation damping. The amount of soil that is mobilized by the impact and contributes to wave propagation increases in stiffer soils, therefore, it is expected to observe larger damping in soils with higher strength. Regardless of what type of damping governs the behavior, damping value  $C$  in the equations can be back-calculated by comparison between the model output and the full-scale experiments or the extensive number of validated numerical simulations using LS-DYNA.

Sum of the inertia forces, damping forces, stiffness resistance and external excitation should satisfy the dynamic equilibrium equation. This provides a way to evaluate the

damping coefficient by matching the predicted and observed behavior. To quantify this damping coefficient  $C$ , an expression is framed based on the known theoretical concepts on dynamic loading. In this formulation, dimensionless coefficients are introduced to correctly relate damping to the significant parameters. These coefficients are then adjusted by comparison with the measured data and numerical results.

In the previous studies, dynamic damping of a foundation has been correlated to the parameters such as foundation dimension, stiffness, and soil shear wave velocity (Wolf and Somaini, 1986). Figure 5-14 indicates the fundamental lumped-parameter model proposed by Wolf and Somaini. In this model, damping coefficients are introduced as functions of the physical properties of soil including shear modulus  $G_s$ , density  $\rho_s$ , the static stiffness  $K$ .

$$C_0 = \frac{b}{c_s} K \mu_0 \quad (5-32)$$

$$C_1 = \frac{b}{c_s} K \mu_1 \quad (5-33)$$

In the above relations, dimensionless coefficients  $\mu_0$  and  $\mu_1$  were determined by applying curve-fitting techniques for a specific component of motion.

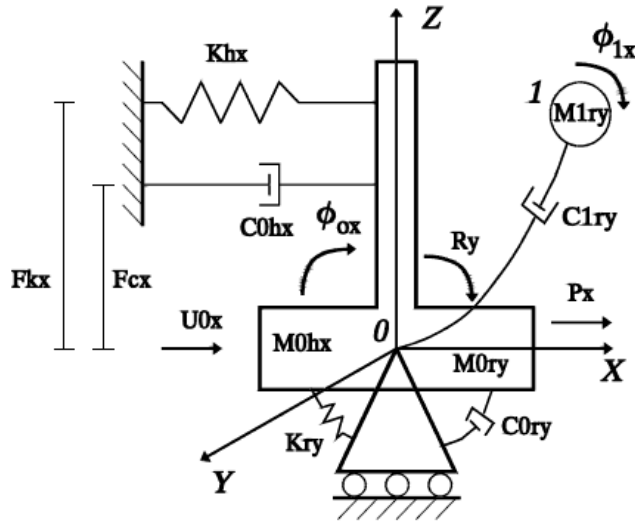


Fig. 1. Soil model.

**Figure 5-14: Soil model presented by Wolf and Somaini**

In this research using a similar approach,  $C$  is correlated to the pile width  $B$ , soil-pile stiffness  $K$ , and soil stiffness which is directly related to the wave velocity  $V_s$ . Damping is inversely proportional to the soil shear wave velocity or soil stiffness. The following expression is proposed:

$$C = f\left(B, K, \frac{1}{V_s}\right) = \alpha \frac{BK}{V_s} \quad (5-34)$$

$$V_s = \sqrt{\frac{G_s}{\rho}} \quad \text{and} \quad G_s = \frac{E}{2(1+\nu)} \quad (5-35)$$

As noted in damping expression, shear wave velocity contributes to damping estimate inversely. This measure can be obtained from shear modulus (Eq. 5-35). Within the scope of this study, in order to limit the input parameters to simple and robust site

investigation data, an equivalent soil shear wave velocity  $V'_s$  is used in damping formulation. Therefore,  $V'_s$  is established using Eq.5-36, where the soil elastic modulus  $E$  is replaced by the soil pressuremeter modulus  $E_0$ . The possible imposed inaccuracy of this simplification is further compensated for by introducing dimensionless coefficient based on real experimental data as well as validated numerical results. Indeed one could write that the shear wave velocity is expressed as follows where  $\rho$  is the soil density:

$$V'_s = \sqrt{\frac{E_0}{2(1+\nu)\rho}} \quad (5-36)$$

Where  $\nu$  is Poisson's ratio. To determine the value of  $\alpha$  in Eq. 5-34, the predictions using the proposed simple method code, TAMU-POST (Group) were compared to the two full scale impact tests and the LS-DYNA simulations; the best agreement was sought. Section 5.7 explains the quantification of the factor  $\alpha$  (*Alpha*).

#### 5.5.4. Mass M

Lumped mass (M) at the nodes adjacent to piles includes three terms: mass of the pile ( $M_p$ ), mass of the beam ( $M_b$ ), mass of the associated soil ( $M_s$ ).  $M_p$  includes mass of pile that contributes most to the resistance; this is taken as the zero shear depth  $D_v$  (defined in the previous section).  $M_b$  includes the mass of the beam element which is  $h$  long.

Mass of the beam and pile are relatively well identified, but there is more uncertainty in estimating the mass of the associated soil. Mass of the soil wedge mobilized due to the impact (Figure 5-15) depends on pile geometry, soil density and soil stiffness.

In this research, a sensitivity analysis was performed to identify the effect of varying the mass on the output of the program (will be discussed in Section 6.2.6). It was found that the mass of soil does not affect the maximum deflection significantly. Moreover, the soil mass value is not considerable compared to the pile, beam and vehicle mass. Therefore, it sounds reasonable to use an approximate estimate of soil mass as given by Eq. 5-37 and to emphasize on the influence of damping factor which plays a more important role on the system performance.

$$M_{soil} = \rho_s B^2 D_v \quad (5-37)$$

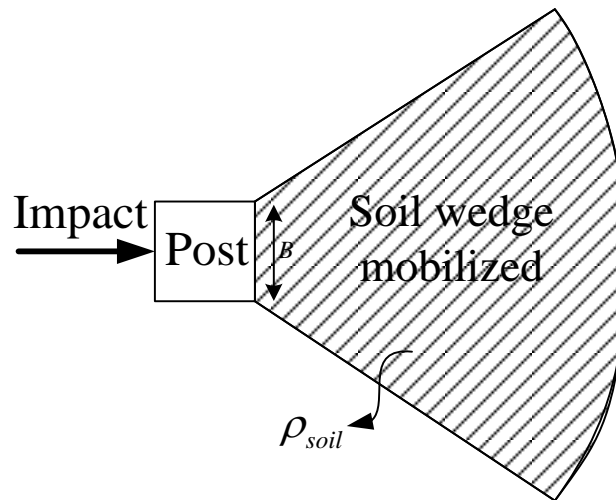


**Figure 5-15: Mobilized soil wedge**

## 5.6. Energy absorption

Severity of vehicle-barrier collisions depends on stiffness of the vehicle and barrier, and the impact speed. The kinetic energy of the approaching vehicle is absorbed in part by the work done to deflect the barrier system and in part by deforming the vehicle. Vehicle deformation is not included in the proposed simple model since the vehicle is modelled as a rigid mass. To account for the vehicle crushing, a reduction factor ( $\kappa$ ) is applied to approach velocity in proportion with the energy absorbed in deforming the vehicle (Eq. 5.38). This reduction factor may depend on the vehicle type and the stiffness of the barrier.

$$V_{design} = \kappa V_{Crushing} \quad (5-38)$$

To quantify the energy absorbed by crushing the front of the vehicle, a large number of FE models including different vehicle types, barrier configurations and soil strengths were analyzed. The energy absorption was quantified by comparing the total kinetic energy of the vehicle and the internal energy of the barrier and soil together during the impact. Let's assume that  $E_{TK}$ ,  $E_{Crush}$  and  $E_{Barrier}$  are the total kinetic energy of the vehicle, the energy expended to crush the vehicle, and the energy absorbed by the deformation of the barrier system (soil-pile-beam), respectively. Ideally the difference between  $E_{TK}$  and  $E_{Crush}$  is the energy that the barrier absorbs during the impact. However, in numerical simulations there are small losses of energy including an



inevitable small hourglass energy and the energy spent in contacts sliding. Neglecting these small effects, Eq. 5-39 can be written as:

$$E_{Soil-Pile} = E_{TK} - E_{Crush} = \frac{1}{2} m V_{modified}^2 = \kappa^2 (\frac{1}{2} m V^2) \quad (5-39)$$

Therefore the reduction factor  $\kappa$  is obtained as follows:

$$\kappa = \sqrt{\frac{E_{TK} - E_{Crushing}}{E_{TK}}} \quad \text{or} \quad \kappa = \sqrt{\frac{E_{Soil-Pile}}{E_{TK}}} \quad (5-40)$$

Table 5-4, Table 5-5 and Table 5-6 summarize the numerical simulations and the corresponding computed velocity reduction factors. In the simulations involving three class of vehicles (medium-duty truck, pickup truck and sedan) and pile groups with various layouts, it was observed that the vehicle class contributes more to the reduction factor than the barrier stiffness. However in the case of the single piles, the barrier and soil stiffness plays a more important role than the vehicle class. Therefore, the recommendations for the velocity reduction factor are made according to the three vehicle classes. For the medium-duty truck (M), pickup truck (P) a crushing factor of 0.8 and for the vehicle class passenger car (C), a crushing factor of 0.4 is suggested.

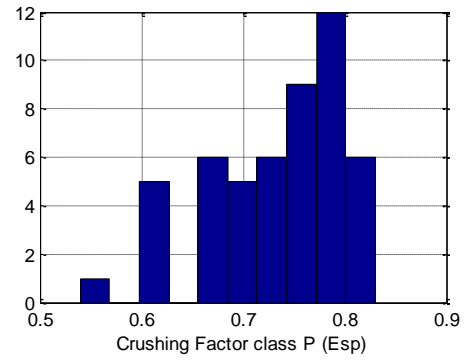
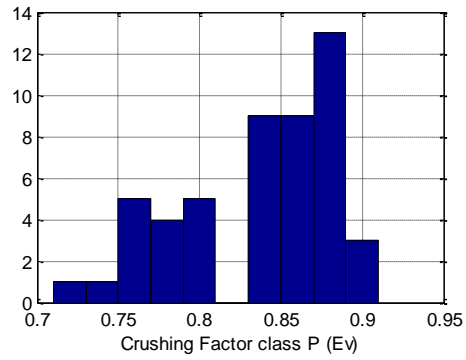
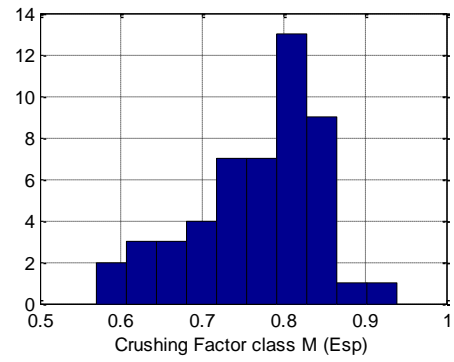
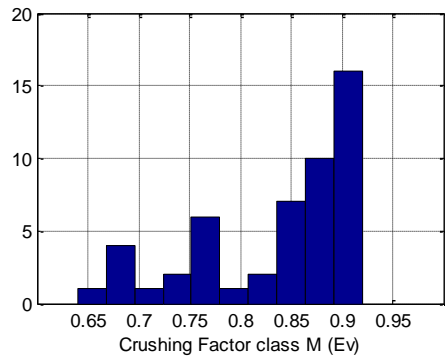


**Figure 5-16: Crushing factor for vehicle classes M and P**

**Table 5-4: Vehicle velocity reduction factor: Medium duty truck (M)**

No. Test	Vehicle Mass (kg)	Vehicle Velocity (m/s)	Vehicle Total Kinetic Energy ETK (kJ)	Barrier total Internal energy ESoilPile (kJ)	Vehicle total Internal energy EV (kJ)	Kapa from ESoilPile	Kapa from EV
1	6800	26.82	1605.60	745.00	654.00	0.68	0.77
2	6800	26.82	1605.60	760.93	670.00	0.69	0.76
3	6800	22.35	1060.00	633.30	353.90	0.77	0.82
4	6800	22.35	1060.00	662.50	275.70	0.79	0.86
5	6800	26.82	1605.60	646.00	723.90	0.63	0.74
6	6800	17.88	627.00	261.30	325.00	0.65	0.69
7	6800	26.82	1605.90	965.00	335.00	0.78	0.89
8	6800	26.82	1605.90	760.00	675.00	0.69	0.76
9	6800	17.88	627.30	201.00	373.00	0.57	0.64
10	6800	22.35	1060.20	676.00	210.00	0.80	0.90
11	6800	17.88	627.30	230.00	343.00	0.61	0.67
12	6800	26.82	1605.60	521.00	836.50	0.57	0.69
13	6800	22.35	1060.20	549.00	373.00	0.72	0.81
14	6800	26.82	1605.60	849.50	575.00	0.73	0.80
15	6800	26.82	1605.60	834.80	629.50	0.72	0.78
16	6800	22.35	1060.00	731.50	277.00	0.83	0.86
17	6800	22.35	1060.00	750.00	211.00	0.84	0.89
18	6800	26.82	1605.60	770.00	643.70	0.69	0.77
19	6800	17.88	627.00	294.00	309.70	0.68	0.71
20	6800	26.82	1605.90	1123.00	282.60	0.84	0.91
21	6800	26.82	1605.90	834.00	631.10	0.72	0.78
22	6800	17.88	627.30	251.00	347.00	0.63	0.67
23	6800	22.35	1060.20	800.00	194.00	0.87	0.90
24	6800	17.88	627.30	301.70	294.00	0.69	0.73
25	6800	22.35	1060.20	682.00	284.50	0.80	0.86
26	6800	22.35	1605.00	1064.00	365.90	0.81	0.88
27	6800	22.35	1605.00	1023.00	374.60	0.80	0.88
28	6800	22.35	1605.00	1056.00	309.37	0.81	0.90
29	6800	22.35	1605.00	1036.00	304.00	0.80	0.90
30	6800	22.35	1605.00	1106.00	284.63	0.83	0.91
31	6800	22.35	1605.00	1040.00	359.70	0.80	0.88
32	6800	22.35	1605.00	919.39	423.00	0.76	0.86
33	6800	22.35	1605.00	1067.00	323.60	0.82	0.89
34	6800	22.35	1605.00	1025.00	294.50	0.80	0.90
35	6800	22.35	1605.00	990.00	329.00	0.79	0.89
36	6800	22.35	1605.00	875.00	407.00	0.74	0.86
37	6800	22.35	1605.00	1162.00	266.00	0.85	0.91
38	6800	22.35	1605.00	1118.50	262.58	0.83	0.91
39	6800	22.35	1605.00	1084.00	299.00	0.82	0.90
40	6800	22.35	1605.00	1007.00	345.00	0.79	0.89
41	6800	22.35	1605.00	1040.00	253.16	0.80	0.92
42	6800	22.35	1605.00	1015.00	337.00	0.80	0.89
43	6800	22.35	1605.00	936.00	274.70	0.76	0.91
44	6800	22.35	1605.00	827.00	433.00	0.72	0.85
45	6800	22.35	1605.00	1172.00	260.46	0.85	0.92
46	6800	22.35	1605.00	1079.00	358.50	0.82	0.88
47	6800	22.35	1605.00	876.00	423.00	0.74	0.86
48	6800	22.35	1605.00	1415.00	268.00	0.94	0.91
49	6800	22.35	1605.00	1105.00	257.60	0.83	0.92
50	6800	22.35	1605.00	1113.00	289.60	0.83	0.91

**Table 5-5: Vehicle velocity reduction factor: Pickup truck (P)**

No. Test	Mass of vehicle Mv (kg)	Velocity of vehicle Vv (m/s)	Vehicle Total Kinetic Energy ETK (kJ)	Barrier total Internal energy ESoilPile (kJ)	Vehicle total Internal energy EV (kJ)	Kapa from ESoilPile	Kapa from EV
1	2300	17.88	383.82	148.00	145.24	0.62	0.79
2	2300	22.35	590.64	224.70	233.60	0.62	0.78
3	2300	22.35	590.00	272.70	167.00	0.68	0.85
4	2300	26.82	843.52	418.10	234.00	0.70	0.85
5	2300	17.88	383.80	149.90	155.38	0.62	0.77
6	2300	26.82	843.50	384.03	218.45	0.67	0.86
7	2300	26.82	843.50	405.14	195.35	0.69	0.88
8	2300	22.35	590.64	209.31	243.46	0.60	0.77
9	2300	17.88	383.80	143.70	166.00	0.61	0.75
10	2300	17.88	383.80	165.04	157.70	0.66	0.77
11	2300	22.35	590.64	277.60	163.00	0.69	0.85
12	2300	17.88	383.80	110.46	188.40	0.54	0.71
13	2300	17.88	383.80	185.50	130.90	0.70	0.81
14	2300	22.35	590.64	256.70	208.00	0.66	0.80
15	2300	22.35	590.64	340.70	149.90	0.76	0.86
16	2300	26.82	843.50	485.40	169.04	0.76	0.89
17	2300	17.88	383.80	188.54	162.44	0.70	0.76
18	2300	26.82	843.50	439.58	206.17	0.72	0.87
19	2300	26.82	843.50	455.00	186.45	0.73	0.88
20	2300	17.88	383.80	169.10	150.21	0.66	0.78
21	2300	26.82	843.50	449.70	228.60	0.73	0.85
22	2300	26.82	843.50	530.00	202.50	0.79	0.87
23	2300	26.82	843.50	502.00	151.70	0.77	0.91
24	2300	22.35	590.70	363.50	137.00	0.78	0.88
25	2300	26.82	843.50	527.00	208.10	0.79	0.87
26	2300	26.82	843.50	479.00	166.00	0.75	0.90
27	2300	17.88	383.30	218.00	136.00	0.75	0.80
28	2300	26.82	843.50	455.00	181.70	0.73	0.89
29	2300	26.82	843.50	490.00	208.00	0.76	0.87
30	2300	17.88	383.30	242.00	111.00	0.79	0.84
31	2300	17.88	383.30	243.90	114.00	0.80	0.84
32	2300	17.88	383.30	242.00	111.00	0.79	0.84
33	2300	26.82	843.50	477.00	196.00	0.75	0.88
34	2300	17.88	383.00	209.00	146.00	0.74	0.79
35	2300	26.82	843.50	481.00	219.00	0.76	0.86
36	2300	26.82	843.50	518.00	152.60	0.78	0.91
37	2300	17.88	383.00	222.50	134.75	0.76	0.81
38	2300	26.82	843.00	511.00	182.00	0.78	0.89
39	2300	26.82	843.50	525.30	220.40	0.79	0.86
40	2300	26.82	843.50	510.00	195.60	0.78	0.88
41	2300	26.82	843.50	562.00	192.00	0.82	0.88
42	2300	26.82	843.50	579.00	195.00	0.83	0.88
43	2300	22.35	590.70	401.00	120.00	0.82	0.89
44	2300	26.82	843.50	554.00	203.00	0.81	0.87
45	2300	17.88	383.50	231.00	133.00	0.78	0.81
46	2300	26.82	843.50	445.00	186.00	0.73	0.88
47	2300	17.88	383.50	253.00	116.00	0.81	0.84
48	2300	17.88	383.50	260.00	104.00	0.82	0.85
49	2300	26.82	843.50	527.00	168.00	0.79	0.89
50	2300	26.82	843.00	385.60	358.32	0.68	0.76

**Table 5-6: Vehicle velocity reduction factor: Passenger car (C)**

No. Test	Vehicle Mass Mv (kg)	Vehicle Velocity Vv (m/s)	Total Kinetic Energy ETK (kJ)	Barrier Internal energy ESoilPile (kJ)	Vehicle Internal energy EV (kJ)	Kapa from ESoilPile	Kapa from EV
1	800	17.88	130.00	39.20	100	0.55	0.48
2	800	22.35	190.90	46.80	167	0.50	0.35
3	800	22.35	190.90	39.90	171	0.46	0.32
4	800	17.88	130.00	24.19	116	0.43	0.33
5	800	17.88	130.00	24.19	116	0.43	0.33

### 5.7. Characterizing damping

Damping represents resistance to deformations when velocities are present. As discussed earlier, damping can be either due to material effects or hysteresis energy consumed by unloading and reloading of the material. Depending on the case either or both types of damping may be most prevalent.

In the damping expression proposed in this work (Eq. 5-34), the *Alpha* factor remains to be determined. This can be done by comparing the TAMU-POST predictions to the available experimental data (two full scale testes) and numerical simulations (about 60 different random cases) and ensuring a best fit. As part of this study, an effort was made to simulate adequately large number of different random cases, described in Section 4. Once the optimum *Alpha* factor is achieved by matching for each experiment and LS-DYNA simulation, a correlation was developed between these alpha values and the influential factors that were identified through analyses.

The analyses suggested that the *Alpha* factor increases primarily with the soil strength. This trend exists for both vehicle classes: the medium-duty truck and the pickup truck P, while the variation is more pronounced for the former than the latter. Figure 5-17 displays the correlation between the damping factor *Alpha* and the soil strength represented by the pressuremeter limit pressure  $P_L$  for two classes of vehicle. The best agreement by a least square approximation was sought.

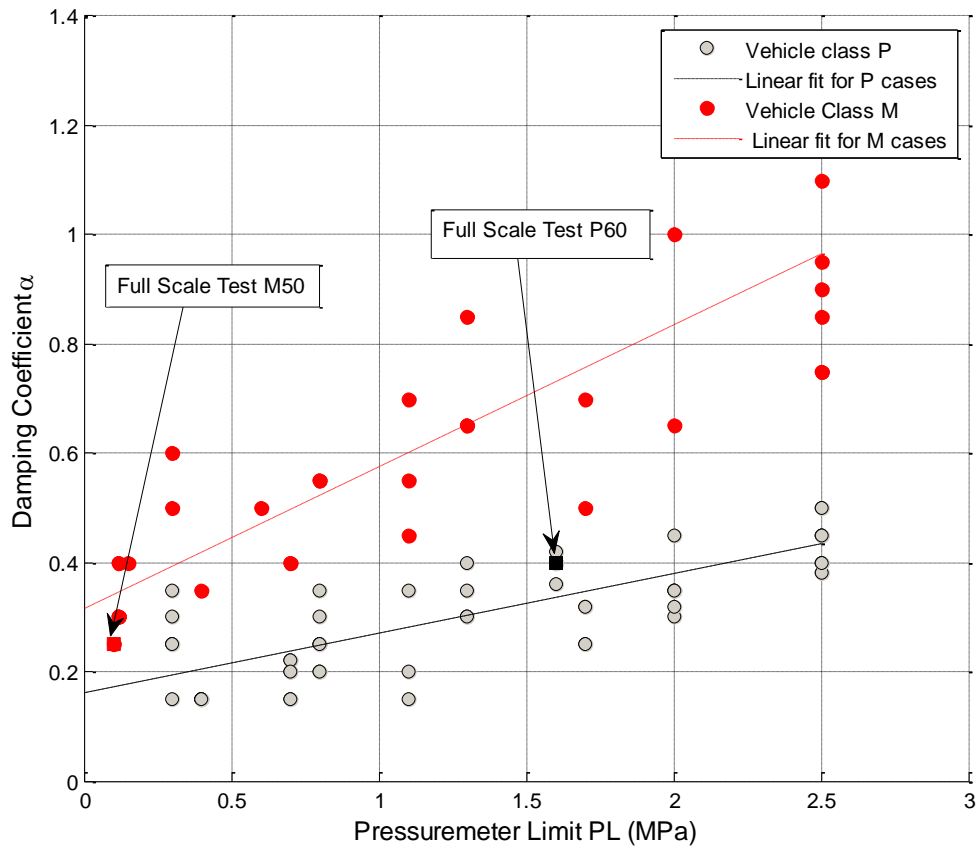


**Figure 5-17: Damping factor *Alpha* versus soil pressuremeter limit pressure  $P_L$**

Figure 5-17 shows that the *Alpha* factor increases with soil strength and the impact level as it was expected. Novak et al. suggests a similar soil behavior in the nonlinear time domain analysis of lateral response of piles observing stronger nonlinear effects in stiffer soils.

As in the case of vehicular impacts studied, with reasonable accuracy for design work, two separate linear equations were derived to characterize the *Alpha* in the damping formulations:

$$\text{For the medium-duty truck M} \quad \alpha = 0.25P_L + 0.3 \quad (5-41)$$

$$\text{For the pickup truck P} \quad \alpha = 0.1P_L + 0.15 \quad (5-42)$$

Later this section, the accuracy of the model to predict the pile deformation using this *Alpha* factor is evaluated, and the following section treats alpha as a random variable and accordingly examines the probabilistic model predictions.

### **5.8. Dynamic penetration**

The model as described above predicts the maximum beam deflection; however the critical measure of interest in design work is the dynamic penetration. As earlier mentioned, it is defined as distance between the front edge of vehicle flatbed and the initial location of the piles at maximum displacement during the impact. To determine this measure additional analyses are necessary to estimate the length  $L_{\text{crushed}}$ :

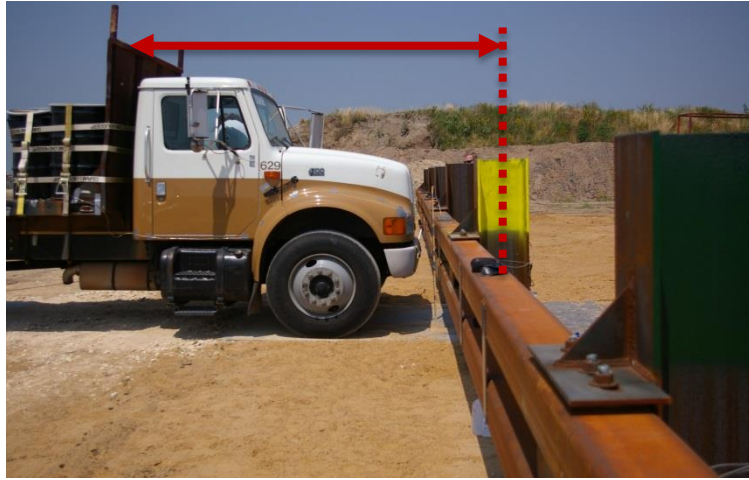


**Figure 5-18: Dynamic penetration**

The length  $L_{\text{crushed}}$  refers to the distance between the crushed position of the bumper and the front edge of the flatbed. Cautious estimates of the crushed length  $L_{\text{crushed}}$  were obtained by crashing numerically each class of vehicle against a rigid wall. Table 5-7 summarizes the results. This table gives the smallest value of  $L_{\text{crushed}}$  and therefore a conservative estimate of the dynamic penetration DP through Eq. 5-43:

$$DP = D_{\text{max}} - L_{\text{Crushed}} \quad (5-43)$$

Where  $D_{\text{max}}$  is the maximum deflection of the beam as given by TAMU-POST (group)

Table 5-7 is embedded in TAMU-POST (Group). As it is noted, large trucks are apparently more stable and exhibit a relatively smaller crushing. And with higher traveling speed, vehicles show more intensive crushing which turns to smaller values of  $L_{\text{crushed}}$ .



**Table 5-7: The obtained  $L_{crushed}$  from the numerical simulations**

	APPROACH SPEED		
	40 mph	50 mph	60 mph
TRUCK	1.9m	1.5m	1.1m
PICKUP TRUCK	1.8m	1.6m	1.4m
SEDAN	1.4m	0.9m	0.4m

LS-DYNA keyword deck by LS-PrePost  
Time = 0.02

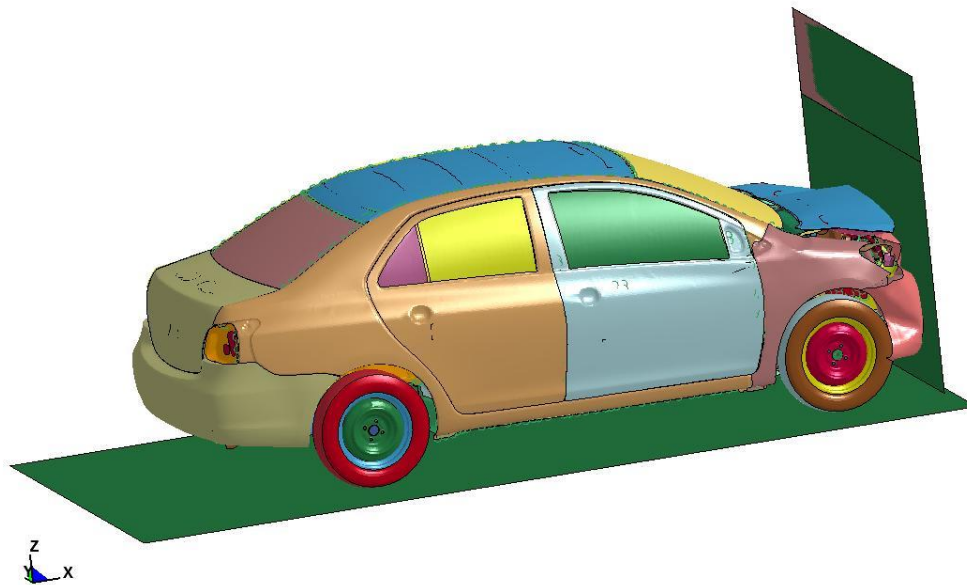


**Figure 5-19: The numerical simulation of a sedan (class C) impacting a rigid wall**

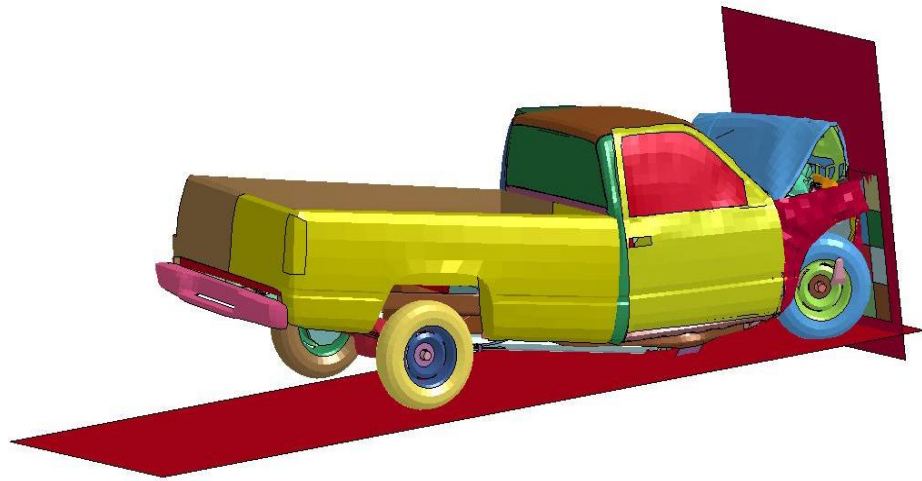


**Figure 5-20: The numerical simulation of a pickup truck (class P) impacting a rigid wall**

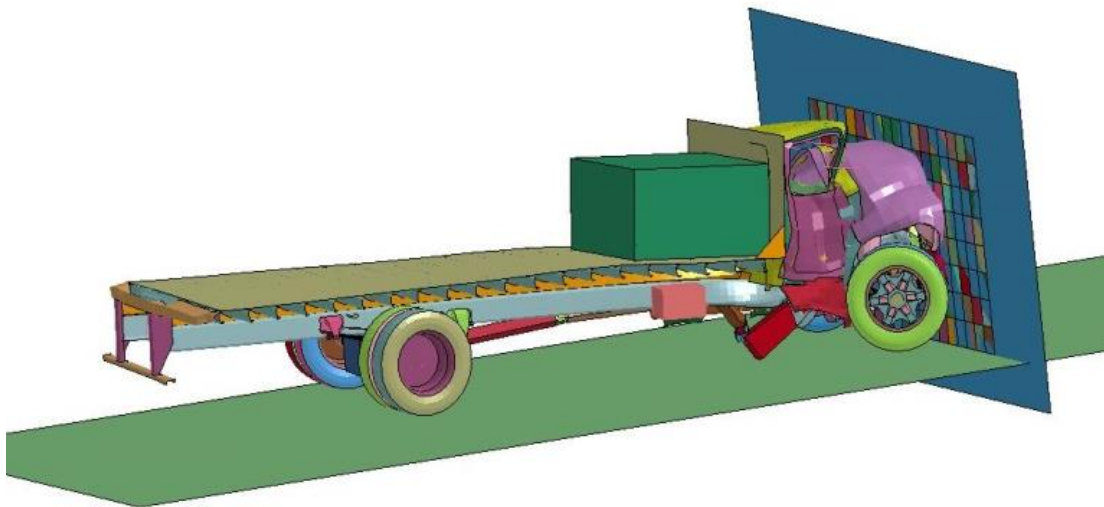


**Figure 5-21: The numerical simulation of a medium duty truck (class M) impacting a rigid wall**

## **6. MODEL VALIDATION AND PARAMETRIC STUDY**

### **6.1. Model validation**

Validation studies are crucial to offer designers and researchers reliable information on the model abilities and limitations. This section investigates the accuracy of the proposed method TAMU-POST (Group) to predict the primary components in design of pile groups. The model predictions including the maximum deflection, maximum bending moment in pile and beam are compared with the full scale tests results previously described in this dissertation as well as the validated LS-DYNA simulations.

In Section 5, it was explained that the space filling technique with Stratified Latin Hypercube Sampling (SLHS) design was used to generate a random collection of impact cases to ensure enough samples are selected from each categories of interest. There is still significant uncertainty about the inputs (such as soil properties) and the model parameters (such as crushing factor) which will be later addressed in a probabilistic study. Additional tests and simulations will help resolve this issue.

#### **6.1.1. Maximum deflection**

The dynamic penetration as the main design criterion is directly determined from the maximum deflection. Therefore first the ability of the program TAMU-POST (Group) is evaluated in terms of the maximum deflection prediction to match the behavior observed in the tests and numerical studies.

The results are reduced to produce the plots shown in Figure 6-1 and Figure 6-2 (log scale). Predicted maximum deflections by the analytical model are plotted versus the measured ones in numerical studies. The impact tests PU60 and M50 are also included.

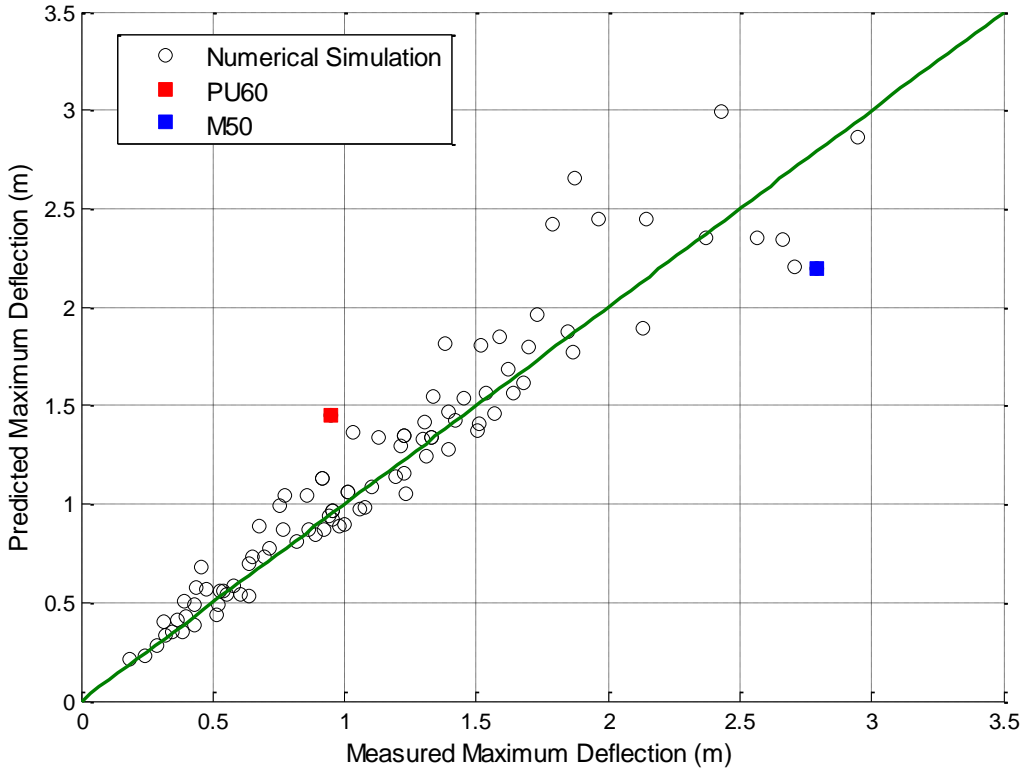


**Figure 6-1: Predicted versus measured maximum deflection**

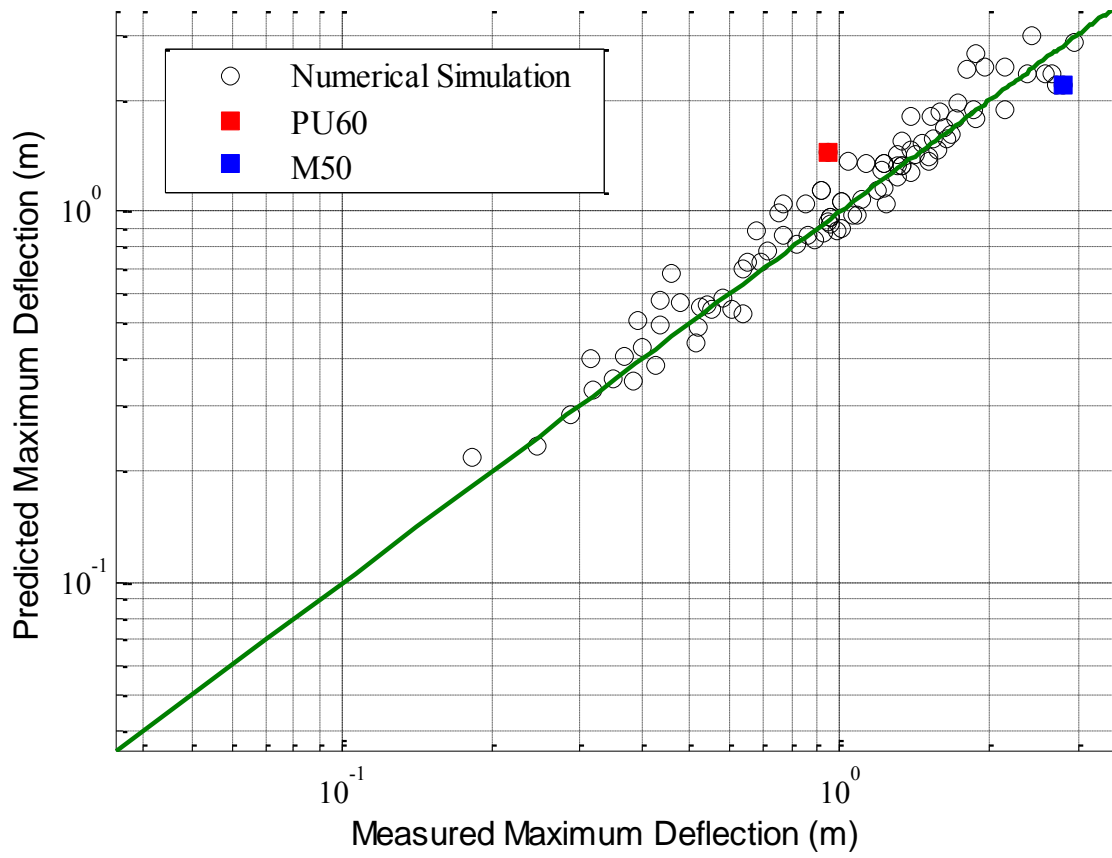


**Figure 6-2: Predicted versus measured maximum deflection (log scale)**

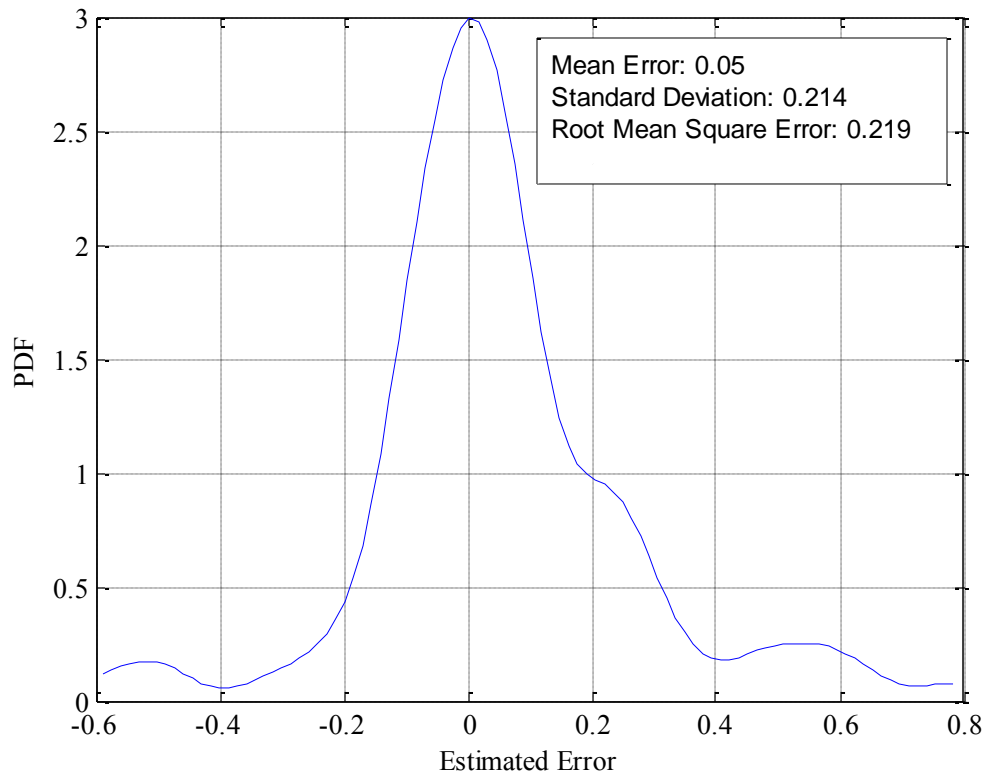


**Figure 6-3: The probability density function of the error in model prediction with respect to the maximum deflection**

TAMU-POST was found to provide reasonable and mostly conservative estimates of the lateral maximum deflection. Figure 6-1 and Figure 6-2 indicate more pronounced agreement between the measured and predicted result for cases with relatively smaller deflections (say less than 2 m). Figure 6-3 shows the probability density function of the error (Predicted deflection – Measured deflection). This figure and the subsequent figure (Figure 6-4) showing the ratio of predicted to measured deflection suggest that the model, while simpler and less computationally intensive than the numerical simulations, results in estimates comparable to those of the experiments and numerical solutions.

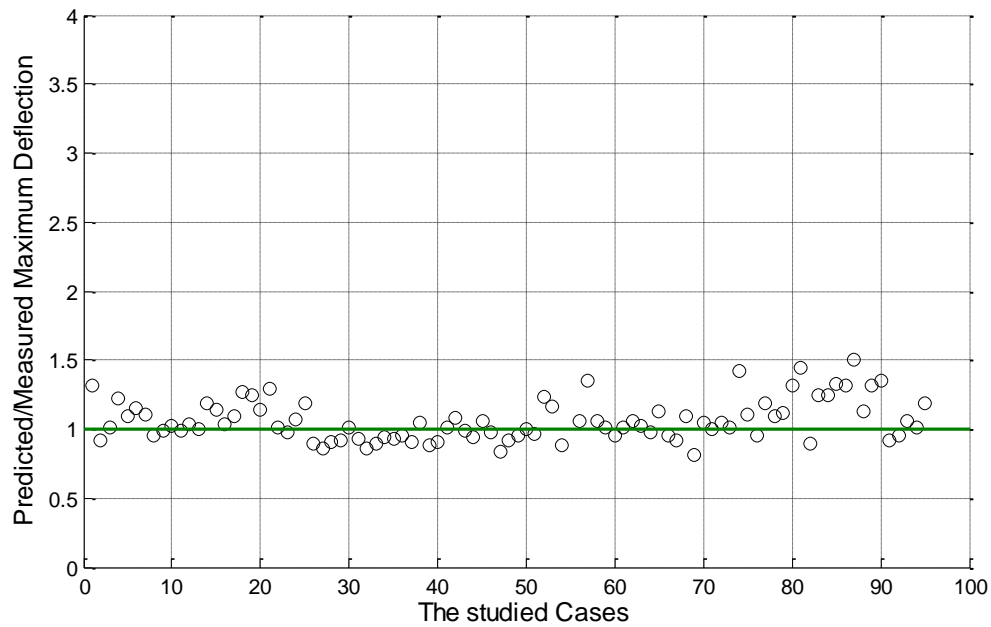


**Figure 6-4: Ratio of predicted over measured maximum deflection for 95 cases**

### **6.1.2. Maximum bending moment in the beam**

To examine further the ability of the model, the other output, maximum bending moment in beam was evaluated through comparison with the numerically obtained beam bending moment. The maximum moment is the largest moment along the length of beam. As plotted in Figure 6-5, the ratio of maximum bending moment predicted by TAMU-POST (Group) to the maximum bending moment obtained in associated simulations tends to increase by soil strength i.e. Limit Pressuremeter  $P_L$ .

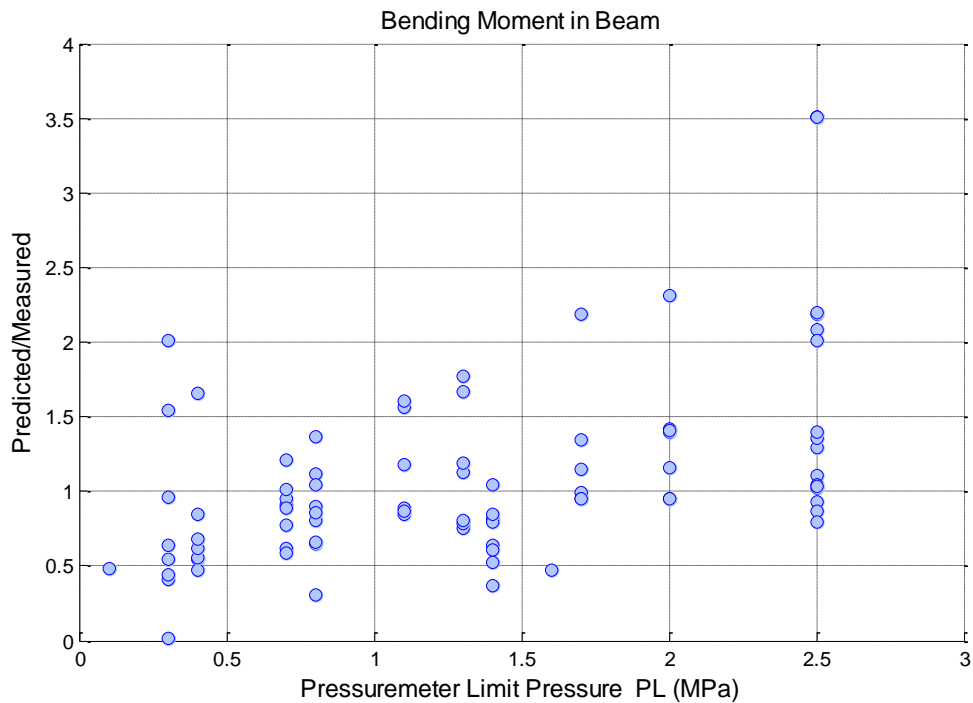


**Figure 6-5: Ratio of predicted over measured maximum bending in the beam versus the soil pressuremeter limit pressure**

Especially in the stiffer soils, as shown in Figure 6-5, TAMU-POST (Group) overestimates the maximum bending moment in beam, and the overestimation rate depends on soil conditions. In contrast, for very low strength soil cases the model predicts less bending moment than the measured data.

This overestimation is believed to attribute to the fact that the model theory neglects the beam becomes plastic under impact. As observed in both experiments and simulations, beam and piles are most likely to exhibit plastic behavior in extreme loading. This issue is continued to be unresolved since the model is not designed to incorporate the structural plasticity. However for design, it is informative to indicate the model performance in moment predictions for a given soil condition. It is important



point out that, the computed bending moment in pile and beam are overestimated and not recommended as design measures. To investigate this, for each soil strength category (with different  $P_{LS}$ ) the mean ratio of predicted to measured moment in beam versus the associated  $P_L$  is plotted in Figure 6-6. The best curve fitted is also included.

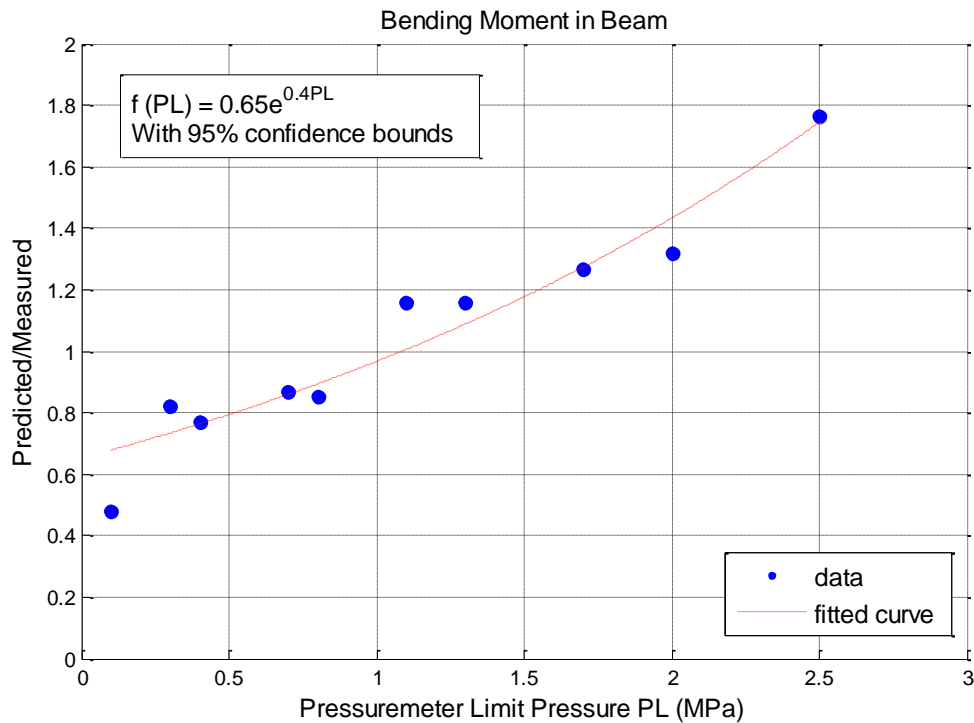


**Figure 6-6: Predicted over measured maximum bending in the beam versus soil pressuremeter limit pressure**

### 6.1.3. Maximum bending moment in the pile

Similar to the beam bending moment predictions, the ratio of predicted to measured moment in the pile (Figure 6-7) suggests that the model overestimates the maximum pile moment. However, this overestimation is less notable in high strength soils. The maximum moment in pile is referred to the largest moment along the length of pile. This

higher moment is due to the fact that the SALLOP approach, that was adopted to calculate the pile moment is essentially for static loading and it relies on the elastic theory. In addition, the input forces for the SALLOP method were chosen based on the impact forces calculated by the program TAMU-POST (Group). It induces a secondary inaccuracy into the moment results.

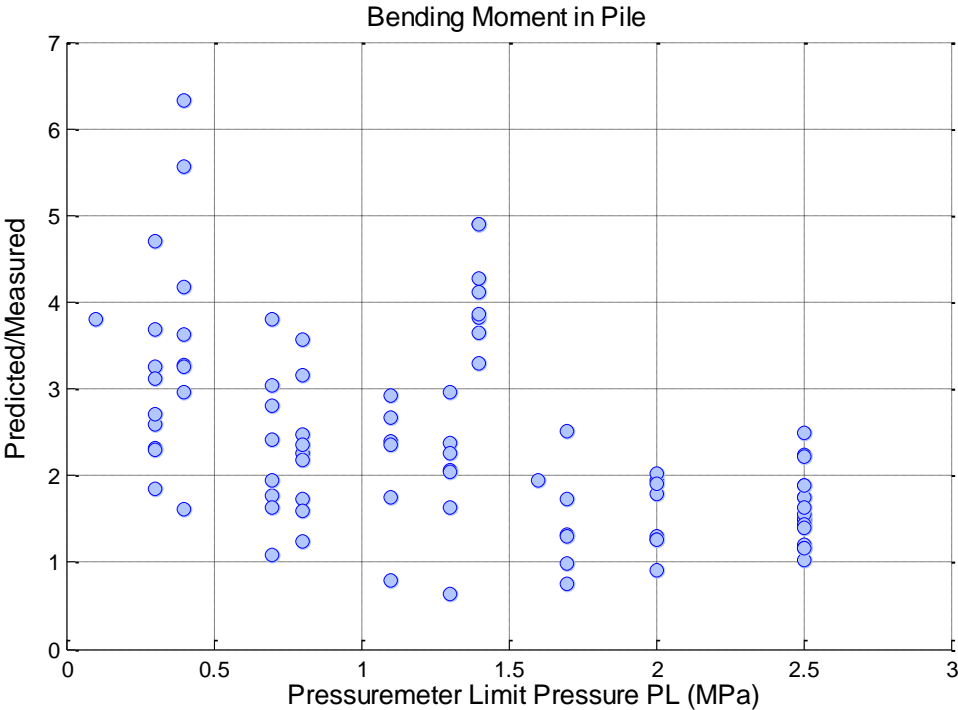


**Figure 6-7: Ratio of predicted over measured maximum bending in the beam versus soil pressuremeter limit pressure**

Again, a plot is provided (Figure 6-8) to give a better insight on the program limitation regarding moment predicting.

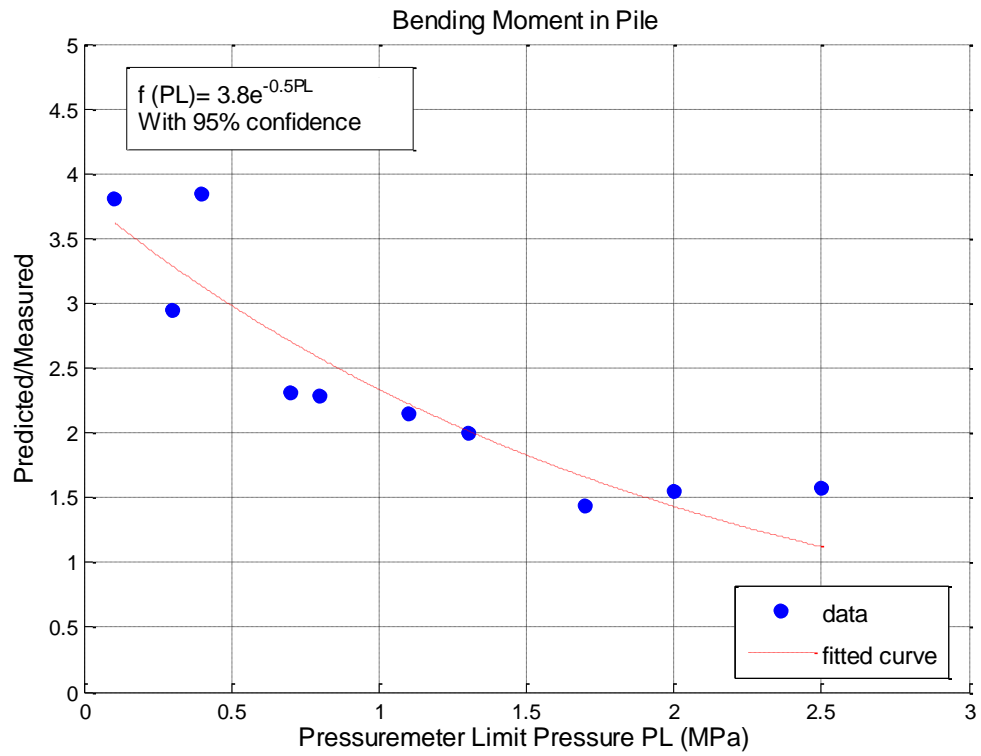


**Figure 6-8: Ratio of predicted over measured maximum bending moment in the beam versus the soil pressuremeter limit pressure**

## 6.2. Parametric study and design insights

It is essential to comprehend the influence of contributing factors on the impact performance of piles to select a pile configuration capable of offering the required resistance against a desired impact level while accepting a predetermined deformation (e.g. 1m for P1 test designation in ASTM F2656). A parametric study on impact response of pile groups offers helpful insights on critical geometric and geomechanic characteristics of pile groups for a functional and economical design. Using the simple analytical approach TAMU-POST (Group), the proposed model that has been earlier proven to compare well to 3D LSDYNA numerical simulations, this section parametrically studies the variation of factors affecting the ultimate resistance of pile groups under impacts. For selected cases numerical data are added and compared to TAMU-POST data points to illustrate the effectiveness of the developed method.

In this analysis, the main parameters including mass and velocity of vehicle ( $M_v$  and  $V_v$ ), soil strength (in terms of soil pressuremeter limit pressure  $P_L$ ), pile embedment depth ( $L$ ), the ratio of pile spacing to the pile width or diameter ( $S/D$ ) are investigated. The analyses are performed considering two different cases: a four-pile (HSS6x6x1/2) under impact of a 2300 kg pickup truck (P) and an eight-pile impacted by a 6800 truck (M).

Additional factors such as the number of piles, varying pile and beam bending stiffness ( $EI_{pile}$  and  $EI_{beam}$ ) are addressed to provide information on contribution of structural elements in response of pile groups subjected to vehicular impacts. As the model theory bases on three main inputs estimation Mass (M), Damping (C) and

Stiffness (K) it seems worthy to examine the sensitivity of the model precision to the primary model inputs M, C and K. This analysis presents the effect of these inputs variation on the model results.

### **6.2.1. Effect of pile spacing and pile embedment depth**

Two important features in pile groups design are pile spacing and embedment depth. To derive insight on the critical pile spacing and depth to resist a given scenario, two extreme cases are studied, S/D and L ranging from 10 to 50 and 1 m to 2.5 m, respectively. Figure 6-9 and Figure 6-10 illustrate how the maximum deflection of the barrier varies by the ratio of pile spacing to the pile width (S/D) having different pile depths for the prescribed cases. These plots offer the critical embedment depth and the corresponding S/D for a given case.

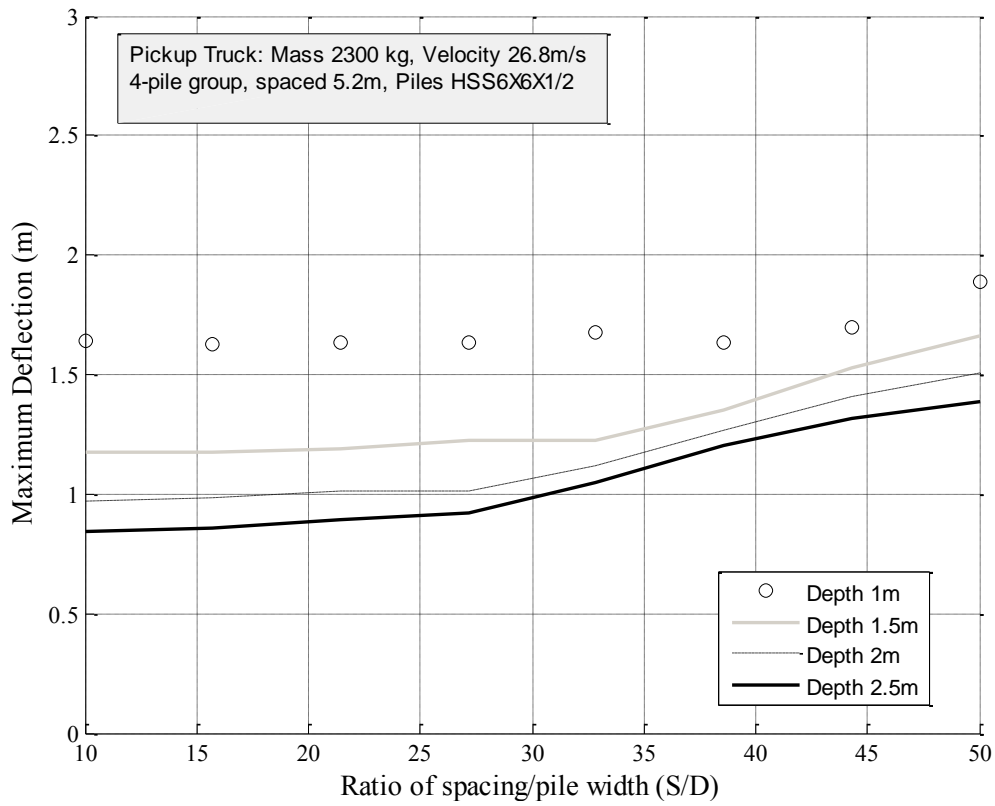


**Figure 6-9: The effect of pile spacing and pile embedment depth for the four-pile group**

For example, for the small piles (HSS6X6X1/2) (Figure 6-9) in the case of 4-pile group, pile depth of 1 m apparently is not enough to resist the impact PU60 no matter of pile spacing. As the depth increases, pile spacing affect slightly the response linearly. After a critical S/D (~26 for this particular case) the deflection increases dramatically. Therefore, given the enough embedment depth is met, this study should be considered to determine the most cost-effective pile spacing for the examined scenario.

Similarly for the large piles (W14X90) in the case of eight-pile group, it is shown that the deflection is linearly affected by the ratio of S/D. For this case of large piles the spacing is reasonably limited to S=20.

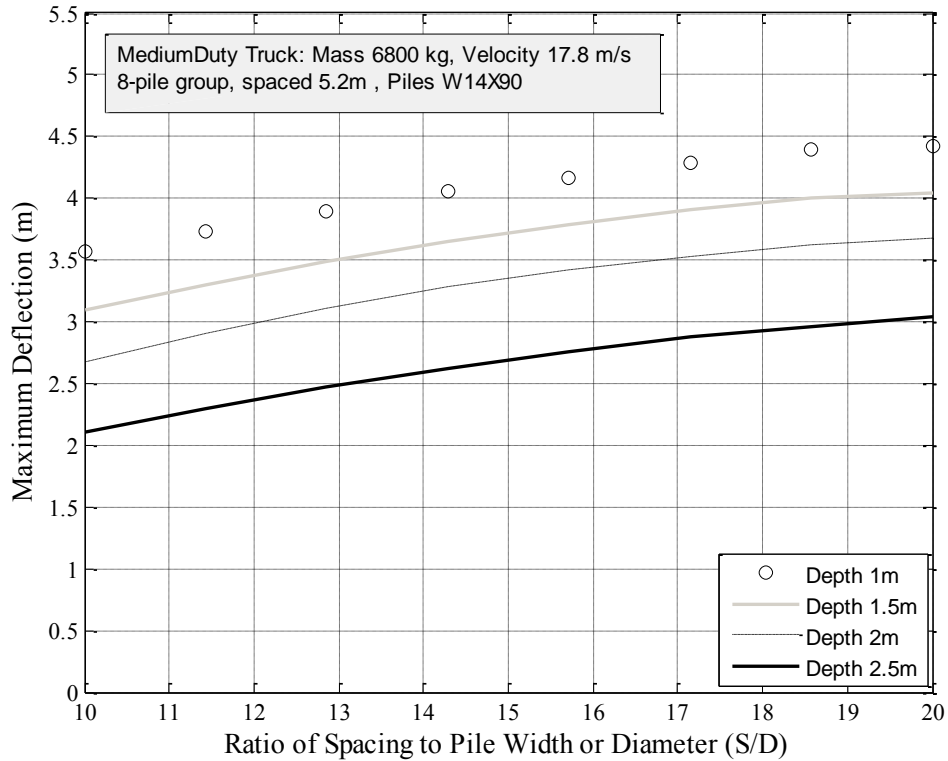


**Figure 6-10: The effect of pile spacing and pile embedment depth for the eight-pile group**

### 6.2.2. Effect of mass and velocity of vehicle

To design anti-ram barrier, it is worthy to examine the resistance of barrier against different extreme impact levels. Figure 6-11 provides information on how vehicle mass and velocity impact the barrier response. As expected, it is shown that the small barrier (four HSS6x6x1/2 piles) is more sensitive to the impact level rather than the larger

barrier of eight I-beam piles. This information allows a reasonable estimation of the barrier performance against any scenarios and threats that are probable based on the risk studies.

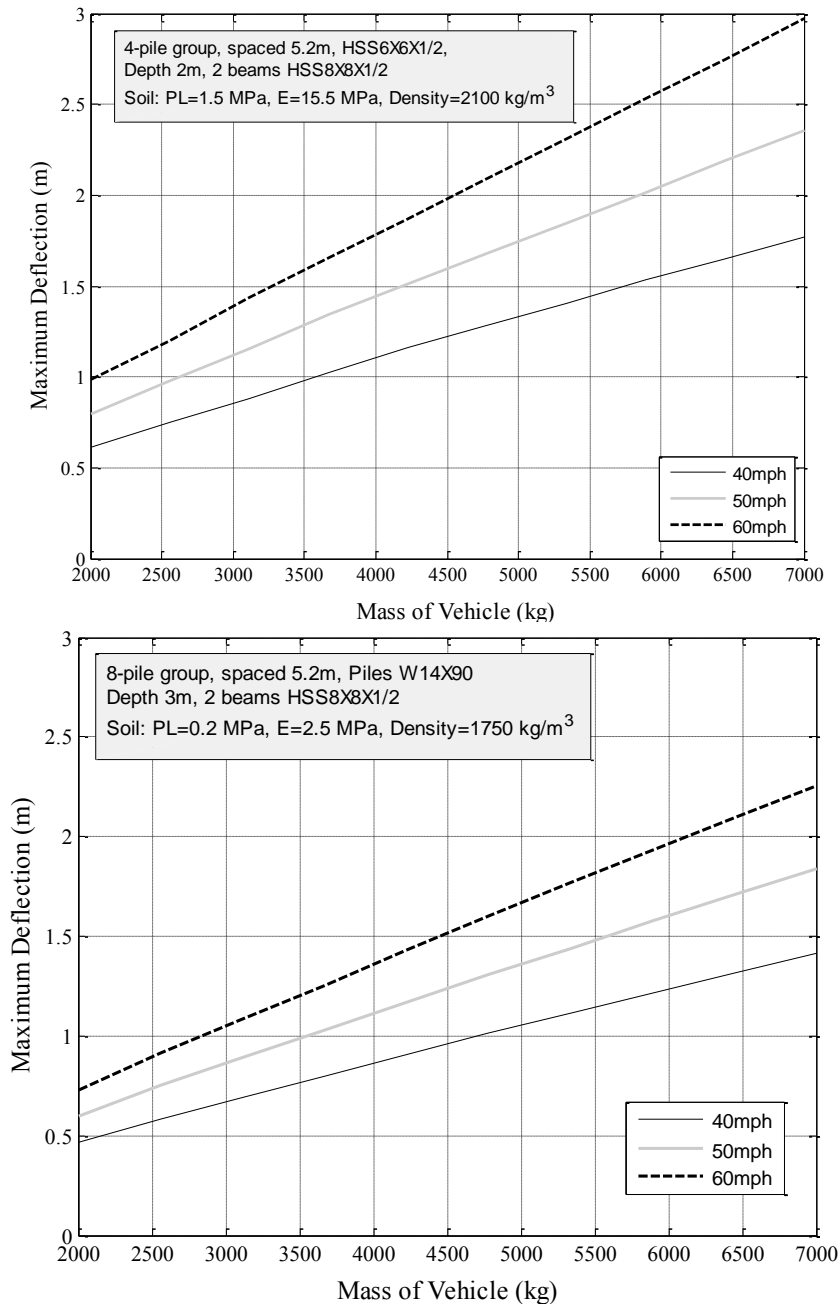


**Figure 6-11: The effect of mass and velocity of vehicle**



### **6.2.3. Effect of soil strength**

The governing role of soil-pile interaction on pile response is well recognized, however, it is hard to conclude on how soil and pile characteristics control the ultimate resistance. To comprehend this, the maximum deflection of two different barriers with different soil strength and pile depth is studied. The soil Pressuremeter Limit Pressure (PL) varies from 0.3 to 2.5 MPa (corresponds to very soft to very hard soil) and the considered depths are 1, 1.5 and 2 m.

As shown in Figure 6-12, it is interesting to notice that increasing the pile depth up to a certain depth significantly improves the performance, in particular, for relatively low strength soils. After a critical depth, the response does not largely get affected by the increased depth. Hereby, for an economic design it is strongly recommended to spot the critical depth for a given soil condition.

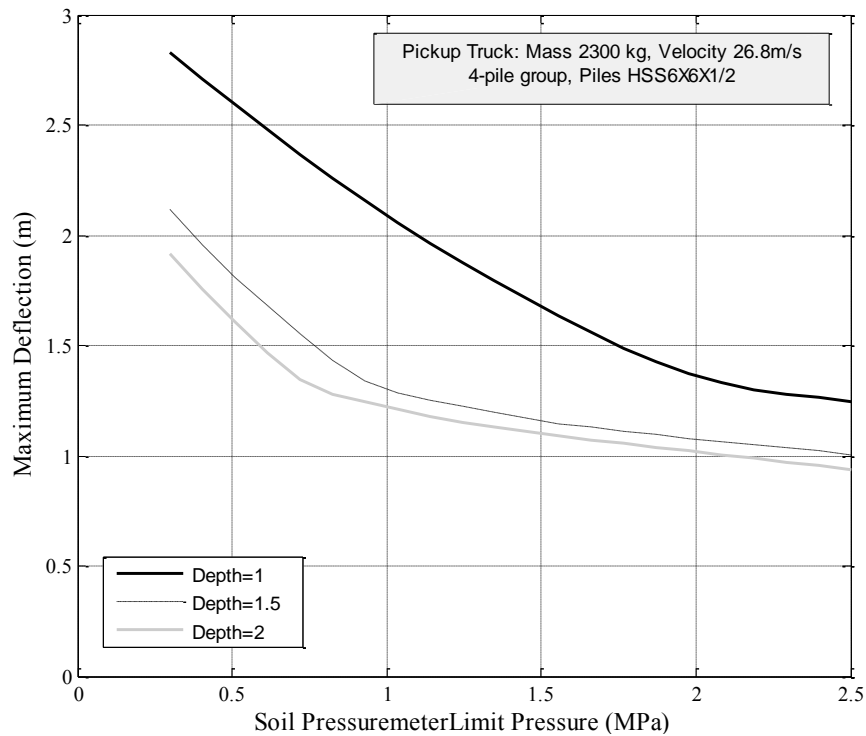


**Figure 6-12: The effect of soil strength and pile embedment depth for the four-pile group**

Soil strength is also projected to be important. Improving soil strength has a pronounced impact on the pile response. This effect gradually becomes less marked for high strength soil. Similar findings are applicable for the eight-pile group under the large impact with a different corresponding critical depth (Figure 6-13).

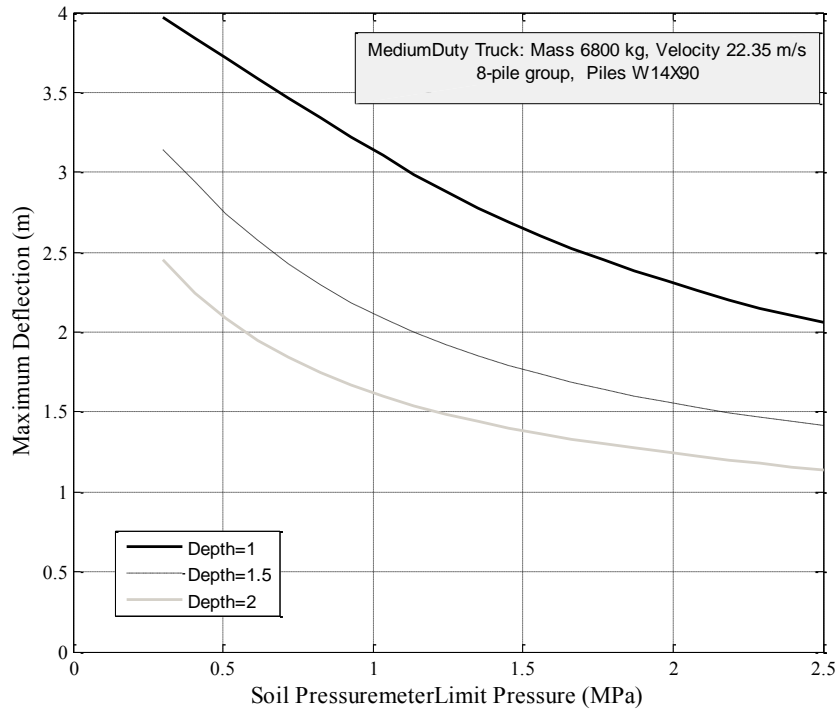


**Figure 6-13: The effect of soil strength and pile embedment depth for the eight-pile group**

#### 6.2.4. Effect of pile and beam bending stiffness

Structural capacity of piles and beams as the other contributing factor needs to be examined. Figure 6-14 and Figure 6-15 illustrate the variation of barrier deflection by bending stiffness of piles and beams for the 4-pile and 8-pile cases.

It is found that as the beam bending stiffness ( $EI$  where  $E$  is elastic modulus and  $I$  is moment inertia) increases, the barrier deflection drops more significantly compared to the case of increase in pile bending stiffness. Therefore, it can be concluded that the beam structural resistance has a greater impact on the response rather than the pile stiffness. The trends shown in the following figures are noteworthy as they suggest the required bending stiffness of piles and beam for the examined cases. For a cost effective

design it is highly recommended to generate the similar comparison to find the optimum pile and beam configurations.

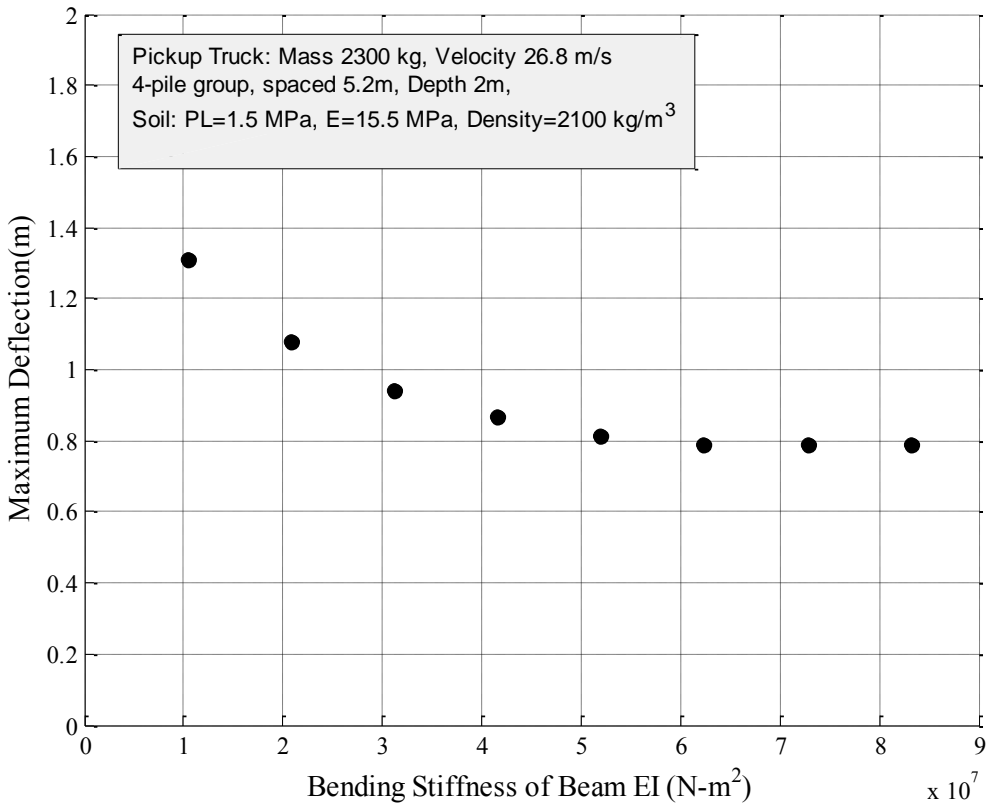


**Figure 6-14: The effect of beam bending stiffness**

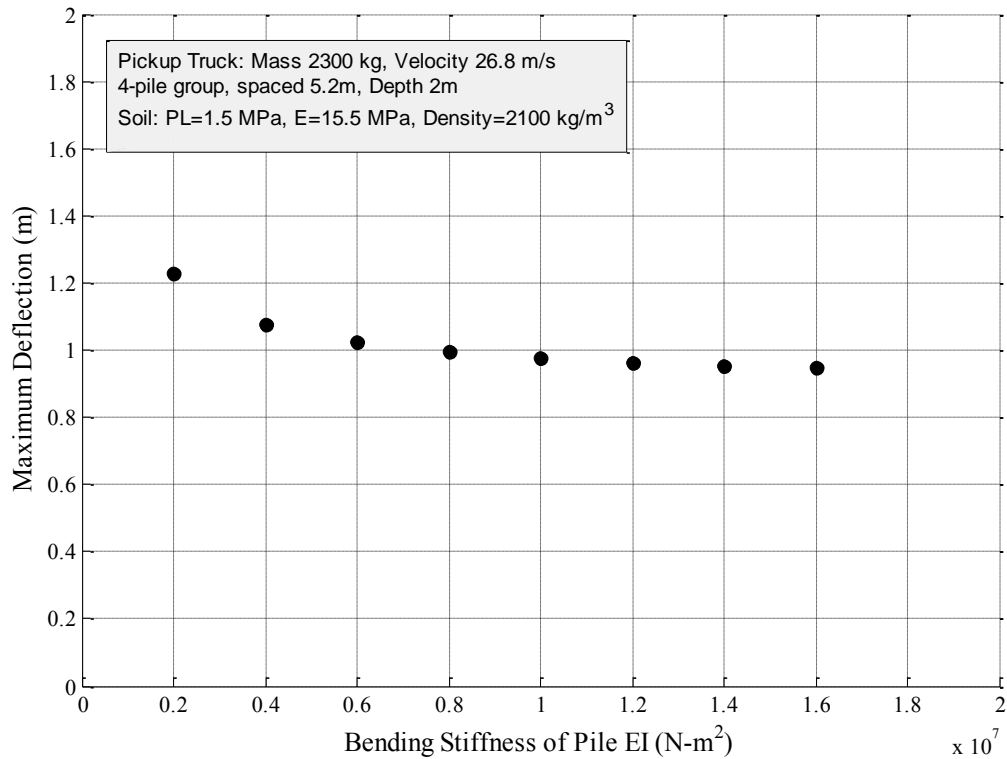


**Figure 6-15: The effect of pile bending stiffness**

### 6.2.5. Number of piles

One of the issues of interest was the effect of number of piles on the impact performance of the barrier. To investigate this, a series of analyses were performed on barriers with different numbers of piles impacted by a pickup truck traveling at 60 mph. The results are displayed in Figure 6-16. As illustrated in this figure,  $D_{max}$  evidently decreases with the pile number. However after a number of piles, for example 6 in this case, maximum deflection tends to remain constant and the response becomes insensitive to increasing number of piles. It is essential to find the number of piles actively contributing to the barrier response for any desired impact level.

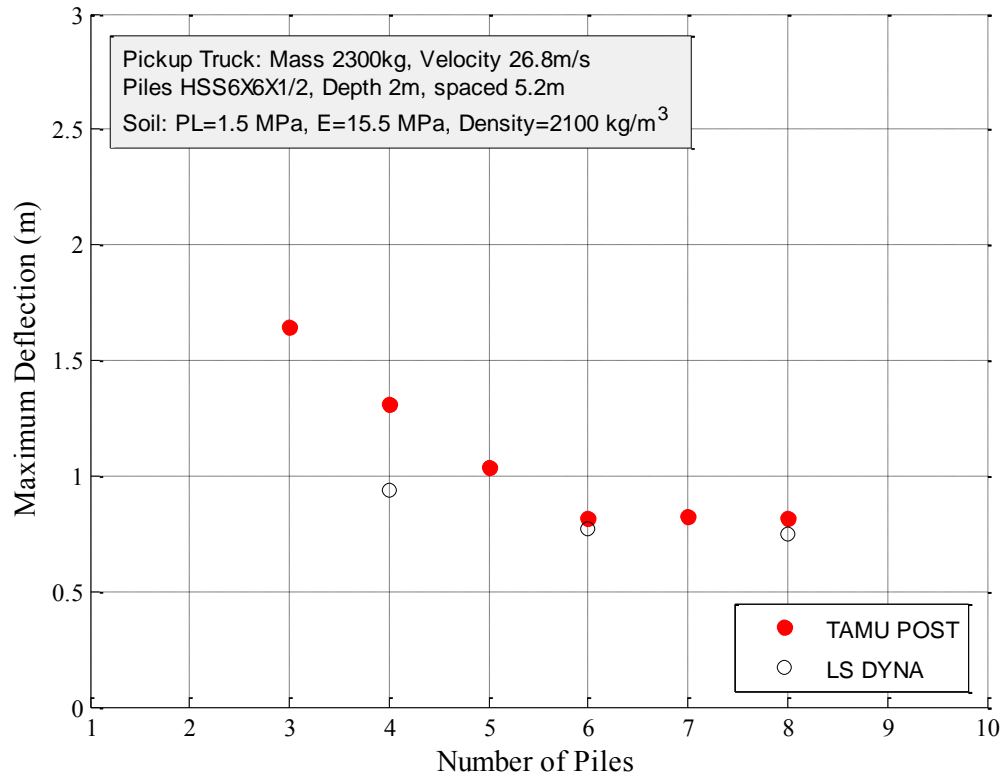


**Figure 6-16: The effect of number of piles**

### 6.2.6. Sensitivity analysis of M, C and K

The proposed model TAMU-POST uses several inputs to estimate the associated damping C, static stiffness K and the involved mass M to solve the main governing dynamic equation. There are inevitable uncertainties in determination of these inputs. It is helpful to understand the sensitivity of the model result to the precision in estimation of these prescribed parameters, M, C and K.

A case of 4-pile group with  $M_0$ ,  $C_0$  and  $K_0$  is considered as the reference. The factors M, C and K are varied ranging from one tenth to ten times of the reference values. In

Figure 6-17, the normalized maximum deflection (the ratio of  $D_{\max}$  to the  $D_{\max}$  of the reference case) is presented versus the normalized factor (0.1 to 10, the ratio of the  $M$ ,  $C$  and  $K$  factor to the associated values of the reference case).

It is found that the model result is primarily affected by the estimated damping. The inherent uncertainties in mass and stiffness determination are found less important.

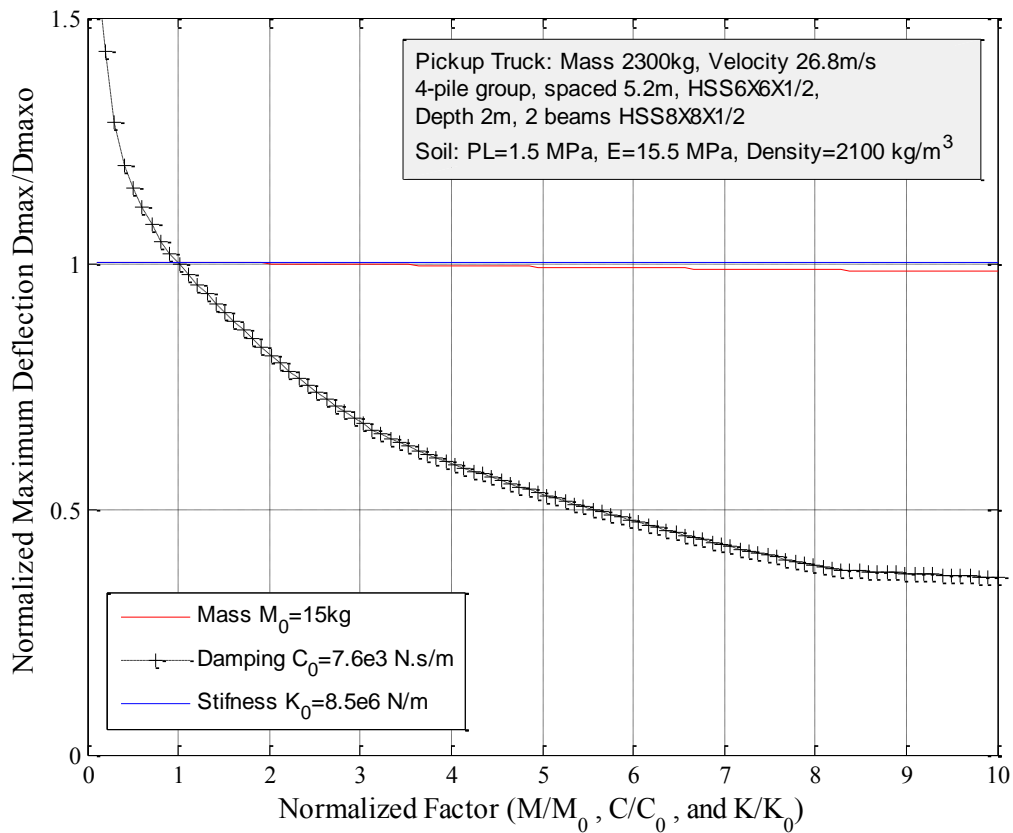


**Figure 6-17: The sensitivity of model result to mass, stiffness and damping estimation**

### **6.3. Reliability analysis of TAMU-POST**

The proposed model so far introduces a deterministic approach. In other words, the model predicts the response of a group of piles for a given set of input parameters and does not address the inherent uncertainties associated with the input parameters including heterogeneity of the soil deposit. On the other hand there is a bias associated with the theoretical model. The method assumes an elastic beam and models the pile and surrounding soil as a single degree of freedom with a dashpot and a spring which do not perfectly represent the real behavior of the system. Due to all these uncertainties the model does not give an absolute answer to the problem. Therefore it is recommended that further research continue to estimate a probability of failure associated with design.

Considering widely different impact scenarios along with the various possible pile configurations there is no single safety factor that can be applied to all impact conditions. For an economic design of such a complicated soil-pile system, it is necessary to perform a simple reliability analysis and quantify probability of failure associated with any potential design. This part of study offers the answer in the form of:

*With this given group of piles there is a probability of  $P$  that this certain truck will be contained.*

Having provided this information, it will be the responsibility of a designer to adopt the associated probability of failure based on the significance of the project. This target probability of success combined with the EXCEL program would be of great help in design of such systems.



In this respect, as a supplement to the deterministic proposed method, a robust Monte Carlo Simulation has been applied to TAMU-POST (Group) to evaluate the model reliability and to consider the randomness of the variables (Fenton & Griffiths, 2008; Ang & Tang, 2007). The theory of MCS is fully explained in many studies (e.g. Hahn and Shapiro, 1968; Morgan et al., 1992 and Rubinstein and Kroese, 2011). Despite simplicity in concept and application, this method provides an unbiased estimate of the probability of failure given sufficiently a large number of samples is considered. This method estimates the cumulative distribution function of the model output for the cases of highly complex model while it maintains the nonlinear essence of the model. It also allows for any nature and magnitude of the input uncertainties described in statistical terms.

In this work, the simplified solution involves varying degrees of uncertainties. These uncertainties correspond to both the input data particularly soil properties and the derived parameters through the model development process such as the crushing factor and *Alpha* factor.

The program TAMU-POST (Group) incorporated with the code of Monte Carlo Method computes the probability of failure for each criterion as follows:

$$P_f = P(y_t \geq y_{allowable}) = \int_F f(x)dx = \int I[y_t \geq y_{allowable}] \cdot f(x)dx \quad (6.1)$$

Where  $y_t$  refers to the computed output (dynamic penetration) and  $y_{allowable}$  denotes the corresponding allowable values. If failure reaches, the indicator  $I$  equals to 1.0.

### **6.3.1. Failure criterion**

This method basically involves running the model where the uncertain input parameters are varied randomly. The important design measure which is the maximum deflection of the beam for the current impact problems (service limit state) is computed using the program TAMU-POST for each set of random samples. Since this research concerns the dynamic penetration of the truck, the maximum deflection minus the  $L_{\text{crushed}}$  (i.e. maximum amount of overpassing of truck with respect to the initial position of the piles) should be limited to one meter. With emphasis of this research on the barrier maximum deflection and the test designation P1 according to the standard ASTM F2656-07, it is defined that the failure occurs when the dynamic penetration exceeds 1 m (the performance-based design). Past impact testing observations proved that the deflection-related design criterion is enough to assure that the structure does not fail due to the material failure and over exceeding capacity. Hereby the probability of failure corresponding to serviceability limit state is estimated.

### **6.3.2. Random variables and the probability distributions**

To capture the spatial variability of the inputs, soil properties including the pressure limit pressure ( $P_L$ ), the elastic modulus ( $E_s$ ) and the density ( $\rho$ ) were candidates as random variables with a lognormal distribution. This distribution is commonly accepted to describe the physical properties of soil in particular the strength parameters. It is worth noting that Poisson's ratio varies within a relatively narrow range (Griffith & Fenton, 2007). So it seems justifiable to neglect Poisson's randomness.

The proper values for coefficients of variation ( $CV = \sigma / \mu$ ) and the standard deviations  $\sigma$  of the geotechnical parameters are commonly estimated using the available data and engineering knowledge. For widely common in-situ testing methods, the literature values of the coefficients of variation are given in Table 6-1 (Kulhawy and Trautmann 1996). These values are corresponding to the measurement uncertainty arising from the systematic testing error (equipment and operator effects) and random testing error. The Pressuremeter test has been found to be largely dependent on type of the boring and the test conditions. In this study, coefficient of variation of 0.2 was assumed for the  $P_L$ . Figure 6-18 illustrates the PDFs of the soil random parameters.

**Table 6-1: Coefficients of variation for in situ testing methods (Kulhawy and Trautmann 1996)**

Test	Equipment	Operation	Random	Range
Standard penetration test	0.05-0.075	0.05-0.75	0.12-0.15	0.15-0.45
Cone Penetration Test (CPT)	0.05	0.1-0.15	0.1-0.15	0.15-0.25
Vane Shear Test (VST)	0.05	0.08	0.1	0.1-0.2
Pressuremeter Test, pre-bored	0.05	0.12	0.1	0.1-0.2
Pressuremeter Test, self-boring (PMT)	0.08	0.15	0.08	0.15-0.25

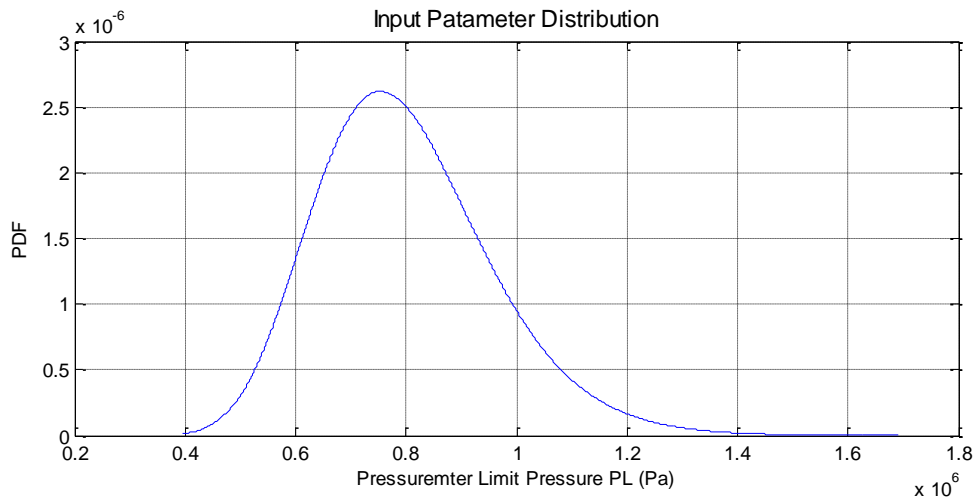


**Figure 6-18: The probability distribution of the random input parameter**

In addition, as earlier discussed, the analytical model uses a crushing factor to account for the energy absorption due to the crushing of the vehicle front part and an *Alpha* factor to calibrate damping  $C$ . Both factors were determined by analyzing a number of numerical simulations and two full scale tests. It is essential to examine the uncertainty in estimation of these model parameters. Therefore the crushing factor and the *Alpha* damping factor are further assumed random variables.

These variables may be correlated or independent. The *Alpha* factor is defined as a function of limit pressure of the soil ( $P_L$ ). Herein, the mean value for the *Alpha* factor was determined using the random  $P_L$  and then an independent distribution for the *Alpha* factor was defined and used in the MCS. Structural parameters including  $S/D$  (the ratio of pile spacing to pile width or diameter), embedment depth, impact level, and pile, beam sections are considered non-random. Table 6-2 summarizes the statistical features of the prescribed distributions.

**Table 6-2: The random variables and their statistical features**

	Parameter	Distribution	Coefficient of variation
Model Parameters	Crushing Factor	Lognormal	0.05
	Alpha Factor	Lognormal	0.1
Soil Properties	PL (MPa)	Lognormal	0.2

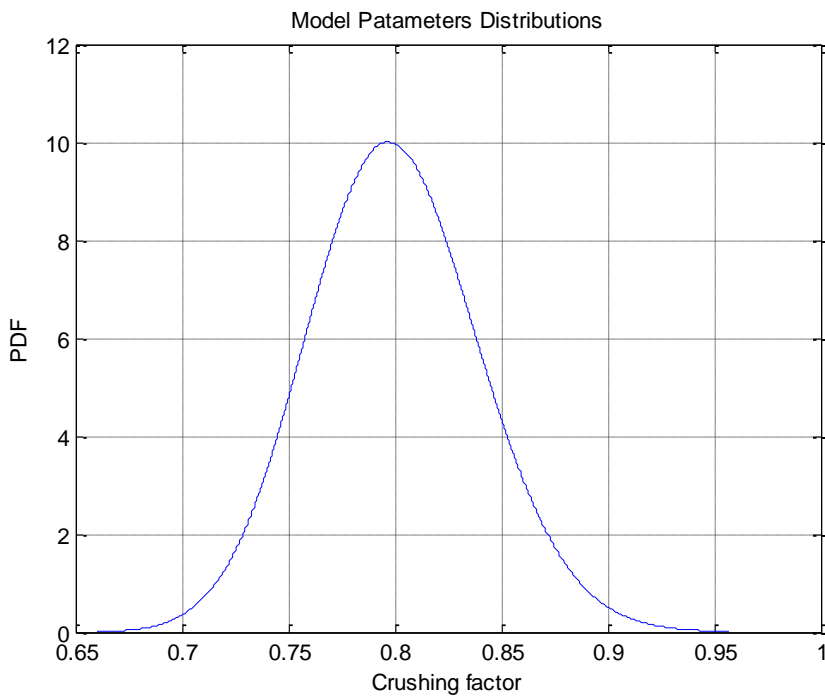


**Figure 6-19: PDE of the model parameter: crushing factor**

### 6.3.3. A design example

As an example, an extreme case is investigated to illustrate the application of Monte Carlo Simulation to design of pile groups. A barrier soil-pile system is considered to stop and redirect a Medium duty truck with a mass of 6800 kg traveling at 60 mph (100

km/h), which is the highest impact level in the ASTM F2656. Soil has a medium strength with the properties as  $PL=0.8$  MPa,  $E_0=10$  MPa and density of  $1900$  kg/m<sup>3</sup>. For the first step, an eight-pile group of W14x90 section, spaced at 5.2 m, connected with a beam of HSS10x10x1/2 is considered. Piles are embedded in soil to a depth of 3 m. Using TAMU-POST the maximum deflection and dynamic penetration are deterministically obtained (Figure 6-20).

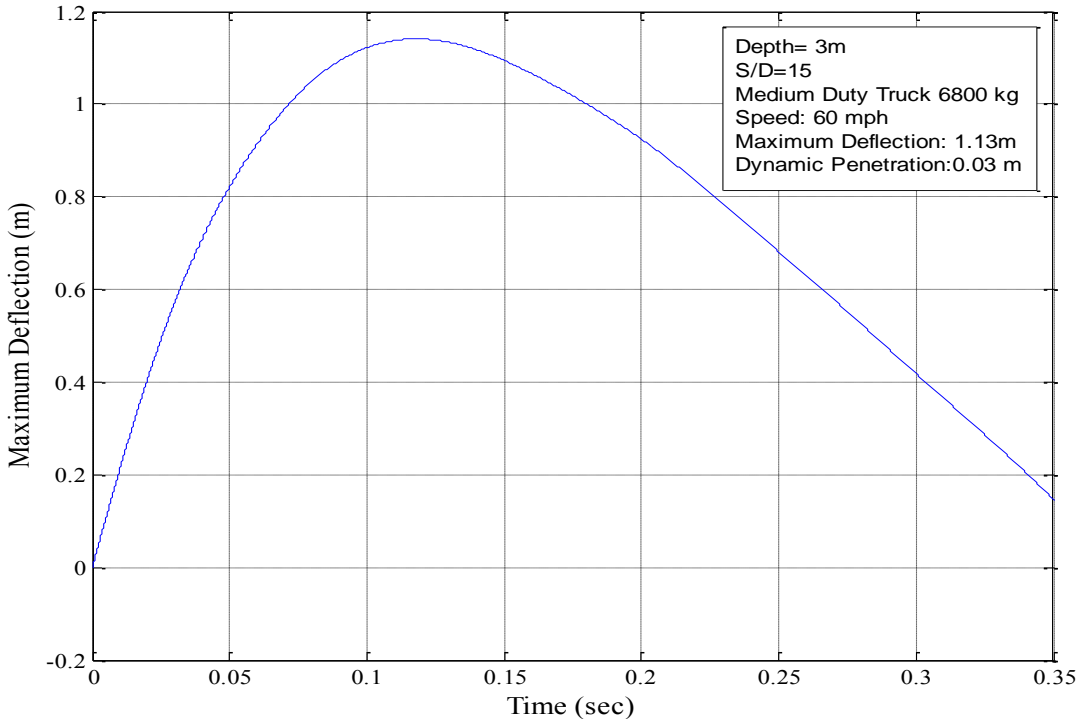


**Figure 6-20: The deterministic response by TAMU-POST**

The dynamic penetration is 0.03 m much less than 1 m, it implies that the soil-pile system is perfectly resisting the impact level M60. Continuing this example, a series of

analyses were conducted to estimate the probability of failure where the uncertainties in the input parameters and the model factors are considered explicitly.

Another question is to obtain the required number of samples which depends on the probability distribution function of the model output and the desired accuracy.

Figure 6-18 shows the results, number of samples as NS=5000 was adopted.

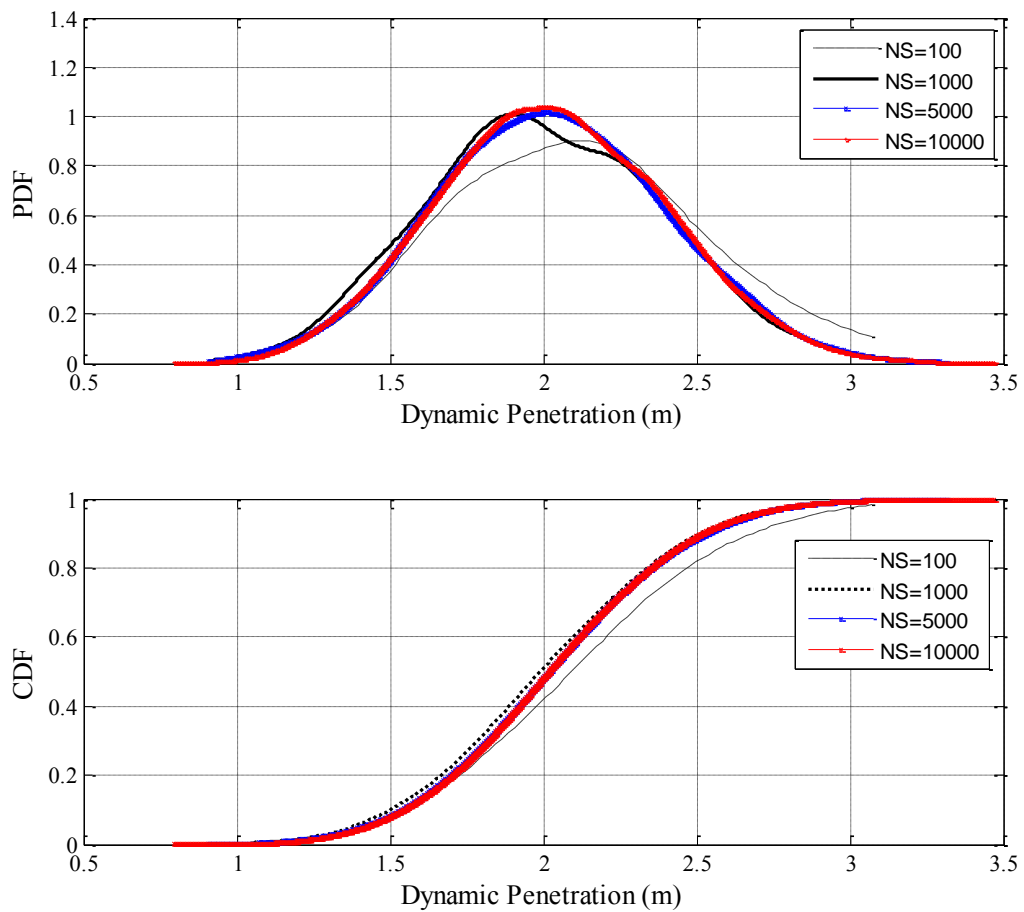


**Figure 6-21: Comparison of MCS results with different numbers of sample**

The analyses have been conducted for a wide range of soil-pile barrier systems; S/D and embedment depth L ranging from 10 to 25 and 1.5 m to 3 m, respectively. The results are gathered in Table 6-3 and illustrated in Figure 6-22 and Figure 6-23

**Table 6-3: The cases studied**

<b>Case</b>	<b>Embedment Depth L (m)</b>	<b>Ratio of pile spacing to pile diameter or width S/D</b>
1	1	15
2	1.5	15
3	2	15
4	2.5	15
5	3	15
6	3	10
7	3	15
8	3	20
9	3	25
10	3	30

As observed in Figure 6-22, embedment depth is one of the governing features, and significantly impacts the dynamic penetration and accordingly the probability of failure. It is worthwhile to pay attention to variation of response and POF for the cases of different depths: a large POF (99%) (corresponding to a safety factor of 0.45) for the case of depth 1m suggests a certain nonfunctional barrier. While POF drops significantly with an increase in depth, it is found that after a certain depth, deeper piles do not improve the performance remarkably. This finding offers a very helpful insight for an economic and safe design.



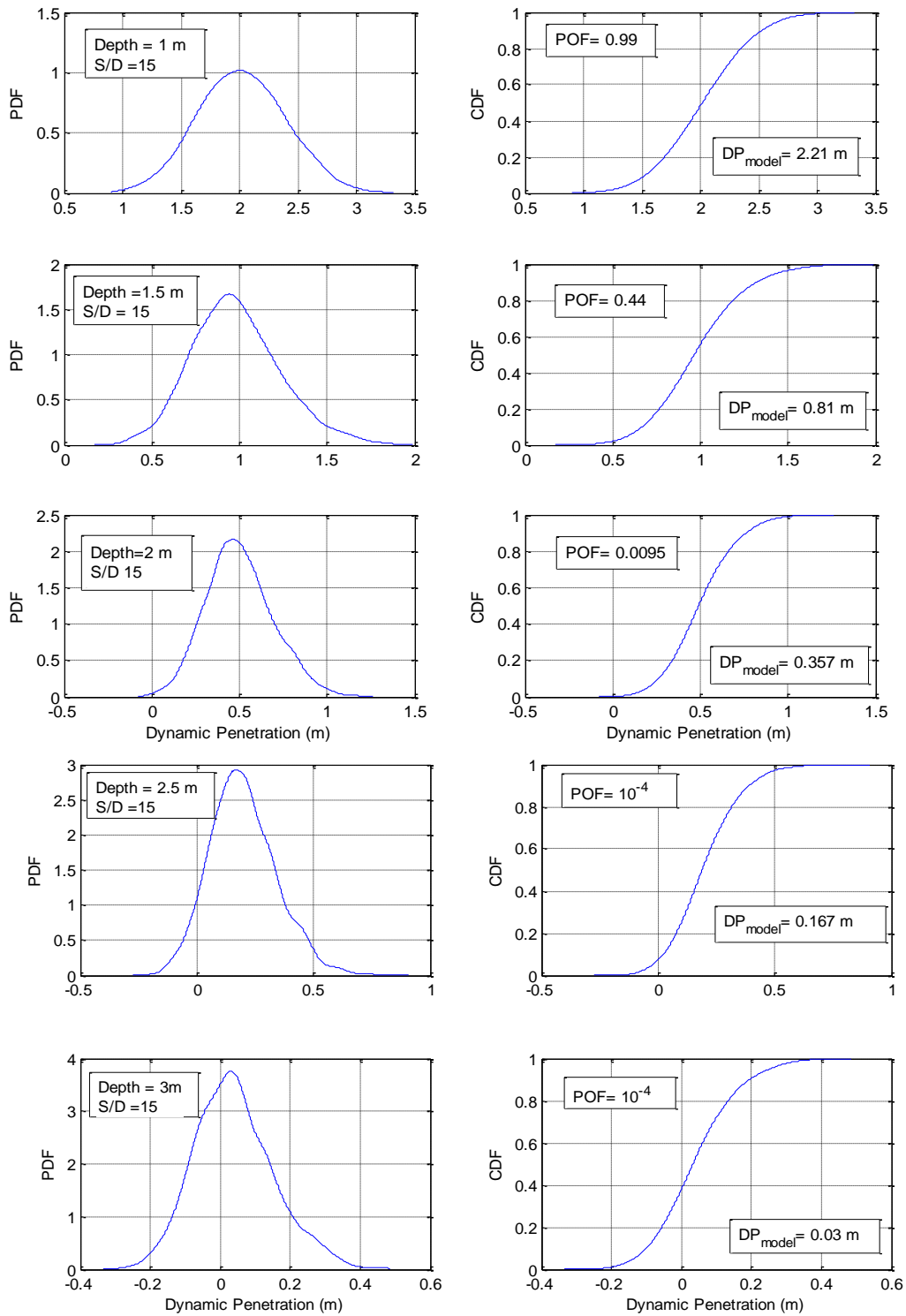


**Figure 6-22: Probability Distribution Function of the dynamic penetration and the associated probability of failure, depth ranging from 1 m to 3 m**

In a companion analysis, a similar case (M60) was analyzed, where the ratio of pile spacing to pile width or diameter varies between 10 and 30. As shown in Figure 6-23, the probability of failure remains small up to a critical S/D, where the dynamic penetration and the associated probability of failure increases drastically from  $10^{-4}$  to 0.014 and then 0.79. It clarifies the importance of the appropriate pile spacing for an economic and safe design of barriers.

In summary, this estimated probability of failure provides a noteworthy insight into the risk associated with any case of interest and assists the designer to characterize the details of the pile system such as pile spacing, embedment depth, pile and beam sectional characteristics for a given design such that the target reliability is achieved.

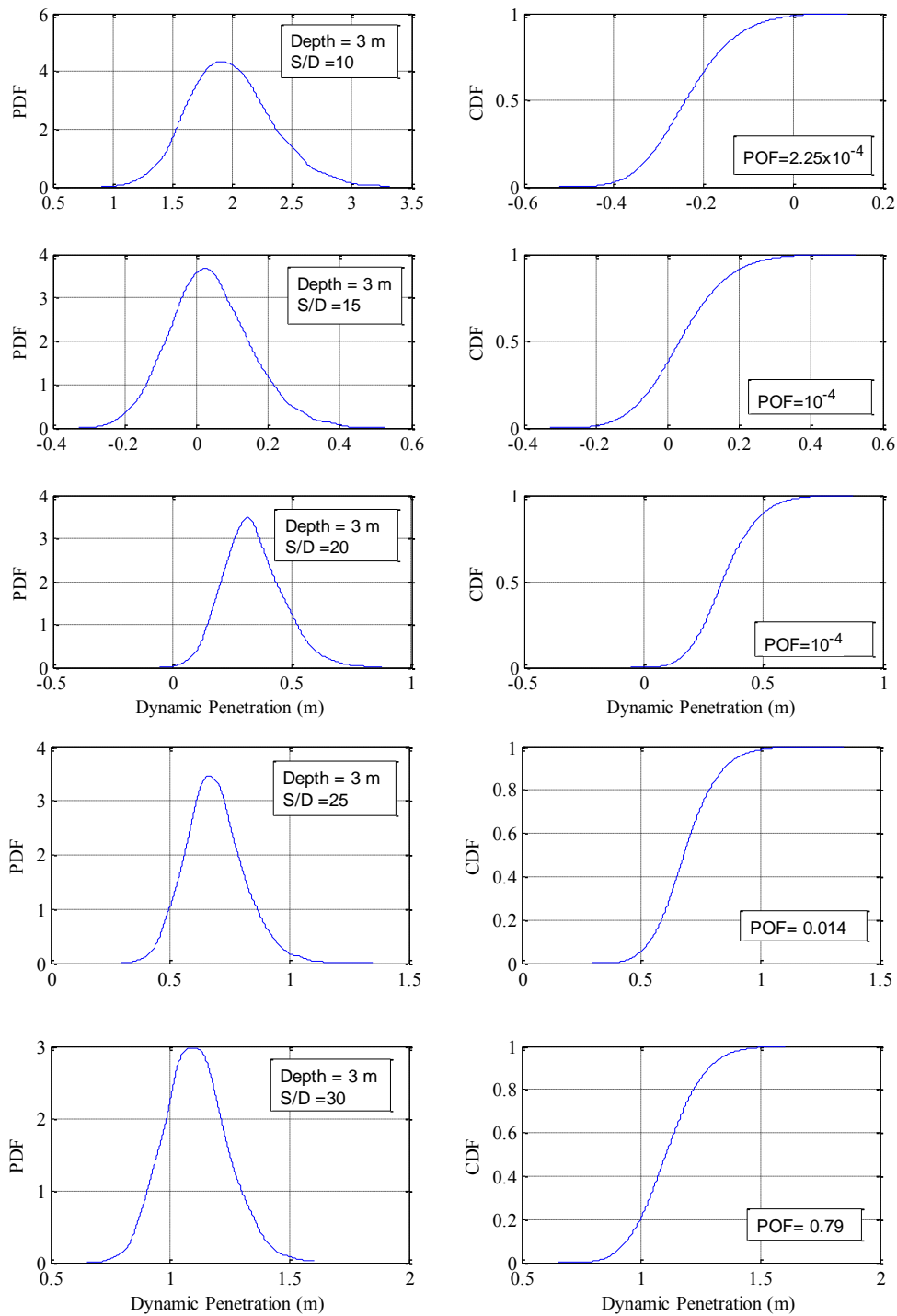


**Figure 6-23: Probability Distribution Function of the dynamic penetration and the associated probability of failure, S/D ranging from 10 to 30**

## 7. SUMMARY AND CONCLUSIONS

This dissertation detailed a combined experimental, numerical and analytical investigation on the impact response of group piles. In this project, a simple but effective analytical solution is developed to predict the performance of in-line piles embedded in any soil type subjected to impact of a vehicle with any given mass and velocity. The solution was then coded in an Excel spreadsheet called TAMU-POST (Group) and MATLAB for the practical use.

A literature review was performed; however very little work was found on soil-pile interaction under impact loading and the impact performance of piles. A series of full scale tests were conducted to compile an adequate database. The experiments were complemented by a similar series of numerical simulations using LS-DYNA. The total datasets collected from the tests and simulations were applied to develop and later verify the proposed analytical model. The following sections present the summaries of the conclusions, implications from the research and at the end present the recommendations for the future study.

### 7.1. Experimental study

Learning from the past experience of the single pile tests, two full scale crash tests and two full scale static tests were performed and analyzed: A group of 8 in-line piles embedded 3 m in loose sand to sustain a 6800 kg truck with an approaching velocity of 80 km/h and a group of four piles embedded 2 m in hard clay, connected together with two beams was designed to arrest a 2300 kg pickup truck with an approaching velocity

of 100 km/h. The results obtained from the conducted identical static tests allowed quantifying the static stiffness. Beams and piles displacements along with the vehicle accelerations during each of the tests were measured using accelerometers, a data acquisition system and high speed cameras. To characterize the soil properties a number of laboratory and in-situ tests were carried out. The main observations are summarized as:

- On average, comparison of the measured static resistance from the tests with the SALLOP method indicated a fairly good agreement. For designing pile groups under impacts, identical full scale static testing is essential to characterize the static resistance of the soil-pile system and compare with the analysis method proposed in the program TAMU-POST (Group).
- A group of four in-line piles with 2 m embedment depth could effectively arrest a vehicle 2300 kg going 100 km/h in hard clay. Preliminary design simulations showed that 2 m depth is the minimum depth necessary to adequately ensure the lateral resistance of the piles.
- In the PU60 test, all piles were observed to bend under the impact loading. One of the critical issues of interest in design work is to assure that the structural elements such as piles, beams and the connections do not break or rupture, especially in high strength soils.
- In the M50 test, a group of eight in-line piles effectively arrested a vehicle up to 6800 kg going 80 km/h in loose sand. The piles located on the edges of the group deflecting in the reverse direction did not carry as much load as those located

within the group. The failure in two of the connections also did not allow for fully transferring the impact load to all the piles.

- The researchers recommend the typical minimum embedment depth for the impact problems with Medium-duty truck (M) and Pickup truck is 3 m and 2 m, respectively. These values may differ for extreme soil conditions.
- The experimental setup and instrumentation used in this testing program offer an efficient approach to record the real behavior of piles and vehicle in similar experimental work.

## **7.2. Numerical study**

Extensive numerical simulations were performed using LS-DYNA prior to the testing program to design the test setup and after the tests to calibrate the models against the experiments. In addition, a series of simulations of various scenarios was performed to augment the datasets that would contribute to develop the analytical method. To best cover all possibilities in sample selection, the space filling technique of “Stratified Latin Hypercube Sampling” (SLHS) was adopted. The main numerical observations can be summarized as:

- The LS-DYNA models results regarding PU60 and M50 tests compared very well to these crash tests and validation of the simulations was carried out successfully in both quantitative and qualitative ways.
- The presented models provide a reliable means for impact simulation of different cases and study of any aspect of the impact mechanism. Within the scope of this

work, particularly soil contribution to the barrier performance and affecting factors are studied. Once one or more finite element models are validated against the full scale tests, those simulations can be reliably applied to study new crash scenarios.

- An Isotropic Elastic Plastic constitutive model using Von Mises yield criteria available in LS-DYNA was used to numerically model the cohesive soil behavior (hard clay in the test PU60). Also, for cohesionless soil, the Joint Rock model modified with Drucker-Prager was found to reasonably characterize the real behavior of the loose sand.
- The parameters including the vehicle mass, vehicle speed, pile spacing, pile width or diameter and soil strength were observed to be the most influential factors on the barrier response.

### **7.3. Analytical study**

A computationally efficient model TAMU-POST (Group) was developed to predict the lateral response of pile groups under impact loading through a nonlinear impact analysis. The proposed model facilitates a direct analysis of a pile group subjected to impact loading with little computational effort.

The model was developed mathematically based on the finite difference solution to the governing differential equation for a beam supported by a group of in-line piles represented by single degrees of freedom with damping, mass, spring and slider. The

coded program called TAMU-POST (Group) was then calibrated against the data bank of full scale experiments and LS-DYNA finite element simulations.

This semi empirical-theoretical model, while simpler and much less computationally intensive than the numerical solutions or the full scale tests, resulted in estimates comparable to those obtained from the experiments and numerical efforts. The easy use of the program and conservative results make the model a useful tool for a good approximate estimation of the pile group deformation under vehicular impacts. The conclusions are summarized as:

- Although the impact response of a pile group is a complicated nonlinear dynamic problem, the simplified mass-spring-dashpot analogy method with calibrated constants for damping gives a remarkably good estimate of the deflection measured in the tests and validated simulations. It was shown that the displacement predicted by TAMU-POST is within +/- 15% from the measured values.
- Approximating the stiffness of the soil-pile system by the simple method SALLOP is an acceptable simplification.
- Recommendations are drawn on how to best obtain the input parameters and to evaluate the precision of predictions using TAMU-POST (Group).
- Damping parameter of soil is greatly affected by soil strength and the level of loading. These effects were included in the analysis. Direct expressions are presented as a function of soil strength (i.e. pressuremeter limit pressure  $P_L$ ) and impact level to estimate the value for damping.



- In the model development process, conservative estimates of the dynamic penetration for the three vehicle classes are derived from the numerically simulations of vehicles impacting fully rigid walls.
- The energy absorption by the vehicle crushing was quantified by comparing the total kinetic energy of the vehicle and the internal energy of the barrier and soil together during the impact.
- As a useful supplement to the deterministic methodology, a reliability analysis is performed to provide insights on the probability of failure associated with any given design case. Using the adequate range of variance for the random input parameters and the model parameters, this study reveals the importance of such probabilistic study to give insights on the design safety.
- It is highly recommended that for a given soil condition and impact level, several cases with various important design measures such as embedment depth and pile spacing be probabilistically analyzed to identify the associated probability of failure. This simple effort indicates the critical design features (i.e. critical depth and critical S/D) that would result in an economic, reliable and admittedly safe design with a very low probability of failure in the range of  $10^{-4}$ .
- In this study, the uncertainties in estimates of soil properties (such as pressuremeter limit pressure  $P_L$ ) and the model parameters (such as crushing factor and *Alpha* factor) were acknowledged.
- It was also found that TAMU-POST (Group) overestimates the maximum bending moment in the pile and beam. The overestimation rate depends on soil

conditions, specifically soil strength. For design purposes, the beam and piles plots which indicate the moment overestimation trends as a function of soil strength are reported in the dissertation.

- A parametric study on impact response of pile groups varying the critical geometric and geomechanic characteristics is performed. In this analysis, the main parameters including mass and velocity of vehicle ( $M_v$  and  $V_v$ ), soil strength (in terms of  $P_L$ ), pile embedment depth ( $L$ ), the ratio of pile spacing to the pile width or diameter ( $S/D$ ), number of piles and pile and beam bending stiffness are addressed. A notable result is that, the ultimate resistance does not improve when any of depth, pile spacing or number of piles varies beyond certain values. These sensitive parameters offer an acceptable range to optimize the design of new and improved soil-pile barrier systems.

The main advantages of the model are listed as:

- It allows for analysis of different loading levels, different piles spacing, any soil conditions, pile and beam cross-sectional properties.
- The effect of soil nonlinearity was captured in the analysis.
- It requires the least number of input parameters that could be easily obtained from common laboratory and in situ tests.
- The probability of failure associated with any design is provided.
- With little computational effort, designer can spot the critical features for a cost effective and functional system design.

- It is easy to use, does not need a special expertise and it takes less than one minute to run the code.

The potential limitations of the proposed model include:

- While it predicts the maximum deflection very well, it does overestimates the bending moment in piles and beams.
- The inherent model error arising from the simplifications applied must be acknowledged.
- The model was based on two full scale tests and about 100 numerical simulations. This limited databank should be extended for a more improved and reliable analysis method.
- The number of piles from 3 to 8 piles and the ratio of S/D ranging from 10 to 50 can be analyzed using this model.

#### **7.4. Recommendations for future studies**

Several mechanisms governing the vehicle- barrier crash, in particular the impact force transmitted to the barrier, energy absorption by vehicle crushing have not been fully resolved. A better understanding of these features helps to incorporate these effects into the piles response estimation model. For this purpose, it is suggested to conduct a large number of numerical simulations with different vehicles, traveling with different velocities and more diverse barrier configurations.

A substantial step to forward this research is to calibrate the properties of the soil material model with the pressuremeter test (PMT).

In extreme loading, car crashes for instance, materials mostly experience large deformations and exhibit nonlinear behavior. The proposed model in this research, as discussed before, incorporated nonlinear springs to account for the soil nonlinearity and employs factors obtained directly from nonlinear observations both experimentally and numerically, to reflect the additional displacements caused by the plastic behavior of piles and beams. To address the structural behavior of piles and beams and the plastic behavior, it seems essential to explore approaches that model plastic failure of pile and beams more directly. For instance a method that considers the degradation of pile and beam elastic modulus as the deformation is progressing would enhance the model precision in bending moment estimation.

To achieve a better insight, a great reliance must be placed on performing more real scale experiments on piles with more protected and accurate instrumentation. These tests can fully replicate various impact scenarios. In this project, most of the strain gauges were damaged and could not be recovered. The more full scale tests are performed, the more reliable numerical models can be developed and validated. These experiments as well as numerical simulations can improve the precision of damping expression and the associated calibrating factor.

Further numerical studies with more refined finite element models and more predictive constitutive models are required to provide information to advance the proposed analytical approach. In order build confidence in modeling soil and soil-pile interaction, it is recommended to study the other numerical approaches embedded in LS DYNA such as Smoothed-Particle Hydrodynamics (SPH) and Multi-Material Arbitrary

Lagrangian-Eulerian (MM-ALE). These approaches are believed to treat large deformation well.

There are uncertainties associated with both material properties and input model parameters as well as the error inherently induced in the model development procedures that require a thorough probabilistic study. In order to quantify the uncertainties in the parameters and the simple model, it is suggested to expand the simple deterministic model to probabilistic demand model using a Bayesian framework and to estimate the fragility (conditional probability of failure of the system given a set of demand variables) of the barrier under a vehicle impact.

## REFERENCES

- Abu-Odeh, A., McCaskey, K.M., Bligh, R.P., Menges, W.L. & Kuhn, D.L. (2015).  
Crash Test and MASH TL-3 Evaluation of the TxDOT Short Radius Guardrail.  
Test Report. 0-6711-1. Project No. 0-6711. Texas A&M Transportation Institute,  
College Station, TX.
- Arrington, D.R., Bligh, R.P. & Menges, W.L. (2011). MASH Test 3-37 of the TxDOT  
31-Inch W-Beam Downstream Anchor Terminal. 9-1002-6. Texas Transportation  
Institute, Houston, TX.
- ASTM Standard D1586, A. S. (2011). ASTM Standard D1586: Standard test method for  
standard penetration test (SPT) and split-barrel sampling of soils. West  
Conshohocken, PA: ASTM International.
- ASTM Standard D2850, A. S. (2003). Standard test method for unconsolidated-  
undrained triaxial compression test on cohesive soils. West Conshohocken, PA:  
ASTM International.
- ASTM Standard D3441-05, A. S. (2005). Standard Test Method for Mechanical Cone  
Penetration Tests of Soil.
- ASTM Standard D4719, A. S. (2007). Standard test methods for prebored pressuremeter  
testing in soils. West Conshohocken, PA: ASTM International.

- ASTM Standard D5778, A. S. (2012). Standard Test Method for Electronic Friction Cone and Piezocone Penetration Testing of Soils. West Conshohocken, PA: ASTM International.
- ASTM Standard D7383, A. S. (2010). Standard test methods for axial compressive force pulse (rapid) testing of deep foundations. West Conshohocken, PA: ASTM International.
- ASTM Standard F2656, A. (2007). Standard test method for vehicle crash testing of perimeter barriers. West Conshohocken, PA: ASTM International.
- Alberson, D. C., Buth, C. E., Briaud, J. L., & Menhes, W. L. . (2007). DOS K12 testing and evaluation of direct embedded pier. College Station, TX: Texas Transportation Institute.
- Alejano, L. R., & Bobet, A. (2012). Drucker–Prager criterion. *Rock Mechanics and Rock Engineering*. 45(6), 995-999. doi: 10.1007/s00603-012-0278-2.
- Allegretti, T., & Pluta, P. (2003). Coast Guard-AWO Bridge Allision Work Group Report. Washington, D.C.
- Ang, A., & Tang, W. (2007). *Probability Concepts in Engineering: Emphasis on Applications to Civil and Environmental Engineering (v.1)*: John Wiley Publishers.

- API. (2002). Recommended Practice for Planning, Designing and Constructing Fixed Offshore Platforms—Working Stress Design.
- Asadollahi, P. M., Lim, S., Mirdamadi, A., Briaud, J., Abuodeh, A., Roesset, J., Norris, R. (2014). Full-Scale Test and Numerical Simulation of a Truck Impacting a Group of Side-by-Side Piles. Proc. Geo-Congress 2014 Technical Papers@sGeo-characterization and Modeling for Sustainability.
- Baguelin, F., Frank, R., & Said, Y. (1977). Theoretical study of lateral reaction mechanism of piles. *Geotechnique*, 27(3), 405-434.
- Baranov, V. (1967). On the calculation of excited vibrations of an embedded foundation. *Voprosy Dynamiki Prochnosti*, 14, 195-209.
- Belytschko T, Tsay CS. ASME, AMD 1981.48:209–31.
- Blaney, G. W. (1974). Dynamic stiffness of piles.
- Bligh, R.P., Seckinger, N.R., Abu-Odeh, A., Roschke, P.N., Menges, W.L.& Heck, R.R. (2004) Dynamic Response of Guardrail Systems Encased in Pavement Mow Strips. Research Report. 0-4162-2. Texas Transportation Institute, College Station, TX.
- Bogard, D., & Matlock, H. (1983). Procedures for analysis of laterally loaded pile groups in soft clay. Paper presented at the Geotechnical practice in offshore engineering.



- Brackin, M.S., Abu-Odeh, A., Buth, C.E., Williams, W.F., Fry, G. & Freeby, G. (2013). Impact Forces from Heavy-Vehicle Collisions with Bridge Piers. Transportation Research Record. 2313. Transportation Research Board, Washington, DC., pp. 42-51.
- Briaud, J. L., & Ballouz, M. (1996). LATWAK: impact test to obtain pile lateral static stiffness. *Journal of geotechnical engineering*, 122(6), 437-444.
- Briaud, J.L. (1997). Sallop: simple approach for lateral loads on piles. *Journal of Geotechnical and Geoenvironmental Engineering*, 123(10), 958-964.
- Briaud, J.L. (2013). *Geotechnical engineering: unsaturated and saturated soils*: John Wiley & Sons.
- Briaud, J. (1992). *The pressuremeter*. Taylor & Francis.
- Broms, B. B. (1964a). Lateral resistance of piles in cohesionless soils. *Journal of the Soil Mechanics and Foundations Division*, 90(3), 123-158.
- Broms, B. B. (1964b). Lateral resistance of piles in cohesive soils. *Journal of the Soil Mechanics and Foundations Division*, 90(2), 27-64.
- Brown, D., & Bollman, H. (1996). Pile group design using COM 624. Paper presented at the Conference on The Design of Bridges for Extreme Events, US Department of Transportation, Federal Highway Administration, Washington DC.

- Brown, D. A., Morrison, C., & Reese, L. C. (1988). Lateral load behavior of a pile group in sand. *Journal of Geotechnical Engineering, ASCE*, 114(GT11), 1261–1276.
- Brown, D. A., & Reese, L. C. (1988). Behavior of a large-scale pile group subjected to cyclic lateral loading: DTIC Document.
- Chopra, A.K. (2001). *Dynamic of Structures: Theory and Applications to Earthquake Engineering*. 2<sup>nd</sup> Edition, Prentice Hall.
- Consolazio, G., Cowan, D., Biggs, A., Cook, R., Ansley, M., & Bollmann, H. (2005). Part 2: Design of Foundations and Structures: Full-Scale Experimental Measurement of Barge Impact Loads on Bridge Piers. *Transportation Research Record: Journal of the Transportation Research Board* (1936), 79-93.
- "Cone Penetration Test Procedure" Retrieved May 2014 from <http://www.geotechdata.info/geotest/cone-penetration-test.html>.
- De Barros, F. C., & Luco, J. E. (1990). Discrete models for vertical vibrations of surface and embedded foundations. *Earthquake Engineering & Structural Dynamics*, 19 (2), 289-303.
- Deeks, A., & Randolph, M. (1995). A simple model for inelastic footing response to transient loading. *International journal for numerical and analytical methods in geomechanics*, 19 (5), 307-329.

- Dezi, F., Gara, F., & Roia, D. (2012). Dynamic response of a near-shore pile to lateral impact load. *Soil Dynamics and Earthquake Engineering*, 40, 34-47.
- Dobry, R., & Gazetas, G. (1988). Simple method for dynamic stiffness and damping of floating pile groups. *Geotechnique*, 38 (4), 557-574.
- Drucker, D. C., & Prager, W. (2013). Soil mechanics and plastic analysis or limit design. *Quarterly of Applied Mathematics*, 10.
- DYNASUPPORT website, "Contact Types" Retrieved April 2014.  
<http://www.dynasupport.com/tutorial/contact-modeling-in-ls-dyna/contact-types>).
- El-Marsafawi, H., Han, Y., & Novák, M. (1992). Dynamic experiments on two pile groups. *Journal of Geotechnical Engineering*, 118 (4), 576-592.
- El Naggar, M., & Novak, M. (1995). Nonlinear lateral interaction in pile dynamics. *Soil Dynamics and Earthquake Engineering*, 14 (2), 141-157.
- El Naggar, M., & Novak, M. (1996). Nonlinear analysis for dynamic lateral pile response. *Soil Dynamics and Earthquake Engineering*, 15 (4), 233-244.
- El-Tawil, Sh., (2004). Vehicle Collision with Bridge Piers. Report Department of Civil and Environmental Engineering, University of Michigan, Ann Arbor, MI, 48109-2125.

FEMA 430. (2003). Federal Emergency Management Agency. Chapter 4, Perimeter security design.

Fenton, G. A., & Griffiths, D. V. (2008). Risk assessment in geotechnical engineering: Wiley.

FHWA publications, Retrieved June 2015 from <https://www.fhwa.dot.gov/publications/publicroads/08nov/04.cfm>.

Focht Jr, J. A., & Koch, K. J. (1973). Rational analysis of the lateral performance of offshore pile groups. Paper presented at the Offshore Technology Conference.

Griffiths, D. V., & Fenton, G. A. (2007). Probabilistic methods in geotechnical engineering (Vol. 491): Springer Science & Business Media.

Hahn, G. J., & Shapiro, S. S. (1968). Statistical models in engineering. In Statistical models in engineering. John Wiley & Sons.

Halling, M. W., Womack, K. C., Muhammad, I., & Rollins, K. M. (2000). Vibrational testing of a full-scale pile group in soft clay. Paper presented at the Proc. 12th World Conference on Earthquake Engineering, Auckland.

Hallquist, J. O. (1976). Procedure for the solution of finite-deformation contact-impact problems by the finite element method: California University, Livermore (USA). Lawrence Livermore Lab.

- Hallquist, J. O. (1993). LS-DYNA3D theoretical manual. Livermore Software Technology Corporation.
- Hallquist, J. O. (2006). LS-DYNA theory manual. Livermore Software Technology Corporation.
- Hallquist, J. O. (2007). LS-DYNA keyword user's manual. Livermore Software Technology Corporation.
- Hallquist, J. O., & Benson, D. (1986). DYNA3D user's manual (nonlinear dynamic analysis of structures in three dimensions). Revision 2: Lawrence Livermore National Lab., CA (USA).
- Hetenyi, M. (1946). Beams on elastic foundation. Ann Arbor, Michigan: The University of Michigan Press.
- Hoare, A., Regan, D. G., & Wilson, D. P. (2008). Theoretical Biology and Medical Modelling. *Theoretical Biology and Medical Modelling*, 5(4).
- Inman, R. L., Helson, J. C., & Campbell, J. E. (1981). An approach to sensitivity analysis of computer models: Part II-ranking of input variables, response surface validation, distribution effect and technique synopsis. *Journal of Quality Technology*, 13(4).

- Kagawa, T., & Kraft, L. M. (1981). Dynamic characteristics of lateral load-deflection relationships of flexible piles. *Earthquake Engineering & Structural Dynamics*, 9(1), 53-68.
- Kaynia, A., & Kausel, E. (1982). Dynamic behavior of pile groups. Paper presented at the 2<sup>nd</sup> Int. Conf. on Numerical Methods in Offshore Piling, Austin, Texas.
- Kuhlemeyer, R. L. (1979). Static and dynamic laterally loaded floating piles. *Journal of the Geotechnical Engineering Division*, 105(2), 289-304.
- Kulhawy, F. K., & Trautmann, C. H. (1996). Estimation of in-situ test uncertainty. *Uncertainty in the geologic environment: from theory to practice*. ASCE Geotechnical Special Publication No. 58, 269-286.
- Lim, S. G. (2011). Development of design guidelines for soil embedded post systems using wide- flange I-beams to contain truck impact. (PhD), Texas A&M University, College Station.
- LS-DYNA R7.1 Keyword Manual, Vol. I, Vol. II, & Vol. III.2014.
- Lysmer, J., & Richart, F. E. (1966). Dynamic response of footings to vertical loading. *Journal of the Soil Mechanics and Foundations Division*, 92(1), 65-91.
- Manna, B., & Baidya, D. (2009). Vertical vibration of full-scale pile—analytical and experimental study. *Journal of Geotechnical and Geoenvironmental Engineering*, 135(10), 1452-1461.

- Marzougui, D., Zink, M., Zaouk, A., Kan, C., & Bedewi, N. (2004). Development and validation of a vehicle suspension finite element model for use in crash simulations. *International Journal of Crashworthiness*, 9(6), 565-576.
- Matlock, H. (1970). Correlations for design of laterally loaded piles in soft clay. *Offshore Technology in Civil Engineering's Hall of Fame Papers from the Early Years*, 77-94.
- Matlock, H., & Reese, L. C. (1960). Generalized solutions for laterally loaded piles. *Journal of the Soil Mechanics and Foundations Division*, 86(5), 63-94.
- McClelland, B., & Focht Jr, J. (1956). Soil modulus for laterally loaded piles. *Journal of the Soil Mechanics and Foundations Division*, 82(4), 1-22.
- McKay, M. D., Beckman, R. J., & Conover, W. J. (1979). Comparison of three methods for selecting values of input variables in the analysis of output from a computer code. *Technometrics*, 21(2), 239-245.
- McKay, M. D., Beckman, R. J., & Conover, W. J. (2000). A comparison of three methods for selecting values of input variables in the analysis of output from a computer code. *Technometrics*, 42(1), 55-61.
- McVay, M. C., Wasman, S. J., Consolazio, G. R., Bullock, P. J., Cowan, D. G., & Bollmann, H. T. (2009). Dynamic soil–structure interaction of bridge substructure subject to vessel impact. *Journal of Bridge Engineering*, 14(1), 7-16.

- Meyer, B. J., & Reese, L. C. (1979). Analysis of single piles under lateral loading: Center for Highway Research, University of Texas at Austin.
- Mirdamadi, A. (2014). Deterministic and probabilistic simple model for single pile behavior under lateral truck impact. (PhD), Texas A&M University.
- Mohan, P., Marzougui, D., & Kan, C. D. (2009). Development and validation of hybrid iii crash test dummy (No. 2009-01-0473). SAE Technical Paper.
- Morgan, M. G., Henrion, M., & Small, M. (1992). Uncertainty: a guide to dealing with uncertainty in quantitative risk and policy analysis: Cambridge University Press.
- National Crash Analysis Center (NCAC). Finite Element Model Archive. FE Models. <http://www.ncac.gwu.edu/vml/models.html>.
- Nguyen, T., Berggren, B., & Hansbo, S. (1988). A new soil model for pile driving and driveability analysis. Paper presented at the 3rd International Conference on Application of Stress-Wave Theory to Piles, Canada.
- Nogami, T. (1980). Dynamic stiffness and damping of pile groups in inhomogeneous soil. Paper presented at the Dynamic Response of Pile Foundations@ sAnalytical Aspects.
- Nogami, T., Jun, O., & Konagai, K. (1991). Nonlinear time domain numerical model for pile group under transient dynamic forces. Paper presented at the Second



International Conference on Recent Advances in Geotechnical Earthquake Engineering and Soil Dynamics (1991: March 11-15; St. Louis, Missouri).

Nogami, T., & Novak, M. (1976). Soil-pile interaction in vertical vibration. *Earthquake Engineering & Structural Dynamics*, 4(3), 277-293.

Nogami, T., Otani, J., Konagai, K., & Chen, H.L. (1992). Nonlinear soil-pile interaction model for dynamic lateral motion. *Journal of Geotechnical Engineering*, 118(1), 89-106.

Novak, M. (1974). Dynamic stiffness and damping of piles. *Canadian Geotechnical Journal*, 11(4), 574-598.

Novak, M., Aboul-Ella, F., & Nogami, T. (1978). Dynamic soil reactions for plane strain case. *Journal of the Engineering Mechanics Division*, 104(4), 953-959.

Novak, M., & F. Grigg, R. (1976). Dynamic experiments with small pile foundations. *Canadian Geotechnical Journal*, 13(4), 372-385.

Novak, M., & Janes, M. (1989). Dynamic and static response of pile groups. XII ICSMFE, 11751178.

Novak, M., & Sharnouby, B. E. (1984). Evaluation of dynamic experiments on pile group. *Journal of Geotechnical Engineering*, 110(6), 738-756.

- O'Neill, M. W. (1983). Group action in offshore piles. Paper presented at the Proceedings of the Conference on Geotechnical Practice in Offshore Engineering.
- O'Neill, M. W., Ghazzaly, O. I., & Ha, H. B. (1977). Analysis of three-dimensional pile groups with nonlinear soil response and pile-soil-pile interaction. Paper presented at the Offshore Technology Conference.
- Ooi, P. S., & Duncan, J. M. (1994). Lateral load analysis of groups of piles and drilled shafts. *Journal of Geotechnical Engineering*, 120(6), 1034-1050.
- Pajouh, M. A., Briaud, J.-L., Alberson, D., Arrington, D., & Mirdamadi, A. (2015). Full Scale Crash Test on a Group of Piles in Clay. Paper presented at the IFCEE 2015.
- Penzien, J. (1970). Soil-pile foundation interaction.
- Potts, D. M., & Zdravkovic, L. (1999). *Finite element analysis in geotechnical engineering: Theory*: Thomas Telford.
- Poulos, H. G. (1971a). Behavior of laterally loaded piles i. single piles. *Journal of Soil Mechanics & Foundations Div.*
- Poulos, H. G. (1971b). Behavior of laterally loaded piles II. Pile groups. *Journal of Soil Mechanics & Foundations Div.*

- Poulos, H. G., & Davis, E. H. (1980). Pile foundation analysis and design.
- Pulikanti, S., & Ramancharla, P. K. (2013). SSI Analysis of Framed Structures Supported on Pile Foundations: A Review.
- Rainer, J. (1975). Damping in dynamic structure-foundation interaction. *Canadian Geotechnical Journal*, 12(1), 13-22.
- Randolph, M. F. (1981). The response of flexible piles to lateral loading. *Geotechnique*, 31(2), 247-259.
- Rao, S. N., Ramakrishna, V., & Raju, G. B. (1996). Behavior of pile-supported dolphins in marine clay under lateral loading. *Journal of Geotechnical Engineering*, 122(8), 607-612.
- Reese, L. C., Cox, W. R., & Koop, F. D. (1974). Analysis of laterally loaded piles in sand. *Offshore Technology in Civil Engineering Hall of Fame Papers from the Early Years*, 95-105.
- Reese, L. C., & Welch, R. C. (1975). Lateral loading of deep foundations in stiff clay. *Journal of the Geotechnical engineering division*, 101(7), 633-649.
- Reese, L. C., Cooley, L. A., & Radhakrishnan, N. (1984). Laterally Loaded Piles and Computer Program COM624G: DTIC Document.

- Reid, J., & Marzougui, D. (2002). Improved Truck Model for Roadside Safety Simulations: Part I—Structural Modeling. *Transportation Research Record: Journal of the Transportation Research Board* 1797: 53-62.
- Roesset, J. M., Whitman, R. V., & Dobry, R. (1973). Modal analysis for structures with foundation interaction. *Journal of the Structural Division*, 99(3), 399-416.
- Rollins, K. M., Peterson, K. T., & Weaver, T. J. (1998). Lateral load behavior of full-scale pile group in clay. *Journal of geotechnical and geoenvironmental engineering*, 124(6), 468-478.
- Rollins, K. M., Johnson, S. R., Petersen, K. T., & Weaver, T. J. (2003). Static and dynamic lateral load behavior of pile groups based on full-scale testing. Paper presented at the The Thirteenth International Offshore and Polar Engineering Conference.
- Rollins, K. M., Lane, J. D., & Gerber, T. M. (2005). Measured and computed lateral response of a pile group in sand. *Journal of Geotechnical and Geoenvironmental Engineering*.
- Rollins, K. M., Olsen, R., Egbert, J., Olsen, K., Jensen, D., & Garrett, B. (2003). *Response, Analysis, and Design of Pile Groups Subjected to Static & Dynamic Lateral Loads: Utah Department of Transportation*.
- Ross, H.E., Sicking, D.L., Zimmer, R.A., Michie, J.D. (1993). "Recommended Procedures for the Safety Performance Evaluation of Highway Features"

National Cooperative Highway Research Program Report 350. (NCHRP 350),  
TRB National Academy Press. Washington, D.C.

Rubinstein, R. Y., & Kroese, D. P. (2011). Simulation and the Monte Carlo method  
(Vol. 707). John Wiley & Sons.

Ruesta, P. F., & Townsend, F. C. (1997). Evaluation of laterally loaded pile group at  
Roosevelt Bridge. *Journal of Geotechnical and Geoenvironmental Engineering*,  
123(12), 1153-1161.

Sheta, M., & Novak, M. (1982). Vertical vibration of pile groups. *Journal of  
Geotechnical and Geoenvironmental Engineering*, 108(GT4).

Silvestri Dobrovlny, C., Arrington, D.R., Bligh, R.P., & Menges, W.L. (2012)  
Development Guidance for Sign Design Standards. 0-6363-1. Texas  
Transportation Institute, College Station, TX.

Smith, E. A. (1962). Pile-driving analysis by the wave equation. *American Society of  
Civil Engineers Transactions*.

“Standard Penetration Test (SPT) procedure“ Website of Geotechnical and Foundation  
Engineering, Retrieved May 2014 from <http://foundationeng.blogspot.com>.

Terzaghi, K. (1955). Evaluation of coefficients of subgrade reaction. *Geotechnique*,  
5(4), 297-326.

Texas A&M Supercomputing Facility. Retrieved June 2015 from <http://sc.tamu.edu/>.

- U.S. State Department, B. o. D. S. (2003). SD-STD-02.01, Revision A, Test method for vehicle crash testing of perimeter barriers and gates. Washington, D.C.
- Veletsos, A. S., & Verbic, B. (1974). Basic response functions for elastic foundations. *Journal of the Engineering Mechanics Division*, 100(2), 189-202.
- Wolf, J., & Hall, W. (1988). Soil-structure-interaction analysis in time domain: A Division of Simon & Schuster.
- Wolf, J. P. (1980). Dynamic stiffness of group of battered piles. *Journal of the Geotechnical Engineering Division*, 106(2), 198-203.
- Wolf, J. P., & Somaini, D. R. (1986). Approximate dynamic model of embedded foundation in time domain. *Earthquake Engineering & Structural Dynamics*, 14(5), 683-703.
- Wu, G., & Finn, W. L. (1997). Dynamic nonlinear analysis of pile foundations using finite element method in the time domain. *Canadian Geotechnical Journal*, 34(1), 44-52.
- Zhu, B., Chen, R., Guo, J., Kong, L., & Chen, Y. (2011). Large-scale modeling and theoretical investigation of lateral collisions on elevated piles. *Journal of Geotechnical and Geoenvironmental Engineering*, 138(4), 461-471.

# APPENDIX A

## SITE CHARACTERIZATION – BORING LOG AND SPT RESULTS

BORING LOG NO. B-1										Page 1 of 1	
<b>PROJECT:</b>					<b>CLIENT: Texas A&amp;M University College Station, Texas</b>						
<b>SITE: Riverside Campus Bryan, Texas</b>											
GRAPHIC LOG	LOCATION	DEPTH (FL)	WATER LEVEL OBSERVATIONS	SAMPLE TYPE	FIELD TEST RESULTS	STRENGTH TEST			WATER CONTENT (%)	DRY UNIT WEIGHT (pcf)	ATTERBERG LIMITS
	See Exhibit A-2					TEST TYPE	COMPRESSIVE STRENGTH	STRAIN (%)			LL-PL-PI
DEPTH											
6.5	<b>SANDY CLAY</b> , dark tan				4-7-8 N=15						
					6-7-7 N=14						
		5			4-6-7 N=13						
	<b>Boring Terminated at 6.5 Feet</b>										
Stratification lines are approximate. In-situ, the transition may be gradual. Hammer Type: Automatic											
<b>Advancement Method:</b> Dry augered to termination depth.			See Exhibit A-3 for description of field procedures. See Appendix B for description of laboratory procedures and additional data (if any).			<b>Notes:</b>					
<b>Abandonment Method:</b> Borings left open at the direction of the client			See Appendix C for explanation of symbols and abbreviations.								
<b>WATER LEVEL OBSERVATIONS</b> <i>No free water observed</i>								Boring Started: 11/18/2013		Boring Completed: 11/18/2013	
						Drill Rig: D50 Track		Driller: Terracon - Roger Bauer			
						Project No.: A1125038		Exhibit: A-1			

THIS BORING LOG IS NOT VALID IF SEPARATED FROM ORIGINAL REPORT. GEO SMART LOG-NO WELL A1125038-GINT-MJ/GPJ

## BORING LOG NO. B-2

Page 1 of 1

<b>PROJECT:</b>	<b>CLIENT: Texas A&amp;M University</b>
<b>SITE: Riverside Campus</b>	<b>College Station, Texas</b>

<b>LOCATION</b> See Exhibit A-2		<b>DEPTH (FL)</b>	<b>WATER LEVEL OBSERVATIONS</b>	<b>SAMPLE TYPE</b>	<b>FIELD TEST RESULTS</b>	<b>STRENGTH TEST</b>			<b>WATER CONTENT (%)</b>	<b>DRY UNIT WEIGHT (pcf)</b>	<b>ATTERBERG LIMITS</b>	<b>PERCENT FINES</b>
<b>DEPTH</b>						<b>TEST TYPE</b>	<b>COMPRESSIVE STRENGTH</b>	<b>STRAIN (%)</b>			<b>LL-PL-PI</b>	

<p><b>SANDY CLAY</b>, dark tan</p>					HP=4.5+							
					HP=4.5+							
		5			HP=4.5+							

6.5 **Boring Terminated at 6.5 Feet**

Stratification lines are approximate. In-situ, the transition may be gradual. Hammer Type: Automatic

<b>Advancement Method:</b> Dry augered to termination depth.	See Exhibit A-3 for description of field procedures. See Appendix B for description of laboratory procedures and additional data (if any). See Appendix C for explanation of symbols and abbreviations.	<b>Notes:</b>
<b>Abandonment Method:</b> Borings left open at the direction of the client		

<b>WATER LEVEL OBSERVATIONS</b>		Boring Started: 11/18/2013
No free water observed		Boring Completed: 11/18/2013
		Drill Rig: D50 Track
		Driller: Terracon - Roger Bauer
		Project No.: A1125038
		Exhibit: A-2

THIS BORING LOG IS NOT VALID IF SEPARATED FROM ORIGINAL REPORT. GEO SMART LOG-NO WELL A1125038-GINT-HM.GPJ



## BORING LOG NO. B-3

Page 1 of 1

<b>PROJECT:</b>	<b>CLIENT:</b> Texas A&M University College Station, Texas
<b>SITE:</b> Riverside Campus Bryan, Texas	

GRAPHIC LOG	LOCATION See Exhibit A-2	DEPTH (FL)	WATER LEVEL OBSERVATIONS	SAMPLE TYPE	FIELD TEST RESULTS	STRENGTH TEST			WATER CONTENT (%)	DRY UNIT WEIGHT (pcf)	ATTERBERG LIMITS		
						TEST TYPE	COMPRESSIVE STRENGTH	STRAIN (%)			LL-PL-PI	PERCENT FINES	
DEPTH	<b>SANDY CLAY</b> , dark tan				5-10-11 N=21								
					3-5-6 N=11								
					4-5-6 N=11								
		5											
		6.5											
	<b>Boring Terminated at 6.5 Feet</b>												

Stratification lines are approximate. In-situ, the transition may be gradual. Hammer Type: Automatic

<b>Advancement Method:</b> Dry augered to termination depth.	See Exhibit A-3 for description of field procedures. See Appendix B for description of laboratory procedures and additional data (if any). See Appendix C for explanation of symbols and abbreviations.	<b>Notes:</b>
<b>Abandonment Method:</b> Borings left open at the direction of the client		

<b>WATER LEVEL OBSERVATIONS</b> No free water observed		Boring Started: 11/18/2013 Drill Rig: D50 Track Project No.: A1125038
		Boring Completed: 11/18/2013 Driller: Terracon - Roger Bauer Exhibit: A-3

THIS BORING LOG IS NOT VALID IF SEPARATED FROM ORIGINAL REPORT. GEO SMART LOG-NO WELL A1125038-GINT-AU.GPJ

# BORING LOG NO. B-4

<b>PROJECT:</b>		<b>CLIENT: Texas A&amp;M University College Station, Texas</b>										
<b>SITE: Riverside Campus Bryan, Texas</b>												
GRAPHIC LOG	LOCATION See Exhibit A-2	DEPTH (FL)	WATER LEVEL OBSERVATIONS	SAMPLE TYPE	FIELD TEST RESULTS	STRENGTH TEST			WATER CONTENT (%)	DRY UNIT WEIGHT (pcf)	ATTERBERG LIMITS	PERCENT FINES
	DEPTH					TEST TYPE	COMPRESSIVE STRENGTH	STRAIN (%)			LL-PL-PI	
6.5	SANDY CLAY, dark tan				HP=3.25							
					HP=4.5+							
		5			HP=4.5+							
	6.5	Boring Terminated at 6.5 Feet										
Stratification lines are approximate. In-situ, the transition may be gradual. Hammer Type: Automatic												
Advancement Method: Dry augered to termination depth.		See Exhibit A-3 for description of field procedures. See Appendix B for description of laboratory procedures and additional data (if any).				Notes:						
Abandonment Method: Borings left open at the direction of the client		See Appendix C for explanation of symbols and abbreviations.										
<b>WATER LEVEL OBSERVATIONS</b>		<b>Terracon</b>				Boring Started: 11/18/2013		Boring Completed: 11/18/2013				
No free water observed						Drill Rig: D50 Track		Driller: Terracon - Roger Bauer				
						Project No.: A1125038		Exhibit: A-4				

THIS BORING LOG IS NOT VALID IF SEPARATED FROM ORIGINAL REPORT. GEO SMART LOG-NO WELL A1125038-GINT-MJ.GPJ


# BORING LOG NO. B-5

<b>PROJECT:</b>	<b>CLIENT: Texas A&amp;M University</b>
<b>SITE: Riverside Campus</b>	<b>College Station, Texas</b>
<b>Bryan, Texas</b>	

GRAPHIC LOG	LOCATION See Exhibit A-2	DEPTH (FL)	WATER LEVEL OBSERVATIONS	SAMPLE TYPE	FIELD TEST RESULTS	STRENGTH TEST			WATER CONTENT (%)	DRY UNIT WEIGHT (pcf)	ATTERBERG LIMITS	PERCENT FINES
						TEST TYPE	COMPRESSIVE STRENGTH	STRAIN (%)				
DEPTH	<b>SANDY CLAY</b> , dark tan				3-3-5 N=8							
					3-8-11 N=19							
		5			4-9-12 N=21							
	6.5											
	<i>Boring Terminated at 6.5 Feet</i>											

Stratification lines are approximate. In-situ, the transition may be gradual. Hammer Type: Automatic

THIS BORING LOG IS NOT VALID IF SEPARATED FROM ORIGINAL REPORT. GEO SMART LOG-NO WELL A1125038-GINT-MJ.GPJ

<b>Advancement Method:</b> Dry augered to termination depth.	See Exhibit A-3 for description of field procedures. See Appendix B for description of laboratory procedures and additional data (if any). See Appendix C for explanation of symbols and abbreviations.	<b>Notes:</b>
<b>Abandonment Method:</b> Borings left open at the direction of the client		
WATER LEVEL OBSERVATIONS <i>No free water observed</i>		Boring Started: 11/18/2013 Drill Rig: D50 Track Project No.: A1125038
		Boring Completed: 11/18/2013 Driller: Terracon - Roger Bauer Exhibit: A-5

**FIELD DENSITY TEST REPORT**

Report Number: A1131064.0010  
 Service Date: 12/02/13  
 Report Date: 12/03/13  
 Task: PO #478260-22, Research Foundation



6198 Imperial Loop  
 College Station, TX 77845  
 979-846-3767 Reg No: F-3272

**Client**

Texas Transportation Institute  
 Attn: Gary Gerke  
 TTI Business Office  
 3135 TAMU  
 College Station, TX 77843-3135

**Project**

Riverside Campus  
 Riverside Campus  
 Bryan, TX

Project Number: A1131064

**Material Information**

Mat. No.	Proctor Ref. No.	Classification and Description	Laboratory Test Method	Lab Test Data		Project Requirements	
				Optimum Water Content (%)	Max. Lab Density (pcf)	Water Content (%)	Compaction (%)
1	A1111007.0045A	Black with red clay	ASTMD698	15.3	107.5	N/A	N/A

**Field Test Data**

Test No.	Test Location	Lift / Elev.	Mat. No.	Probe Depth (in)	Wet Density (pcf)	Water Content (pcf)	Water Content (%)	Dry Density (pcf)	Percent Compaction (%)
<b>PO# 478260-22</b>									
1	Static	Final	1	8	124.9	17.5	16.3	107.4	99.9
2	West	Final	1	10	122.8	15.2	14.1	107.6	100+
3	East	Final	1	10	127.8	13.6	11.9	114.2	100+

Datum: Serial No: 7415 Std. Cnt. M: 608 Std. Cnt. D: 1584

Comments:

## **APPENDIX B**

### **THE IN-SITU AND LABORATORY TESTS**

#### **Pressuremeter Test PMT**

Pressuremeter test (PMT) an in situ stress-strain test was developed in France in late 1950s Louis Menard to obtain information on soil characterization for both granular and cohesive soils. The PMT (as shown in Figure B-1, Briaud, 1992) consists of drilling a borehole to a desired depth, inserting an inflatable cylindrical probe and expanding the probe while recording the pressure and corresponding change in volume (or radius). This test data provides a relatively accurate means to determine the p-y curve used in design of laterally loaded deep foundations. Moreover, using PMT data and empirical equations bearing capacity and settlement analyses can be performed for shallow foundations. The primary advantage of PMT test is that it permits to replicate different load sequences such as rapid inflation for impact loading and unload-reload cycles for cyclic loading. (Briaud 1992).

Three major types for PMT testing equipment are available: preboring or Menard-type pressuremeter, self-boring, and the push-in pressuremeters. In the self-boring pressuremeter, the probe is equipped with the drilling equipment that bores into the soil to avoid the decompression of soil due to preboring. In the push-in PMT, the probe is pushed into the soil and the displacement takes place during the insertion. Herein, the most common method preboring PMT is addressed.

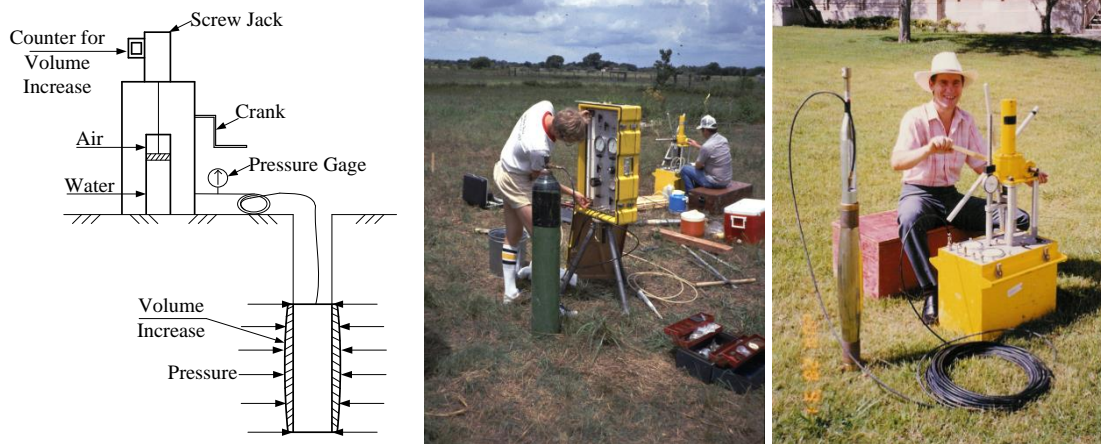


**Figure B-1: TEXAM and Menard Pressuremeters**

A typical PMT result as a stress strain curve presented in Figure B-2 has three distinct phases: the initial curved portion (phase I) attributed to the expansion of probe to reach full contact with the borehole sides, the linear portion (phase II) representing the onset of plastic behavior and the nonlinear portion (phase III) indication of plastic behavior until a limit pressure is reached.

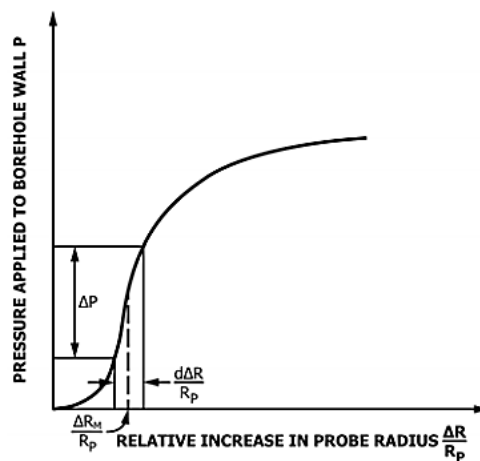


**Figure B-2: Typical PMT test result: pressure vs relative increase in radius**

Useful information on the soil properties can be inferred from this test such as the modulus  $E_o$  so called the first load modulus and the pressuremeter limit pressure  $P_L$  (Figure B-3). An unload-reload loop is often addressed close to the point  $P_y$  to obtain the reload modulus  $E_r$ .

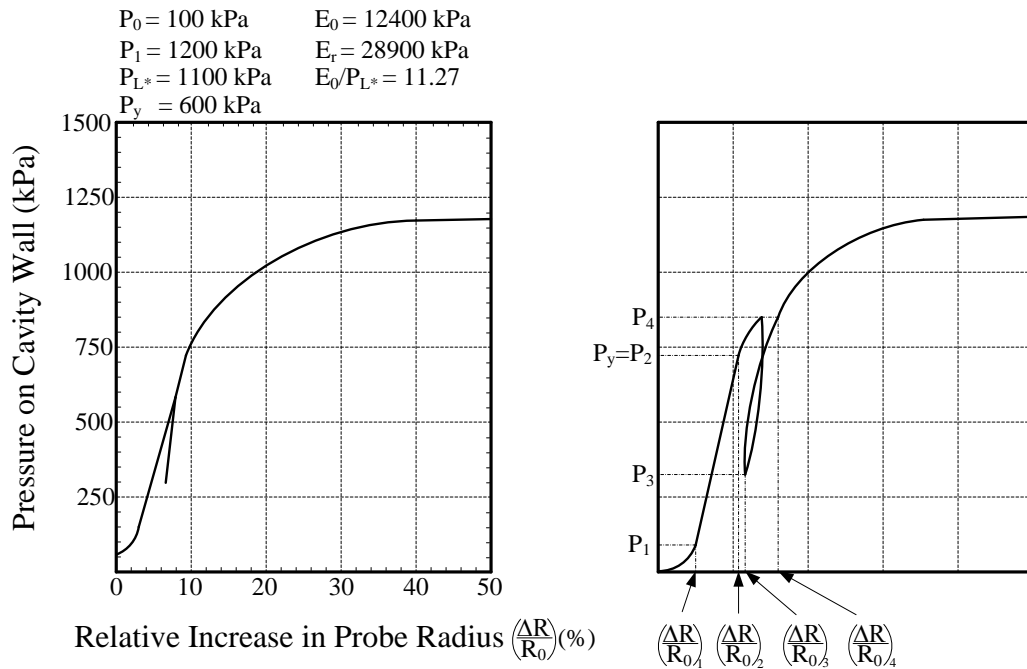


**Figure B-3: Pressuremeter test result**

PMT test result largely depends on the drilling process and the disturbance of the borehole walls. To minimize the disturbance and ensure the full contact between the probe and hole sides, the diameter of the borehole should be slightly larger than the PMT probe and improved techniques should be applied to make the borehole. The following recommendations are suggested if  $D_1$ ,  $D_2$ , and  $D_3$  denote the diameter of the drilling tool, of the deflated probe, and of the borehole before inflation of the probe respectively:

$$D_2 < D_1 < 1.03D_2$$

$$1.03D_2 < D_3 < 1.20D_2$$

The most commonly recommended method for preparing the borehole is the wet rotary method. In this case the rotation of the drill bit should be slow (about 60 rpm) and the circulation of the drilling mud should also be slow. The bottom of the borehole should be at least 1 m deeper than the PMT location to allow any cuttings not transported up to the surface to settle at the bottom of the hole. Other methods can be used as shown in Table B-1.

**Table B-1: Guidelines for PMT borehole preparation (ASTM D4719-07)**

Soil	Type	Rotary Drilling With Bottom Discharge of Prepared Mud	Pushed Thin Wall Sampler	Pilot Hole Drilling and Subsequent Sampler Pushing	Pilot Hole Drilling and Simultaneous Shaving	Hand Auger in the Dry	Hand Auger with Bottom Discharge of Prepared Mud	Driven or Vibro-Driven Sampler
Clayey Soils	Soft	2 <sup>B</sup>	2 <sup>B</sup>	2	2	NR	1	NR
	Firm to Stiff	1 <sup>B</sup>	1	2	2	1	1	NR
	Stiff to Hard	1	2	1	1	NA	NA	NA
Silty Soils	Above GWL <sup>C</sup>	1 <sup>B</sup>	2 <sup>B</sup>	2	2 <sup>B</sup>	1	2	2
	Under GWL <sup>C</sup>	1 <sup>B</sup>	NR	NR	2 <sup>B</sup>	NR	1	NR
Sandy Soils	- Loose and Above GWL <sup>C</sup>	1 <sup>B</sup>	NR	NR	2	2	1	2
	-Loose and Below GWL <sup>C</sup>	1 <sup>B</sup>	NR	NR	2	NR	1	NR
	-Medium to Dense	1 <sup>B</sup>	NR	NR	2	1	1	2
Sandy Gravels or Gravelly Sands Below GWL	Loose							
	Dense	2	NA	NA	NA	NA	NA	NR
Weathered Rock		NR	NA	NA	NA	NA	NA	NR
		1	NA	2 <sup>B</sup>	NA	NA	NA	1

A 1 is first choice, 2 is second choice, NR is not recommended and NA is nonapplicable.

B – Method applicable only under certain conditions. C – GWL is ground water level. D – Pilot hole drilling required beforehand.



Prior to the main test, two calibrations should be conducted: Volume and Pressure calibrations. In pressure calibration, probe is tested to determine the amount of pressure  $P_c$  required to inflate the probe in the air. In membrane resistance calibration, probe is also calibrated to determine the amount of volume  $V_c$  necessary to inflate the probe in a tight fitting thick steel tube. The PMT test can be performed in increments of either pressure or volume, however, increase in volume is preferred since unlike the pressure increase there is no need to approximate the limit pressure  $P_L$ . The data reduction consists of converting the raw data into the corrected pressure and corresponding relative increase in borehole radius using the calibration  $P_c$ ,  $V_c$  and applying the confinement pressure adjustment (Briaud 1992).

### **Standard Penetration Test (SPT)**

Standard Penetration Test is a simple and inexpensive, thus extensively used in situ testing method to provide information of soil properties especially granular deposits such as sands and gravels. However, some countries such as Brazil have extended the use of SPT testing for soft soils (silt and clay) (Briaud 2013). This method also allows for a disturbed soil sample. SPT testing procedure consists of insertion of a sampler into the soil dropping a rigid 623N hammer from a height of 0.76 m and counting the number of blows required to advance the split-barrel sampler for three 0.15 m penetrations (over depth interval of 0.15 m to 0.45 m). The N-value, the indication of the penetration resistance of soil, is reported as sum of blows number for the last two 0.15 m drives. This  $N_{SPT}$  should be adjusted to a constant energy level (60% of the theoretical energy

N60). Additionally the normalization to an overburden stress level and accounting for different drop heights and rod length might be necessary (ASTM Standard D1586). In this study, the consulting firm Terracon Inc. performed the SPT tests in the field.

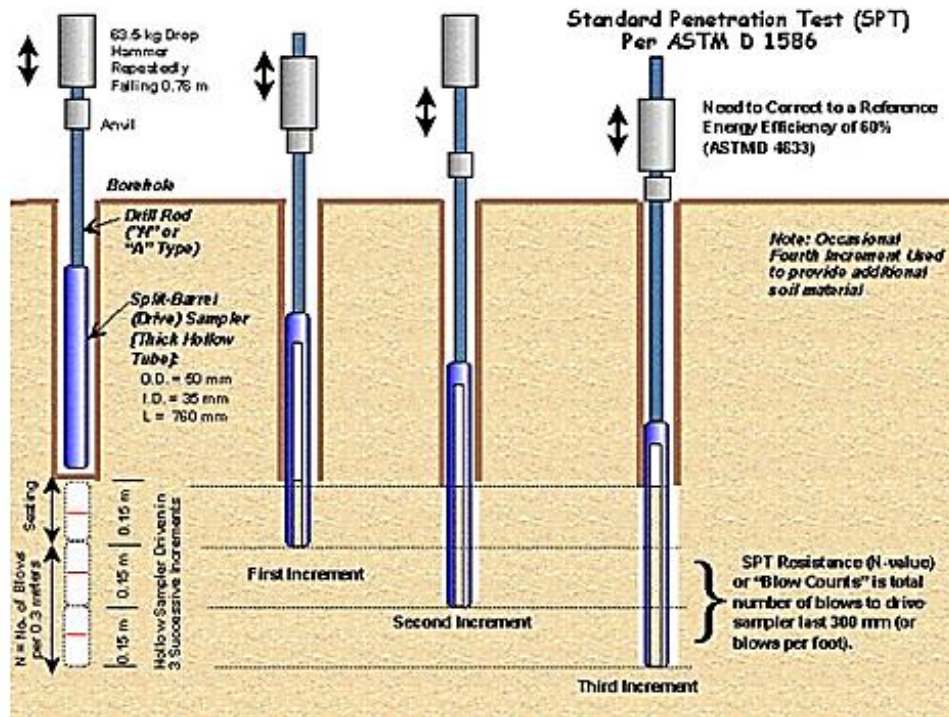
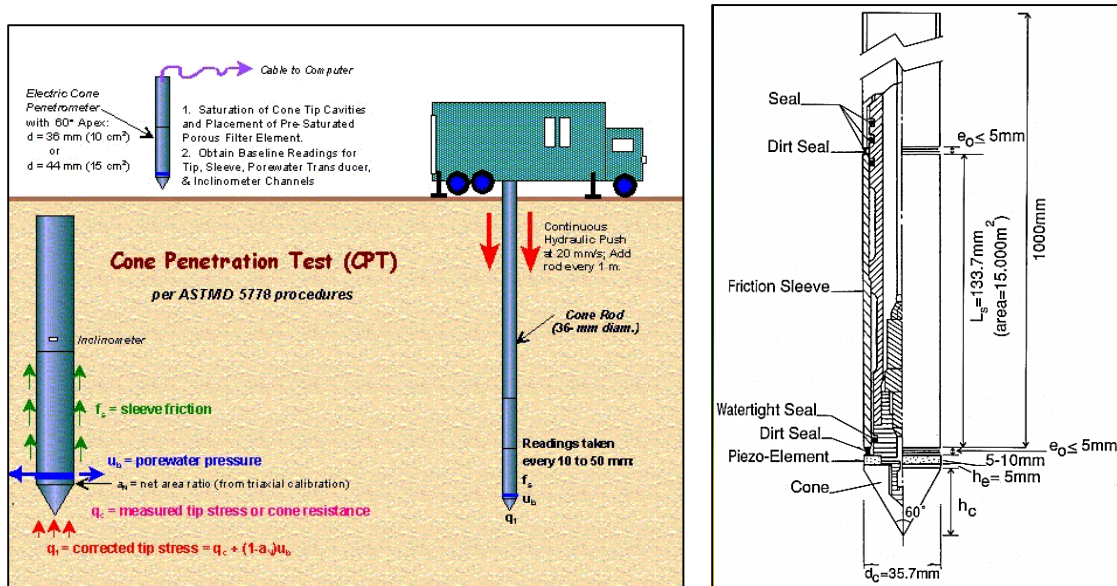


Figure B-4: The Standard Penetration Test (SPT) procedure (Retrieved from the website: Geotechnical and Foundation Engineering)

### Cone Penetration Test

Cone Penetration Test a common simple and efficient in situ testing method provides a detailed continuous record of cone resistance including tip and sleeve friction and porewater pressure. This test is a valuable means to determine the subsurface stratigraphy and in sequence engineering properties of soil. The test consists of penetrating an instrumented cone (either mechanical type or electrical type

penetrometer) attached to a rod into the soil and recording cone, sleeve resistance and porewater pressure. Additional sensors may be included in the cone to monitor useful data such as temperature, shear wave velocity and electrical conductivity. The standard test methods of mechanical cone penetration test and electronic friction cone and piezocone penetration testing are covered in ASTM D3441-05 and ASTM D5778 – 07, respectively.



**Figure B-5: CPT testing setup and an example of a mechanical cone penetrometer**

### Unconsolidated Undrained Triaxial Test (UU)

This test provides information to determine the undrained compressive strength of soil in terms of the total stress. The specimen under a certain confining fluid pressure is sheared in compression while no drainage is permitted. The UU test strength is applicable to cases that involve highly rapid loading (ASTM Standard D2850).

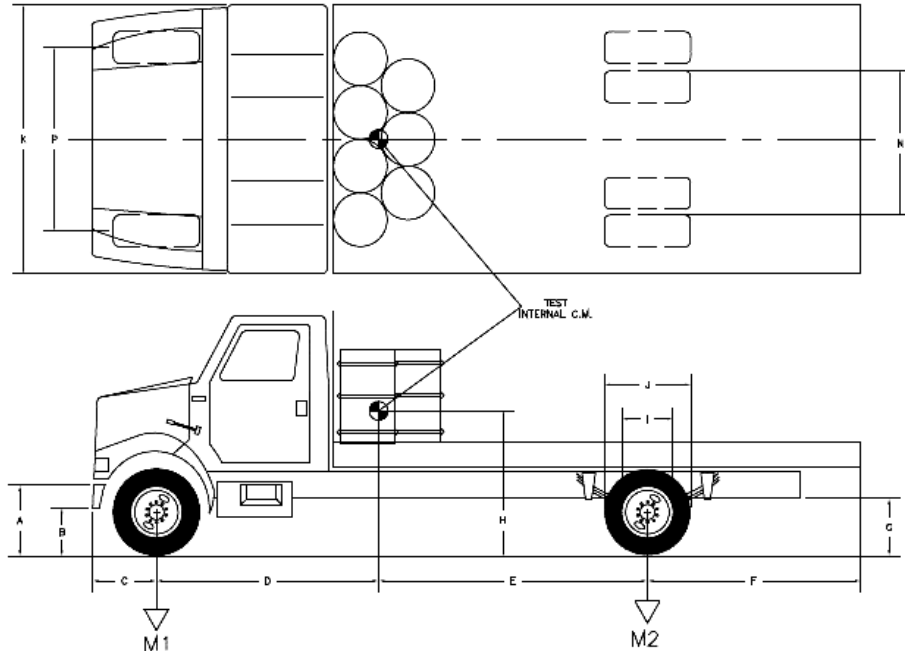
## APPENDIX C

### TEST VEHICLE PROPERTIES AND INFORMATION

DATE: 2010-05-27 TEST NO.: 400951-SNL24 VIN NO.: 1HTSCABN41H369576

YEAR: 2001 MAKE: International MODEL: 4700

TIRE SIZE: 275/80R22.5 ODOMETER: 145741



**GEOMETRY (inches)**

A 31.5 B 20.5 C 30.5 D 103.5 E 102.5 F 111.5 G 29.0  
 H \_\_\_\_\_ I 23.5 J 39.5 K 94.0 L 80.5 N \_\_\_\_\_ D+E = 206

Allowed Range for Wheelbase (D+E) = 208 ± 20 inches

**MASS DISTRIBUTION (lb)**

LF	3770	RF	3730	LR	3910	RR	3660
<u>MASS (kg)</u>		<u>CURB</u>		<u>TEST INERTIAL</u>			
M <sub>1</sub>		6340		7500			
M <sub>2</sub>		5800		7570		Allowed Range	
M <sub>Total</sub>		12,140		15,070		for Inertial Wt. =	
						15000 ± 309 lb	

**Figure C-1: Vehicle properties for the test 400951-SNL24**

Date: 2013-12-12 Test No.: 478260-USD22

Year: 2000 Make: Chevrolet

Tire Inflation Pressure: 60 PSI Odometer: 190363

Describe any damage to the vehicle prior to test:

• Denotes accelerometer location.

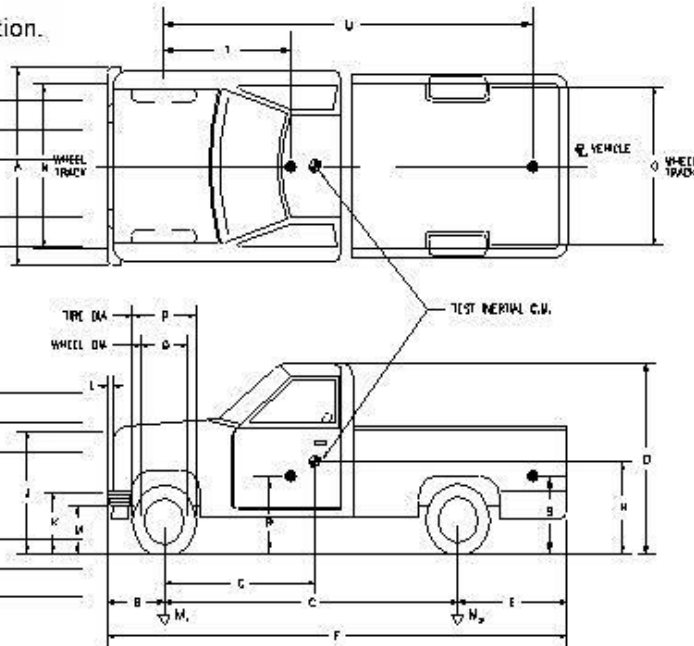
NOTES:

Engine Type: V8  
 Engine CID: 5.7 liter  
 Transmission Type:

Auto  
 Manual

Optional Equipment:

Dummy Data:  
 Type: No dummy  
 Mass:  
 Seat Position:



Geometry ( inches )

A	74.00	E	50.00	J	43.00	N	63.00	R	28.75
B	34.00	F	216.00	K	26.00	O	64.50	S	34.50
C	132.00	G	60.46	L	3.50	P	29.50	T	57.50
D	72.25	H	—	M	17.00	Q	17.50	U	132.00

Mass

( lb )	Curb	Test Inertial	Gross Static
M <sub>1</sub>	2674	2745	2745
M <sub>2</sub>	1951	2320	2320
M <sub>Total</sub>		5065	5065

Mass Distribution

( lb ): LF: 1433 RF: 1312 LR: 1145 □

Figure C-2: Vehicle properties for the test 478260-USD22

## **APPENDIX D**

### **USER'S MANUAL FOR TAMU-POST (GROUP)**

TAMU-POST (Group) is an analysis program that can evaluate the response of a group of in-line piles, connected by a beam, embedded in any type of soil, and subjected to horizontal vehicle impact. TAMU-POST has been developed at Texas A&M University under the direction of Professor Jean-Louis Briaud in collaboration with the Texas A&M Transportation Institute (TTI). The project was sponsored by the United States Department of States. The development of TAMU-POST (Group) benefited from the prior development of TAMU-POST (Single) dealing with single pile impacts. The use of the TAMU-POST (Group) program requires some basic knowledge in soil mechanics and structural principles.

TAMU-POST (Group) has been framed in an excel spreadsheet to facilitate its use in practice. Software requirements are Windows XP and later, Microsoft Office. The user's manual provides step-by-step instructions to input the data, run the program, and analyze a group of piles subjected to vehicle impact. The program was verified against two full scale experiments: an impact test against a group of eight in-line piles in loose sand connected by a beam and an impact test on a group of four in-line piles in hard clay connected by a beam. It was also compared to a large number of numerical simulations performed using LS-DYNA. The main features of TAMU-POST (Group) include:

- It can analyze a group of in-line piles hit by any vehicle class within the common range (i.e. small car passenger C with a mass of 800 kg, Pickup Truck P with a mass

of 2300 kg and Medium duty truck M with a mass of 6800 kg) with any approaching velocity within the common range (i.e. 40 mph, 50 mph, and 60 mph).

- The number of piles can vary from three to eight and the impact can be on any of the piles or on the beam, between the piles.
- The soil type can be clay, sand or soft rock with any soil strength. Soil strength is categorized from 1 = low strength to 5 = high strength in this report.
- TAMU-POST does require soil input data. The program requires Pressuremeter data (limit pressure and modulus). If PMT data is not available, data from the other common tests (Standard Penetration Test SPT or Cone Penetration Test CPT or Undrained Triaxial Test UU) can be used; the program will convert the data from these tests to the PMT data through empirical correlations.
- The ratio of the pile spacing (center to center) to the pile width (perpendicular to the impact) can vary from 5 to 50.
- The piles and beam can have any cross section and can be made of any material but all piles must be identical. Note that the failure mechanisms such as cracking in concrete material or fracture in wooden material have not been studied. Therefore, if concrete or wood are used, special attention should be paid to ensure providing the material strength prior to yielding.
- TAMU-POST (Group) predicts the maximum deflection of the beam and the dynamic penetration very well but tends to overestimate the bending moment in the pile and the beam.

The graphical user-interface features of the TAMU-POST (Group) include:

- Both SI units and American customary units can be used.
- The barrier layout, number of piles, and node number allocation can be selected from the pre-drawn sketches.
- The most important outputs (i.e. maximum deflection, dynamic penetration, maximum bending moment in the beam and pile) are presented and compared to the criteria right below the input selection to help the user optimize the design.
- TAMU-POST does not give a result if the input parameters are not correctly provided (for example if the number of piles does not lie between 3 and 8).
- Other outputs (i.e.: the beam moment envelop, the impact force on the impact node,...) are presented in a separate sheet.

### **TAMU-POST Structure**

The primary objective of developing TAMU-POST (Group) was to reduce the complexity of the dynamic soil-pile-beam interaction problem during an impact on a group of piles and to automate the calculations in a fast, efficient and simple manner. The calculations for a new case take at most one minute to complete. The Excel Spreadsheet program includes eight pages that guide the user from the beginning to the end of the response analysis.



### **The Input Pages (Vehicle, Pile, Beam, Soil and Layout)**

The required parameters are input into the main code through the Input Pages. The input parameters describe the features of the barrier such as structural properties of the piles and beams, geotechnical data, piles layout as well as the vehicle mass and approaching velocity. For convenience, the unit system can be switched between the SI system and the American customary system. If the input data is entered incorrectly (i.e. negative value or value out of the suggested ranges) the cells with the incorrect data become red and the program does not work. To facilitate the design procedure, a table including a summary of the results (e.g. maximum displacement of the impact point, maximum bending moment in the piles and the beam) is embedded in each input page. If the user does change any input parameter, the program reruns immediately so that the user can inspect the effect of that parameter on the response of the barrier.

### **The Solver Page**

The computation core is also included in the Excel program to provide the user an insight into the theoretical calculations performed by the program. The solver page shows the matrices generated by solving the governing differential equation using the finite difference method (refer to the Section 5 for more information). The program computes the displacement, velocity, moment and acceleration for all the nodes at the posts and at half span of the beam so that the user has access to all the data for any point of concern in addition to the impact node.

### Detailed Results Page

This page displays the important outputs. According to the ASTM F2656-07, a successful barrier design is reached if, upon impact, the front edge of the flat bed of the truck does not pass the initial location of the barrier more than one meter. Therefore the most important output to design a new barrier is the maximum deflection at the impact point and the dynamic penetration. The next most important output is the maximum bending moment in piles and beam. Other parameters such as the impact force at the impact point and the beam moment envelop are presented. If any other parameter at any other node is of interest, the user can easily refer to the solver page and look for that parameter.

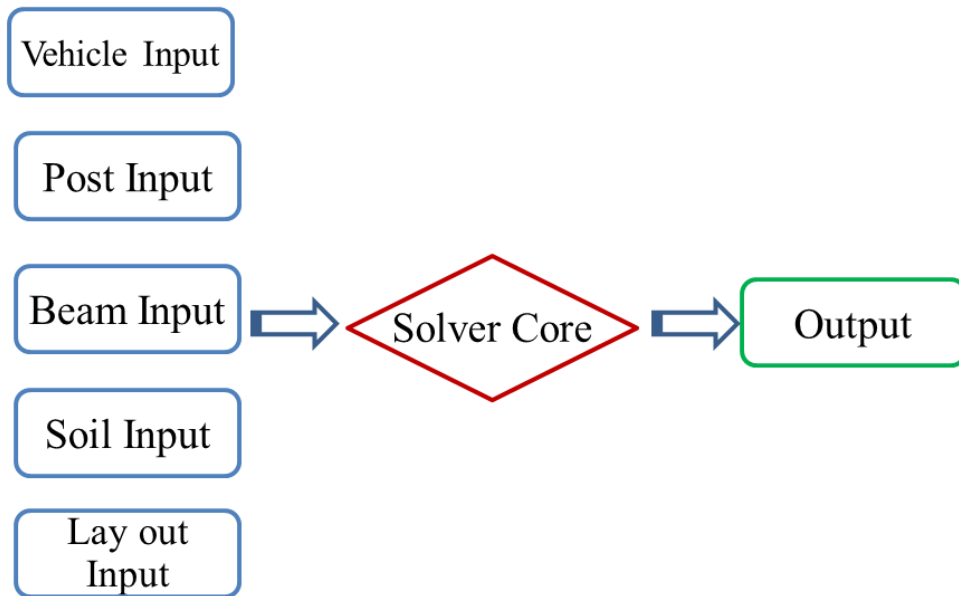


**Figure D-1: The structure of the program TAMU-POST (Group)**

## Using TAMU-POST (Group)

TAMU-POST (Group) is used to design a group of piles and beam system in a given soil to capture a truck with a certain mass and approaching with a certain velocity. The process consists of choosing a system and checking if the system can stop the vehicle within a predefined distance. The geotechnical properties of the soil are input (PMT, CPT, SPT or Undrained Triaxial test). Given the soil properties, the designer must choose the number of piles, the spacing between piles, and the structural properties of the beam and the piles. Then the program is run and the output gives the response of the system. If any of the criteria are not met, the user can try another possible pile-beam system.

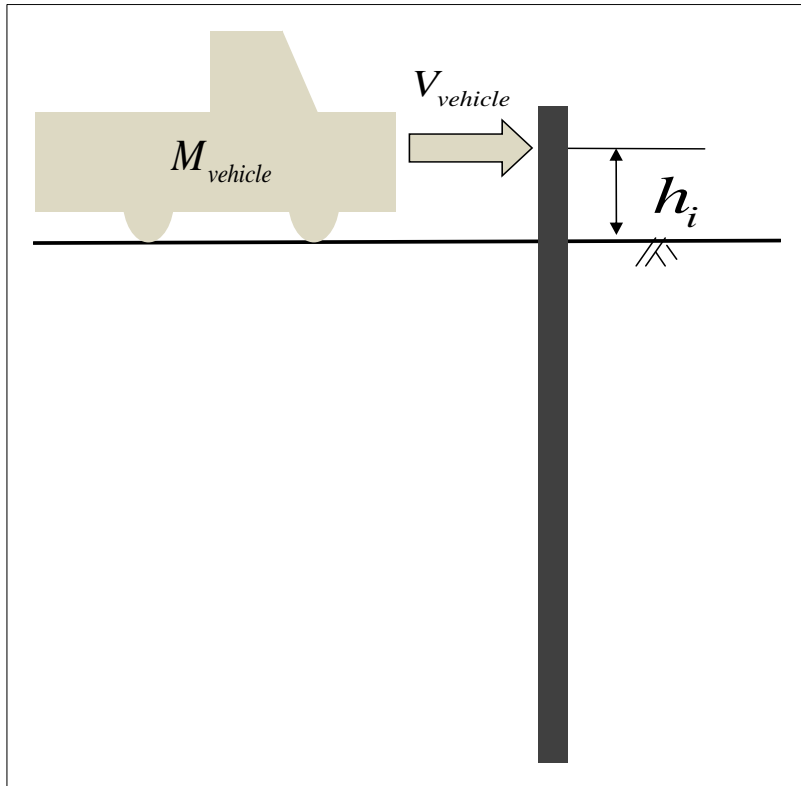
There are two ways to get the program to run a case: automatic or manual. Automatic means that anytime the user changes an input quantity the program starts running and a new set of answers is output. Manual means that once all parameters are input, the user can start the program manually. To select and switch from one to the other, you can access “*Calculation Options*” under the “*Formulas*” tab on the top bar of the Excel program. If you select “*Manual*” after filling out the input pages, click on “*Calculate Now*” and the program will run. You can also select the “*Automatic*” option from the same menu. The general procedure involves the following steps:

### **Input Page “Vehicle”**

Provide the input data associated with the vehicle:

- Insert the vehicle class (See Table D-1)
- Insert the approaching velocity of the vehicle ( $V_v$ )
- Insert the total Mass of the vehicle ( $M_v$ )
- Insert the height of impact ( $h$ )

Based on the vehicle type and the approaching velocity, estimate  $L_{crushed}$  (See Table D-2). This regards the crushing of the vehicle during impact. Table D-2 gives a conservative estimate of this crushing length based on simulations of impact against a rigid wall. See the full report for more details on  $L_{crushed}$ .



Vehicle		
Vehicle Class (See Table 1)	P	
Velocity of the Vehicle, $V_v$	<b>mph</b>	<b>m/s</b>
		17.88
Mass of the Vehicle, $M_v$	<b>lb</b>	<b>kg</b>
		2300
Impact Height, $h_i$	<b>ft</b>	<b>m</b>
		0.7
Lcrushed (See Table 2)	<b>m</b>	
	1.8	

**Figure D-2: The input data for the Vehicle**

**Table D-1: Test designations according to the ASTM Standard F2656-07**

Test Vehicle/Minimum Test Inertial Vehicle	Mass, kg (lbm)	Minimum Test Velocity km/h (mph)	Permissible Speed Range km/h (mph)	Kinetic Energy KJ (ft-kips)	Condition Designation
Small passenger car (C)	1100 (2430)	65 (40)	60.1-75.0	179 (131)	C40
		80 (50)	75.1-90.0	271 (205)	C50
		100 (60)	90.1- above	424 (295)	C60
Pickup truck (P)	2300 (5070)	65 (40)	60.1-75.0	375 (273)	PU40
		80 (50)	75.1-90.0	568 (426)	PU50
		100 (60)	90.1- above	887 (613)	PU60
Medium-duty truck (M)	6800 (15000)	50 (30)	45.0-60.0	656 (451)	M30
		65 (40)	60.1-75.0	1110 (802)	M40
		80 (50)	75.1-above	1680 (1250)	M50
Heavy goods vehicle (H)	29500 (65000)	50 (30)	45.0-60.0	2850 (1950)	H30
		65 (40)	60.1-75.0	4810 (3470)	H40
		80 (50)	75.1-above	7280 (5430)	H50

**Table D-2: Estimation of the Lcrushed upon the vehicle type and approach speed**

Crushing Length of Vehicle Table	Approach speed		
	40 mph	50 mph	60 mph
Truck	1.9m	1.5m	1.1m
Pickup truck	1.8m	1.6m	1.4m
Sedan	1.4m	0.9m	0.4m
		↓	
<b>Lcrushed</b>	<b>1.8</b>		

### **Input Page “Pile”**

Provide the structural input data associated with the piles (Figure D-3). It is assumed that the piles are identical in material and section.

- Input the descriptive section type of the piles
- Input the total length of the piles, (L)
- Input the embedded length of the piles, (D)
- Input the width of the piles, (B)
- Input the Young's modulus of the piles material, ( $E_{pile}$ )
- Input the moment of inertia of the piles, ( $I_{pile}$ )
- Input the mass per unit length of pile, ( $M_{pile}$ )
- Input the yield strength of the pile material, ( $F_{y_{pile}}$ )
- Input the ultimate strength of the pile material, ( $F_{u_{pile}}$ )
- Input the plastic section modulus of the piles, ( $Z_{pile}$ )

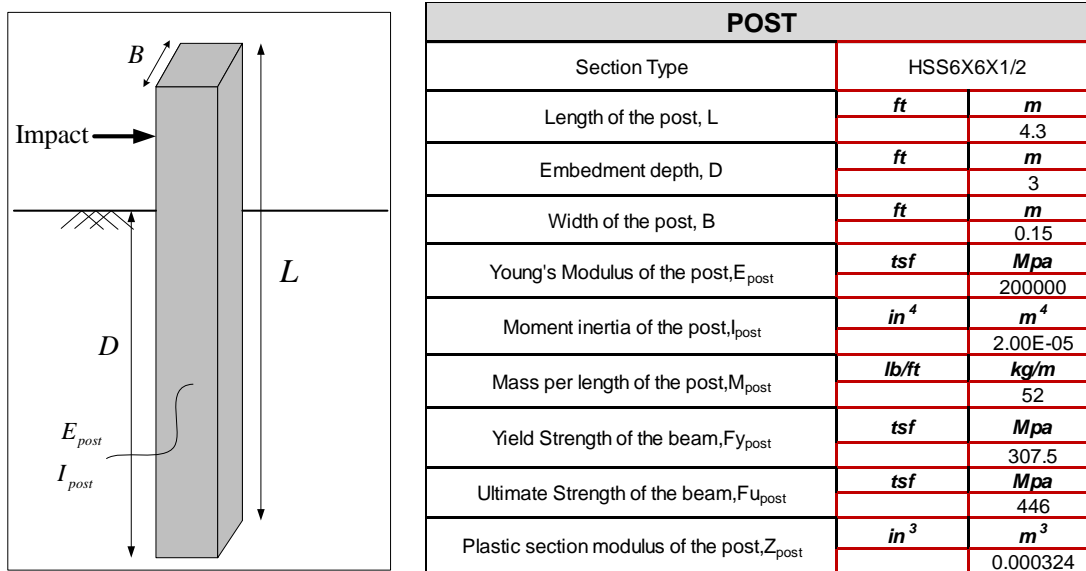


**Figure D-3: The input page “Pile”**

### Input Page “Beam”

Provide the structural input data associated with the beam (Figure D-4):

- Input the section type of the beam
- Input the Young's modulus of the beam material ( $E_{beam}$ )
- Input the moment inertia of the beam ( $I_{beam}$ )
- Input the mass per unit length of the beam ( $M_{beam}$ )
- Input the yield strength of the beam material, ( $F_{y_{beam}}$ )
- Input the ultimate strength of the beam material, ( $F_{u_{beam}}$ )
- Input the plastic section modulus of the beam, ( $Z_{beam}$ )



<b>Beam</b>		
Section Type	HSS10X10X1/2	
Young's Modulus of the beam, $E_{beam}$	<b>tsf</b>	<b>Mpa</b>
		200000
Moment inertia of the beam, $I_{beam}$	<b>in<sup>4</sup></b>	<b>m<sup>4</sup></b>
		0.000052
Mass of the beam per length, $M_{beam}$	<b>lb/ft</b>	<b>kg/m</b>
		73
Yield Strength of the beam, $F_{ybeam}$	<b>tsf</b>	<b>Mpa</b>
		307.5
Ultimate Strength of the beam, $F_{ubeam}$	<b>tsf</b>	<b>Mpa</b>
		446
Section Modulus of the beam, $Z_{beam}$	<b>in<sup>3</sup></b>	<b>m<sup>3</sup></b>
		0.000614

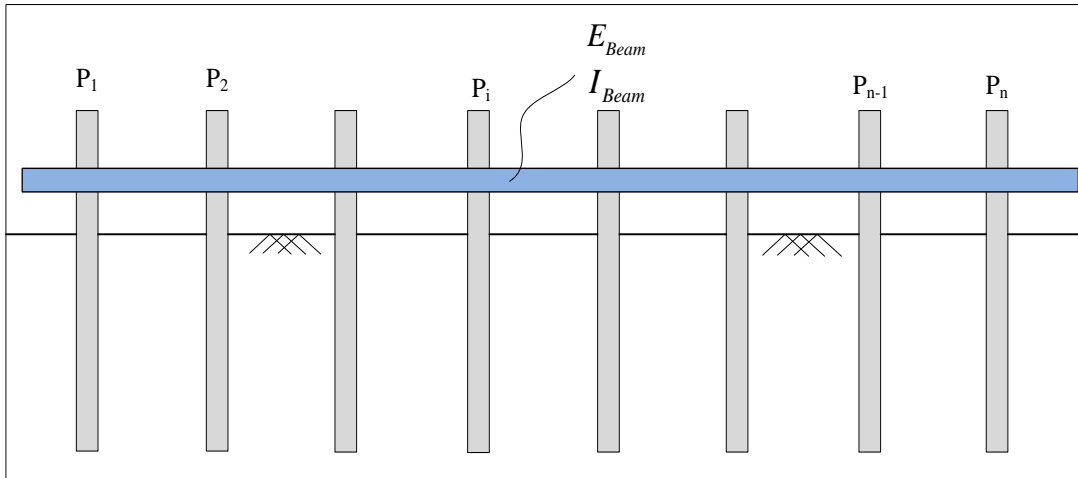


**Figure D-4: The input page “Beam”**

## Input Page “Soil”

Provide the input data associated with the soil (Figure D-5):

- Input the type of soil: Clay, Sand
- Input the Poisson’s ratio of the soil.
- Input the average pressuremeter limit pressure  $P_L$  (PMT) within the stressed zone if available.
- Input the average pressuremeter modulus,  $E$  (PMT) within the stressed zone if available.
- Input the average Standard Penetration Test blow count per foot  $N$  (SPT) within the stressed zone if available. In this case the SPT  $N$  value will be transformed into a PMT limit pressure  $P_L$  and a PMT modulus  $E$  automatically based on correlations recommended by Briaud (2013).
- Input the average tip resistance of the CPT ( $q_c$ ) within the stressed zone if available. In this case the CPT  $q_c$  value will be transformed into a PMT limit pressure  $P_L$  and a PMT modulus  $E$  automatically based on correlations recommended by Briaud (2013).
- Input the average undrained shear strength ( $S_u$ ) within the stressed zone if available. In this case the  $S_u$  will be transformed into a PMT limit pressure  $P_L$  and a PMT modulus  $E$  automatically based on correlations recommended by Briaud (2013).

Soil		
	Soil Type	Sand
	Poisson's ratio	0.35
	Unit weight $\gamma_{soil}$	<b>pcf</b>
		<b>kN/m<sup>3</sup></b>
		18
<b>PMT</b>	Limit Pressuremeter PL <sub>(PMT)</sub>	<b>tsf</b>
		<b>Mpa</b>
		0.4
	Pressuremeter Modulus, E <sub>(PMT)</sub>	<b>tsf</b>
		<b>Mpa</b>
		5
<b>SPT</b>	Standard Penetration Test blow counts <sub>(SPT)</sub>	
	Limit Pressuremeter PL <sub>from SPT</sub>	
	Pressuremeter Modulus, E <sub>from SPT</sub>	
<b>CPT</b>	Tip Resistance <sub>(qc)</sub>	
	Limit Pressuremeter PL <sub>from qc</sub>	
	Pressuremeter Modulus, E <sub>from qc</sub>	
<b>Su</b>	Undrained Shear Strength <sub>(Su)</sub>	
	Limit Pressuremeter PL <sub>(PMT) from Su</sub>	
	Pressuremeter Modulus, E <sub>from Su</sub>	

**Figure D-5: The input page “Soil”**

### **Input Page “Layout”**

- Input the number of the piles, based on the options presented in the embedded figures (Figure D-6 and Figure D-7).
- Input the center to center spacing between the piles (S).
- Input the node number which will be subjected to the impact based on the embedded figure in the page.

Layout of Piles		
Number of piles	4	
Space between the piles	<i>ft</i>	<i>m</i>
		5.2
The node under impact	8	

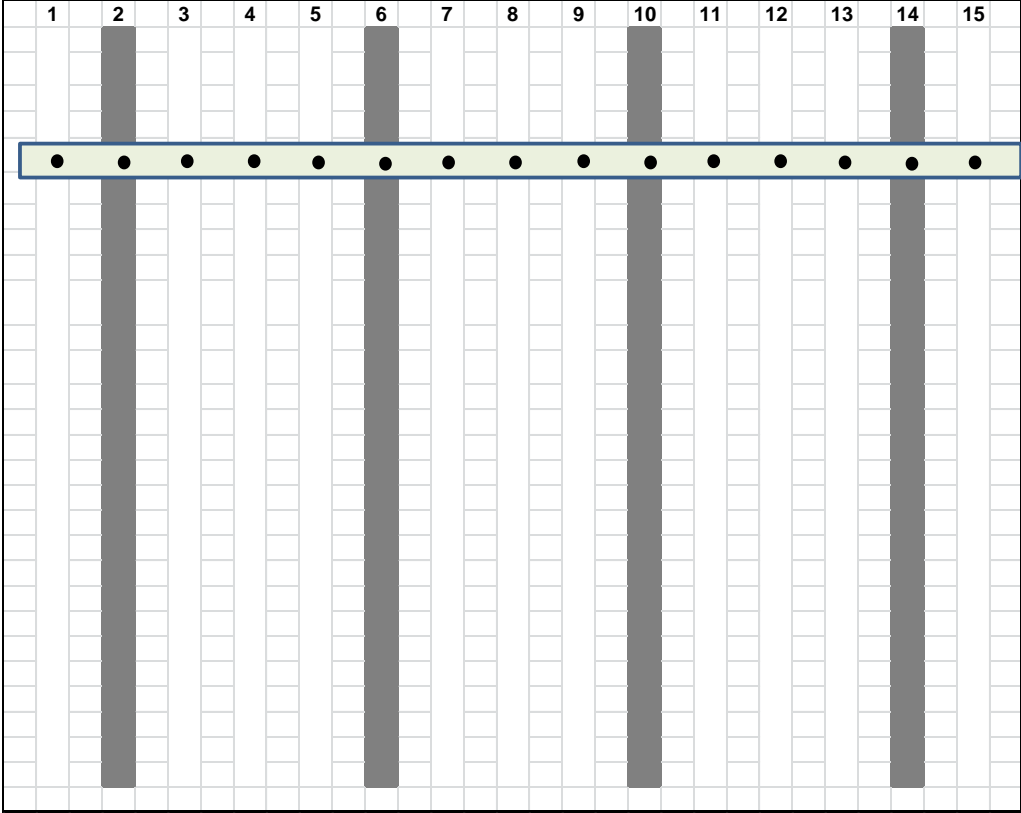
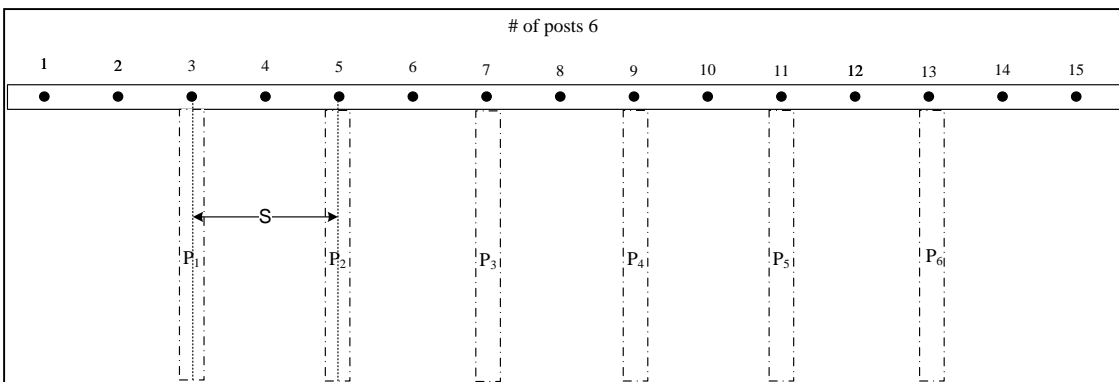
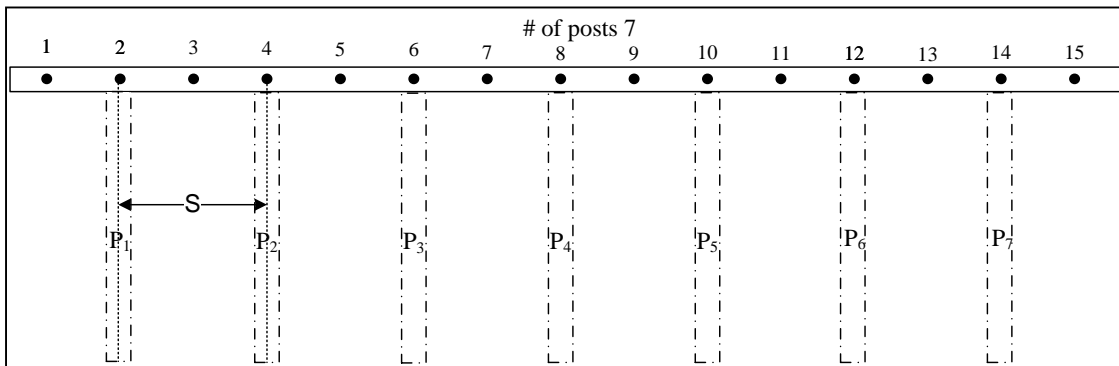
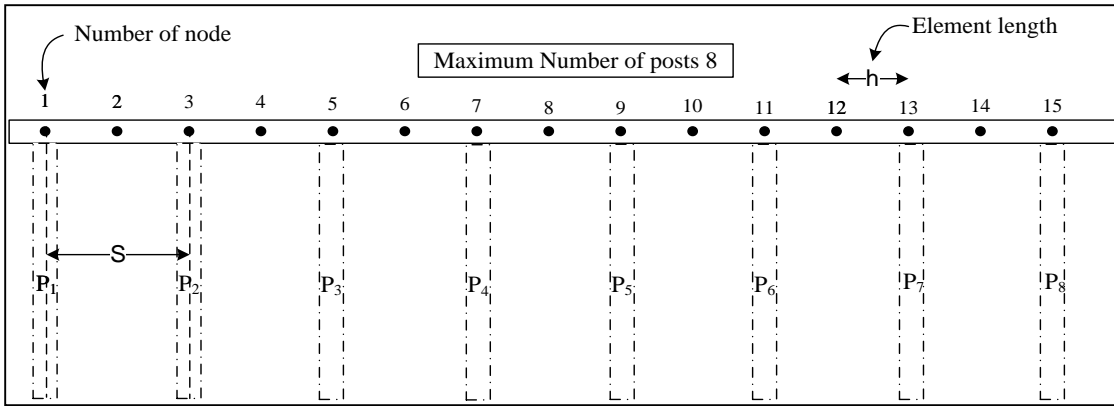
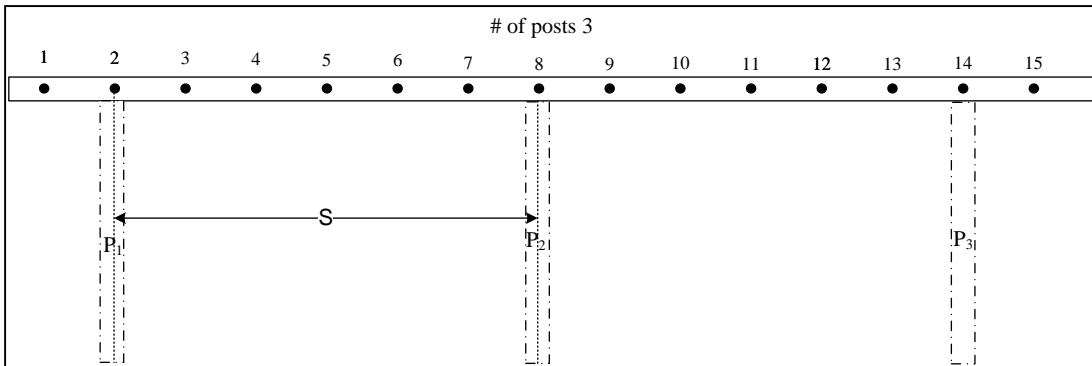
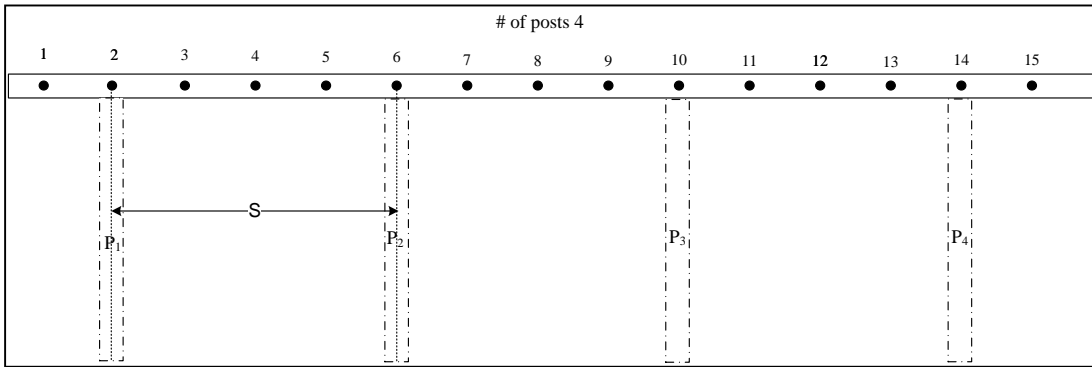
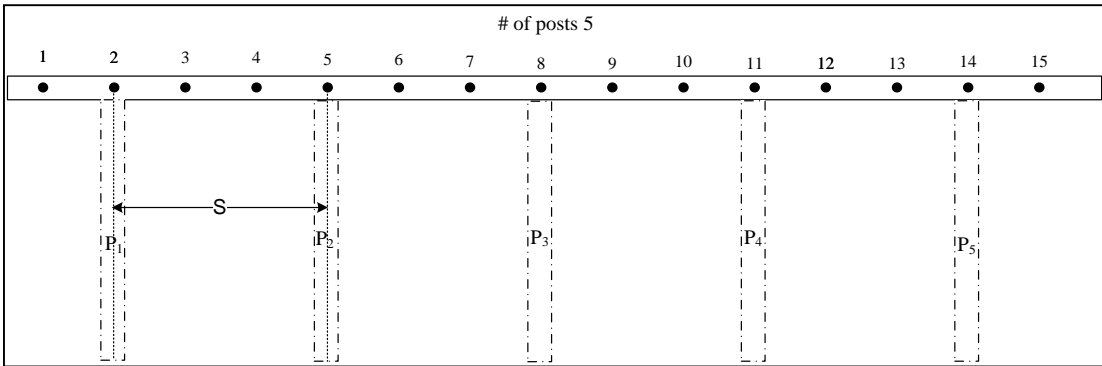


Figure D-6: The visual selection of layout

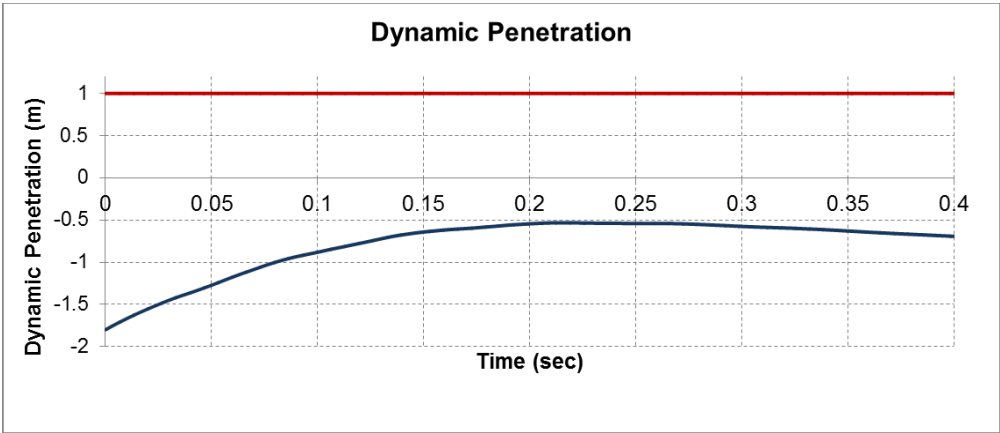
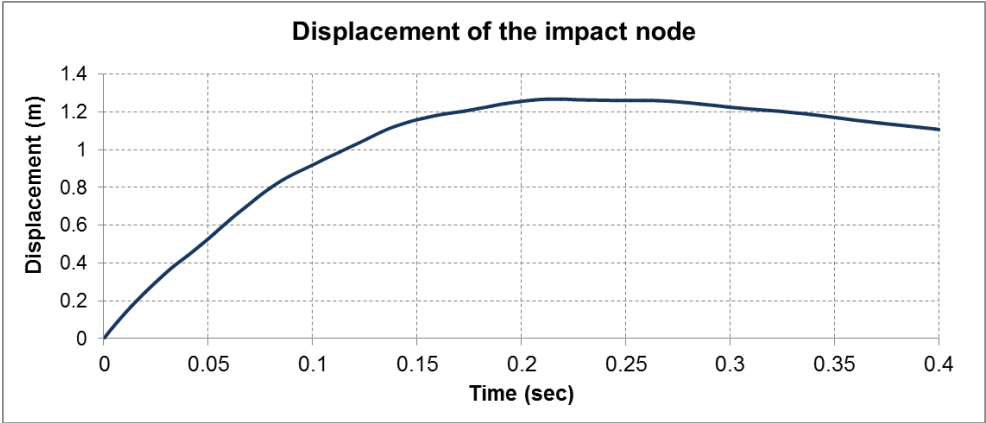




**Figure D-7: The nodes allocated to the piles and the mid span points**

### Detailed Results

This page includes the results for the displacement at the point of impact, the bending moment of the beam at the point of impact, and the impact force at the point of impact (Figure D-8).



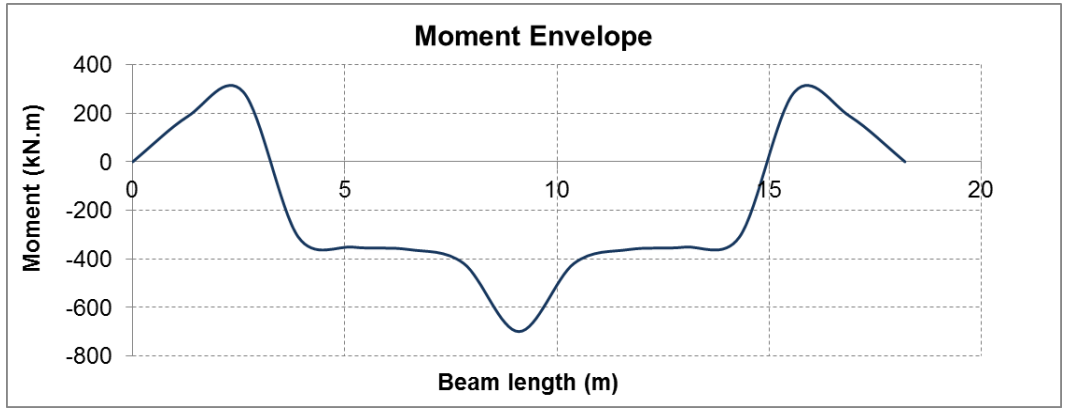
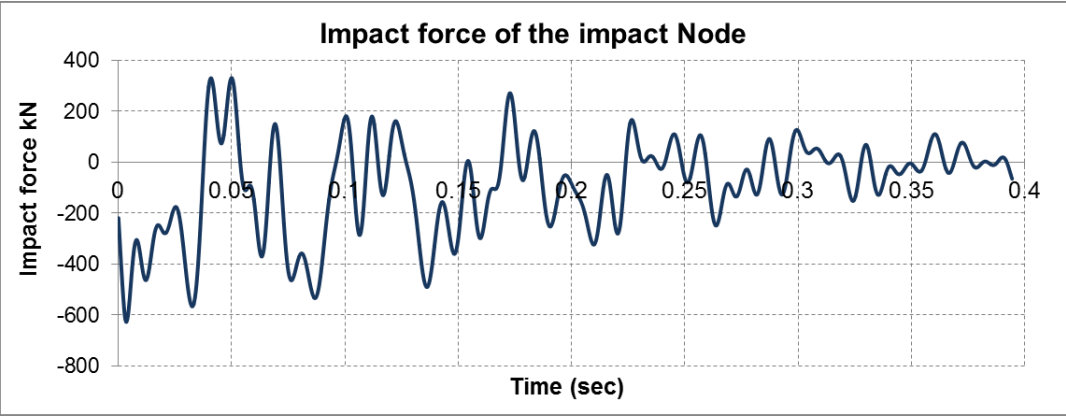


**Figure D-8: The detailed results**



## APPENDIX E

### MATLAB CODE (MONTE CARLO SIMULATION AND TAMU-POST)

```
%Monte Carlo Simulation and computing the probability of failure

NS=5000;

% Identify the random variables: Crushing factor
m1 = 0.8;
cv1=0.05;
v1=(cv1*m1)^2;
mu1 = log((m1^2)/sqrt(v1+m1^2));
sigma1 = sqrt(log(v1/(m1^2)+1));
X1 = lognrnd(mu1,sigma1,NS,1);
x1=linspace(min(X1),max(X1),NS);

% Identify the random variables: Pressuremeter Limit pressure PL
m2 = 0.8e6;
cv2=0.2;
v2=(cv2*m2)^2;
mu2 = log((m2^2)/sqrt(v2+m2^2));
sigma2 = sqrt(log(v2/(m2^2)+1));
X2 = lognrnd(mu2,sigma2,NS,1);
x2=linspace(min(X2),max(X2),NS);

for tt=1:NS
Fac_Vv=X1(tt);
PL_PMT=X2(tt);
Es=1e7;
rho=1900;

% Calling TAMU-POST(Group) to calculate the deterministic maximum DP
[MDispTD1,Dyn_PenD1,alphaD1]=TAMUFUNCTIONM1(0.8,0.8e6,1e7,1900);

% Calling TAMU-POST(Group) to calculate the probabilistic maximum DP
[MDispT1,Dyn_Pen1,alpha1]=TAMUFUNCTIONM1(Fac_Vv,PL_PMT,Es,rho);
MDis1(tt)=MDispT1;
Dyn_Penn1(tt)=Dyn_Pen1;
alpha_m1(tt)=alpha1;
end

save('CASEM1PL_5000.mat','MDis1','Dyn_Penn1','alpha_m1','MDispTD1','
Dyn_PenD1','alphaD1')
```

```

load('CASEM1PL_5000.mat')
% Plotting the PDF and CDF, estimating the probability of failure

figure (3)
subplot(2,1,1)
myFit_Dyn_Pen1=fitdist(Dyn_Penn1.', 'kernel');
index1=linspace(min(Dyn_Penn1),max(Dyn_Penn1),NS);
plot(index1,pdf(myFit_Dyn_Pen1, index1))
xlabel('Dynamic Penetration (m)', 'fontsize',12);
ylabel('PDF', 'fontsize',12);
grid on
subplot(2,1,2)
Y1=cdf(myFit_Dyn_Pen1,index1);
plot(index1,Y1)
xlabel('Dynamic Penetration (m)', 'fontsize',12);
ylabel('CDF', 'fontsize',12);
grid on
I1=find(index1<=1);
ps1=Y1(length(I1));
pof1=1-ps1;

figure (4)
subplot(2,1,1)
myFit_MDispT1=fitdist(MDis1.', 'kernel');
index11=linspace(min(MDis1),max(MDis1),NS);
plot(index11,pdf(myFit_MDispT1, index11))
xlabel('Maximum Deflection (m)', 'fontsize',12);
ylabel('PDF', 'fontsize',12);
grid on

subplot(2,1,2)
Y11=cdf(myFit_MDispT1,index11);
plot(index11,Y11)
xlabel('Maximum Deflection (m)', 'fontsize',12);
ylabel('CDF', 'fontsize',12);
grid on

```

```

%% Analysis of the group pile system using Multi Degrees of Freedom
%-----
function[MDispT,Dyn_Pen,alpha]=TAMUFUNCTIONM1(Fac_Vv,PL_PMT,Es,rho)
%-----
% Input Data
%-----
load LCrushed

dt=1e-5;
nt=40000;
t=(1:nt)*dt;
%-----
% Vehicle
Mv=6800; % Mass of the Vehicle(kg)
Vv=26.8; % Velocity of the vehicle (m/s)
%-----
% Lay out of the Piles
np=8; % Number of posts
nn=15; % Number of nodes
s=5.2; % Space between the piles (m)
Lmat=zeros(1,15); % Matrix associated with pile layout
no_impact=8; % number of the node under impact
if (np==8)
    Lmat(1)=1; Lmat(3)=1; Lmat(5)=1; Lmat(7)=1;Lmat(9)=1;
    Lmat(11)=1;Lmat(13)=1;Lmat(15)=1;
end
if (np==7)
    Lmat(2)=1; Lmat(4)=1; Lmat(6)=1; Lmat(8)=1;Lmat(10)=1;
    Lmat(12)=1;Lmat(14)=1;
end
if (np==6)
    Lmat(3)=1; Lmat(5)=1; Lmat(7)=1; Lmat(9)=1;Lmat(11)=1;
    Lmat(13)=1;
end
if (np==5)
    Lmat(2)=1; Lmat(5)=1; Lmat(8)=1; Lmat(11)=1;Lmat(14)=1;
end
if (np==4)
    Lmat(2)=1; Lmat(6)=1; Lmat(10)=1; Lmat(14)=1;
end
if (np==3)
    Lmat(2)=1; Lmat(8)=1; Lmat(14)=1;
end
%-----
% Soil-Pile-Beam parameters
% Soil
ks=2.3*Es; % Stiffness property for soil MDOF
(N/m2)
Pu=PL_PMT; % Ultimate static resistance (N/m2)
PL_PMT
nu=0.49; % Possion Ratio of soil

% Pile

```

```

Bp=0.35; % Width of pile (m)
Ip=4.16E-04; % Moment Inertia of the pile (m4)
Ep=2.00E+11; % Elastic Modulus of pile (N/m2)
D=1; % Embedment depth, (m)
H=1; % Height of impact (m)
L=D; % length of the pile (m)
Lp=3.4;
M_length_pile=135;
Mpile=M_length_pile*Lp; % Mass of the pile (kg)
fy=250e6;
Zp=2.57E-03;
Mp_pile=fy*Zp;

% Beam
Bb=0.25; % Width of beam (m) 8in=0.2m
Mb=92.95; % Mass per length of the beam
Eb=2.00E+11; % Elastic Modulus of beam (N/m2)
Ib=1.07E-04; % Moment Inertia of the beam
Zb=9.94E-03; % section modulus of the beam
fy=250e6; % Yield Strength of the steel, Sybeam
Mp_beam=fy*Zb; % yield moment (N.m)

% SDOF equivalent parameters
% SALLOP for Ks and Pu
L0=(4*Ep*Ip/ks)^0.25;
a1=atan(1/(1+2*H/L0))*L0;
b1=L^2/(3*(L+2*H));
a2=L0^2*ks/(2*(L0+H));
b2=L^2*ks/(4*L+6*H);
if L>=3*L0
    Dv=atan(1/(1+2*H/L0))*L0; % Dv zero shear depth
    Ks=L0^2*ks/(2*(L0+H));
else if L<=L0
    Dv=L^2/(3*(L+2*H));
    Ks=L^2*ks/(4*L+6*H);
else
    Dv=b1-(b1-a1)*(L/L0-1)/2;
    Ks=b2-(b2-a2)*(L/L0-1)/2;
end
end
Mpile=M_length_pile*Dv; % Mass of the pile (kg)
Hou=0.75*Pu*Bp*Dv; % Failure load of the pile SALLOP
yf=Hou/Ks; % failure displacement (m)

% Damping
Vs_PMT=(Es/(2*(1+nu)))/rho)^0.5;
Cs_gs=Bp*Ks/Vs_PMT;

m5=0.25*Pu/10^6+0.3;
cv5=0.1;
v5=(cv5*m5)^2;
mu5 = log((m5^2)/sqrt(v5+m5^2));
sigma5 = sqrt(log(v5/(m5^2)+1));

```

```

alpha=lognrnd(mu5,sigma5,1,1);
Cs_g=alpha.*Cs_gs;

% Mass
Ms=rho*Bp*Dv*1*Bp;

h=s/2; % Length of the elements
if (np==5)
    h=s/3;
elseif (np==4)
    h=s/4;
elseif (np==3)
    h=s/6;
end

LmatMass=ones(1,15);
Lmat1=Lmat;
LmatMass(1)=0.5;
LmatMass(15)=0.5;

Mp=Lmat1*Ms+Lmat1*Mpile+LmatMass*Mb*h;
Mp(no_impact)=Mv;

Cg=Lmat*Cs_g;

K=Lmat*Ks;
yf=Lmat*yf; % yield displacement

%% -----
% Main code
e=Eb*Ib/h^3;
cg=Cg/2/dt;
MP=Mp/dt^2;

y=zeros(nn,nt);
v=zeros(nn,nt-1);
acc=zeros(nn,nt-2);
Mom=zeros(nn,nt);
y(no_impact,1)=-dt*Vv*Fac_Vv;

for i=2:nt;
    kfac=ones(1,nn);
    cfac=ones(1,nn);
    mfac=ones(1,nn);
    f=zeros(1,nn);

    for j=1:nn
        if(abs(y(j,i))-abs(y(j,i-1)))>=0 %separation check
            if (abs(y(j,i))>yf(j))
                f(j)=-sign(y(j,i))*K(j)*yf(j); % failure load
                kfac(j)=0;
            end
        end
    end
end

```

```

        else
            f(j)=0;
        end
    else
        f(j)=0;
        kfac(j)=0;
        cfac(j)=0;
    end
end
m=MP;
k=kfac.*K;
mc_g=m+cfac.*cg;
cm_g=cfac.*cg-m;

% main stiffness matrix
emk=zeros(nn,nn);
emk(1,1)=-2*e+2*m(1)-k(1);
emk(1,2)=4*e;
emk(1,3)=-2*e;
emk(2,1)=2*e;
emk(2,2)=-5*e+2*m(2)-k(2);
emk(2,3)=4*e;
emk(2,4)=-e;
for l=3:nn-2;
    emk(1,l-2)=-e;
    emk(1,l-1)=4*e;
    emk(1,l)=-6*e+2*m(l)-k(l);
    emk(1,l+1)=4*e;
    emk(1,l+2)=-e;
end
emk(nn-1,nn-3)=-e;
emk(nn-1,nn-2)=4*e;
emk(nn-1,nn-1)=-5*e+2*m(nn-1)-k(nn-1);
emk(nn-1,nn)=2*e;
emk(nn,nn-2)=-2*e;
emk(nn,nn-1)=4*e;
emk(nn,nn)=-2*e+2*m(nn)-k(nn);

% Displacement
y(:,i+1)=(emk*y(:,i)+cm_g(:).*y(:,i-1)+f(:))./mc_g(:);

%Velocity
for j=1:nn;
    v(j,i)=(y(j,i)-y(j,i-1))/dt;
end

% Moment
for j=2:nn-1;
    Mom(j,i)=(y(j+1,i)-2*y(j,i)+y(j-1,i))/h^2*Eb*Ib;
end
end
end

```

```

% Acceleration
for j=1:nn;
    for i=1:nt-2;
        acc(j,i)=(y(j,i+2)-2*y(j,i+1)+y(j,i))/dt^2;
    end
end

% Bending Moment in Pile
NCpile=7;
if (np==7||np==5||np==3)
    NCpile=8;
elseif (np==4)
    NCpile=6;
end
nsmooth=500;
accs=zeros(1,nt-2+nsmooth);
accs(nsmooth+1:nt-2+nsmooth)=acc(NCpile,1:nt-2);
Accs=smooth(accs,nsmooth);

HOUP=Mp(NCpile).*max(abs(Accs(:)));
zmaxL0=Dv/L0;
MP1=HOUP.*L0.*exp(-zmaxL0).*sin(zmaxL0)+HOUP.*H.*exp(-
zmaxL0).*sin(zmaxL0)+cos(zmaxL0));
MP2=HOUP.*H+HOUP.*Dv+(HOUP.*L+2.*HOUP.*H)./L.^3).*Dv^3-
((2.*HOUP.*L+3.*HOUP.*H)./L.^2).*Dv^2;
if L>=3*L0
    Moment_pile_max=MP1;
else if L<=L0
    Moment_pile_max=MP2;
else
    Moment_pile_max=MP2+(MP1-MP2)*(L/L0-1)/2;
end
end

%% -----
% Post processing
set(0,'defaultAxesFontSize',10);
set(0,'defaultAxesFontName','times');

nsmooth=500;
moms=zeros(1,nt+nsmooth);
moms(nsmooth+1:nt+nsmooth)=Mom(no_impact,1:nt);
Moms=smooth(moms,nsmooth);

MDispT=max(y(no_impact,1:nt));
L_Crushed=LCrushed(1,3);

Dyn_Pen=MDispT-L_Crushed;

end

```